Dinucleating Ligands with Intramolecular Hydrogen Bonding Groups for Effective Phosphodiester Hydrolysis.

A Thesis submitted for the Degree of

Doctor of Philosophy

by

Daniela Natale

School of Chemistry
University of Edinburgh
King's Building
West Main Road
Edinburgh, EH9 3JJ

May 2008

Abstract

An important challenge in chemistry is the hydrolysis of nucleic acids under mild conditions with an efficiency that approaches that of natural enzymes. In the synthesis of small and efficient artificial catalysts it is important to understand how catalysis occurs under biological conditions and to create compounds for practical applications such as artificial restriction enzymes, therapeutic agents and tools in gene therapy.[1,2] In many cases, the extraordinary activity of natural nucleases arises from an active site where the combination of metal ions and acid/base residues provides specific coordination and hydrogen bonding interactions.[3]

In this work, twelve mono and dinucleating dipicolylamine(dpa)-based ligands have been designed and synthesized to investigate the catalytic activity of their corresponding zinc complexes toward the hydrolysis of phosphodiester bonds of RNA model substrates.

The identity and stoichiometry of the metal complexes in solution were evaluated by potentiometric pH titrations, in water and/or in the binary solvent mixture DMSO:H_2O (67%:33%), for four potentially dinucleating dpa-based ligands: *N,N,N',N'*-tetrakis[(2-pyridyl)methyl]-2,6-diamino-*p*-nitrophenol (LOH), *N,N,N',N'*-tetrakis[(6-amino-2-pyridyl)methyl]-2-hydroxy-1,3-diaminopropane (LOH'), 1,3-Bis[bis(pyridin-2-ylmethyl)amino]-propan-2-ol (L^1OH) and *N,N,N',N'*-tetrakis[(6-amino-2-pyridyl)methyl]-2,6-diamino-*p*-nitrophenol (L^1OH').

Results showed that all ligands in the presence of Zn(II) are able to form mononuclear and dinuclear complexes but their stability is strongly affected by the presence of the amino groups in the dipicolylamine core and dependent on the nature of the bridging unit (phenol or alcohol group). In general, the ligand L^1OH' forms the less stable zinc complexes and mainly mononuclear species, wherease LOH' forms the most stable dinuclear complexes. The introduction of hydrogen bonding functionalities also affects the basicity of the ligands, which is enhanced, and decreases the pK_a of a zinc-bound water molecule by *ca.* two pK_a units.

The catalytic efficiency of metal complexes of the ligands with four amino hydrogen bonding groups (L^1OH' and LOH') has been tested on small RNA models and the mechanism of catalysis was investigated with the help of inhibition, solvent

kinetic isotope effect (SKIE) and computational studies. The cleavage rate of HPNPP, an activated RNA model, as well as the more stable substrate UpU, is accelerated a million fold over the uncatalyzed reaction in water, at 25°C and neutral pH.[4] The catalytic ability of dinickel(II), dicobalt(II), dicopper(II) and dicadmium(II) complexes of the ligand LOH' was also investigated and found to follow the order: Ni(II) >> Co(II) > Zn(II) > Cd(II) >> Cu(II).

The X-Ray crystal structure of the complex [Zn_2(LOH')] with 4-nitrophenol phosphate reveals that the phosphodiester dianion binds the complex by bridging the two Zn(II) atoms and hydrogen bonding the four amino groups. These last set of interactions are responsible for the enhanced reactivity of the most active dinuclear zinc catalyst for phosphodiester hydrolysis reported to date.

MS and ^{13}C-NMR experiments show that this complex is also able to activate atmospheric CO_2 to form an insoluble carbonate complex. The fixation of carbon dioxide was, however, only observed with Zn(II) and Co(II) complexes showing that the reactivity reflects geometrical preferences of the metal complex and the different mechanism of catalysis.

Catalytic studies on the reactivity of zinc complexes of the ligand L^1OH' reveal that in this case mononuclear and dinuclear complexes are equally effective to promote the hydrolysis of HPNPP. The results show that hydrogen bonding interactions with the metal-free dipycolylamine unit in the mononuclear zinc complex are catalytically important and they enhance the catalytic activity by two orders of magnitude compared to the former reported most effective mononuclear Zn(II) complex for HPNPP hydrolysis.

Interestingly, the zinc complexes of L^1OH' are not able to fix atmospheric CO_2 indicating that such small catalysts are selective for phosphodiester hydrolysis as they do not react with CO_2 to form carbonate.

In summary, the results presented in this thesis suggest that the cooperation of metals and hydrogen bonding interactions can be applied to substantially activate metal complexes for phosphate hydrolysis.

To my dad.

Acknowledgements

I would like to start this thesis by acknowledging those people who, in one way or another, have contributed to the achievement of this important goal in my life.

First of all, I'm extremely indebted to my supervisor Dr. Juan C. Mareque Rivas for his support, guidance and help during these years and preparation of this thesis. His constant presence, constructive advice and words have been an important reference point professionally and personally during my studies.

I wish also to thank Prof. Francesco Salvatore, my supervisor during my undergraduate years in Naples. His belief in me as a student and as a person has contributed deeply to my self-ambition. Furthermore, I'm thankful to him for also being a good friend, for giving me constantly advices and help with the potentiometric experiments together with Prof. Liberato Ciavatta who I'm also thankful to, for his relevant suggestions during our collaboration and my visits in Naples. I would like to thank Prof. Angela Lombardi from the University of Naples for being strongly supportive during the application and selection process for this PhD position; I'm sure her kind words have played an important role.

Special thanks go to Dr. Nicholas H. Williams form the University of Sheffield for being extremely kind and welcoming during my visits there. Many, many thanks also to Dr. G. Feng for being an excellent and patient teacher during the time I was learning about kinetic experiments and for being always helpful whenever I asked.

A special thanks goes to Dr. Juraj Bella who helped me with the NMR experiments. His smiles and nice company have made everlasting and, sometimes, frustrating experiments an enjoyable time.

I want to express my sincere gratitude to Prof. P. Sadler and Prof. S. Chapman for allowing me to have access to the spectrophotometer in their respective laboratories. I would like to express my thanks to Dr. Andrew Turner for patiently teaching me all I know about Computational Chemistry and for always being available to help me with this difficult area of Chemistry.

Many thanks to my present and former colleagues Pilar, Ganesh, Manish, Laurent, Jordan, Angeles, Jose, Emiliano and Praba for making the lab a nice working environment. A special thanks to Pili, my labmate and flatmate during these

years in Edinburgh but, most important, my best friend. Her presence and friendship have made this difficult time abroad one of the best periods of my life. I will never forget how much she made me laugh and how good I felt in every single moment spent together. Same for Mariaki, my other best friend. Although the youngest of us, she always knew the right words to say in my happy and bad moments. I will miss that, and our long speeches! I will miss both. Their presence in Edinburgh was for me of an inestimable value. Thanks again to both! You will be my best friend forever.

During this period I have met other special people, now my special friends, to whom I want to say thanks. First of all Alex who since my first day in Edinburgh had helped me to make me feel welcome and part of a group. No words can express what his company and friendship has meant to me during these years. Thanks also to Ale, my best Italian friend in Edinburgh, for being there when I need it and for never being tired to listen my endless speeches in my mother tongue! Thanks to Agos for being so unique and for always making me see the easier side of the life. I'm very happy to be his friend, I will never meet again anybody like him.

I would like to thanks also Chiara and Davide for being such a good friends to me and for making me feel at home with their presence. I really appreciated their genuine friendship and I wish to see them often in the future. Many thanks to Oscar, Jordi, Giai, Isa, Iria, Mike, Cecile, Wolfango, Irene, Andrea, Pekka, Miriam, Michele, Ana and all people have contributed to make Edinburgh an unforgettable city.

A special thanks to Malcolm and Ann for making so enjoyable my last two months in Edinburgh when feeling at home would have been very important for me in that period. I couldn't be luckier.

I cannot forget to mention and to thanks my longest friends: Enza and Lore. Our friendship and love hasn't changed at all during these years of my absence in Naples. Deeply thanks to both, for being my friends in the past, in the present and surely in the future.

I would like to thanks also my new friends: Silvia, Varsha and Caroline. They have welcomed me in Bern since my first day. Their friendly presence is an important factor in this new chapter of my life.

Thanks also to Dr. Jens Stein, my new supervisor in Bern, for being so patient during the writing up of this thesis and for making such an enjoyable time working with him.

I wish I could thanks Suor Joseph, my chemistry teacher during the high school time. Her passion for science made me love this subject since the first day. She first has believed in me as a student and today I know, whenever she is, she is proud of me.

I would like to thanks Antonio, my love, for understanding my need of professional affirmation and for loving me so much; without his support I might never started this PhD. During these years he was always present and patient although the distance didn't help; he was there when I lost all my securities and hopes, he helped me to go through this moment. Grazie! I couldn't be where I am without your love.

Finally, I'm deeply grateful to my sister Roberta and my mum, the most important people of my life. No words can fully express how much I love them, how difficult it was staying far from them and how important it was for me to have their support during this time. This thesis is also for them whom, together with my beloved dad, have believed in myself and sacrificed their needs to see this day come true. We missed so many moments all together but the pride in their eyes will comfort me everyday of my life.

Grazie papà, thanks to your love, your princess is finally a Doctor. I won't save the world but I will do my best in my little.

Declaration

I hereby declare that, except where specific reference is made to other sources, the work contained in this thesis is the original work of my own research since the registration of the PhD degree in September 2004, and any collaboration has been clearly indicated. This thesis has been composed by myself and has not been submitted, in whole or in part, for any other degree, diploma or other qualification.

Abbreviations

ADP	Adenosine diphosphate
AP	Alkaline phosphatase
ApA	Adenylyl(3'-5')adenosine
Arg	Arginine
Asn	Asparagine
Asp	Aspartic acid
ATP	Adenosine triphosphate
BAPMAE	2-[Bis-(6-amino-pyridin-2-ylmethyl)-amino]ethanol
BNP	*Bis-para*-nitrophenol phosphate
Bpy	Bipyridine
CA	Carbonic anhydrase
cAMP	2',3'-Cyclic adenosine monophosphate
DCM	Dichloromethane
DFT	Density Functional Theory
DIP	4,7-Diphenyl-1,10-phenanthroline
DMP	Dimethyl phosphate
DMSO	Dimethyl sulfoxide
DNA	Deoxyribonucleic acid
Dpa	Dipicolylamine
DTPB	1,4,7-Triazaheptane
E. Coli	Escherichia coli
EtOAc	Ethyl acetate
HCA	Human carbonic anhydrase
His	Histidine
HNP	Protonated *para*-nitrophenol
HPNPP	2-Hydroxypropyl-4-nitrophenyl phosphate
HPTB	1,3-Diamino-2-hydroxypropane
Im	Imidazole
ISE	Ion-selective electrodes
M_{im}	Monoisotopic Mass
MS	Mass Spectrometry
NMR	Nuclear Magnetic Resonance spectroscopy

NP	Nitrophenolate anion
NPP	Nitrophenyl phosphate
OBAN	Oligonucleotide based artificial nuclease
ODN	Oligodeoxyribonucleotides
PAP	Purple acid phosphatase
PEI	Polyethylene imine
PNA	Peptide nucleic acid
RNA	Ribonucleic acid
RNase	Ribonuclease
RT	Room temperature
Ser	Serine
SNase	Staphylococcal nuclease
TACH	*cis,cis*-Triaminocyclohexane
TACN	1,4,7-Triazacyclononane
THF	Tetrahydrofuran
TPA	Tris[(2-pyridyl)-methylamine]
Tren	Tris(2-aminoethyl)amine
Trien	Triethylenetetramine
Trp	Tryptophan
Tyr	Tyrosine
UpPNP	Uridine-3'-4-nitrophenyl phosphate
UpU	Uridyl(3'-5')uridine

Contents

Chapter 1 – INTRODUCTION

1.1 Phosphodiester bonds: properties and occurrence in nature.

Phosphate esters are phosphoric acid derivatives (Fig. 1) formed by condensation reactions of this with alcohols.

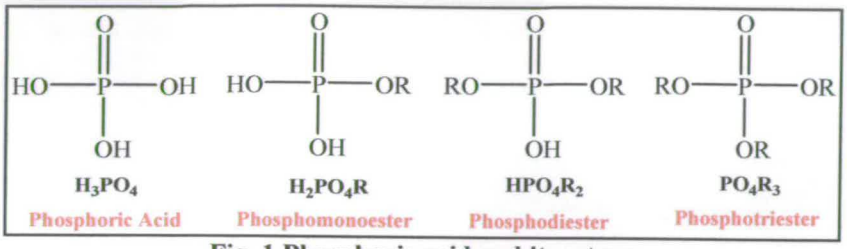

Fig. 1 Phosphoric acid and its esters.

Many important bio-molecules contain a phosphate group, and the enzymatic reactions that hydrolyze or transfer these groups are involved in important biological functions. For example, the presence of the phosphodiester bond in genetic materials (DNA and RNA are phosphodiesters) (Fig. 2) is well-known.

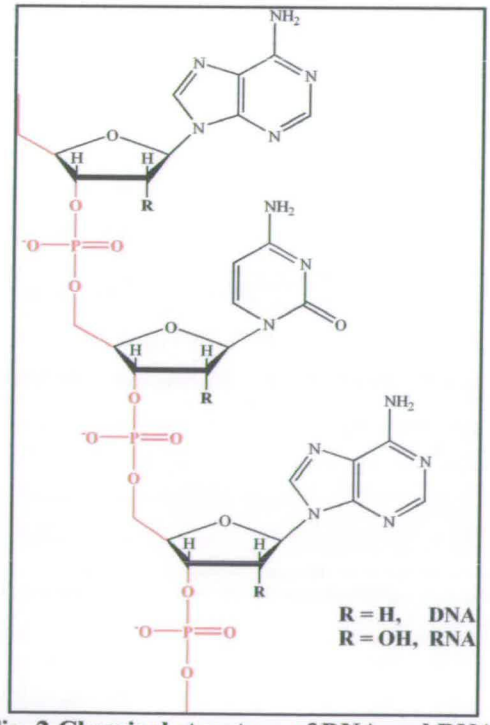

Fig. 2 Chemical structure of DNA and RNA.

Phosphates can also be found in coenzymes, in energy reservoir molecules and

as intermediates in biochemical transformations (ATP and ADP, phospholipids, carbohydrate catabolism, *etc.*).

The vital task of maintaining the integrity of genetic material is accomplished by the phosphodiester bond which, despite its thermodynamic instability to hydrolysis, kinetically, is remarkably stable. Thus, the half-life for hydrolysis of a phosphodiester bond in DNA at pH 7 and 25°C has been estimated to be in the range of 10-100 billion years and 110 years for RNA.[5] RNA is hydrolyzed much more readily due to the presence of the 2'-hydroxyl on the ribose ring.

Phosphodiester linkages are the most stable chemical bonds found in biological molecules. To facilitate other important cellular processes, however, some natural enzymes are able to cleave nucleic acids with reaction rate accelerations as large as 10^{16} fold. How these enzymes achieve so large rate enhancements is not fully understood.

Given the importance of phosphate esters in biology, there is considerable interest in understanding the details of their enzymatic hydrolysis.

1.2 Cleavage of Nucleic Acids: nucleases and related enzymes.

Generally, enzymes that hydrolyze chemical bonds are called *hydrolases*. Each type of hydrolase is identified with the name of its substrate. In this way, the class of enzymes involved in cleaving the phosphodiester bonds of nucleic acids are called *nucleases* (Fig. 3).

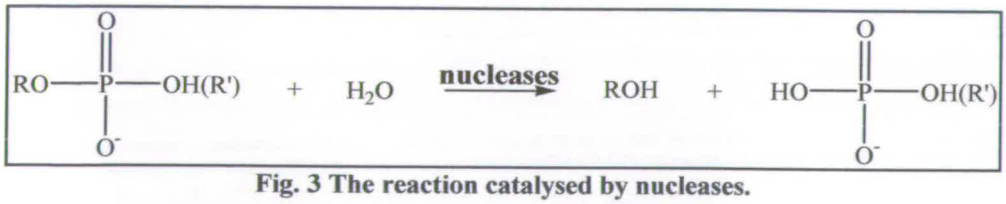

Fig. 3 The reaction catalysed by nucleases.

The first examples of nucleases were isolated in the late 1960s from *Escherichia coli* by Arber and co-workers.[6] Following this work, other scientists have isolated and characterized different nucleases. In many of the reported

structures, one or more metal ions are frequently found in the active site. The most common are divalent cations such as Mg^{2+}, Zn^{2+}, Ca^{2+}, Fe^{2+} and Mn^{2+}. Despite considerable efforts, the exact mechanistic roles of these metals are not well understood. For example it is not clear how, in this class of enzymes, the metal(s) help the enzyme to achieve the extraordinary catalytic activities they exhibit.

Analysis of crystal structures and detailed kinetic studies of different metallophosphohydrolases have shown that in addition to the metal, the hydrolysis of phosphate ester bonds is catalyzed using functional groups of amino acids.

Among the class of phosphohydrolases, *Purple Acid Phosphatase*, *Alkaline Phosphatase*, *Staphylococcal Nuclease* and *P1 Nuclease* are the best characterized examples.

1.2.1 Purple Acid Phosphatases.

Purple Acid Phosphatases (PAP) are enzymes that catalyze the hydrolysis of phosphate monoesters under acidic conditions but not of internucleotide phosphate diester linkages. The exact physiological function of PAP is still unknown, but most probably they are involved in degradative biological processes.

The name is due to their characteristic intense purple colour which results from a tyrosine-Fe(III) charge transfer at $\lambda_{max} = 500$ nm. Generally, the active site of PAP consists of a binuclear metal ion site with two irons or one iron and one zinc or manganese. The common iron centre is always trivalent (Fe(III)) and the other metal is divalent and varies with the source of enzyme. Mammalian PAPs usually have Fe(III)-Fe(II) centres, whereas PAPs isolated from plants most typically have Fe(III)-Zn(II) or Fe(III)-Mn(II) centres.

Many physical and spectroscopic methods have been used to characterize this active site and to date the accepted picture has seven invariant amino acids ligands (three histidines, two aspartates, one asparagine and one tyrosine) coordinating the binuclear metal centre (Fig. 4).

The mechanism of catalysis remains to be fully elucidated, but it is accepted that the two metal ions act cooperatively.

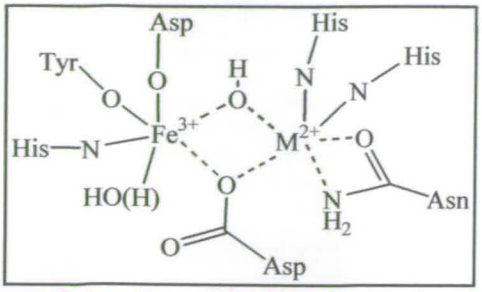

Fig. 4 Proposed structure of the binuclear active site of PAP.

It is also accepted that the acidic pH optimum for this class of enzymes is probably due to the deprotonation of the iron-bound water molecule. This is necessary to form either the nucleophile or to act as a general base to deprotonate a potential nucleophilic water molecule. The substrate binds as a phosphomonoester and it has been proposed that it binds only to the divalent metal ion (Fig. 5).[7]

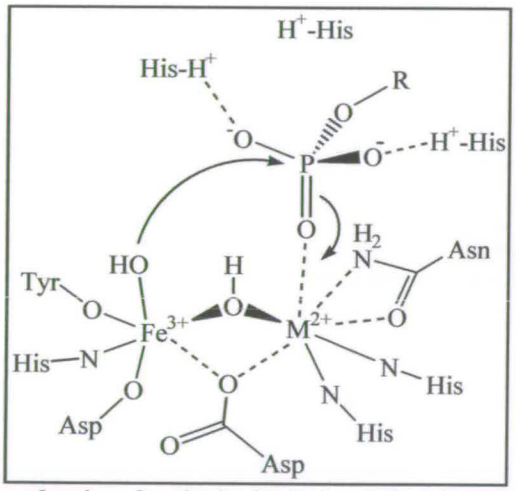

Fig. 5 Proposed mechanism for the hydrolysis of phosphomonoesters by PAP.

1.2.2 Alkaline Phosphatase.

Alkaline Phosphatases (APs) are metallo-hydrolases capable of cleaving non-specifically monophosphoesters, or transferring the phosphoryl group to an alcohol. This class of enzymes mainly share three characteristics: optimal activity at pH > 7, low substrate specificity and a requirement for Zn(II) ions. They are found in both prokaryotes and eukaryotes. In *E. coli* the active site has two Zn(II) ions approximately 4 Å apart and one Mg(II) ion. The Zn(II) ions are the catalytically active species, whereas the magnesium, which does not participate directly in

catalysis provides a general base in the form of a Mg(II)-hydroxide to deprotonate the nucleophile.

The active sites of all the APs share this trimetallic centre and an arginine residue that probably has a role in binding and in stabilizating the reaction transition state. The interactions between the substrate in the reaction transition state and the binuclear zinc centre appear to be as shown in Fig. 6.[8]

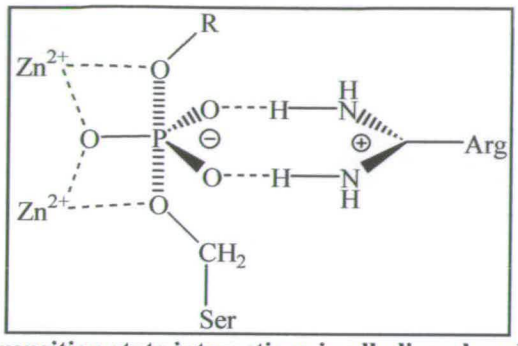

Fig. 6 Transition state interactions in alkaline phosphatases.

In contrast to other metallophosphatases, the reaction catalyzed by alkaline phosphatase involves a covalent intermediate between the phosphate and a serine residue that acts as nucleophile at the phosphorus. X-ray crystallographic data showed that the two Zn(II) ions are located in close proximity of the serine residue, and that they do not share any bridging ligand. However, when the substrate binds this is stabilized by hydrogen bond interactions with the arginine residue and coordination bonds with both zinc ions. The magnesium ion enhances the activity but it is not indispensable for catalysis. AP is a prototypical bimetalloenzyme and by far the most studied metallophosphohydrolase. A mechanism has been proposed for its hydrolytic activity (Fig. 7).[9]

First of all, the hydrolysis of the phosphomonoester is achieved via a two-step nucleophilic displacement mechanism. During these steps the Zn(II) ions act cooperatively and activate the nucleophile (in this case the serine residue) for the attack at the phosphorus and a water molecule to displace the phosphate group from the serine. Each of these steps results in inversion at the phosphorus centre leading to overall retention of configuration.

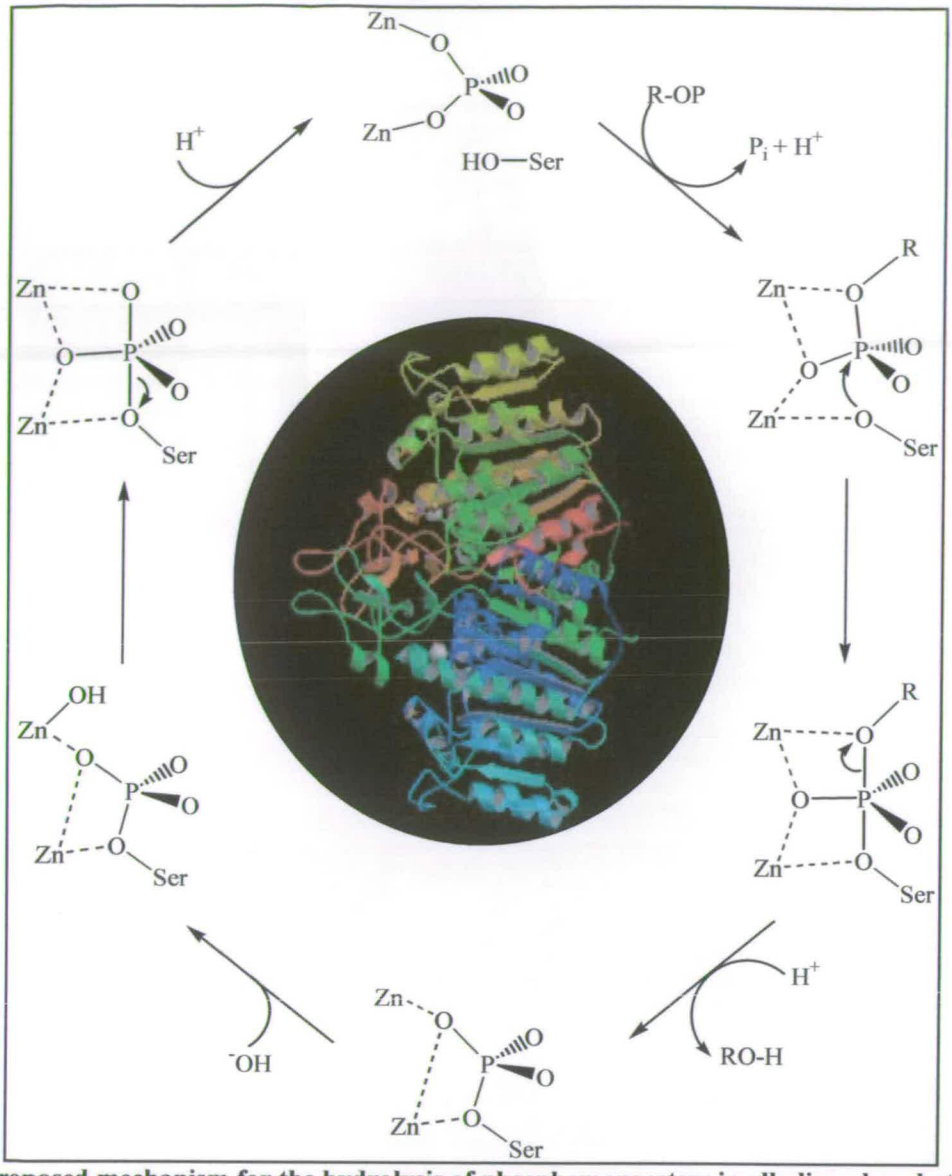

Fig. 7 Proposed mechanism for the hydrolysis of phosphomonoesters in alkaline phosphatase.[9]

1.2.3 Staphylococcal Nuclease.

Staphylococcal Nuclease (SNase) is an enzyme able to hydrolyze phosphodiester linkages in DNA and RNA. Compared to the uncatalyzed mechanism, the reaction is accelerated by as much as 10^{16} which is one of the largest values known for enzymatic rate acceleration.

The active site contains a Ca(II) ion, two arginines and a glutamate. The proposed hydrolytic mechanism proceeds with inversion of configuration following the in-line nucleophilic attack by water. Water is activated by coordination to the Ca(II) ion and probably deprotonated by the glutamate residue. The two arginines

stabilize the bound substrate through hydrogen bonds, and facilitate the departure of the leaving group by protonation (Fig. 8).[10]

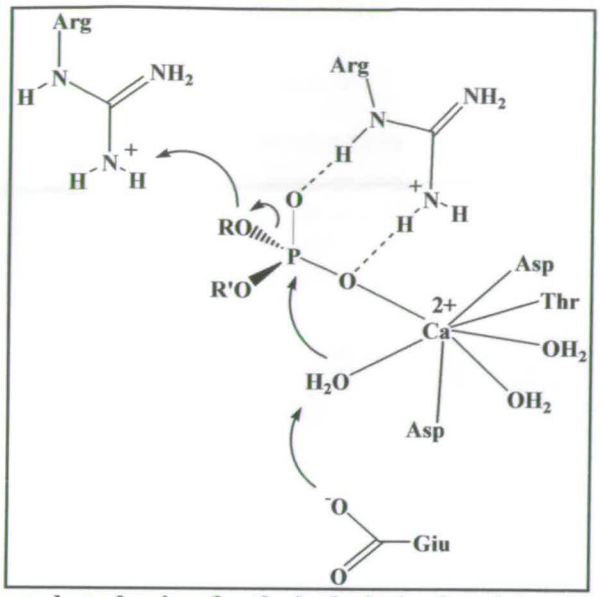

Fig. 8 Proposed mechanism for the hydrolysis of nucleic acids in SNase.

1.2.4 P1 Nuclease.

P1 nuclease is an enzyme that hydrolyzes single-stranded DNA and RNA and also removes a terminal phosphate group of an oligonucleotide acting as a phosphomonoesterase. For this, it requires three Zn(II) ions and the reaction proceeds with inversion of configuration at the phosphorus centre.

The details of the active site have been revealed by X-ray crystallography.[11] These studies suggest that the three Zn(II) ions are 5-coordinate with approximately trigonal-bipyramidal coordination geometries of three oxygen atoms and two nitrogen atoms (Fig. 9). In the trizinc cluster, it is possible to identify a binuclear zinc unit less accessible to RNA or DNA phosphate groups than the third metal ion, which is directly involved in catalysis.

This unit is bridged by an aspartate residue and a water (or hydroxide) molecule to keep the two Zn(II) ions at a distance of 3.2 Å while the third metal is coordinated by two solvent molecules. The inversion of configuration at the phosphorus during hydrolysis indicates an in-line displacement mechanism.

The attacking nucleophile might be the water bridging Zn1 and Zn3 ions or one of the Zn2-bound water molecules.

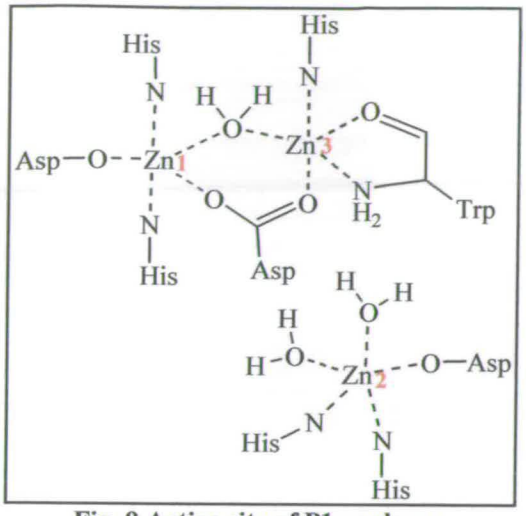

Fig. 9 Active site of P1 nuclease.

1.3 Mechanism of catalysis and the role of the metal ion.

Phosphodiesters are extremely stable in water and in general, their hydrolysis involves a phosphoryl transfer reaction which begins with the deprotonation and activation of a nucleophile and finishes with protonation of a leaving group (Fig. 10a). The mechanism of hydrolysis of phosphodiesters can be of two types: 1) a two-step addition-elimination mechanism with a phosphorane intermediate, or 2) concerted with no intermediate and simultaneous bond formation to the nucleophile and bond fission to the leaving group. Several studies have shown that phosphodiester cleavage proceeds through the concerted mechanism,[12] presumably through a trigonal-bipyramidal transition state (Fig. 10b).

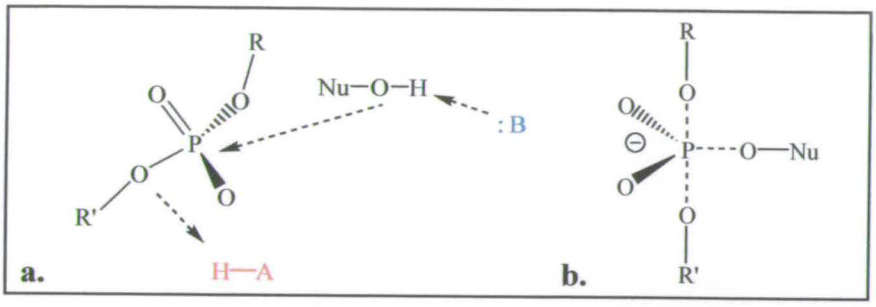

Fig. 10 Mechanism of phosphodiester bond cleavage (a) and the Transition State generated (b).

One important way to promote this reaction is by compensating the negative charge. In contrast, cleavage of monoesters depends strongly on the leaving group reactivity, which supports a dissociative mechanism with extensive bond cleavage to the leaving group and little bond formation to the nucleophile in the transition state. Triesters are cleaved mainly via an associative mechanism as their reactivity is sensitive to the nature of the nucleophile.[12] In this case the transition state has more advanced bond formation to the nucleophile than bond breaking to the leaving group (Fig. 11).

The hydrolysis of phosphodiesters by natural nucleases is often facilitated using one or more metal ions. The extraordinary reactivity of these enzymes is probably due to the cooperation of these metal ions, water molecules bound to them and/or second sphere amino acid residues

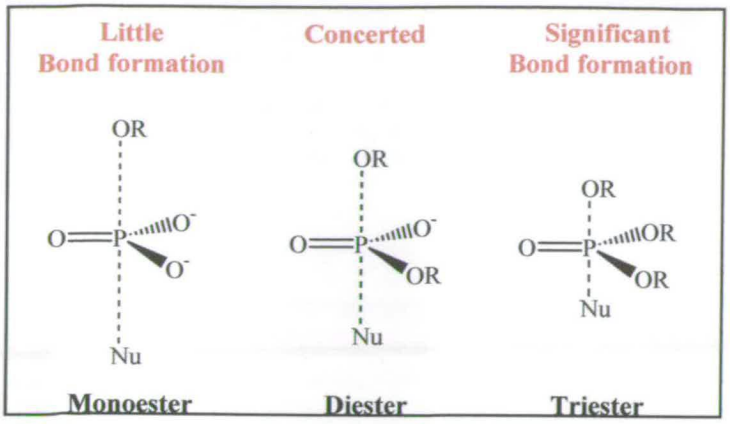

Fig. 11 Transition state models for the hydrolysis of phosphomonoesters, diesters and triesters.

There are different general strategies to cleave the phosphodiester bonds. A common one is the generation of a nucleophile by Lewis-acid activation or by proton abstraction by a basic group. Electrostatic activation of the substrate and stabilization of the transition state and/or leaving group are other frequent strategies. However, the exact mechanism of catalysis and the precise role of the metal ion in this and similar enzymes remain uncertain.

Different properties make a metal ion suitable and powerful for the hydrolysis of phosphodiesters. First of all, a positively charged metal ion can stabilize the negative charge distribution of the substrate in the transition state. This electrostatic effect can be exerted not only by direct contact with the substrate but also indirectly by activating functional groups or solvent molecules in the immediate environment in the active site. For example, a metal ion can cause pK_a shifts of potential nucleophilic species to provide the nucleophile at neutral pH.

It is accepted that a metal ion can catalyze the cleavage of phosphodiesters by using three different catalytic strategies: general base catalysis by deprotonating a nucleophilic functional group or providing a metal-bound hydroxide as nucleophile itself (Fig. 12a-b), electrophilic and general acid catalysis (Fig. 13c-d, Fig. 14). These mechanisms are not mutually exclusive and the combination of these and/or the involvement of different metal ions is also likely.

When the metal-coordinated water or hydroxide is the general acid or base catalyst (Fig. 12b and Fig. 14), the activation mode provided by the metal is called indirect or outer sphere. Instead, the direct activation modes (Fig. 12a, Fig. 13b, c) are classified as inner sphere modes.

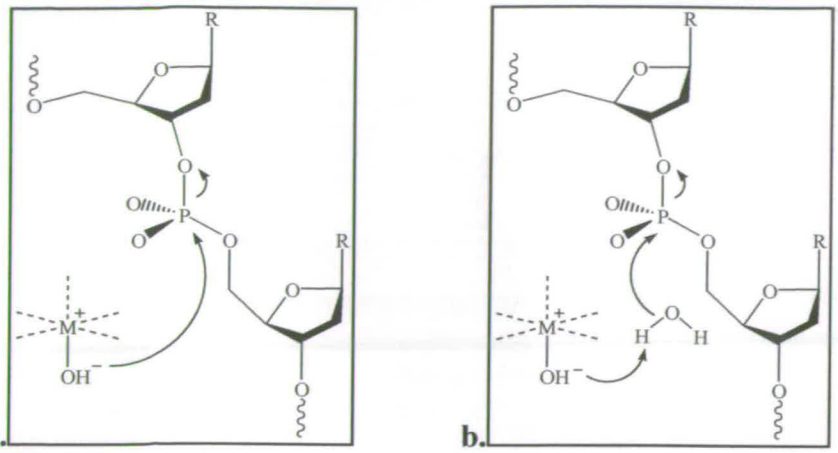

Fig. 12 Metal(II)-bound hydroxide acting as nucleophile (a) or as a general base (b).

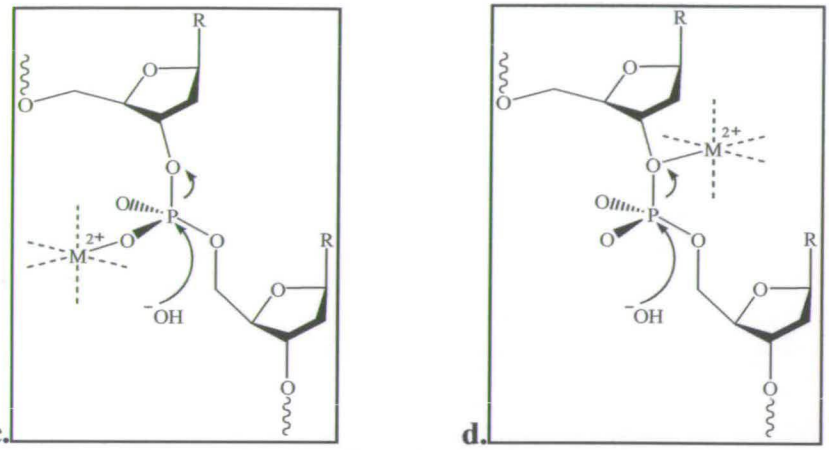

Fig. 13 Metal(II) ion acting as a Lewis acid binding a non-bridging oxygen of the substrate (c) or activating the leaving group (d).

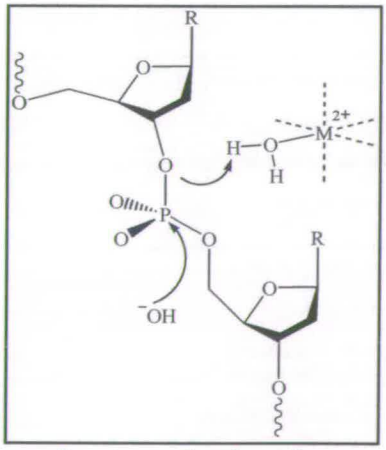

Fig. 14 A metal(II)-bound water molecule acting as a general acid.

Metals that are suitable for this task are hard Lewis acids (to bind the hard oxygen of the phosphate), kinetically labile (to exchange ligands very rapidly) and

with high positive charge density (to reduce the negative charge of the phosphodiester bond).

1.4 Synthetic nucleases.

The development of synthetic, low molecular weight mimics of nucleases is an area of considerable current interest. There are several reasons for this interest. First of all, the creation of a simple model system that mimics structural and functional features of this class of enzymes facilitates detailed mechanistic studies. In addition to this, potential applications in medicine and biotechnology have been envisioned for such artificial nucleases. Among these, the important task of genome sequencing could benefit from using synthetic nucleases. Presently most of the natural restriction enzymes are able to recognise and cleave 4, 6 or 8 base sequences yielding too many fragments that are not easy to separate. It is obvious that a system able to recognise and hydrolyze a sequence of longer bases would be of great utility, as it would yield bigger fragments easier to isolate and analyze. Moreover the synthesis and use of metal based nucleases could also be helpful in interpreting the precise role of metals in natural nucleases providing valuable information for understanding the chemistry involved in the active site. Finally, these systems can also find applications in environmental chemistry as reagents against phosphodiester containing pesticide and nerve gas compounds.

Artificial nucleases are simple chemical structures designed to imitate the active site of natural nucleases. The catalytic activity of such structures is guaranteed by including a minimal set of interactions. The synthetic models created to date, however, do not reach the catalytic efficiency of enzymes and higher reactivities are needed to fulfill any of their potential applications.

Just as in natural nucleases, hydrolytic rather than oxidative cleavage is desirable as it avoids the damage caused by the diffusion of free radicals produced during oxidative cleavage. For the hydrolysis of phosphodiesters under mild conditions, metal ions and metal complexes are the most efficient non-enzymatic reagents currently available. Obviously DNA and RNA are the most interesting

substrates to test the catalytic activities of such artificial nucleases but unfortunately their incredible resistance to cleavage makes difficult or impossible to perform any mechanistic investigations on such substrates. For this reason, kinetic experiments are routinely done on activated models, usually phosphodiesters with good leaving groups. These studies are easier, faster and in general more informative but mechanistic extrapolations to natural substrates have to be done with caution, as there may be differences in the reaction pathways adopted by natural and activated substrates. The most widely used DNA model is bis-*para*-nitrophenyl phosphate (BNP) (Fig.15a). This substrate has two good leaving groups and its spontaneous hydrolysis in water at 25°C has been estimated to be 1.6×10^{-11} s^{-1} (half life > 1300 years).[13] For RNA, the most used activated model is hydroxypropyl-*para*-nitrophenyl phosphate (HPNPP) (Fig.15b).

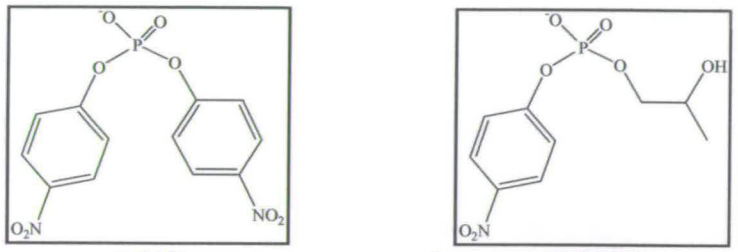

a. BNP **b. HPNPP**

Fig. 15 Activated models of DNA (left) and RNA (right) in hydrolysis reactions.

This compound contains an intramolecular nucleophile and its reaction is quite fast even at room temperature. In addition, the reaction with BNP or HPNPP is easily followed by UV-vis spectroscopy due to the release of *p*-nitrophenolate, which has a maximum absorbance at $\lambda = 400$ nm.

Small dinucleotides and natural RNAs are sometimes used as substrates. They are less resistant to hydrolysis than DNA due to the presence of the 2'-hydroxyl group on the ribose ring and experiments can be run in a reasonable time.

1.4.1 Free ions and mononuclear metal complexes.

Many enzyme-based studies have demonstrated that the metal ion can play a fundamental role in catalysis.[14] Thus, it is not surprising that aqua complexes of

metal ions can promote hydrolysis of phosphodiester bonds. The choice of metals that are physiologically accessible to natural enzymes is rather limited. In contrast, chemists have access to a bigger number of potentially ideal candidates as artificial catalysts. Among these, zinc, copper, cobalt, iron and lanthanide ions are used the most and give better reactivities. Usually their aqua complexes are scarcely reactive toward the hydrolysis of nucleic acids with the only exception of trivalent lanthanide ions.

A systematic investigation on the kinetic parameters of such ions in the cleavage of DNA has shown similar reactivity among the lanthanide series but different affinity under the same conditions.[15] A peculiar case is cerium, which can reach a stable tetravalent oxidation state and it is much more reactive (20 to 1000 times more efficient) than any other trivalent lanthanide ions.[16] Despite their reactivity, free aqueous lanthanides ions are not suitable to create new catalysts to hydrolyze nucleic acids. There are two main reasons for this: 1) they are very similar to the biologically relevant Ca(II) ion and then very toxic for biological systems; 2) they have a tendency to precipitate around pH = 9 so they need to be encapsulated in a ligand. This has proved to be difficult due to the lability of lanthanide complexes. When stable complexes can be prepared, a large excess of the complexing agent has to be used to ensure the necessary solubility. Moreover, the nuclease activity is often lower than that of free aqueous lanthanide ions. The problem is associated with the preference of lanthanides for oxygen donor anionic groups. Anionic ligands ensure an efficient binding but decrease the total positive charge on the complex producing an inhibitor effect during catalysis. Despite these important problems, some significant advances have been made and some lanthanide complexes have proven to be extraordinarily effective at promoting transesterification of phosphodiesters. Generally, the most successful compounds among these complexes include those with macrocyclic ligands such as Schiff bases, crown ethers, azacrowns and polyaminocarboxylate derivative.[17]

One of the first examples of an effective lanthanide-based artificial nuclease was reported by Morrow in 1992. This hexadentate ligand (Fig. 16) forms stable complexes with Eu(III) and efficiently promotes the transesterification of RNA oligomers at neutral pH.[18]

Since then similar Schiff base complexes have been reported to efficiently cleave different types of phosphodiesters[19], RNA[20] and DNA[21]. However, in many cases the reactivity of these complexes is lower than that of the corresponding free lanthanide ion. One exception is the Ce(IV)-EDTA complex, which is able to cleave DNA via a hydrolytic pathway whereas the free ion is unreactive.[22]

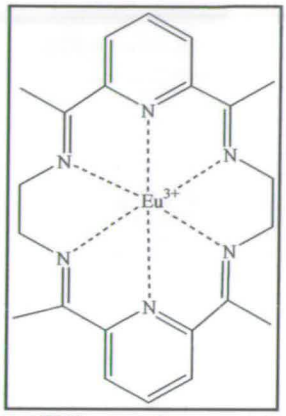

Fig. 16 Macrocyclic Europium(III) complex reported by Morrow *et al.*.[18]

Compared to lanthanides, the nuclease activity of mononuclear complexes of transition metals has been investigated more extensively. Several of these artificial mononuclear metallonucleases have focused on Co(III), Cu(II) and Zn(II) complexes but only a few have been reported to work efficiently.

An early example of a Co(III)-based artificial nuclease was reported by Spiro *et al.* in 1969.[23] This was a Co(III) complex of triethylenetetramine (trien) and it was shown that it is able to hydrolyze phosphomonoesters. Following this work many other researchers have studied and published mononuclear cobalt-based catalysts with general formula $[N_4Co(OH_2)_2]$ in which N_4 indicates a tetraamine ligand.[24] The reactivity of such complexes is highly sensitive to the structure of the polyamine ligand.

Chin has shown that with an appropriate tetraamine ligand a cobalt complex can lead to a billion fold rate acceleration in the hydrolysis of an activated phosphodiesters (BNP).[25] He reported that a very stable *cis*-diaqua cobalt complex $[(cyclen)Co(III)(OH_2)_2]$ (Fig. 17) is able also to hydrolyze the inactivated phosphodiester dimethyl phosphate (DMP) at neutral pH by providing Lewis acid activation and intramolecular metal hydroxide activation simultaneously.[26]

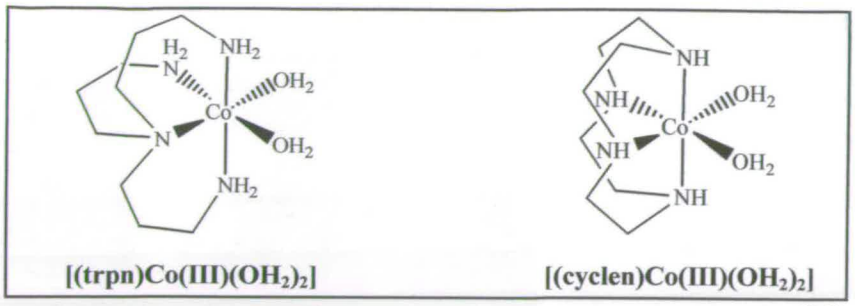

Fig. 17 Mononuclear Co(III)-based catalysts reported by Chin *et al.*.[25,26]

Similar ligands have also been used in early examples of mononuclear artificial nucleases with Zn(II) and Cu(II) ions. The structure of some of these polyamine ligands are shown in Fig. 18.

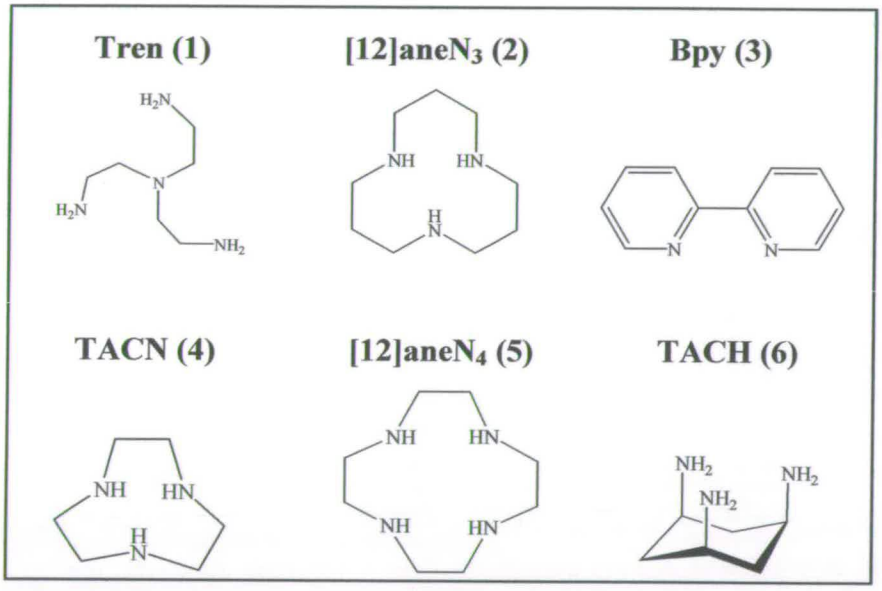

Fig. 18 Structures of some polyamine ligands used for the formation of mononuclear Zn(II) and Cu(II) catalysts for the hydrolysis of nucleic acids or their activated models.

When Tren and Bpy were used to coordinate zinc or copper, the nuclease activity observed was quite disappointing and only $Cu(bpy)^{2+}$ was able to cleave DNA but via an oxidative rather than hydrolytic mechanism.[27] As for Co(III), the polyamine cyclen ([12]aneN$_4$) forms the most reactive catalysts. Zn(II) complexes of [12]aneN$_3$ and [12]aneN$_4$ (Fig. 18) have been reported to enhance the reactivity over the background reaction by 46 and 550 fold, respectively. The greater activity of the triazocyclododecane is mainly due to two factors: 1) occupation of fewer binding

sites on the metal ion and 2) lower acidity of the metal-bound water molecule, which allows the generation of the nucleophile at physiological pH.[28]

The effect that the nature of the ligand has on the overall reactivity of the complex was investigated by Tonellato *et al.*.[29] Their results show that the number of coordinating atoms on the ligand and its favoured coordination geometry dictates the ability of the zinc complex toward the hydrolysis of phosphodiesters. What they observed is that triamino ligands that prefer a facial or tripodal coordination mode are the most reactive, and it was suggested that this is because in this geometry the complexes bind the substrate better. Moreover, like in previous reports by Koike and Kimura,[28] the reactivity of these systems is also modulated by the nucleophilicity of the metal-bound water molecule.

Copper complexes have often been used for oxidative rather than hydrolytic cleavage of nucleic acids due to their redox properties, but some efforts have been made to develop copper-based complexes able to hydrolytically cleave phosphodiesters. The first attempt was reported in 1996 by Burstyn and Hegg.[30] The ligand used in this case was a polyamine derivative of a cyclohexane framework (TACH, Fig. 18). This TACH-Cu(II) complex is able to cleave DNA. However the same experiments carried out in the absence of oxygen showed reduced reactivity indicating the simultaneous occurrence of a secondary oxidative mechanism.

A subsequent report contradicts this result and shows that the same TACH-Cu(II) complex is able to cleave DNA with high rate independently of the presence of oxygen.[31] Finally, another example of mononuclear Cu(II) complex that efficiently cleaves DNA has been reported by Cowan *et al.*.[32] The ligand used is the natural aminoglycoside neamine (Fig. 19).

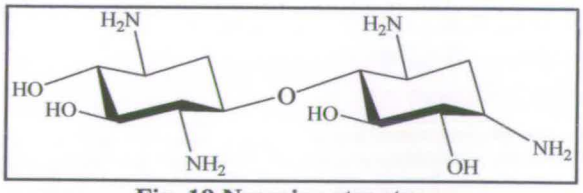

Fig. 19 Neamine structure.

Most recent studies are now focused on the modification and functionalization of these or similar simple mononuclear complexes with auxiliary functionalities.

The expectation is that this strategy will provide more sophisticated and effective catalysts.

1.4.2 Dinuclear and polynuclear metal complexes.

Inspired by natural nucleases, numerous research groups have expanded the synthesis of biomimetic metal complexes to bi- and polynuclear compounds.[33] Several dinuclear complexes have been synthesized and shown to be better catalysts for the cleavage of nucleic acids or related model compounds than their mononuclear analogues.[34]

While there has been significant progress in this area,[35] the mechanism for the cooperative interaction of metal ions in promoting hydrolytic phosphodiester cleavage is not well understood. It is believed, however, that the precise spatial localization of the ions is mandatory to ensure multiple interactions with the substrate and/or nucleophile and consequently, to simultaneously take advantage of several of the activation modes by which metal ions can promote the hydrolysis of phosphate esters (Lewis acid, leaving group and nucleophile activation). On the basis of this observation, a series of bimetallic complexes have been synthesized and investigated as catalysts for the cleavage of phosphodiesters.

A common strategy exploited in some of the most successful bimetallic synthetic nucleases makes use of a bridging alkoxide unit to hold together two metal complexes. One example was reported in 1995 by Komiyama and co-workers, which uses bis(pyridinylmethyl)amine (DPA) as metal coordination unit.[36] They showed that a dizinc(II) complex of the tetrapyridyl ligand *N,N,N',N'*-tetrakis[2-(pyridyl)methyl]-2-hydroxy-1,3-diaminopropane can hydrolyze diribonucleotides under mild conditions. The hydrolytic activity of this dinuclear complex is greater than that of the corresponding mononuclear analogue, which appears to be inactive (Fig. 20).

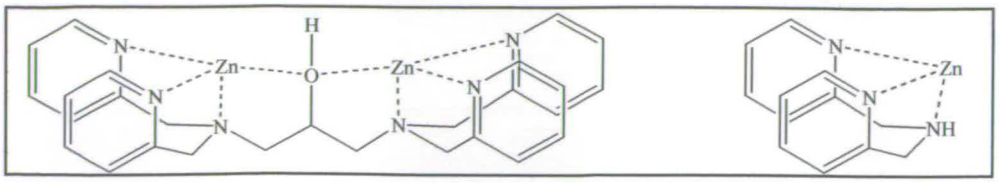

Fig. 20 Structure of a DPA-based dizinc and monozinc catalytic site. The remaining coordination sites can be occupied with H_2O, OH^- or the phosphate ester substrate.

A few years later the same group compared the reactivity of this dinuclear system with that of a trimetallic complex with three DPA units as ligands (Fig. 21). They found that the three metal ions act cooperatively and the catalytic activity is three times greater that the bimetallic one.[37]

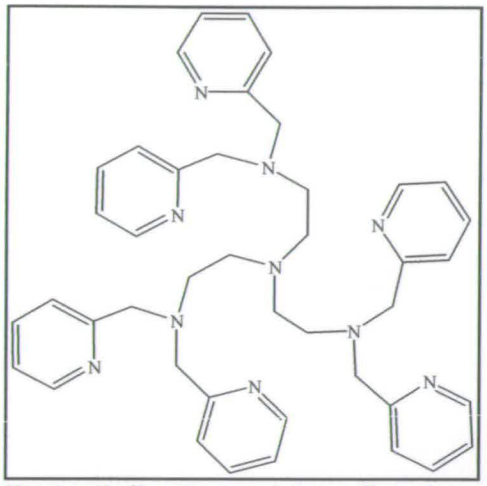

Fig. 21 Trimetalic bis(pyridinylmethyl)amine-containing ligand reported by Komiyama *et al.*[37]

A bridging alkoxide unit has also been used by Morrow and co-workers[38] to hold two zinc-cyclen complexes in close proximity (Fig. 22). In this case the dinuclear system is also a much better catalyst for the cleavage of different phosphate diesters than the corresponding mononuclear complex. The related dinuclear Cd(II) complex is even more reactive toward HPNPP cleavage while the Cu(II) has very low cleavage activity.[39]

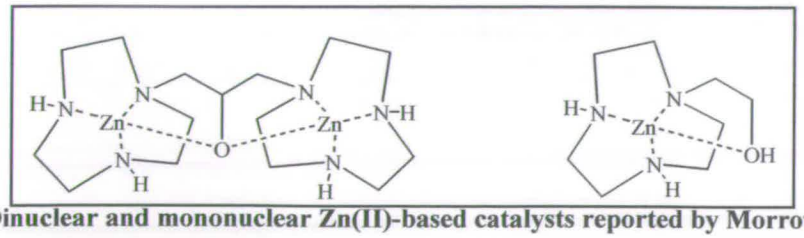

Fig. 22 Dinuclear and mononuclear Zn(II)-based catalysts reported by Morrow *et al.*.[38]

Moreover the catalytic activity observed in the dinuclear zinc complex is greater than the reactivity expected for the same system in which the two chelating units act independently. This suggests cooperativity between the two metal ions. The bridging alkoxide group seems to play a fundamental role, as changing this unit results in the loss of metal ion cooperativity.[40] Thus, the linker alkoxide makes the metals form a dense positively charged core in which the Zn(II) cations cooperate towards binding anions.

The high activity of this dinuclear catalyst is mainly due to the effective interaction of this positively charged core with the anionic transition state produced during the cleavage of phosphodiesters. The entity of stabilization on the barrier of the transition state, from the free catalyst and the substrate (k_{cat}/K_M), changes upon the effect of changing the substrate structure. The largest value (ΔG = 9.6 kcal/mol) is observed for the simplest RNA model HPNPP compared to UpPNP (ΔG = 7.2 kcal/mol) and UpU (ΔG = 9.3 kcal/mol) (Fig. 23).

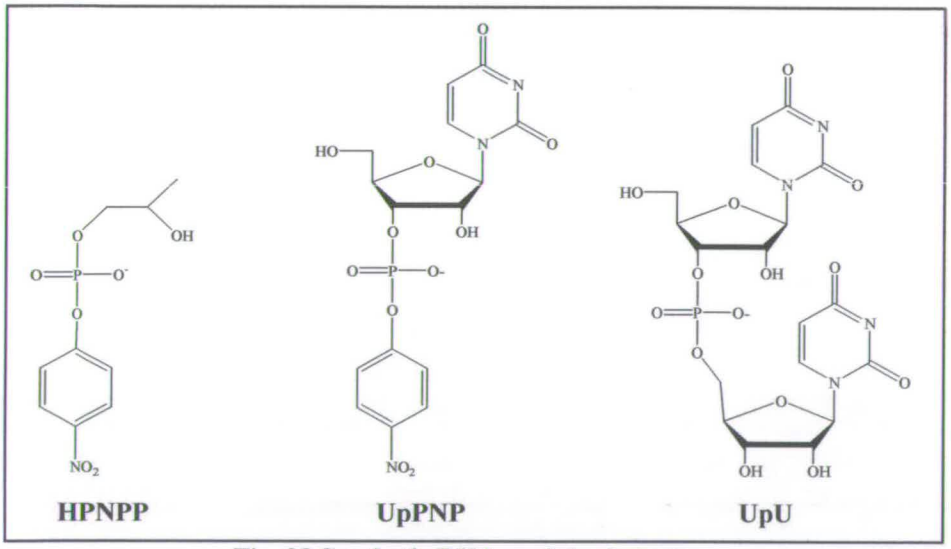

Fig. 23 Synthetic RNA model substrates.

This effect has been attributed to the more bulky structure of these latter substrates that restricts a closer approach to the cationic core. Moreover the observation that the TS in the cleavage of UpU is 2.1 kcal/mol more strongly stabilized compared to UpPNP is probably due to the interaction of the metal complex with the strongly basic C-5' oxyanion leaving group. With the more acidic *para*-nitrophenol leaving group in UpPNP this interaction is unfavored.[41]

An earlier example of cooperativity between two metal centres has been reported by Scrimin and co-workers in 1999.[42] They used a different strategy and a more sophisticated spacer: two azacrown-functionalied α-amino acid units incorporated in appropriate positions of an α-helix-forming heptapeptide (Fig. 24). This ligand binds two Zn(II) ions and its nuclease activity has been tested with the RNA model HPNPP. The dinuclear complex is more reactive than the corresponding mononuclear (5-fold rate acceleration) as evidence for cooperativity. The postulated mechanism involves the binding of the substrate to one zinc ion and activation of the intramolecular nucleophilic hydroxide by the second metal (Fig. 25).

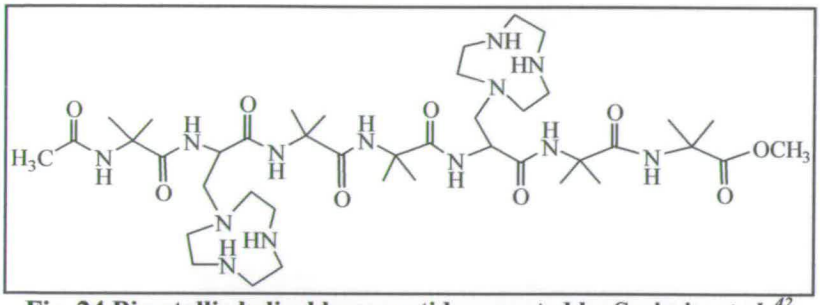

Fig. 24 Bimetallic helical hexapeptide reported by Scrimin *et al.*.[42]

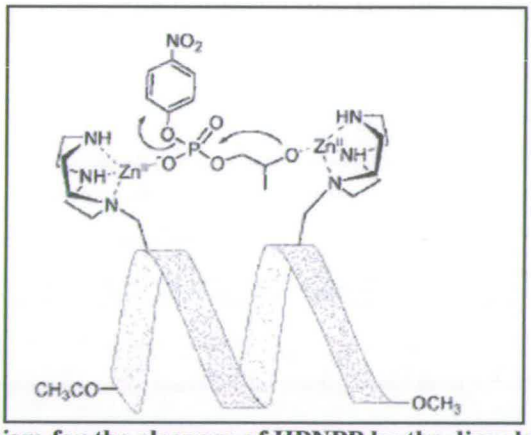

Fig. 25 Proposed mechanism for the cleavage of HPNPP by the dinuclear hexapeptide complex.

Few examples of dinuclear catalysts using metals other than Zn(II) have been reported. Among these, the dinuclear Cu(II) complex of the ligand shown in Fig. 26 is able to cleave plasmid DNA. Its reactivity is significantly greater than that of a mononuclear analogue, which was essentially inactive.[43]

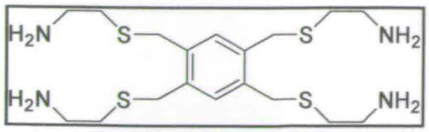

Fig. 26 Structure of a dinuclear Cu(II) artificial nuclease.

A few years later, two trinuclear copper-based catalysts for the cleavage of dinucleotides have been reported by Anslyn and co-workers.[44] The effective trinuclear Cu(II) complex of **L3A** (Fig. 27) shows interesting substrate specificity depending on the type of phosphate diester linkage (2'-5' or 3'-5') and sequence. The corresponding dinuclear complex shows very little selectivity indicating that the three Cu(II) ions are necessary for the found substrate specificity.

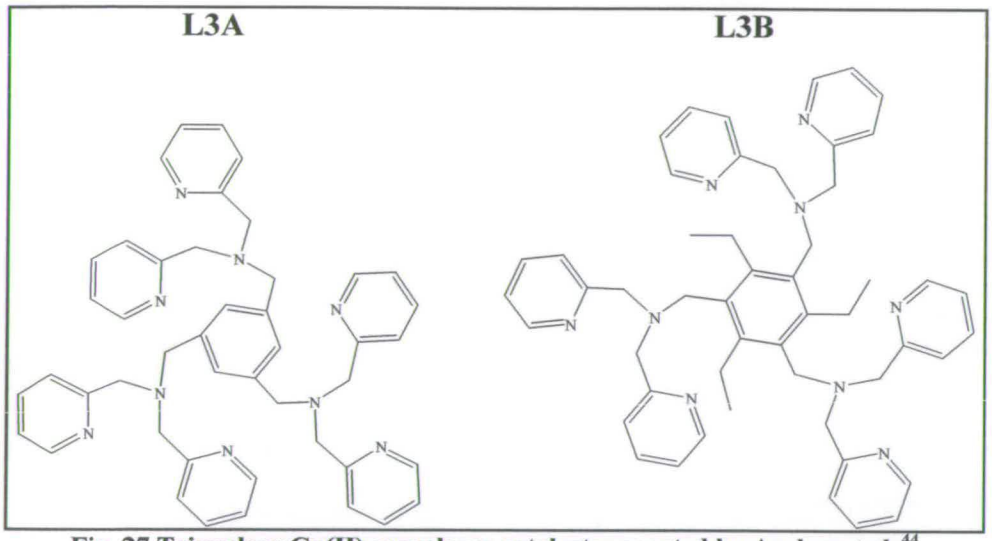

Fig. 27 Trinuclear Cu(II) complexes catalysts reported by Anslyn *et al.*.[44]

Efficient catalysis due to the synergistic action of metal centres has also been observed in polymetallic nuclease models based upon functionalized calix[4]arene scaffolds.[45] Recently, Cu(II) complexes of [12]aneN_3 ligating units have been inserted in the calix[4]arene ring at different distances between them by attachment to 1,2 or 1,3 positions (Fig. 28).[46]

The catalytic activity of such complexes for the cleavage of HPNPP in water was analyzed and compared with mononuclear controls which were found to be less efficient. Moreover, the 1,2-vicinal bimetallic catalyst (1-Cu_2) is much more efficient than its 1,3-distal regioisomer complex (2-Cu_2) in which the cooperativity between

the metal ions is not observed. It is interesting to note that in this case the catalytic activity of the trimetallic complex is slightly lower than that of 1-Cu_2.

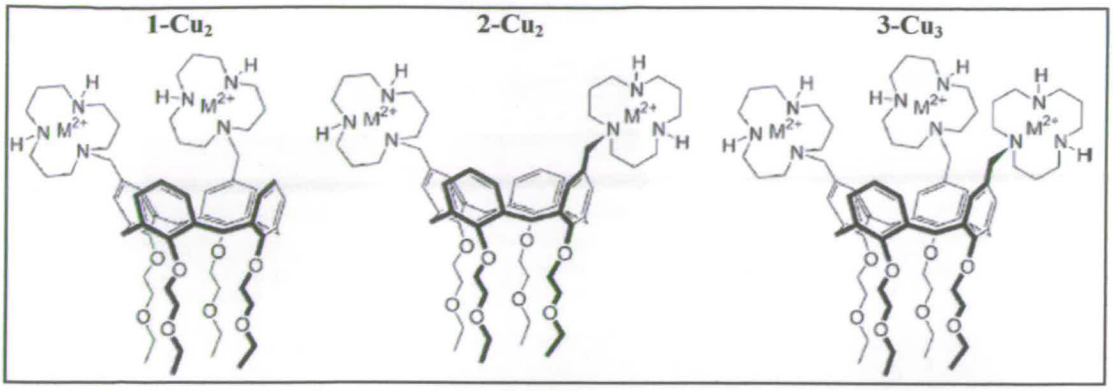

Fig. 28 Calix[4]arene-based artificial metallo-nucleases reported by Ungaro *et al.*.[46]

Fe(III) is present in the active site of some phosphatases but it has been scarcely employed to obtain artificial nucleases. Interestingly, the few Fe(III) complexes reported in the literature with hydrolytic DNA cleavage activity are binuclear.[47,48] The ligands used were benzimidazolylmethyl derivates of 1,3-diamino-2-hydroxypropane (HPTB) and of 1,4,7-triazaheptane (DTPB) (Fig. 29).

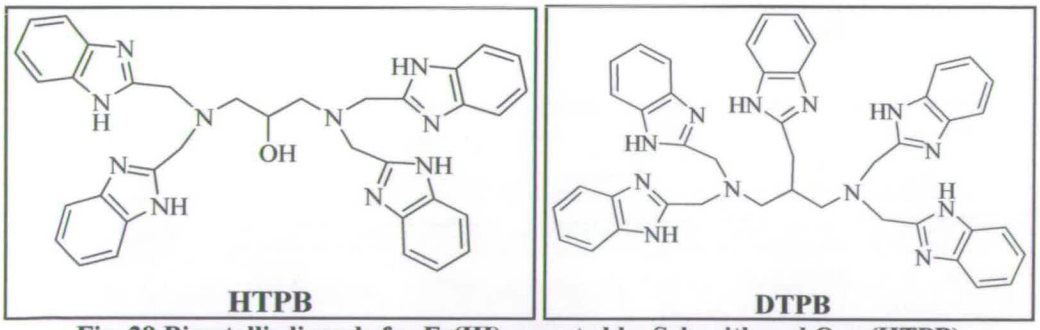

Fig. 29 Bimetallic ligands for Fe(III) reported by Schnaith and Que (HTPB) and Liu (DTPB).[47,48]

In comparison to biologically relevant transition metals, the ability of lanthanide ions to readily catalyze the hydrolysis of DNA is notable. This efficiency results from the conjunction of higher oxidation state and charge density, coordination number and rapid ligand exchange rates. These characteristics make the lanthanide ions well-suited to be catalytic centres in the development of artificial enzymes.

One of the first examples of dinuclear Ln(III) complexes was published in 1996 by Schneider and co-workers.[49] The ligand was a 30-membered azacrown macrocycle (Fig. 30) and binds two Eu(III) or Pr(III) ions. However, the activity of the binuclear Ln(III) complexes formed was only two-fold that of the free metal ion.

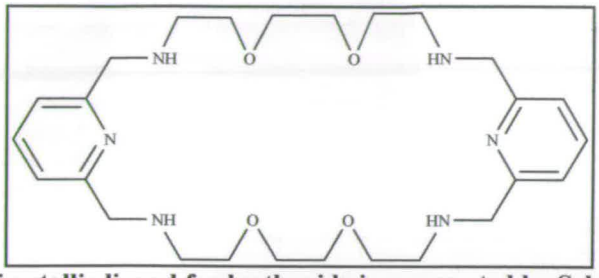

Fig. 30 Bimetallic ligand for lanthanide ions reported by Schmeider.[49]

More effective are the Er(III) dinuclear complexes of a Schiff base-containing macrocycle (Fig. 31) developed by Zhu and co-workers.[50] Unfortunately the high reactivity is counterbalanced by low affinity for the substrate so that high concentrations of complex are required to obtain a fast degradation of the DNA.

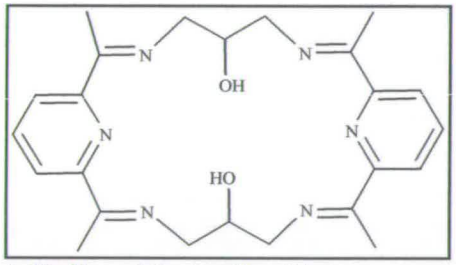

Fig. 31 Bimetallic ligand for lanthanide ions reported by Zhu.[50]

Very recently Morrow and co-workers have studied and compared the catalytic reactivity of mononuclear and dinuclear Eu(III) complexes toward cleavage of HPNPP.[51] The septadentate ligand used (Fig. 32) forms a stable complex with Eu(III) at neutral pH, and at higher pH generates a dimeric complex in which each Eu(III) centre is nine-coordinate and linked by a pair of bridging *cis*-hydroxide ligands. The dinuclear complex appears to be quite a good catalyst for the hydrolysis of HPNPP although there is only a small difference in the stabilizations of the TS compared with the corresponding mononuclear analogue.

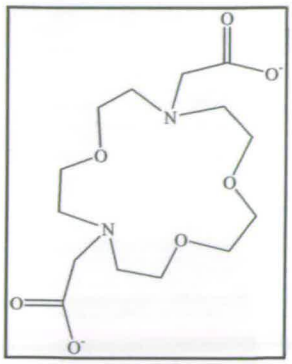

Fig. 32 1,7-Diaza-4,10,13-trioxacyclopentadecane-N.N'-diacetic acid ligand used by Morrow *et al.* to form mononuclear and dinuclear lanthanides complexes.[51]

The absence of cooperativity between the two Eu(III) centres is probably due to the non rigidity of the complex as well as the absence of more than a single binding site on each metal for interaction with the substrate. Clearly, ensuring an intrametallic distance similar to the active site of natural enzymes in dinuclear complexes is necessary but often not sufficient to create an efficient catalyst for phosphodiester hydrolysis.[52]

However this area of research is still relatively new and how a polynuclear metal complex can promote effective phosphodiesters hydrolysis is not fully understood. New and more sophisticated strategies are continually tested in view to reach improved efficiency.

1.4.3 Mononuclear metal complexes with auxiliary H-bonding groups.

Several examples of synthetic metal complexes which promote the hydrolysis of nucleic acids or of phosphate esters models have been reported but their activity is still much lower than that of the corresponding enzymes. The high reactivity of nucleases is due to the cooperation of metal ions and functional groups of the amino acid side chains present in the active site, but so far there have been only a few examples of applying this approach to synthetic nucleases.

In some cases the effect(s) associated with the second sphere groups, in particular those capable of acting as H-bond donors with metal-bound water and/or phosphate substrates, were found to be remarkable. For example, Chin and co-workers published a work in which they compared the reactivity of the Cu(II)

complexes **1** and **2** (Fig. 33) for hydrolyzing 2',3'-cyclic adenosine monophosphate (2',3'-cAMP).[53] In this work they showed that the amino groups in **1** lower the pK_a of the metal-bound water molecule and enhance its reactivity by ca. 2,000-fold compared to **2** by acting as a hydrogen bond donors to the Cu-bound species. Similarly, binding of a phosphate ester to Cu(II) with simultaneous H-bonding to one ammonium group (Fig. 34) have resulted in a remarkable acceleration, *ca.* 10^7-fold, in the hydrolysis of the activated phosphate diester bis-*p*-nitrophenyl phosphate presumably due to the additional electrostatic activation of the phosphate provided by N-H---O-P H-bonding.[54]

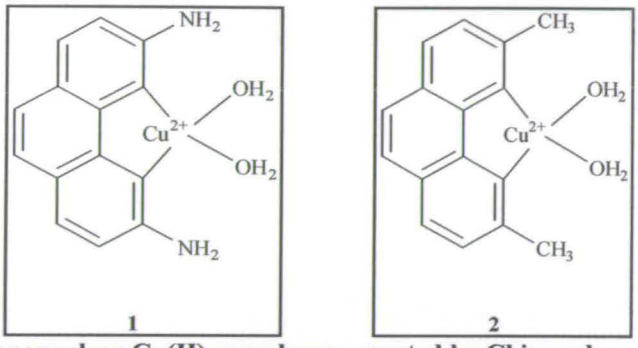

Fig. 33 Mononuclear Cu(II) complexes reported by Chin and co-workers.[53]

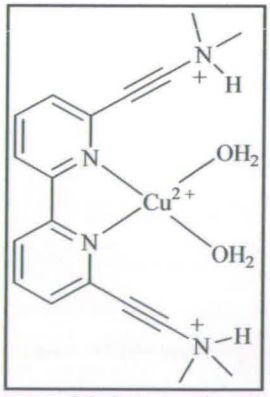

Fig. 34 Monometallic synthetic nuclease with intramolecular H-bonding reported by Krämer.[54]

Comparable effects have been observed for Zn(II) complexes. Anslyn and co-workers have reported that ammonium and guanidinium groups incorporated in monometallic Zn(II) complexes of terpyridine-based ligands (Fig. 35) impart rate enhancements as large as 3300-fold in promoting the hydrolysis of the RNA dimer adenylyl(3'→5')phosphoadenine (ApA) than a control complex without the functional hydrogen bonding features.[55] A possible reason for the enhanced reactivity

has been proposed to be double activation of the phosphate by coordination to the zinc center and to one of the guanidinium fragments, followed by Zn–OH general-base-promoted delivery of the 2'-OH group.

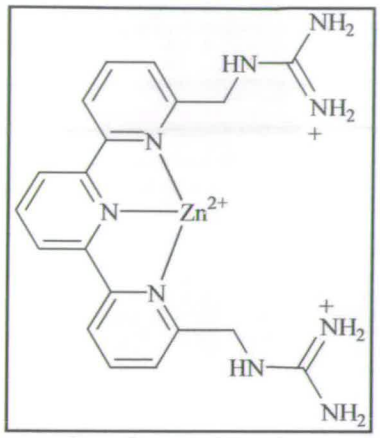

Fig. 35 Monometallic Zn(II) complex of terpyridine incorporating guanidinium groups.[55]

More recently, a monometallic Zn(II) complex with the (6-amino-2-pyridylmethyl)amine unit and a coordinating nucleophilic alcohol arm (Fig. 36) was reported to cleave BNP 750 times faster than the corresponding complex without the 6-amino H-bonding functionality.[56]

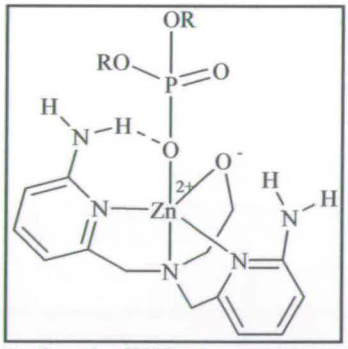

Fig. 36 Proposed intermediate for the BNP cleavage by monometallic Zn(II) complex involving an intracomplex nucleophilic attack.[56]

In this study the BNP cleavage reaction involves an intracomplex nucleophilic attack of the metal-bound alkoxide on the metal coordinated phosphate diester. The two amino groups of the ligand are in the right position to form H-bonds with the metal coordinated substrates thus providing additional Lewis acid activation.

In this lab, ligands derived from TPA (tris[(2-pyridyl)-methylamine]), with 6-amino and 6-neopentylamino groups were shown to exhibit excellent properties for

catalyzing hydrolysis of phosphate esters. For example, these ligands afford more stable monometallic complexes due to their tetradentate nature, and therefore catalysts can be used in lower concentrations. The tripodal nature of the ligands also allows the introduction of more functionally important hydrogen bonding groups. $[(L)Zn(OH_2)]^{2+}$ metal complexes of such modified ligands have zinc-water units which are considerably more acidic than that of $[(tpa)Zn(OH_2)]^{2+}$.[57] This aspect is important because it should facilitate the generation of nucleophilic hydroxide ions at low pH. Remarkably, the magnitude of this effect, as much as 2 pK_a units, was found to be at least as large as that exerted by major changes in the first coordination sphere of the Zn(II) ion, such as lowering its coordination number or changing anionic by neutral ligands. Moreover, the zinc-water acidity progressively increases as the number of amino hydrogen bonding groups increases, and with three amino hydrogen bonding groups the catalytic activity of this mononuclear complex is greater than that of the most effective dinuclear Zn(II) complexes lacking auxiliary hydrogen bonding groups.

The structurally characterized $[(L)Zn(OH)]^{+}$ (Fig. 37) complex exhibits intramolecular N-H----OH-Zn H-bonding, which correlates well with the observed properties.[57b]

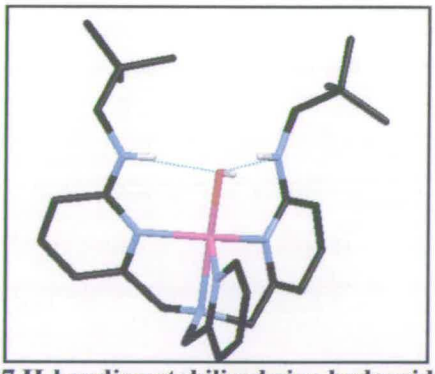

Fig. 37 H-bonding stabilized zinc hydroxide.[57b]

This result suggests that H-bonding microenvironments may be at least as important as the first coordination sphere in facilitating the generation of the nucleophile species at low pH values. It also suggests that ligand environments that are not ideal to achieve very acidic zinc-water units can do so when supported by local H-bonding groups. Moreover, zinc complexes of these ligands were found to

bind phosphates more tightly than the corresponding complexes without the H-bonding groups, a feature that should contribute towards increasing the electrophilicity of the bound phosphate.

This monometallic Zn(II) complex was shown to be considerably more efficient at catalyzing hydrolysis of HPNPP than the related complex without hydrogen bonding groups,[58] ca. 10^4 times more reactive. In fact their catalytic activities are greater than that of the most efficient dinuclear Zn(II) complex reported to date, and several orders of magnitude better than any monometallic transition metal complex lacking H-bonding groups despite the tetradentate nature of the ligand.

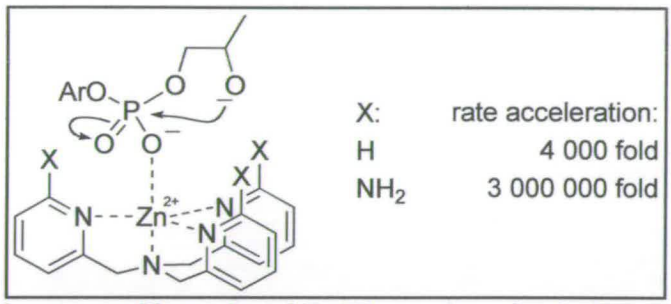

Fig. 38 Reactivity of monometallic tpa-based Zn(II) complexes for the hydrolysis of HPNPP.[58b]

The rate enhancement caused by multiple H-bonding groups in these monometallic zinc complexes is of the same magnitude as that of the metal itself.[58a]

In conclusion, the synthesis of simple and robust artificial phosphate ester hydrolytic agents with metal ions and groups capable of forming intramolecular H-bonds with water and/or substrate is a promising strategy to obtain efficient synthetic nucleases. It would be interesting to investigate the effects arising from these intramolecular H-bonds and the cooperativity of two metals; to explore this aspect is one of the objectives of this thesis.

1.4.4 Metal free artificial nucleases.

Although using metals is a common strategy in this area of reasearch, attempts to create metal free artificial nucleases have also been made. These efforts are inspired by some natural enzymes which despite lacking metals cleave phosphodiester bond by exploiting hydrogen bonding and general acid-base

catalysis. Most of the metal-free artificial nucleases reported to date are aimed at mimicking the catalytic centre of RNAse, which contains two histidine residues.[59] Among these metal-free artificial nucleases, cyclodextrin with pendant imidazole groups[60], polyamine[61], guanidinium compounds[62], sapphyrine[63] and polyethylene imine derivatives[64] give the best results.

In 1989, Anslyn and Breslow described the use of a cyclodextrin with two pendant imidazole groups as catalysts for the hydrolysis of a phosphodiester.[60] The mechanism of catalysis involves the addition of water to the substrate by the proton-assisted addition to the phosphate anion group. The ImH^+ protonates not only the leaving groups but also the phosphate anion of the substrate (Fig. 39) forming a phosphorane intermediate.

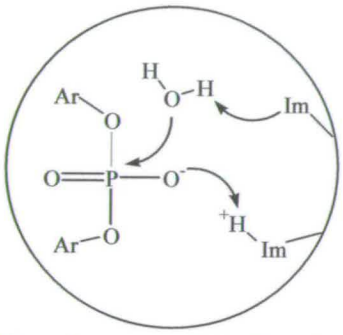

Fig. 39 A top view of the addition of water to the substrate by a proton-assisted addition mechanism in the cyclodextrin-bis(imidazole) reported by Anslyn and Breslow.[60]

Similar acid-base catalysis was observed during the hydrolysis of RNA with diamine and oligamines, which involve two (or more) amino residues connected by $(CH_2)_n$ (n = 2 or 3) chains.[61] The catalytic activity of such amines is due to the formation of monocations at neutral pH. The hydrolysis is achieved by intramolecular acid-base cooperation between the neutral amino residue and the ammonium cation (Fig. 40). The amino group pulls a proton from the 2'-hydroxyl group of the ribose to allow its attack on the phosphorus atom, and the positively charged ammonium centre assists the reaction by interacting with the phosphorus-bound oxygen.

The provision of an intramolecular general base group in addition to electrostatic complementarity of the binding site for the trigonal-bipyramidal

phosphate intermediate makes a bis(guanidinium) receptor able to accelerate the transesterification of the phosphodiester HPNPP.

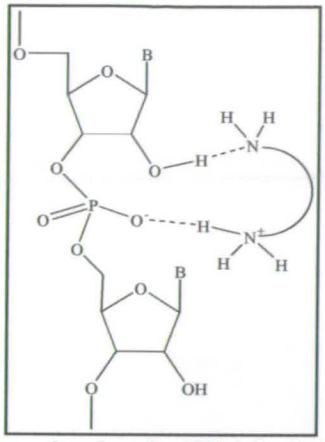

Fig. 40 Proposed mechanism for RNA hydrolysis by diamines.[61]

This approach has been used by Hamilton and co-workers[62a] on a series of mono- and di- substituted guanidinium catalysts. The most efficient catalyst is one in which the internal functional groups have the greatest basicity (Fig. 41).

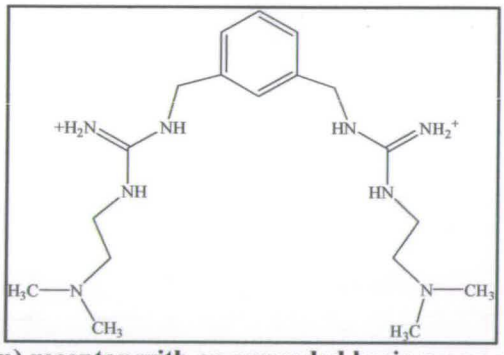

Fig. 41 Bis(guanidinium) receptor with an appended basic group used by Anslyn *et al.*.[62a]

The acceleration over the rate of the uncatalyzed reaction is 290-fold in acetonitrile. More recently, the role of general-acid catalysts in phosphoryl-transfer reactions has been studied also in water. Anslyn and co-workers have designed and synthesized a phosphodiester with an intramolecularly coordinated guanidinium group.[62b] The proton transfer between the guanidinium group and a phosphodiester oxygen has been confirmed by the proton inventory technique. Their results showed that a single guanidinium group can impart a 40-fold rate enhancement towards phosphodiester hydrolysis.

One of the most efficient metal free catalysts able to cleave RNA in water have been reported only a few years ago.[62c] This efficient catalyst is a tris(2-aminobenzimidazoles) derivate (Fig. 42) and represents the only case in which the activity of 1 mM catalyst concentration is comparable to that of many metal complexes.

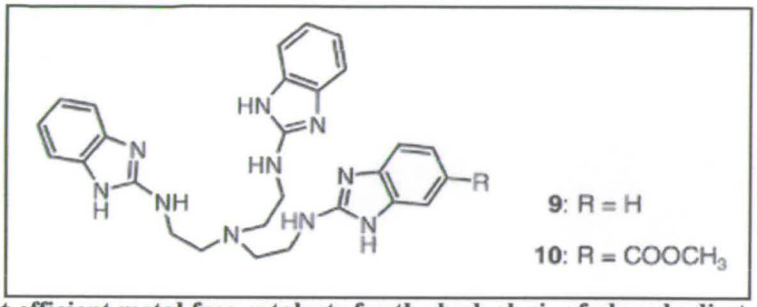

Fig. 42 Most efficient metal free catalysts for the hydrolysis of phosphodiesters in water.

A more sophisticated but efficient metal-free catalyst has been reported very recently.[64] This system (Fig. 43), a modified polyethylene imine (PEI) with alkyl, benzyl and guanidinium groups, in absence of a metal gives a rate acceleration up to 10^4 fold for the cleavage of HPNPP in water.

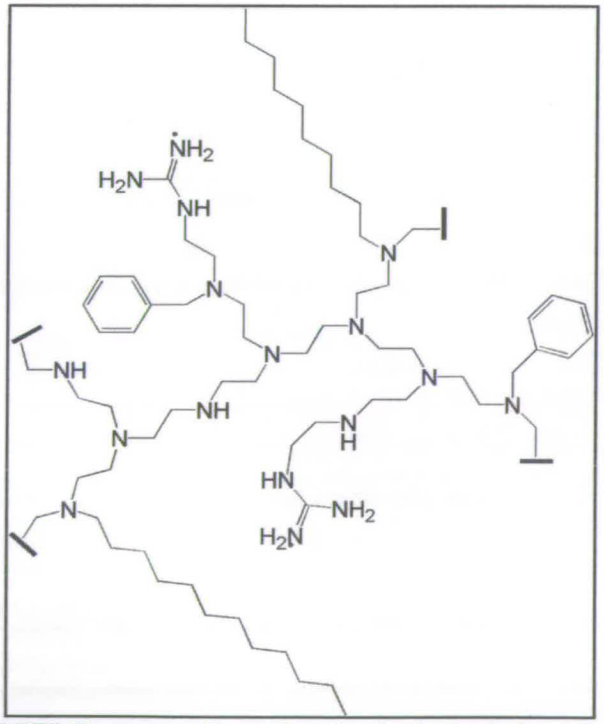

Fig. 43 Modified PEI ("synzymes") catalyst for the hydrolysis of phosphodiesters.[64]

The catalyst reaches maximum catalytic activity at pH ≈ 7.85, exhibits multiple turnovers per polymer molecule and exerts a synergistic effect. Thus, the catalytic activity is higher when the derivatizations (alkyl chain and guanidinium groups) are combined than what it would have been obtained by simply adding the contribution of each single modification.

More often, metal-ion independent artificial nucleases have been conjugated to special secondary or tertiary structures (oligodeoxyribonucleotides, ODN, or peptide nucleic acid, PNA) in order to obtain an increased reactivity and selectivity.[65]

1.4.5 Metal based catalysts conjugated to DNA/RNA recognition units.

A different strategy to create more reactive and selective artificial nucleases involves the conjugation of catalytically-active metal complexes to units with high affinity for nucleic acids. There are different ways by which a molecule can bind and recognize DNA or RNA. First of all, looking at the primary structure of a nucleic acid, the sugar-phosphate backbone and the nucleotide-bases appear to be potential sites for covalent or metal coordination bonds. When the bases hydrogen-bond to form the double-stranded helix structure, another three possible recognition modes are made available: intercalation between the base pairs and major and minor groove recognitions. For DNA substrates, the most common strategy used in the design of artificial nuclease is the conjugation of active metal complexes to small and flat aromatic molecules able to form π-π interactions (Fig. 44).

Many examples of metal complexes connected to intercalator groups have been reported and efficiently used for the oxidative cleavage of DNA.[66] In contrast hydrolytically-active agents using this strategy are rather rare. The first example was reported in 1987 by Barton and co-workers.[67] In this case, metal-activated hydrolytic cleavage of DNA was obtained in the presence of $Ru(DIP)_2^{n+}$ (DIP= 4,7-diphenyl-1,10-phenanthroline) (Fig. 45). The ruthenium intercalator was used as the DNA binding moiety to deliver the metal-coordinated nucleophile to the phosphate backbone for its hydrolysis.

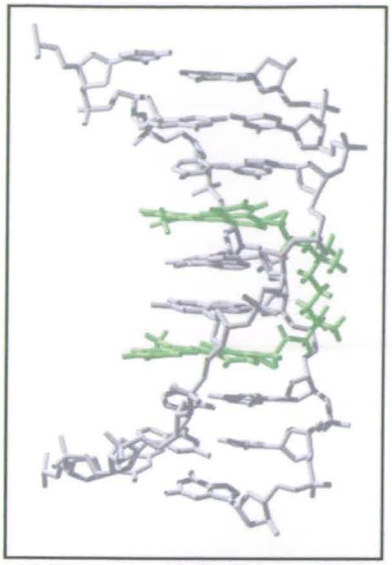

Fig. 44 Example of DNA intercalation.[68]

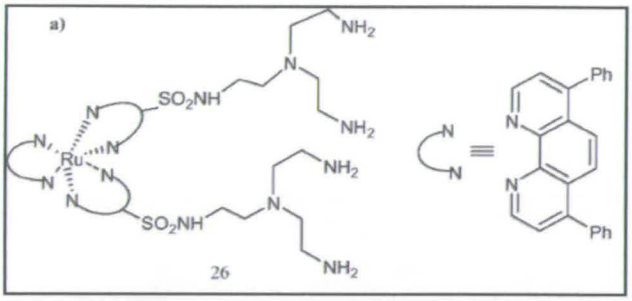

Fig. 45 $Ru(DIP)_2^{n+}$ intercalator used by Barton *et al.* for the cleavage of DNA.

The cleavage efficiency was only modest (after 5 h at 37°C, pH 8.5, ≈ 40% of DNA is cleaved) and it decreases in the order Cu(II) > Co(II) > Zn(II) ≈ Cd(II) ≈ Pb(II).

The same group, ten years later, studied the hydrolytic activity of a mononuclear zinc-peptide complex appended to a rhodium-based intercalator (Fig. 46).[69]

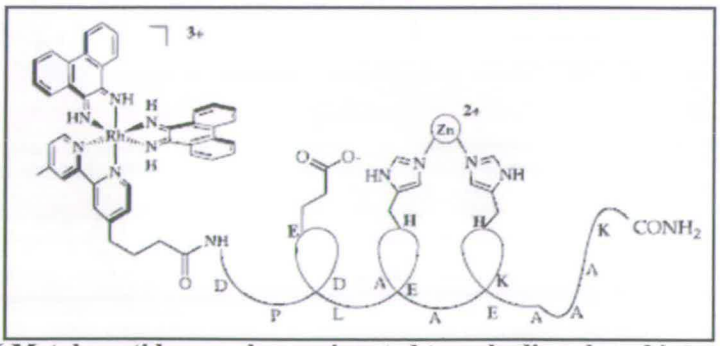

Fig. 46 Metal-peptide complex conjugated to a rhodium-based intercalator.

The rhodium complex contains phenanthrenequinone diimine ligands and in the presence of stoichiometric Zn(II) is able to cleave DNA at micromolar concentrations.

More recently Zagotto *et al.*[70] have studied a series of *cis,cis*-triaminocyclohexane zinc complexes conjugated to an anthraquinone intercalator moiety with alkyl spacers of different lengths (Fig. 47). The presence of the anthraquinone unit led to a 15-fold acceleration in the hydrolysis of DNA compared with the complex lacking the intercalator (**b**, Fig. 47).

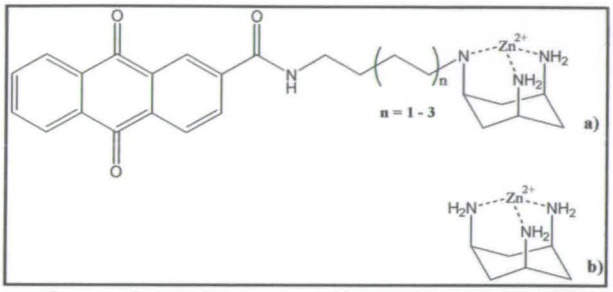

Fig. 47 Zinc complex-anthraquinone conjugates (a) and control compound (b).[70]

Moreover, the length and the flexibility of the spacer were found to play a fundamental role in the activity of the catalyst; short spacers seem to prevent the correct folding of the metal complex to reach the phosphate backbone (Fig. 48).

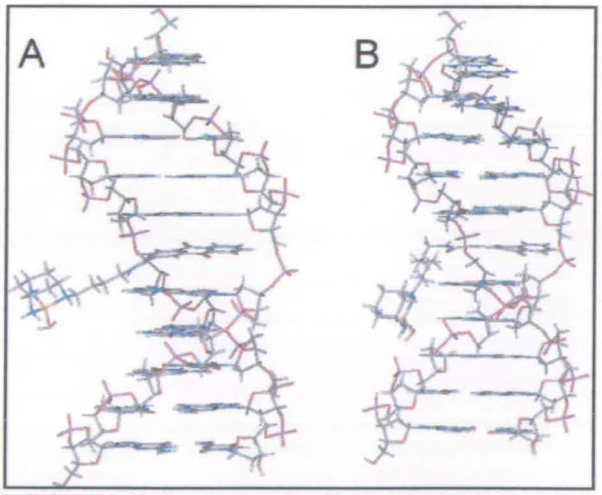

Fig. 48 Calculated structures for the intercalation of a complex with a shorter (A) and a longer (B) spacer.[70]

Other attempts to create artificial nucleases able to selectively cleave nucleic acids have exploited conjugation of catalysts to antisense oligodeoxynucleotides and

PNA. These recognition units are able to form duplex or triplex structures with RNA and DNA. One example of oligonucleotide based artificial nuclease (OBAN) has been reported by Strömberg and co-workers.[71] The oligonucleotide unit has a sequence complementary to that of the target RNA and it is attached via a linker to a cleaving agent, in this case a Zn(II) complex of a 2,9–dimethylphenanthroline derivative (Fig. 49).

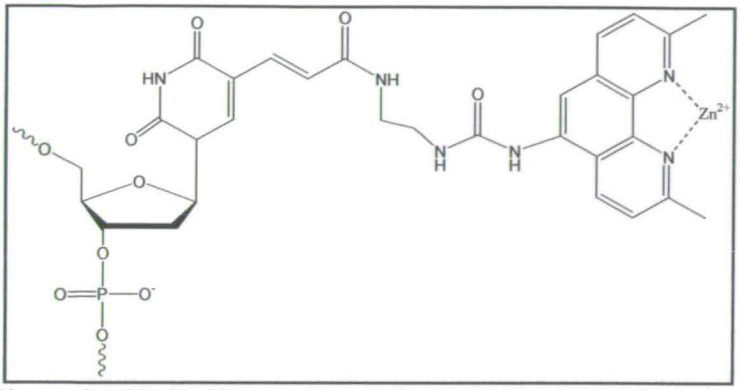

Fig. 49 Oligonucleotide Zn(II) complex conjugated reported by Strömberg *et al.*.[71]

The same metal complex has also been attached to a PNA unit.[72] This PNA-neocuproine-Zn(II) derivative (Fig. 50) specifically cleaves a synthetic RNA target with efficiency as high as was reported for the zinc-cleaving unit alone.[73]

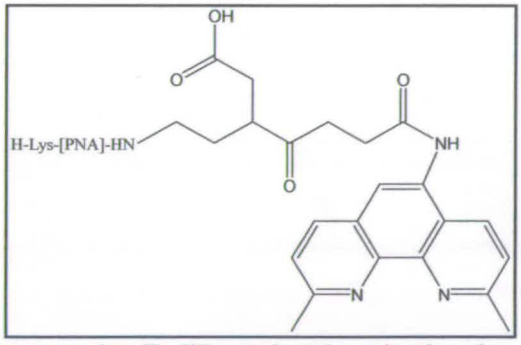

Fig. 50 PNA-neocuproine-Zn(II) catalyst for selective cleavage of RNA.[72]

Antisense oligonucleotides and PNA have also been used to increase the efficiency and selectivity of metal-free artificial nucleases.[74,75] One of the most effective and selective organocatalysts obtained to date was created by attaching *tris*(2-aminobenzimidazole) to DNA oligonucleotides (Fig. 51).[76]

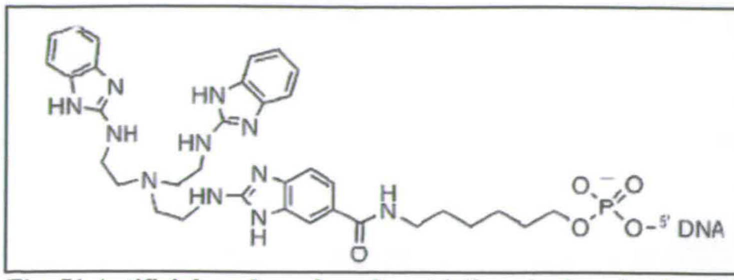

Fig. 51 Artificial nuclease based on *tris*(2-aminobenzimidazole) conjugated to DNA oligonucleotides.[76]

Compared with RNA hydrolytic cleavage, cleaving DNA with high sequence selectivity is rarer. The only example known to date is the zinc finger peptide reported by Nomura and Sugiura (Fig. 52).[77]

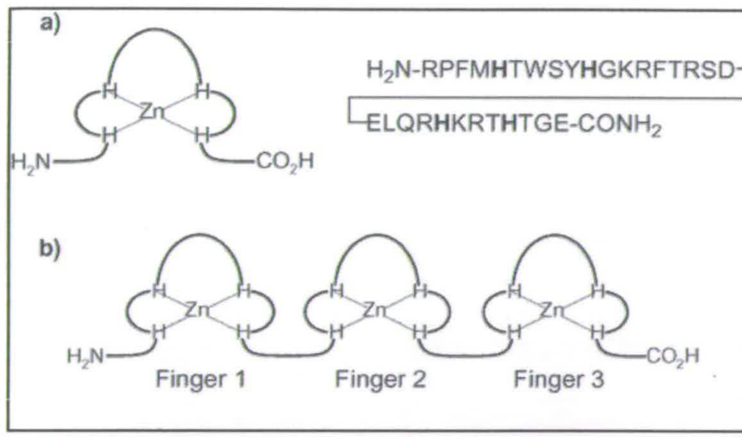

Fig. 52 Schematic representation of the zinc finger based nuclease prepared by Nomura and Sugiura.[77]

The single zinc-finger motif (**a**, Fig. 52) cleaves the DNA with no sequence selectivity that instead is achieved only with the alignment of three-tandem zinc-fingers (**b**, Fig. 52).

Chapter 2 - Methods

2.1 Potentiometric Titrations.

The stability constants (or equilibrium constants) of metal complexes in solution are important parameters and their estimation is necessary in order to understand and explain the properties and behaviour of metal complexes in solution. Different techniques have been developed to estimate the stability constants of metal complexes. One of the most successful and widely employed method is to carry out potentiometric pH titrations. This methodology is based on the use of ion-selective electrodes (ISEs) made of liquid or polymeric membrane materials which respond selectively to the activity or concentration of a certain ion in solution detecting the potentials that arise at the glass/solution interface.[78]

In a pH-electrode the potential, E, measured in mV, is in the absence of current flow directly correlated with the activity of hydrogen ions as described from the Nernst equation (Eq.1):

$$E = E° - \frac{RT}{nF}\ln\{H^+\} \qquad \textbf{Eq.1}$$

where R, T, n and F are respectively the gas constant (8.314 J mol^{-1} K^{-1}), the temperature (in K), the number of valence electrons per mole (1 for H^+) and the Faraday constant (96485 C). E° is constant but its value varies with temperature and electrode. Many electrodes do not follow the ideal slope of the Nernst equation. This deviation is taken into account by introducing the variable "s" (Eq.2), which refers to the electrode sensitivity.

$$E = E° - \frac{sRT}{nF}\ln\{H^+\} \qquad \textbf{Eq.2}$$

When the ionic strength of the solution is controlled by a non-reacting electrolyte at high concentration and the temperature is kept constant, the activity can be substituted by the concentration (Eq.3):

$$E = E° - \frac{sRT}{nF} \ln[H^+] \qquad \textbf{Eq.3}$$

As pH = - log $[H^+]$, Eq.3 becomes:

$$E = E° + SpH \qquad \textbf{Eq.4}$$

where S (electrode slope) and $E°$ are two variables that must be determined each time during the electrode calibration process.[79] Once the electrode is calibrated, very accurate potentiometric pH measurements can be used to determine the protonation and equilibrium constants of ligands and their metal complexes.

Potentiometric titrations are a good way to characterize the speciation in solution. However, this methodology is suitable only when the degree of complex formation is sensitive to the concentration of H^+.

During a typical titration an acid solution of a ligand at known pH, in the presence and absence of a metal ion, is titrated in small increments with a standardized base solution and the pH is recorded. Typically, the pH is varied between 2 and 12, as these represent the lower and upper limits for accurate pH measurement with a glass electrode. For a general chemical reaction (Eq.5), the equilibrium constant at a given temperature and ionic strength is defined as the ratio between the concentrations of the species in solution (Eq.6).

$$a\,A + b\,B \rightleftharpoons c\,C + d\,D \qquad \textbf{Eq.5}$$

$$K_c = \frac{[C]^c[D]^d}{[A]^a[B]^b} \qquad \textbf{Eq.6}$$

Protonation and complex formation equilibria can be expressed in terms of the stepwise and overall stability constanst. The stepwise constants (K) refer to equilibria in which one Lewis acid, such a proton or a metal ion, is combined with a basic donor group (ligand, L^{n-}) (Eq.7).

$$H^+ + L^{n-} \rightleftharpoons HL^{(n-1)-} \qquad K_1 = \frac{[HL^{(n-1)-}]}{[H^+][L^{n-}]} \qquad \textbf{Eq.7}$$

The resulting species may then react with another proton to give the successive stepwise constant (Eq.8) and so on.

$$H^+ + HL^{(n-1)-} \rightleftharpoons H_2L^{(n-2)-} \qquad K_2 = \frac{[H_2L^{(n-2)-}]}{[H^+][HL^{(n-1)-}]} \qquad \textbf{Eq.8}$$

The overall constants are indicated with the symbol β. They express the equilibrium between a fully deprotonated ligand and a different number of protons or metal ions (examples in Eq.9 and 10).

$$H^+ + L^{n-} \rightleftharpoons HL^{(n-1)-} \qquad \beta_1 = \frac{[HL^{(n-1)-}]}{[H^+][L^{n-}]} \qquad \textbf{Eq.9}$$

$$2H^+ + L^{n-} \rightleftharpoons H_2L^{(n-2)-} \qquad \beta_2 = \frac{[H_2L^{(n-2)-}]}{[H^+]^2[L^{n-}]} \qquad \textbf{Eq.10}$$

Stepwise and overall constants are therefore related to each other (Eq.11).

$$\beta_1 = K_1;\ \beta_2 = K_1 * K_2;\ \beta_3 = K_1 * K_2 * K_3;\ ....;\ \beta_n = K_1 * K_2 * ... K_n. \qquad \textbf{Eq.11}$$

The equilibrium constants and the species distribution of these general acid-base equilibria are then calculated by solving the equations of mass-balance with the aid of specifically designed software such as Hyperquad[80] and Hyss[81]:

$$T_A = [A] + \sum_i a_i \beta_i [A]^{a_i} [B]^{b_i} ... \quad T_B = [B] + \sum_i a_i \beta_i [A]^{a_i} [B]^{b_i} ... \qquad \textbf{Eq.12}$$

2.2 Kinetic Analysis.

Kinetic studies are useful tools to address and interpret mechanistic questions. A kinetic analysis deals with rates of chemical reactions and how these can be explained in terms of reaction mechanisms. During a kinetic experiment the rate of a chemical process is measured by following the concentration change of a reactant or a product as a function of the time. The rate of a reaction is in fact defined as the ratio between the change in concentration, ΔC, of a given compound in the time Δt (Eq.13).

$$\text{rate} = \frac{\Delta C}{\Delta t} \qquad \textbf{Eq.13}$$

As the rate may vary with the time, it is usually defined as the derivative of the concentration with respect to time (Eq.14) and its value will be positive if the concentration of the compound increases and negative if it decreases.

$$\text{rate} = \pm\frac{d[\text{concentration}]}{dt} \qquad \textbf{Eq.14}$$

Rates and concentrations are then related, and this relation can be expressed mathematically in the form of a general equation called the "rate law" (Eq.15):

$$v = k[A]^a[B]^b... \qquad \textbf{Eq.15}$$

where k is the rate constant and the powers a, b, ... are the *order* of the reaction with respect to A, B, ...

The term *order* refers to the molecularity of the reaction and indicates the number of molecules involved in forming the product. Empirically the *overall order* of the reaction is given by the sum of the powers to which each concentration term in the rate equation is raised ($a + b + ...$) and it is usually denoted with the symbol n.

In the simplest case in which two molecules A and B react to form a product P, the rate constant is expressed as in Eq.17.

$$A + B \longrightarrow P \qquad \textbf{Eq.16}$$

$$v = -\frac{dA}{dt} = -\frac{dB}{dt} = \frac{dP}{dt} = k[A][B] \qquad \textbf{Eq.17}$$

The reaction is second-order overall but first order in A and first order in B. The unit of the rate constant *k* depends on the order of the reaction. If the rate is proportional to the concentration of a single compound, *k* is a first-order rate constant and the units are sec^{-1}:

$$A \longrightarrow P \qquad \textbf{Eq.18}$$

$$v = k[A] \qquad \textbf{Eq.19}$$

It is also useful to know how the concentration depends on time. This information can be obtained integrating the differential form of the rate law (Eq.20) between t_0 and t.

$$\int_{A_0}^{A} -\frac{d[A]}{A} = k_{t_0} \int_{t_0}^{t} dt \qquad \textbf{Eq.20}$$

The solution of such integral shows an exponential dependence of the concentration of the reacting species A as a function of time (Eq.21).

$$[A] = A_0 e^{-kt} \qquad \textbf{Eq.21}$$

The rate represents the instantaneous slope of a graph of concentration *versus* time and the plot of the logarithm of [A] (Eq.22) *versus t* is linear (Fig. 53):

$$\ln[A] = -kt + \ln A_0 \qquad \textbf{Eq.22}$$

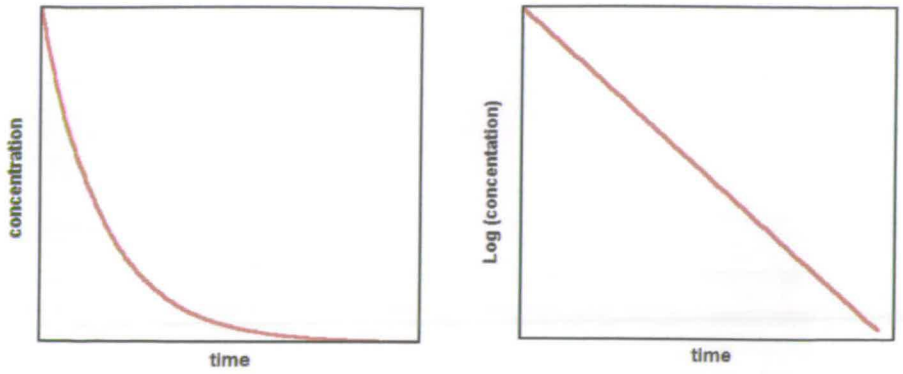

Fig. 53 Concentration change against time and its linear plot for a first order reaction.

However not all reactions follow Eq.19. For example, reactions catalyzed by enzymes usually obey the Michaelis-Menten equation (Eq.23):

$$v = \frac{V_{max}[A]}{K_M + [A]} \qquad \textbf{Eq.23}$$

where V_{max} and K_M are constants that refer to the catalyst efficiency and specificity respectively.

The Michaelis-Menten equation assumes that the enzyme combines with the substrate, S, to form a short-life intermediate enzyme-substrate complex, ES. This complex is then converted into the product making the enzyme available for further reactions with other substrate molecules (Eq.24).

$$E + S \underset{k_{-1}}{\overset{k_1}{\leftrightarrow}} ES \xrightarrow{k_2} E + P \qquad \textbf{Eq.24}$$

The mechanism in this case is more complex and consists of three elementary steps characterized by the corresponding rate constant: k_1, k_{-1} and k_2. The Michaelis-Menten equation is obtained using the steady-state approximation, that is, the concentration of the ES complex does not change appreciably with time (Eq.25).

$$\frac{d[ES]}{dt} = k_1[E][S] - k_{-1}[ES] - k_2[ES] = 0 \qquad \textbf{Eq.25}$$

At any time the initial concentration of the enzyme, $[E]_0$, is given by the sum of free and bound enzyme:

$$[E]_0 = [ES] + [E] \quad \Rightarrow \quad [E] = [E]_0 - [ES] \qquad \textbf{Eq.26}$$

The substitution of this expression for [E] into the Eq.25 leaves [ES] as the only unknown:

$$[ES] = \frac{k_1[E]_0[S]}{k_1[S] + k_{-1} + k_{cat}} \qquad \textbf{Eq.27}$$

The catalytic step of the overall reaction is the one in which the product is formed:

$$ES \xrightarrow{k_2} E + P \qquad \textbf{Eq.28}$$

and for such reason the corresponding rate constant k_2 is written as k_{cat}. The velocity of such process is given by:

$$V = k_{cat}[ES] \qquad \textbf{Eq.29}$$

k_{cat} is also called the "turnover number" and represents the maximum number of molecules of substrate that the enzyme can convert into product per second.

The Michaelis-Menten equation (Eq.30) is obtained by combining equations 27 and 29.

$$V = \frac{k_{cat}[E]_0[S]}{[S] + K_M} \qquad \textbf{Eq.30}$$

K_M is the Michaelis-Menten constant, defined as:

$$K_M = \frac{k_{-1} + k_{cat}}{k_1} \qquad \textbf{Eq.31}$$

K_M also represents the dissociation constant of the complex ES and therefore is a measure of the affinity of the enzyme for the substrate.

Enzyme-catalyzed reactions reach saturation, that is, the reaction rate increases linearly as the concentration of substrate increases and then levels off when it reaches the limiting maximum value V_{max}, which is the enzyme's maximum rate (Fig. 54). Here the enzyme is saturated and further addition of substrate does not produce rate acceleration.

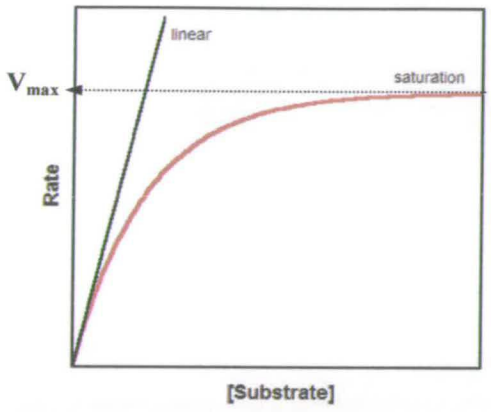

Fig. 54 Typical behaviour of the rate in an enzyme catalyzed reaction as a function of substrate concentration.

The maximum value of the rate, V_{max}, is given by:

$$V_{max} = k_{cat}[ES] \qquad \textbf{Eq.32}$$

and the Michaelis-Menten equation can be written as follows:

$$V = \frac{V_{max}[S]}{[S] + K_M} \qquad \textbf{Eq.33}$$

In this way, K_M can also be interpreted as the concentration of substrate which gives a rate of half the maximum possible value ($V_{max}/2$).

The kinetic parameters k_{cat} and K_M are experimentally determined mainly using the "initial rate" and "pseudo-first order" methods. The method of the "initial rates" is particularly useful in the case of very slow reactions which are only followed less than 5% towards completion. The substrate is used in large excess so that the

reaction is in a steady-state and the concentration of the complex ES remains practically constant over time (d[ES]/dt = 0). The concentration against the time is a linear plot and the slope of this line is equal to k_{cat}.

The "pseudo-first order" method is generally used for fast reactions and is based on having an excess of the catalyst (i.e. [E] >> [S]). In this way, during the course of the reaction only the concentration of the substrate changes significantly while the enzyme concentration remains practically constant. The reaction is followed for a long period to allow the equilibrium condition to be reached. The kinetic parameters are finally obtained using the progress curves.

The rate of a catalyzed reaction may be sometimes reduced if a number of substances, known as *inhibitors*, are present in the reaction mixture. The inhibition process is assumed to proceed essentially as the Michaelis-Menten catalytic process. In other words the enzyme (E) is inactivated by forming a complex with the inhibitor (I), an intermediate complex (EI), which is in equilibrium with E and I according to Eq.34.

$$E + I \underset{K_i}{\leftrightarrow} EI \xrightarrow{k_2} E'(\text{inactive}) \qquad \textbf{Eq.34}$$

In this way, the rate of inactivation is given by

$$v = k_2[EI] = \frac{V[I]}{K_i + [I]} \qquad \textbf{Eq.35}$$

in which $V = k_2[E]$ is the limiting rate of inactivation at saturating concentration of inhibitor.[82]

There are different types of inhibitors. Two extreme classes are the *irreversible* and *reversible inhibitors*. The first type of inhibitors bind irreversibly to the catalyst and decrease its activity to zero. In the second case the catalyst is reversibly inhibited by non-covalent interactions with I. This last class is further divided into four subclasses according to the particular apparent Michaelis-Menten parameters that they affect:

1. *Competitive* (unchanged V, increased K_M).

   In this case the inhibitor and the substrate compete for the same catalytic site. When the inhibitor binds to the catalyst, an inactive complex EI is formed, which is unable of further reaction. In this case an additional equilibrium needs to be considered:

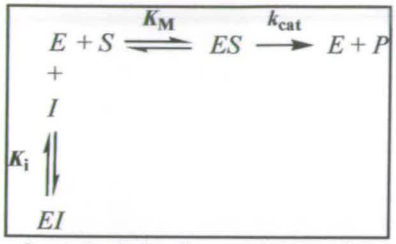

Fig. 55 Mechanism of catalysis in the presence of competitive inhibitors.

The rate equation is now given by

$$v = \frac{[E]_0[S]k_{cat}}{[S] + K_M\left(1 + \frac{[I]}{K_i}\right)} \qquad \textbf{Eq.36}$$

The effect of a competitive inhibitor is only on K_M which is increased by a factor of $(1 + [I]/K_i)$ whereas V_{max} remains unchanged.

2. *Non-competitive* (decreased V, unchanged K_M).

   The inhibitor and the substrate bind simultaneously to the catalyst but they do not compete for the same binding site:

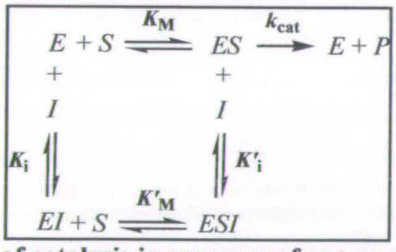

Fig. 56 Mechanism of catalysis in presence of non-competitive inhibitors.

Non-competitive inhibition is observed when $K_M = K'_M$. In this case the reaction rate is given by:

$$v = \frac{[E]_0[S]k_{cat}/(1+[I]/K_i)}{[S]+K_M} \qquad \textbf{Eq.37}$$

K_M remains unchanged and k_{cat} is lowered by a factor of $(1 + [I]/K_i)$.[83]

3. *Mixed* (decreased V, increased K_M).

   Mixed inhibition represents a general case of non-competitive inhibition. If the dissociation constant of S from ES (K_M) is different than that from ESI (K'_M), V and K_M are decreased and increased respectively by the following factors:

$$V^{app} = \frac{V}{1+([I]/K_i)} \qquad K_M^{app} = \frac{K_M(1+([I]/K_i))}{1+([I]/K_i)} \qquad \textbf{Eq.38}$$

4. *Uncompetitive* (V and K_M decreased by the same amount).

   When the inhibitor is able to bind to the Michaelis-Menten complex ES but not to the free catalyst (E), an uncompetitive inhibition occurs.

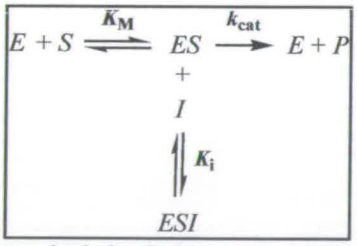

Fig. 57 Mechanism of catalysis in the presence of uncompetitive inhibitors.

In such case, the inhibitor decreases the apparent values of V and K_M by the same factor $(1+[I]/K_i)$ and the rate law appears to be as in Eq.39.

$$v = \frac{[E]_0[S]k_{cat}/(1+[I]/K_i)}{[S]+(K_M/(1+[I]/K_i))} \qquad \textbf{Eq.39}$$

Deviations from the Michaelis-Menten equation are also observed for two other main reasons. The first possibility is *substrate inhibition*. In such case the

enzyme (or more generally the catalyst) is able to bind a second molecule of substrate leading to a complex ES_2 that is catalytically inactive (Fig. 58).

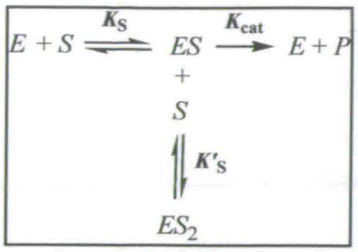

Fig. 58 Mechanism of catalysis with substrate inhibition.

Substrate inhibition becomes important at high substrate concentrations, where the rate law is given by:

$$v = \frac{[E]_0[S]k_{cat}}{K_S + [S] + \frac{[S]^2}{K'_S}} \qquad \textbf{Eq.40}$$

At low concentration, the rate is still expressed as usual by $v = [E]_0[S]k_{cat}/K_S$. Typical rate curves in the presence and absence of substrate inhibition are showed in Fig. 59.

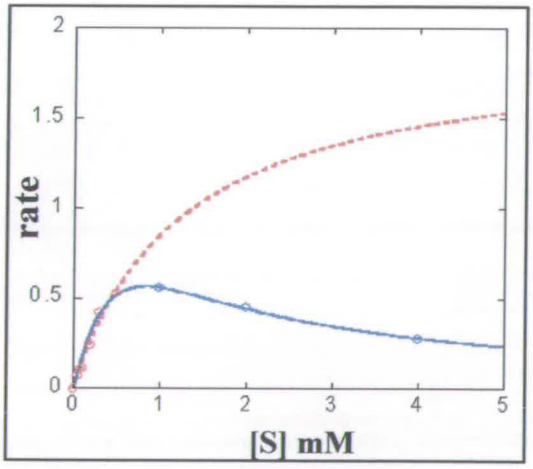

Fig. 59 Substrate inhibition curve (blue) and Michaelis-Menten curve (red).

Other possibilities are substrate activation (the complex ES_2 formed is more active than ES) and product inhibition. Here the product formed is able to bind to the

enzyme itself, sequestering the enzyme and thereby making it unavailable for reacting again with the substrate.

There are many other factors (e.g., concentration, temperature or pH) that influence and characterize the behaviour of a catalyst. Knowledge of their effects on the rate law provides important and essential evidence about the mechanism. A satisfactory mechanism can be deducted only after a careful kinetic investigation has been carried out.

2.3 Computational Methods.

The structure and properties of chemical systems can also be studied and predicted with the aid of theoretical methods. With the rapid increase of computer power and the decrease of their cost, computational chemistry has become 'affordable' to many research groups as a way to complement and/or explain experimental results.

Computational models have at the present an important role in the development of practical applications and in the understanding of crucial mechanistic questions that cannot be studied directly by experiments. Accurate theoretical calculations, usually supported by experimental data, are sometimes essential to resolve important chemical problems.

The starting point and the base of the any computational method is the Schroëdinger equation:

$$H\Psi = E\Psi \qquad \textbf{Eq.41}$$

in which E is the energy of a particle, Ψ is the wave function which characterizes the particle's motion and H is a mathematical operator called the *Hamiltonian*. The Hamiltonian operator reflects the contribution of kinetic and potential energies to the total energy. By resolving the Schroëdinger equation it is possible to calculate different properties that depend upon the electronic distribution, e.g. a chemical reaction involving the breakage and formation of bonds. However, this equation can

be analytically solved only for a system with a single particle, such one electron, and approximations need to be included in the method in order to get an useful insight into the chemistry of systems with more than an electron. Different approximate computational methods have been developed and they can be classified in the simplest way as *ab initio* and *empirical or semi-empirical* methods.

As it is intuitive from the Latin meaning of the name, the *ab initio* methods are derived directly from theoretical principle and they do not need to include any experimental data. The simplest type of *ab initio* calculation makes use of the Hartree-Fock approximation that is based on the Born–Oppenheimer and orbital approximations. In this method, the nuclei are considered fixed and the contribution to the total energy is only electronic. It is also assumed that the N-electron Schroëdinger equation can be solved using a linear combination of a set of approximate one-electron wave functions (basis set). The solution obtained is then iteratively optimized until convergence is reached.

A subclass of the *ab initio* methods is the DFT method (Density Functional Theory method). This is considered an alternative to Hartree-Fock. The DFT method could also be classified as semi-empirical method because in its theoretical calculations parameters derived from experimental data are often included. The starting point of a DFT method is the electron density rather than the wave function.

Semi-empirical and empirical methods are also based on the Hartree-Fock assumption but they consider only the valence electrons and make use of some experimental data. These methods are used for studying large molecules where the enormous number of calculations would make the *ab initio* method too expensive in terms of time and computer resources.

Computational chemistry has an interdisciplinary character and for such reason a wide range of computational tools and methods are available at the present. The desired accuracy grade and the intrinsic characteristics of the chemical system dictate the choosing of the most appropriate computational method.

Chapter 3 - Ligand design and synthesis

3.1 Introduction.

A convenient way to design a new catalyst is by taking inspiration from nature. As mentioned in Chapter 1, metalloenzymes achieve their extraordinary catalytic efficiency due to a careful choice of functional groups and metal(s) in the active site. The intrinsic properties of the metal ion, such as its geometric preference (number, type and arrangement of the ligand binding site) and redox properties, play an important role in its ability to cleave phosphate ester bonds. However, the chemical characteristics of the ligand used to form the catalytic complex are even more fundamental. The structure and steric factors of the ligand can dramatically influence not only metal binding but also how the resulting complex captures and activates the substrate.

In this work, different ligands have been chosen and prepared. All of them share a common metal binding unit: the chelating fragment dipicolylamine (Fig. 60).

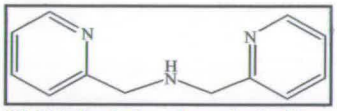

Fig. 60 Dipicolylamine chelating unit.

3.1.1 Dipicolylamine-based ligands.

Bis(2-pyridylmethyl)amine or dipicolylamine (dpa) is a well-known ligand, which was first reported by Kabzinska in 1964.[84] This ligand and its derivatives are able to form stable complexes with Zn(II) and other transition metal ions.[85] For example, $[Zn(dpa)]^{2+}$ can coordinate biologically-relevant anions such phosphates with high affinity ($K \geq 10^7$ M^{-1}) in aqueous solution.[86] This important property has been exploited for the development of complexes capable of recognizing and sensing phosphorylated species.[87] Mono and dinuclear metal complexes with dpa units have also been studied as artificial nucleases, leading to quite effective catalysts.[88]

The good phosphate binding and hydrolysis properties of metal complexes of dpa in water, associated with their easy functionalization were important factors in our ligand design process. In terms of functionalization of dipicolylamine structures, our group and others have incorporated amino hydrogen bonding groups adjacent to

the pyridine nitrogen (Fig. 61). This is important because the incorporation of amino groups in this position of pyridine-based ligands has been recently shown to be functionally important in terms of yielding more effective catalysts for phosphate diester hydrolysis.[89]

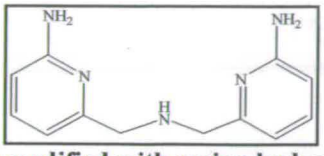

Fig. 61 Dipicolylamine unit modified with amino hydrogen bonding donor groups.

An important aspect causing this effect is that in general, the cooperativity between H-bond groups and metal ions leads to complexes with increased phosphate binding affinity.[90] An example is the $[Zn(tpa)]^{2+}$ complex (tpa = tris-(2-pyridylmethyl)amine) in which the introduction of two amino H-bond donor functionalities led to higher affinity for phenyl phosphate than the complex without the hydrogen bonding groups. Interestingly, the magnitude of the effect observed was comparable to that of the generally more effective dinuclear receptors.[91] Moreover, the tpa ligand functionalised with hydrogen bonding groups afforded Zn(II) complexes in which the pK_a of a water-bound molecule is substantially decreased, providing a potential nucleophile at physiological pH.[92] The Zn(II) complex of tpa with three amino groups was found to be a very effective catalysts for phosphate ester hydrolysis in which the contribution of the hydrogen bonding groups was similar to that of the metal itself (*ca.* 1000-fold rate acceleration). This result was further tested by examining the catalytic activity of a mononuclear complex with two auxiliary hydrogen bonding functionalities with that of the corresponding dinuclear complex. It was found that the activated substrate HPNPP was effectively hydrolysed, and that the activity of both catalysts was very similar.[93]

In essence, these studies showed that a poor mononuclear catalyst can reach the efficiency of a good dinuclear catalyst due to the cooperation between the metal and H-bond groups. In other words, the introduction of a second metal or hydrogen bonding functionalities can be equally effective towards increasing the efficiency of mononuclear catalysts (Fig. 62).

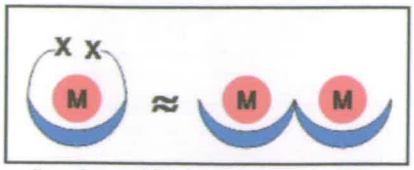

Fig. 62 Effect of the introduction of H-bond groups (X) or a second metal ion (M) in a mononuclear catalyst.

3.1.2 Ligand design.

Considering these important results, it seemed interesting to explore if the reactivity of Zn(II) complexes with the dpa binding unit can be enhanced even further by linking them. For this, three different central spacers were considered leading to three potentially-dinucleating ligands (Fig. 63, LOH', L^1OH' and L^2OH').

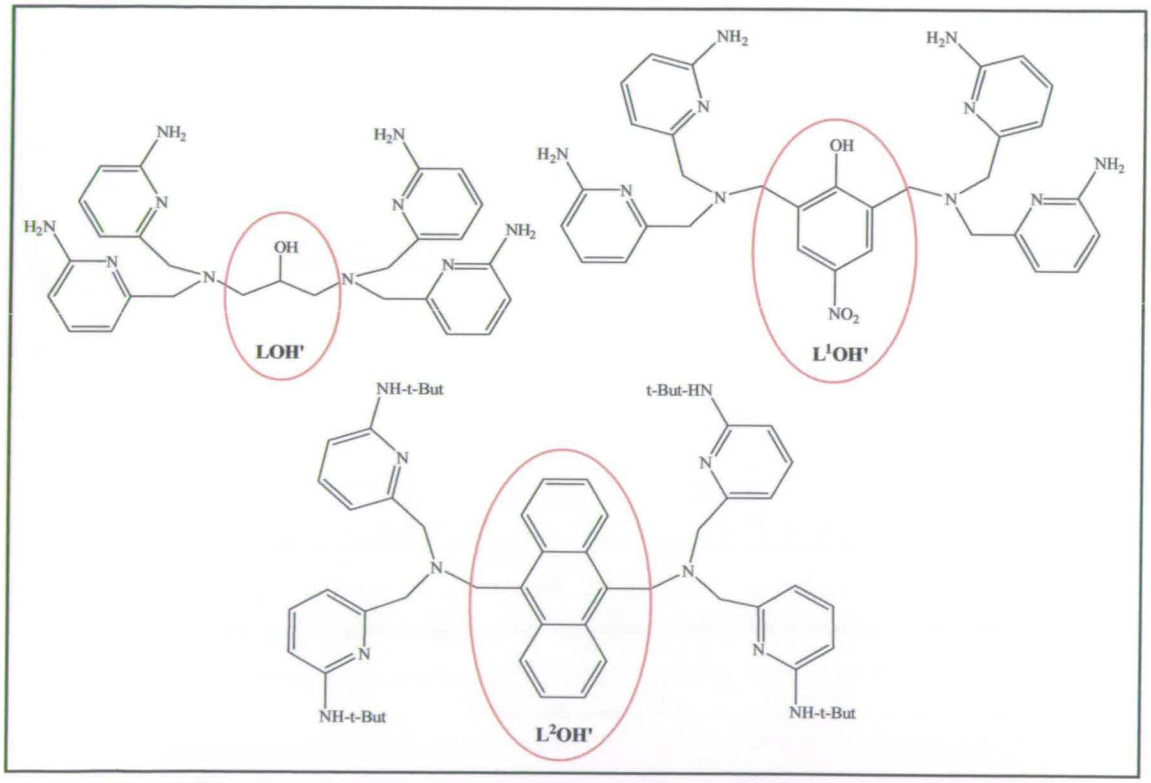

Fig. 63 Dinuclear ligands with H-bonding groups synthesized during this work.

The linkers bring together the two N3 donor sets of dpa and create semi-rigid dinucleating ligands. The different electronic and geometric properties imparted by the linker units on to the metal complex allowed us to explore differences in reactivity, stoichiometry and metal complex speciation. In fact, despite the general

dinucleating nature of the ligand structures, the formation of mononuclear metal complexes cannot be excluded as reported in different examples in the literature.[94]

To fully investigate, understand and compare the origin of the catalytic properties of these metal complexes towards the cleavage of activated phosphodiesters (cooperativity metal/metal, metal/H-bonding and two metals/ H-bonding groups), a series of mono and dinucleating ligands with and without H-bond functionalities was also synthesized (see Table 1). It is important to note that prior to the work described in this thesis, the potential benefits of combining two metals and hydrogen bonding groups had not been investigated (Fig. 64).

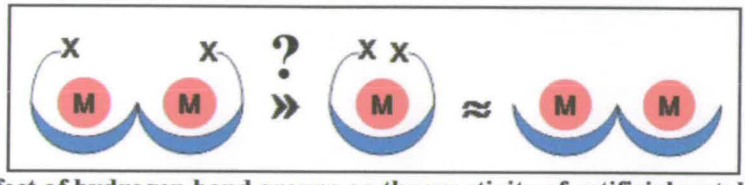

Fig. 64 Effect of hydrogen bond groups on the reactivity of artificial metal nucleases.

Only very recently, and after publication of part of this thesis, one example of a positive synergistic effect between metals and hydrogen bonding groups was explored and observed in a phosphate receptor.[95]

Table 1 – Series of ligands synthesized and cooperative interactions involved.

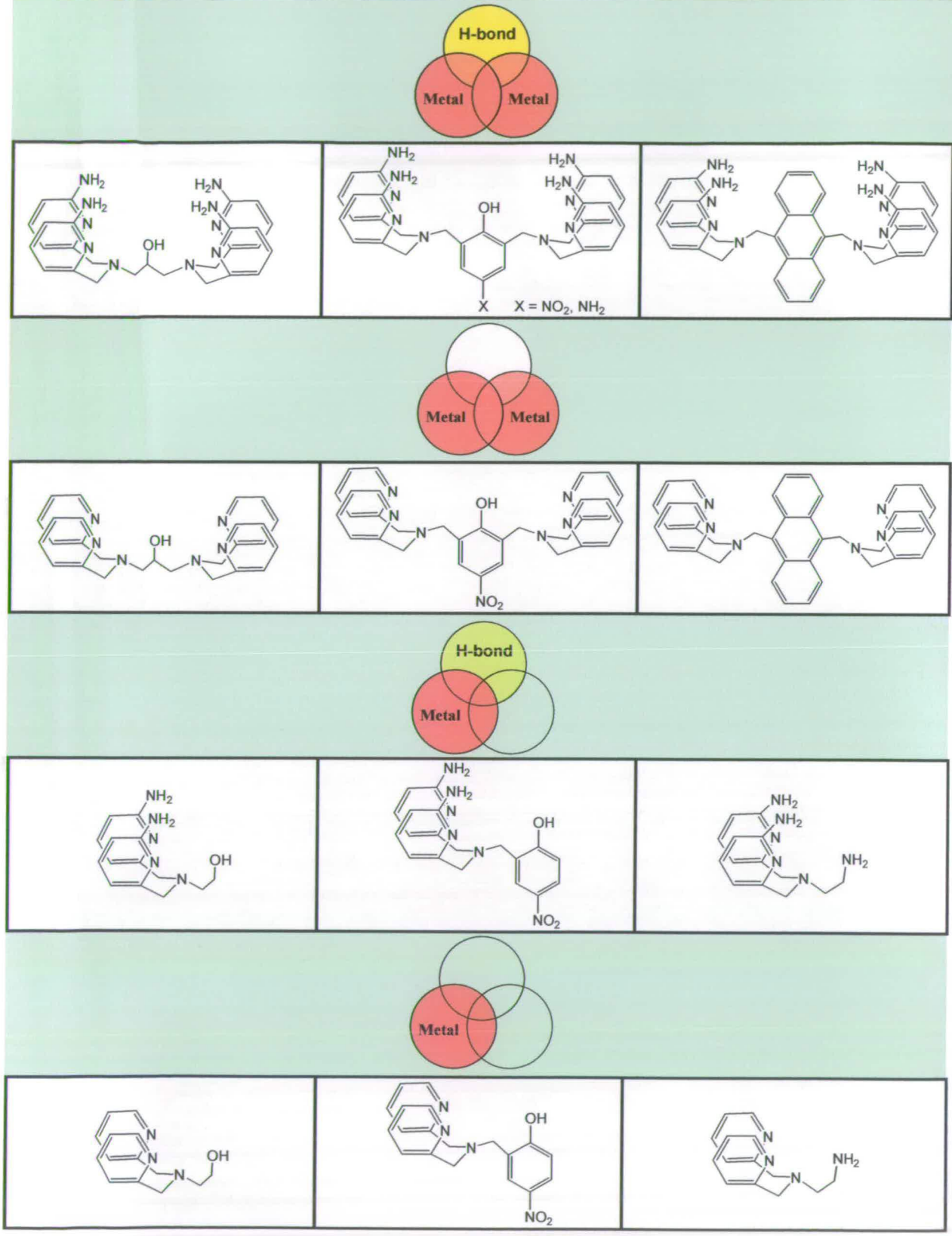

3.2 Results and discussion.

3.2.1 Dinucleating ligands with amino H-bonding donors.

The synthesis of the dinucleating ligands with amino hydrogen bonding groups was accomplished in different steps, summarized in Fig. 65. The strategy involves initially the synthesis of *N*-[6-(bromomethyl)-2-pyridyl] pivalamide (**A**, Fig. 65) from the commercially available 2-amino-6-methylpyridine according to a published procedure.[99] The reaction proceeds in two steps leading to the desired product in high purity after flash chromatography, although the yield is quite low (*ca.* 43%). Two equivalents of **A** were then reacted with 1,3-diamino-2-propanol in acetonitrile to form the ligand LOH'. After 15h under reflux, the reaction affords the crude pivaloylamido containing material as brown oil, which was then purified by flash chromatography. The amino groups were finally deprotected by acid hydrolysis and the pure product obtained in 56% yield. The ligands L^1OH' and L^2OH' were synthesized starting from a common unit, bis(pivalolylamido-2-pyridyl)methylamine (**NH-(Py(*t*-But))$_2$**). This dpa unit functionalized with pivalolylamido hydrogen bonds groups in the pyridine 6th position is obtained by reacting **A** with benzyl amine and following cleavage with H_2 (g) in the presence of Pd/C. The product was obtained in high purity and yield (> 87%) and used without any further purification for the next two reactions.

The synthesis of 9,10-bis[(6-pivalolylamido-2,2'-dipicolylamino)methyl] anthracene (L^2OH') was accomplished in one step by reacting the chelating unit **NH-(Py(*t*-But))$_2$** with the commercially available 9,10-bis(chloromethyl)anthracene. The pure product was isolated in 56% yield after purification with flash chromatography. The deprotection of the amino groups in the pyridine rings, which would lead to the desired final ligand, was unsuccessful. The hydrolysis reaction was attempted both under acid and basic conditions. The reasons for the failure of such final step are still not understood. Finally, the last dinucleating ligand synthesized was L^1OH' (*N,N,N',N'*-tetrakis [(6-amino-2-pyridyl)methyl]-2,6-diamino-*p*-nitrophenol). The synthetic procedure requires a two-step reaction to produce 2,6-bis(bromomethyl)-4-nitrophenol[96] which proceeds with 48% yield. This was then reacted with two equivalents of **NH-(Py(*t*-But))$_2$** in acetonitrile under reflux for 20h.

The product was finally subjected to acid hydrolysis during five days to remove the *tert*-butyl protecting groups and the final ligand was obtained as a yellow solid in 79% yield.

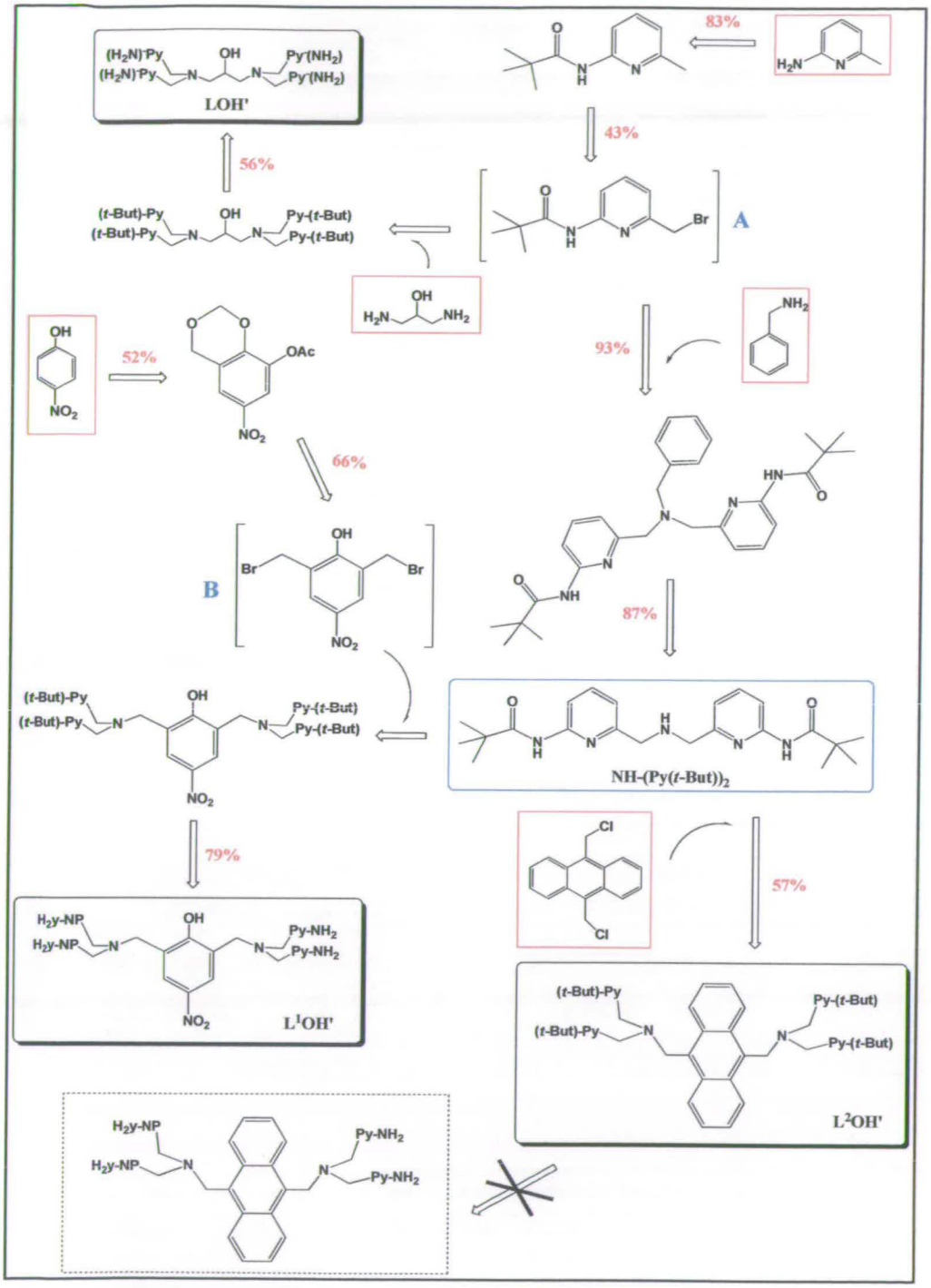

Fig. 65 Synthetic procedure for dpa-based dinucleating ligands with amino H-bonding groups.

3.2.2 Dinucleating ligands without amino H-bonding donors.

The synthesis of the dpa-based dinucleating ligands without the amino hydrogen bonds functionalities was accomplished in the same general way described previously. However in this case the number of steps involved is lower as the majority of the ligands can be prepared from commercially available chemical products. The only exception is the nitrophenol bridging unit, which as shown in Fig. 66 involved a preliminary two-step reaction.

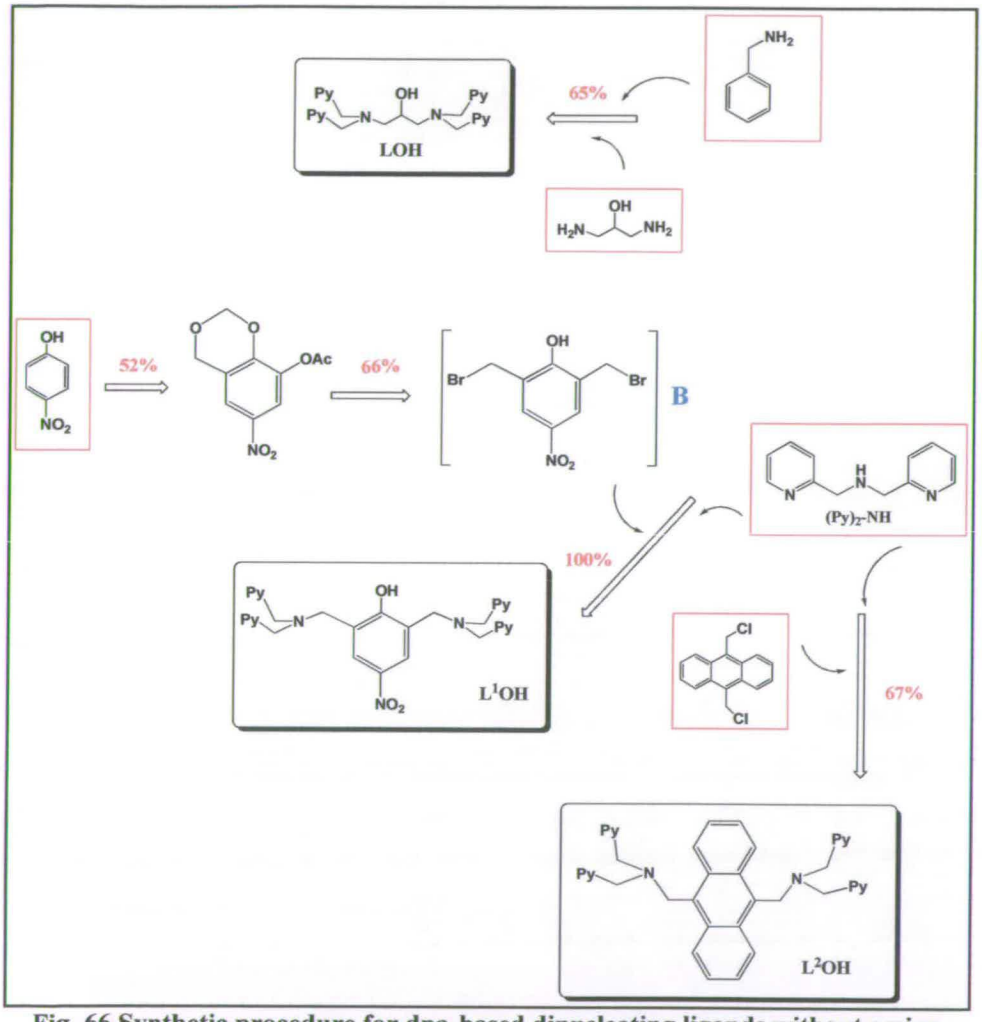

Fig. 66 Synthetic procedure for dpa-based dinucleating ligands without amino H-bonding groups.

The ligand LOH was synthesized by reacting four equivalents of 2-picolyl chloride with 1,3-diamino-2-propanol in the presence of hexadecyltrimethylammonium chloride. After 24h, the crude product is obtained as an orange oil. This was purified by flash chromatography on alumina to afford the pure

ligand in 65% yield. L^1OH was prepared in high yield (*ca.* 100%), by mixing one equivalent of 2,6-bis(bromomethyl)-4-nitrophenol (unit **B**, Fig. 66) with two equivalents of di-(2-picolyl)amine in acetonitrile. The pure product was at the end obtained after extraction in NaOH (*aq.*) and used without further purification.

Finally, the synthesis of L^2OH was carried out in anhydrous DMF at room temperature and isolated in 67% yield adopting a literature procedure.[97]

3.2.3 Mononuclear ligands with and without amino H-bonding donor groups.

In order to fully estimate the cooperativity effects of metal ions and H-bonding in dinuclear metal complexes, the corresponding mononuclear ligands with and without amino H-bonding donor groups have also been synthesized. The overall schemes are shown in Fig. 67 and Fig. 68.

The synthesis of mononuclear ligands without amino groups is usually accomplished in one-step reaction starting from commercial products (Fig. 67). The only exception is the 2-[bis(2-pyridil)methyl]amino-ethylamine ligand (L^5OH), which requires a further step in which the *N*-(*N*-bromoethyl)-phthalimide residue is cleaved off with hydrazine in absolute ethanol to give the amino group.

The ligand L^3OH was synthesized in water by mixing two equivalents of 2-picolylchloride and one of ethanolamine. After one overnight under reflux, the mixture was extracted and the crude product was isolated as red oil. This oil was further purified on basic alumina to give the pure product in 62% yield. The ligand 2-[bis(2-pyridil)methyl]amino-ethylamine was obtained by following the procedure reported in literature.[98]

When hydrogen bond functionalities are introduced in the position 6 of the pyridyl ring, each reaction is extended by at least two additional steps (Fig. 68). As in the case of the synthesis of dinucleating ligands with amino hydrogen bonding groups, the preparation of 2-bromomethyl-6-pivalamidopyridine (unit **A**, Fig. 65) and **NH-(Py(*t*-But))$_2$** represents the starting point of the synthetic procedure.

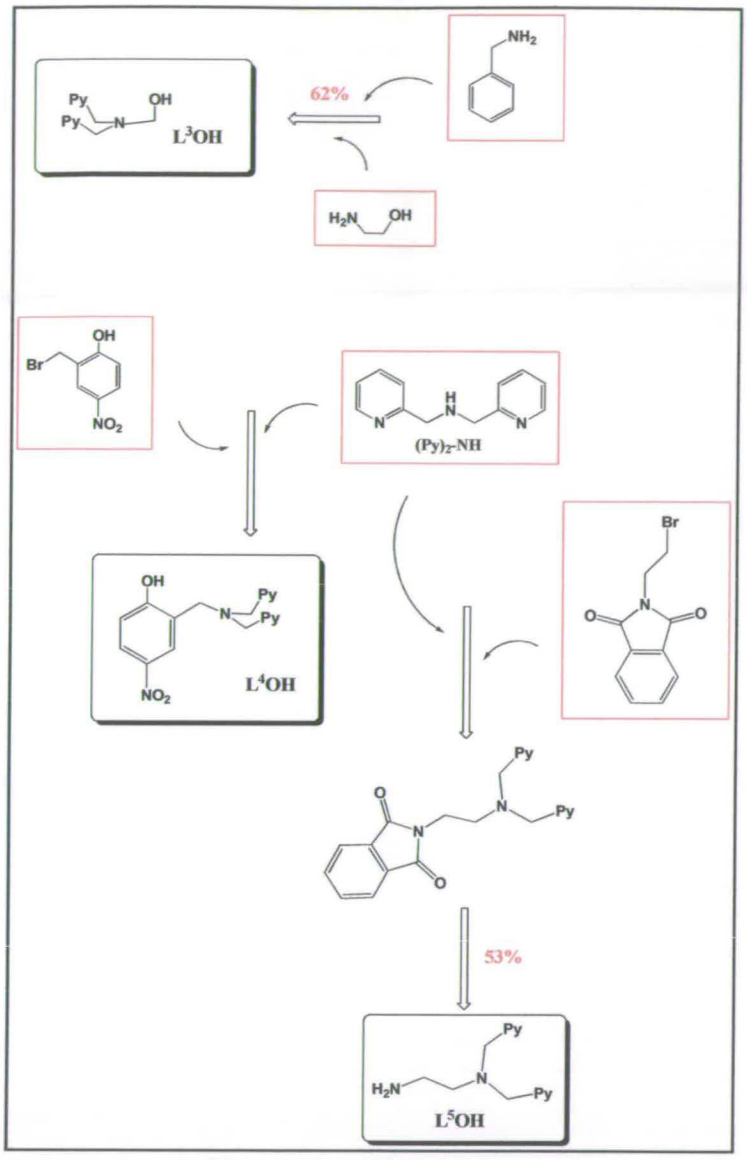

Fig. 67 Synthetic procedure for dpa-based mononuclear ligands without amino H-bonding groups.

Thus, L^3OH' was prepared from the reaction of ethanolamine with 2-bromomethyl-6-pivalamidopyridine followed by acidic hydrolysis, as reported in ref.89c. The ligands L^4OH' and L^5OH' were synthesized using as starting material the chelating unit **NH-(Py(*t*-But))$_2$** and 2-bromomethyl-4-nitrophenol and *N*-(2-bromoethyl)-phthalimide respectively. The amino groups were finally deprotected with acid or basic hydrolysis.

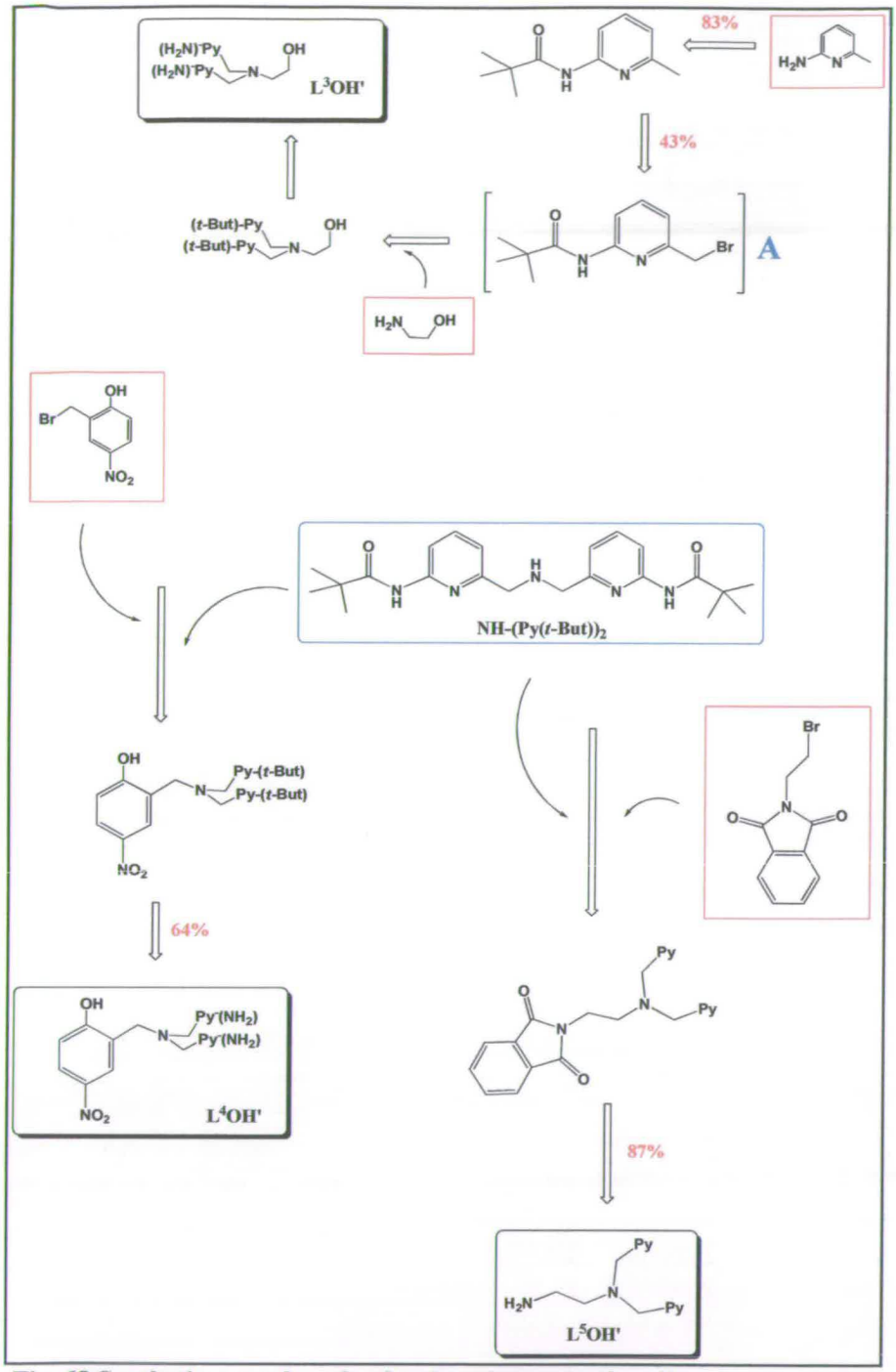

Fig. 68 Synthetic procedure for dpa-based mononuclear ligands with amino H-bonding groups.

3.3 Experimental details.

3.3.1 General.

Reagents were obtained from commercial sources and used as received unless otherwise noted. Solvents were dried and purified under N_2 by using standard methods and were distilled immediately before use. All compounds were prepared under N_2 unless otherwise mentioned. 2-(Pivalolylamido)-6-(bromomethyl)pyridine was synthesized according to a literature procedure.[99] NMR spectra were obtained using a Bruker DPX 200 at 20 °C. ^{13}C and ^{1}H chemical shifts are referenced with respect to the carbon and proton resonances of the solvent. Mass spectra were performed on a micromass Platform II system operating in Flow Injection Analysis mode with the electrospray method. Elemental analyses were carried out by the microanalysis service provided by the School of Chemistry at the University of Edinburgh.

3.3.2 Bis(6-pivalolylamido-2-pyridyl)methyl amine.

To a CH_3CN solution (350 mL) of 2-(pivalolylamido)-6-(bromomethyl) pyridine[99] (5 g, 18 mmol) was added benzylamine (0.99 g, 9 mmol) and Na_2CO_3 (4.77 g, 45 mmol). The resulting mixture was heated at reflux (T = 80°C) overnight after which it was allowed to cool to room temperature. The solvents were evaporated under vacuum and the residue was re-dissolved in DCM (30 mL) and washed with NaOH 1 M (2 x 15 mL). The DCM layer was separated, dried with Na_2SO_4, filtered and the organic solvent was removed under vacuum to afford the crude material as dark yellow oil (4.04 g, Yield 93% from benzylamine).

The crude product (4.04 g, 8.4 mmol) was dissolved in CH_3OH (100 mL) and reacted with H_2 (g) in the presence of Pd/C (10 wt % on carbon) (1 g) for 24 h after which the Pd was filtered and the solvent was removed under vacuum to afford the pure product as a pale brown sticky solid (3.17 g, Yield 87%).

^{1}H-NMR ($CDCl_3$, 200 MHz) δ_H/ppm 8.74 (s, 2H), 8.12 (d, J = 8 Hz, 2H,), 7.62 (t, J = 8 Hz, 2H), 6.94 (d, J = 8 Hz, 2H), 4.14 (s, 4H), 3.45 (s, 1H), 1.32 (s, 18H).

Reaction scheme:

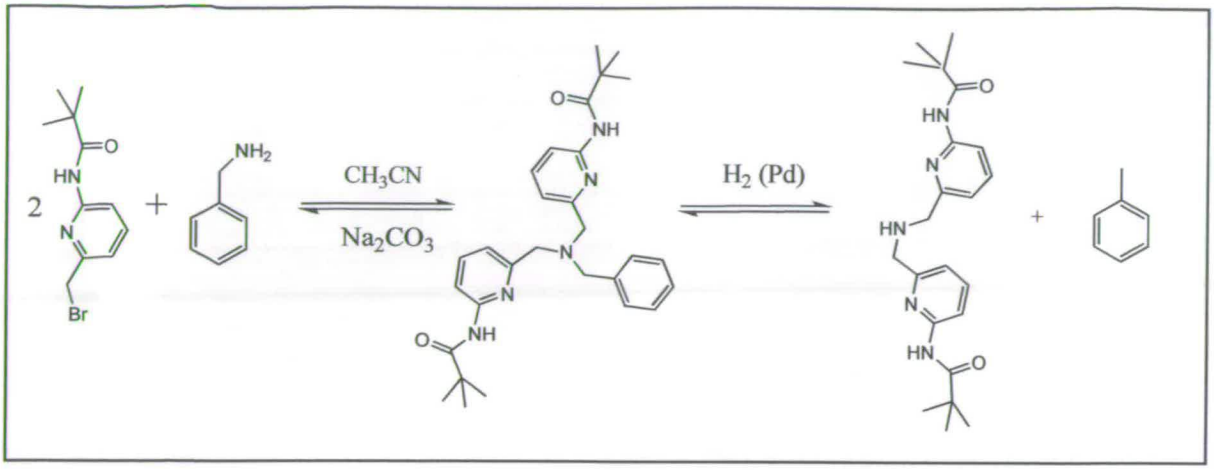

3.3.3 2,6-Bis(bromomethyl)-4-nitrophenol.

1 ***Synthesis of 8-acetoxymethyl-6-nitro-1,3-benzodioxene:***

To a hot mixture (T = 60°C) of paraformaldehyde (6 g, 10 mmol), acetic acid (25 mL) and concentrated sulfuric acid (11 mL) was added 4-nitrophenol (7 g, 50 mmol). The mixture was kept to reflux for 35h after which it was allowed to cool to room temperature. Water (50 mL) and K_2CO_3 (27.6 g, 200 mmol) was added to the solution to neutralize it, giving a colorless solid which was then filtered off, washed with cold water and left to dry for about 1h. The product was recrystallized from ethanol (100 mL) (6.22 g, 52% from 4-nitrophenol).

^{1}H-NMR ($CDCl_3$, 200 MHz) δ_H/ppm 8.21 (s, 1H), 7.92 (s, 1H), 5.39 (s, 2H), 5.17 (s, 2H), 4.97 (s, 2H), 2.18 (s, 3H).

2 ***Synthesis of 2,6-bis(bromomethyl)-4-nitrophenol:***

To a solution of concentrate HBr (48%) (42 mL) was added 8-acetoxymethyl-6-nitro-1,3-benzodioxene from "*step 1*" (6.22 g, 5.8 mmol) and the resulting mixture was heated at reflux for 6 h. The mixture was then allowed to cool to room temperature, filtered and the solid was washed with cold water, dried and recrystallized from chloroform (5.54 g, Yield 66% from 8-acetoxymethyl-6-nitro-1,3-benzodioxene).

^{1}H-NMR ($CDCl_3$, 200 MHz) δ_H/ppm 8.22 (s, 2H), 4.56 (s, 4H).

Reaction scheme:

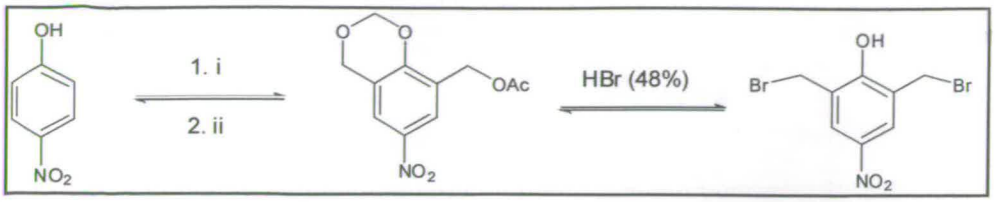

(i) = Paraformaldehyde, Acetic Acid, H_2SO_4 (conc.); (ii) = K_2CO_3(aq).

3.3.4 N,N,N',N'-tetrakis[(6-amino-2-pyridyl)methyl]-2-hydroxy-1,3-diamino-propane (LOH').

To a solution (100 mL) of 2-(pivalolylamido)-6-(bromomethyl)pyridine[99] (2 g, 7.38 mmol) in CH_3CN was added 1,3-diamino-2-propanol (0.165 g, 1.8 mmol) and Na_2CO_3 (0.96 g, 9.14 mmol). The resulting mixture was heated at reflux for 15 h after which it was allowed to cool to room temperature. The solvents were evaporated under vacuum, the residue was re-dissolved in DCM (40 mL) and washed with water (20 mL). The DCM layer was separated, dried with Na_2SO_4, filtered and the organic solvent was removed under vacuum to afford the crude material as brown oil. This oil was further purified by flash chromatography on neutral alumina (8:2 DCM:EtOAc). The pure product was dissolved in 2 M HCl (aq) (75 mL) and the solution was refluxed at 100 °C for 20 h. After cooling to room temperature, NaOH (1 M) was added until a precipitate is formed. The product was extracted with DCM (3 × 50 mL) and the organic fractions were dried over Na_2SO_4. The solvent was evaporated under vacuum to afford the product as a pale yellow/brown solid (0.51 g, Yield 56 % from 1,3-diamino-2-propanol).

The material was characterised as $L{\cdot}H_2O$: Found C 61.0, H 6.8, N 25.92; calc. for $C_{27}H_{36}N_6O_2$: C 60.88; H, 6.81; N, 26.3). MS (ES +) *m/z* found 515.1 (100%), calc. for LH_2^+ 515.3 (100%).

^{1}H NMR (CD_3OD, 360.1 MHz, 293 K) δ/ppm 7.40 (t, J = 8 Hz, 4H), 6.71 (d, J = 8 Hz, 4H), 6.43 (d, J = 8 Hz, 4H), 3.6 (s, 8H), 2.6 and 4.0 (m, 4H and 1H).

^{13}C NMR (CD_3OD, 90.5 MHz) δ/ppm 161.3, 159.1, 140.5, 114, 109.3, 69.5, 62.5, 61.0.

Reaction scheme:

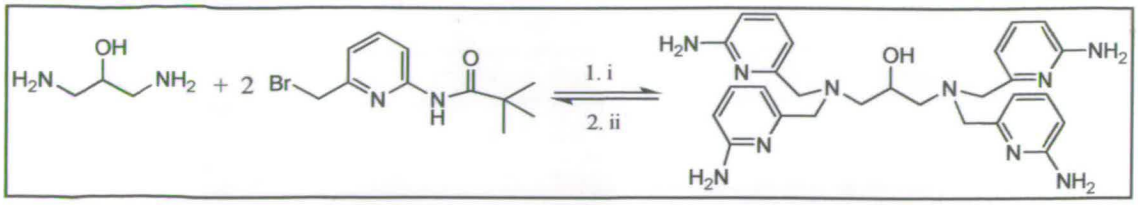

(i)= CH_3CN, Na_2CO_3, Δ; (ii) = 2N HCl_{aq}, Δ.

3.3.5 N,N,N',N'-tetrakis[(6-amino-2-pyridyl)methyl]-2,6-diamino-p-nitrophenol (L^1OH').

To a solution of bis(6-pivalolylamido-2-pyridyl)methylamine (1.87 g, 4.7 mmol) in CH_3CN (80 ml) was added Na_2CO_3 (5 g, 47 mmol) and the mixture stirred for 5 min. Then 2,6-bis(bromomethyl)-4-nitrophenol[100] (0.76 g, 2.35 mmol) was added and the reaction refluxed at 70°C for 20 h after which it was allowed to cool down to room temperature and the Na_2CO_3 filtered off. The solvent was evaporated under vacuum and the residue redissolved in DCM (50 ml) and extracted with water (2 x 25 ml). The organic layers were collected, dried with $MgSO_4$, filtered and the solvent removed under vacuum to afford the crude material as a yellow solid (1.75 g, Yield 78%).

^{1}H NMR ($CDCl_3$, 200 MHz,) δ/ppm 8.46 (s, 2H), 8.14 (d, J = 8 Hz, 4H), 8.08 (s, 4H), 7.62 (t, J = 8 Hz, 4H), 7.08 (d, J = 8 Hz, 4H), 3.80 (s, 4H), 3.78 (s, 8H), 1.31 (s, 36H). MS (ES+) *m/z* 980 ($M^+ + Na^+$, 100%), 958 (M^+, 25%).

This product (1.75 g, 18 mmol) was dissolved in CH_3OH (60 ml) and NaOH 1M (30 ml) was added. The mixture was refluxed at 80°C under stirring for 5 days. The solvent was evaporated under vacuum, the residue redissolved in water (30 ml) and the pH was adjusted to acid with HCl 3 M. This solution was then extracted with DCM (3 x 50 ml). The water layer was separated, the pH adjusted to basic (pH ≈ 11-12) with NaOH 1 M and extracted with DCM (3 x 50 ml). The organic layers were collected, dried with $MgSO_4$ and evaporated under vacuum. The solid was finally washed with CH_3OH. The evaporation of the solvent under vacuum affords the final product as a yellow solid (0.76 g, Yield 79%).

^{1}H-NMR (CD_3OD, 350 MHz) δ/ppm 8.07 (s, 2H), 7.32 (t, J = 7.3 Hz, 4H), 6.72 (d, J = 7.3 Hz, 4H), 6.35 (d, J = 7.3 Hz, 4H), 3.53 (s, 12H).

^{13}C-NMR (CD_3OD, 90 MHz,) δ/ppm 178.4, 160.4, 158.2, 139.1, 131.9, 128.0, 127.3, 112.5, 108.0, 61.4, 56.3. MS (ES-) *m/z* 620 (M^-, 100%).

Reaction scheme:

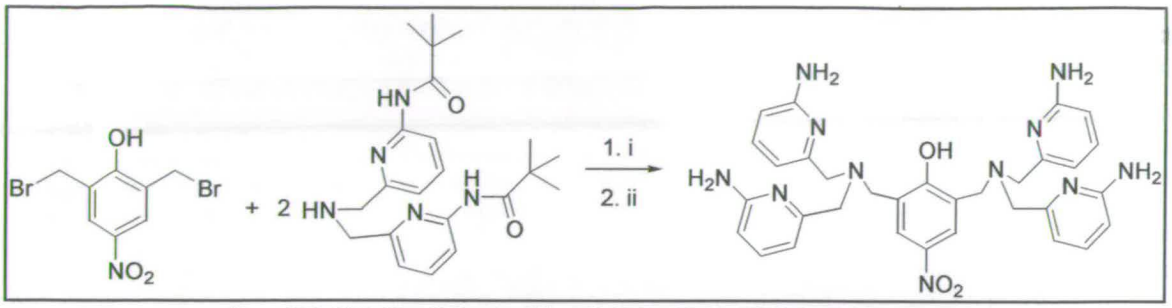

(i) = CH_3CN, Na_2CO_3, Δ; (ii) = 1M $NaOH_{aq}$, H_2O/CH_3OH, Δ.

3.3.6 9,10-Bis[(6-pivalolylamido-2,2'-dipicolylamino)methyl] anthracene (L^2OH').

To a THF solution (20 mL) of bis(6-pivalolylamido-2-pyridyl)methylamine (0.5 g, 0.5 mmol) was added 9,10-bis(chloromethyl)anthracene (0.068 g, 0.25 mmol) and Na_2CO_3 (0.26 g, 2.5 mmol). The resulting mixture was heated at reflux (T = 80°C) for 20 h after which it was allowed to cool to room temperature. The solvent was evaporated to afford the crude material as a yellow solid (0.35 g, Yield 56%). This crude product was purified by flash chromatography on silica gel (**1.** DCM 100% **2.** CH_3OH 100%). The pure product (0.20 g, 0.2 mmol) was redissolved in CH_3OH (30 mL) and NaOH 1M (10 mL). The resulting mixture was heated at reflux (T = 80°C) for 3 days. The following step was unsuccessful as well as the hydrolysis under acidic conditions.

^{1}H-NMR ($CDCl_3$, 200 MHz) δ_H/ppm 8.47 (m, 4H), 8.11 (s, 4H), 8.08 (d, J = 8 Hz, 4H), 7.56 (m, 4H), 7.51 (t, J = 8 Hz, 4H), 7.03 (d, J = 8 Hz, 4H), 4.64 (s, 4H), 3.82 (s, 8H), 1.38 (s, 36 H).

MS (ES +) *m/z* 997.6 (M^+, 40%), 600.2 (M^+ - 398, 50%), 398.1 (M^+ - 600, 100%).

Reaction scheme:

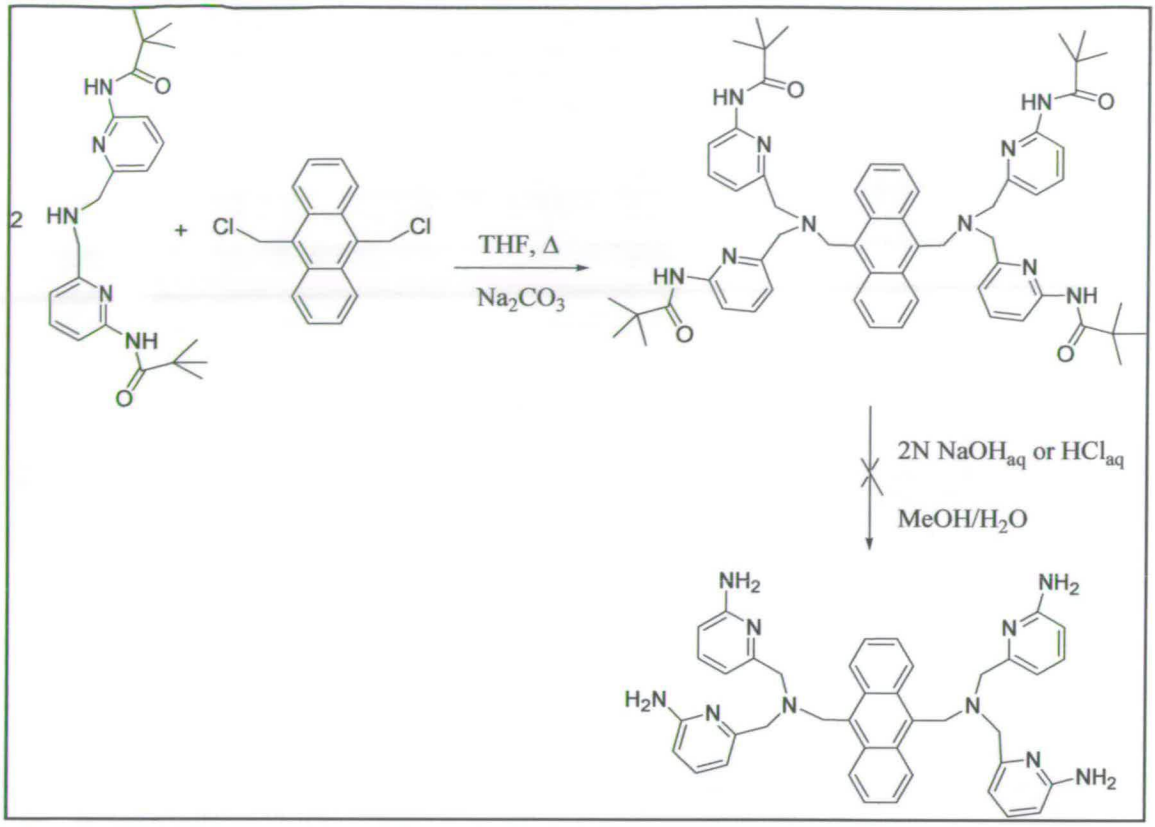

3.3.7 N,N,N',N'-tetrakis[(2-pyridyl)methyl]-2-hydroxy-1,3-diamino-propane (LOH).

To a water solution (25 mL) of 2-picolyl chloride hydrochloride (98%) (3 g, 18.3 mmol) was added 5M NaOH (4 mL). At the same time, to a solution of NaOH 5 M (3 mL) was added 1,3-diamino-2-propanol (0.41 g, 4.55 mmol) and incorporated to the reaction mixture with hexadecyltrimethylammonium chloride (0.02 g, 0.062 mmol). The resulting mixture was left under stirring at room temperature for 24h after which it was extracted with DCM (3 x 30 mL). The DCM layer was separated and washed with water (2 x 40 mL). The organic layer was dried with $MgSO_4$, filtered and the solvent was removed under vacuum to afford the crude material as orange oil. The crude product was purified by flash chromatography on neutral alumina (98%:2%, DCM:CH_3OH followed by 100% CH_3OH). Yield 65%.

^{1}H NMR ($CDCl_3$, 200 MHz) δ/ppm 8.49 (d, J = 8 Hz, 4H), 7.57 (t, J = 8 Hz, 4H), 7.35 (d, J = 8 Hz, 4H), 7.10 (t, J = 8 Hz, 4H), 3.88 (s, 12H), 3.42 (s, 1H).

Reaction scheme:

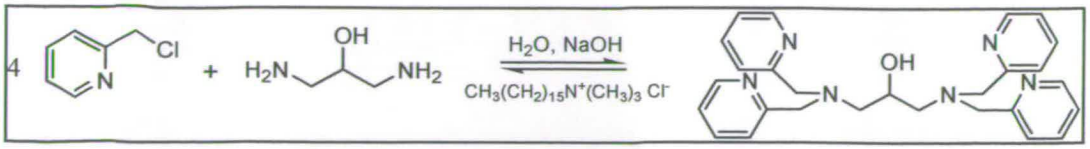

3.3.8 N,N,N',N'-tetrakis[(2-pyridyl)methyl]-2,6-diamino-p-nitrophenol (L^1OH).

To a solution (60 mL) of 2,6-bis(bromomethyl)-4-nitrophenol (0.19 g, 0.6 mmol) in CH_3CN was added di-(2-picolyl)amine (0.24 g, 1.2 mmol) and Na_2CO_3 (1.27 g, 12 mmol). The resulting mixture was heated at reflux (T = 80°C) for 18 h after which it was allowed to cool to room temperature and the Na_2CO_3 was filtered. The solvent was evaporated under vacuum, the residue was redissolved in DCM (20 mL) and extracted with NaOH 1M (20 mL). The organic layer was separated, dried with Na_2SO_4, filtered and the solvent removed under vacuum to afford the final product (0.34 g, Yield 100%).

^{1}H-NMR ($CDCl_3$, 200 MHz) δ_H/ppm 8.55 (d, J = 8 Hz, 4H), 8.21 (s, 2H), 7.66 (t, J = 8 Hz, 4H), 7.48 (d, J = 8 Hz, 4H), 7.13 (t, J = 8 Hz, 4H), 3.94 (s, 8H), 3.89 (s, 4H). MS (ES +) m/z 584.0 ($M^+ + Na^+$ 100%).

Reaction scheme:

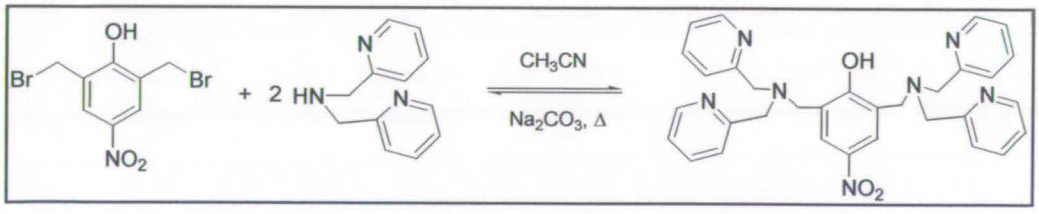

3.3.9 9,10-Bis[(2,2'-dipicolylamino)methyl]anthracene (L^2OH).

This ligand was synthesized as described in the literature[97] by mixing 9,10-bis(chloromethyl) anthracene (0.5 g, 1.83 mmol) with two equivalents of 2,2-dipicolylamine (0.7 g, 3.57 mmol) in DMF (20 ml) and in the presence of K_2CO_3 (0.4 g, 3.87 mmol) and keeping the reaction at 60°C for 3 days.

^{1}H NMR ($CDCl_3$, 600 MHz) δ_H/ppm 8.52 (d, J = 4.6 Hz, 4H), 8.41 (dd, J = 3.3, 6.9 Hz, 4H), 7.56 (m, 4H), 7.43 (dd, J = 3.1, 7.4 Hz, 4H), 7.29 (d, J = 7.8 Hz, 4H), 7.05 (dd, J = 5.4, 7.0 Hz, 4H), 4.64 (s, 4H), 3.98 (s, 8H).

MS (ES +) m/z 623.1 ($M^+ + Na^+$ 100%).

Reaction scheme:

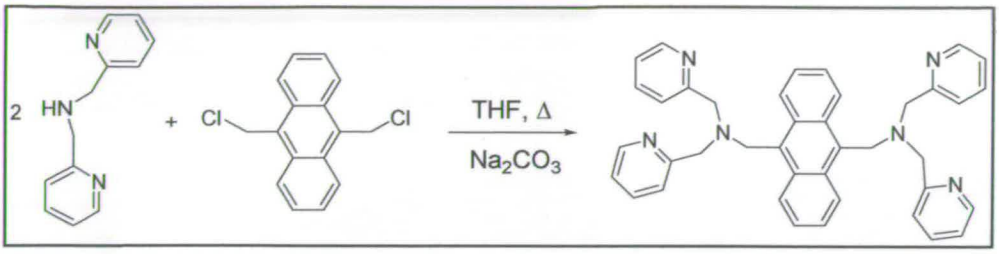

3.3.10 2-[Bis(2-pyridyl)methyl]amino ethanol (L^3OH).

To an aqueous solution (10 ml) of 2-picolylchloride (2.05 g, 12 mmol) was added ethanolamine (0.377 ml, 6.25 mmol). The mixture was stirred and heated at 60°C, and then a solution of NaOH in water (1 g, 25 mmol in 5ml) was added drop wise. The reaction was left overnight. After cooling at room temperature, the mixture was extracted with $CHCl_3$ (3 x 20 ml) and the combined organic phase was dried with $MgSO_4$. Following evaporation of the solvent afforded the product as a red oil. Purification was carried out by absorbing the product onto basic alumina followed by elution with methanol to give the desired product as a dark yellow oil (0.94 g, Yield 62 %).

^{1}H-NMR ($CDCl_3$, 200 MHz) δ/ppm 8.52 (d, J = 8 Hz, 2H), 7.60 (t, J = 8 Hz, 2H), 7.34 (d, J = 8 Hz, 2H), 7.13 (t, J = 8 Hz, 2H) 3.94 (s, 4H), 3.67 (t, J = 6 Hz, 2H), 2.89 (t, J = 6 Hz, 2H).

MS (ES +) 244.2 (M^+, 100%), ($M^+ + Na^+$, 266.2 (70%)).

Reaction scheme:

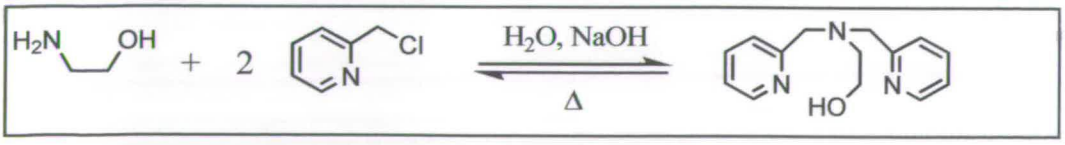

3.3.11 2-[Bis(2-pyridylmethyl)aminomethyl]-4-nitrophenol (L^4OH).

This ligand was prepared according to the procedure described in literature[101] by adding 2-bromomethyl-4-nitrophenol (0.5 g, 2 mmol) to a THF solution (10 ml) of *N,N*-bis(2-pyridylmethyl)amine (0.4 g, 2 mmol) in the presence of triethylamine (0.4 ml, 2 mmol). The reaction was kept at RT for one day.

^{1}H-NMR ($CDCL_3$, 200 MHz) δ/ppm 8.55 (d, J = 8 Hz, 2H), 8.07 (m, 2H), 7.64 (t, J = 8 Hz, 2H), 7.27 (d, J = 8 Hz, 2H), 7.18 (t, J = 8 Hz, 2H), 6.94 (d, J = 6 Hz, 1H), 3.91 (s, 4H), 3.84 (s, 2H).

Reaction scheme:

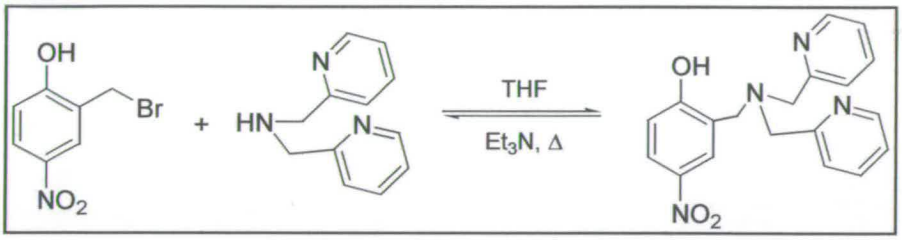

3.3.12 2-[Bis(2-pyridyl)methyl]amino-ethylamine (L^5OH).

The ligand L^5OH was synthesized following the procedure published[102].

^{1}H-NMR ($CDCl_3$, 200 MHz) δ/ppm 8.56 (d, J = 8 Hz, 2H), 7.64 (t, J = 8 Hz, 2H), 7.35 (d, J = 8 Hz, 2H), 7.15 (t, J = 8 Hz, 2H) 4.45 (t, J = 6.4 Hz, 2H), 3.99 (s, 4H) 3.62 (t, J = 8 Hz, 2H), 2.64 (br s, 2H).

Reaction scheme:

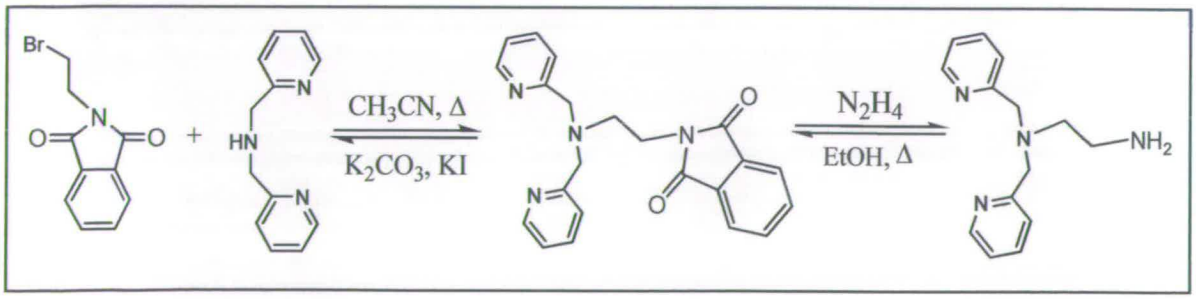

3.3.13 2-[Bis(6-amino-2-pyridyl)methyl]amino-ethanol (L^3OH').

The ligand was prepared from the reaction of ethanolamine with 2-bromomethyl-6-pivalamidopyridine followed by acidic hydrolysis as reported in ref.90c.

^{1}H-NMR ($CDCl_3$, 250 MHz) δ/ppm 7.23 (dd, J = 7.9, 7.3 Hz, 2H), 6.56 (d, J = 7.3 Hz, 2H), 6.25 (d, J = 7.3 Hz, 2H), 4.76 (br s, 5H), 3.61 (s, 4H), 3.54 (t, J = 5.0 Hz, 2H), 2.69 (t, J = 5.0 Hz, 2H).

^{13}C-NMR ($CDCl_3$, 63 MHz,) δ/ppm 158.3, 157.6, 138.2, 112.8, 107.0, 59.9, 59.6, 56.4.

MS (ES+) *m/z* 274 (M^+ + 1, 100%).

Reaction scheme:

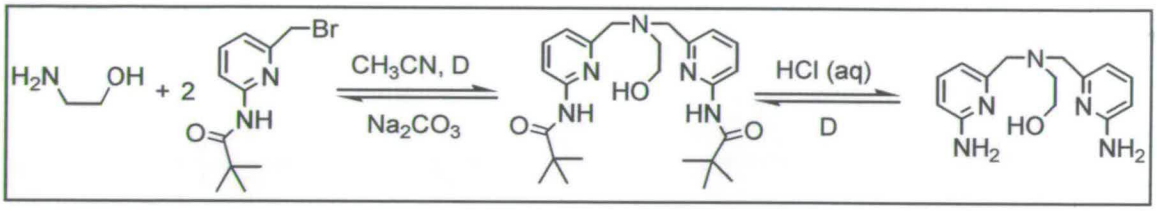

3.3.14 2-[Bis(6-amino-2-pyridylmethyl)aminomethyl]-4-nitrophenol (L^4OH').

This ligand was prepared in THF (80 ml) according to the procedure used for the ligand L^4OH but reacting bis(6-pivalolylamido-2-pyridyl)methyl amine (0.8 g, 2 mmol) instead than di-(2-picolyl) amine. The resulting product was first characterized by NMR spectroscopy and then hydrolyzed under basic conditions (15 ml NaOH 1 M, T = 80°C, 36h).

^{1}H-NMR ($CDCL_3$, 360 MHz) δ/ppm 8.30 (br s, 2H), 8.10 (m, 5H), 7.65 (t, J = 9 Hz, 2H), 6.94 (m, 4H), 3.83 (s, 4H), 3.81 (s, 2H), 1.36 (s, 18H).

^{13}C-NMR ($CDCL_3$, 360 MHz) δ/ppm 178.3, 164.5, 156.7, 152.3, 141.1, 120.4, 127.6, 126.7, 124.6, 119.2, 117.8, 113.3, 59.4, 56.9, 40.9, 28.5.

The final product appears as a yellow solid (Yield 64%). ^{1}H-NMR (CD_3OD, 200 MHz) δ/ppm 7.96 (m, 2H), 7.32 (t, J = 6 Hz, 2H), 6.79 (d, J = 8 Hz, 1H), 6.54 (d, J = 6 Hz, 2H), 6.37 (d, J = 6 Hz, 2H), 3.72 (s, 2H), 3.61 (s, 4H).

Reaction scheme:

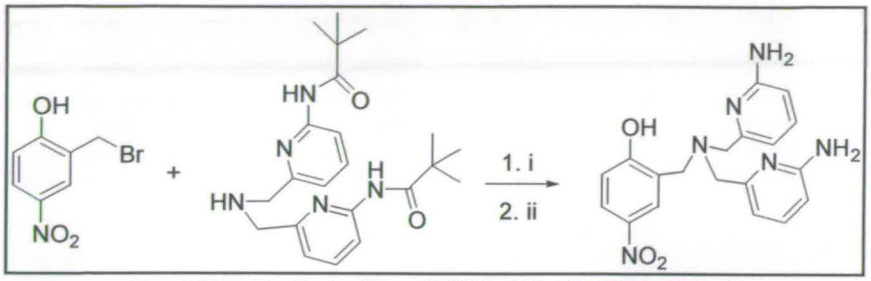

(i) = THF, Et_3N, Δ; (ii) = 2M NaOH, H_2O/CH_3OH, Δ.

3.3.15 2-[Bis(6-amino-2-pyridyl)methyl]amino-ethylamine (L^5OH').

This ligand was synthesized in CH_3CN (15 ml) by reacting bis(6-pivalolylamido-2-pyridyl)methyl amine (0.7 g, 1.77 mmol) with *N*-(2-bromoethyl)-phthalimide (0.44 g, 1.77 mmol) in the presence of K_2CO_3 (0.6 g, 4 mmol) and KI (0.03 g, 0.2 mmol). The reaction mixture was allowed to reflux for five days. After cooling, the solid was removed by filtration and the solvent evaporated under vacuum. The brown oil was purified by column chromatography on silica gel using ethyl acetate as the eluent. The concentration of the second fraction produced the pure product as yellow oil. This latter was dissolved in dry absolute ethanol (17 ml) containing 0.15 ml of $N_2H_4 \cdot H_2O$ (3 mmol) and allowed to reflux for 3 h. The mixture was left to cool down and 3 ml of HCl (37% w/w) were added. The reaction was stirred at RT for 1h to allow the formation of a white precipitate. The solid was removed by filtration and the volume of the solvent concentrated to a few millilitres under vacuum. The solution was made basic by adding NaOH 1 M. The solution was finally extracted with DCM (3 x 5 ml). The organic layers were collected and dried with $MgSO_4$. Evaporation of the solvent afforded the intermediate product (0.16 g, 0.36 mmol) (Step 1 in the reaction scheme) which was dissolved in 15 ml of HCl 2 M. The reaction was kept at reflux (T = 95°C) for two days and then extracted with DCM

(3 x 20 ml). The pH of the water layer was made basic by adding NaOH 2 M and extracted with DCM (3 x 20 ml). Evaporation of the organic solvent afforded the pure product as a yellow oil (0.085 g, Yield 87%).

^{1}H-NMR ($CDCl_3$, 200 MHz) δ/ppm 7.37 (t, J = 7.6 Hz, 2H), 6.67 (d, J = 7.2 Hz, 2H), 6.36 (d, J = 8.2 Hz, 2H), 4.45 (t, J = 7.6 Hz, 2H) 3.76 (s, 4H), 3.61 (t, J = 7.6 Hz, 2H).

Reaction scheme:

1st step:

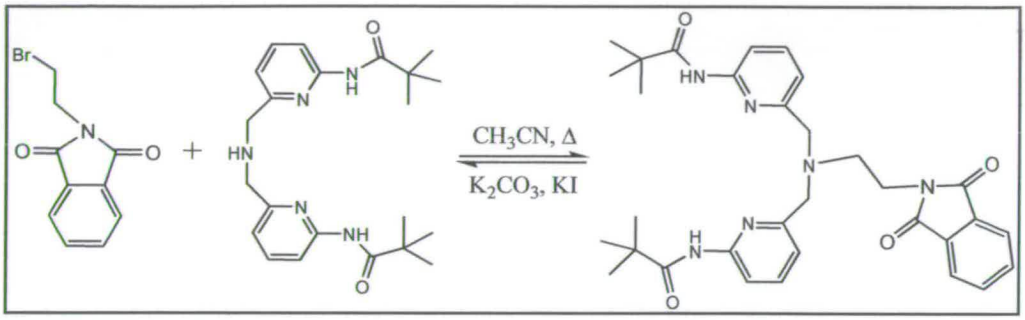

2nd step:

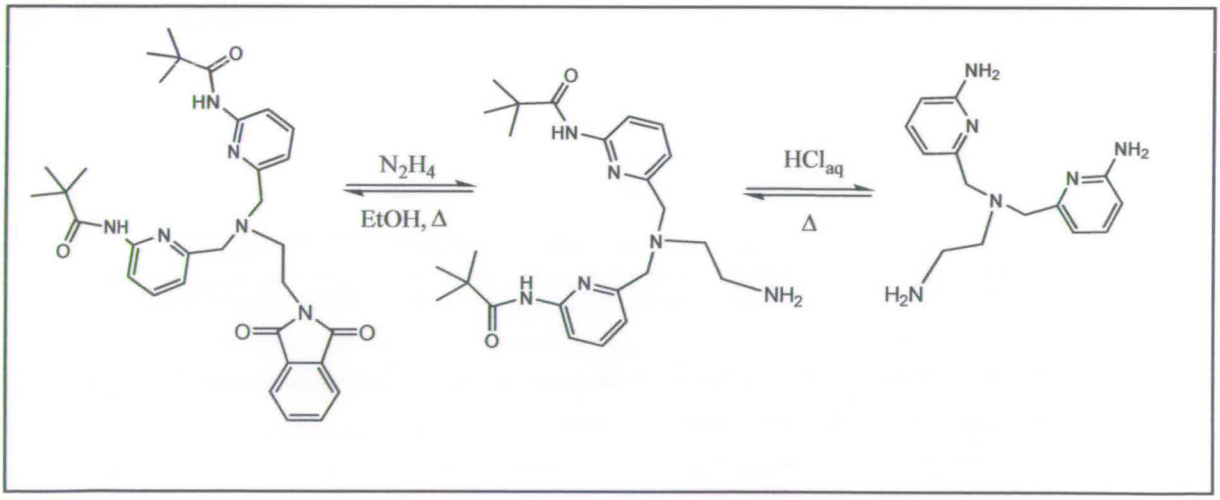

3.3.16 N,N,N',N'-tetrakis[(6-amino-2-pyridyl)methyl]-2,4,6-triamino-phenol.

To a methanolic solution (25 mL) of *N,N,N',N'*-tetrakis[(6-amino-2-pyridyl)methyl]-2,6-diamino-*p*-nitrophenol (0.26 g, 0.4 mmol) was added Pd/C (10 wt

% on carbon) (0.1 g). The resulting mixture was left under H_2(g) for an overnight after which the Pd was filtered and the solvent was evaporated under vacuum to afford the final product as a black oil (0.15 g, 63%). MS (ES +) *m/z* 592.2 (M^+ + 1, 100%).

Reaction scheme:

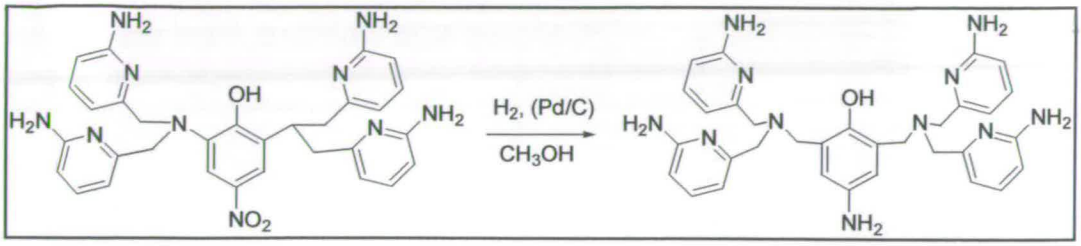

Chapter 4 – Equilibria and Complex Formation in Solution

4.1 Introduction.

The catalytic activity of metal complexes for the hydrolysis of phosphodiesters can be evaluated properly only if the identity of the complexes present in solution is known. For this, the determination of protonation and complex formation constants is important, and therefore, it represents a necessary preliminary investigation.

The ligands LOH and L^1OH (Fig. 69) and their derivatives with amino hydrogen bonding groups in the 6-position of pyridine (LOH' and L^1OH') have been synthesized as models of the active sites of natural nucleases.

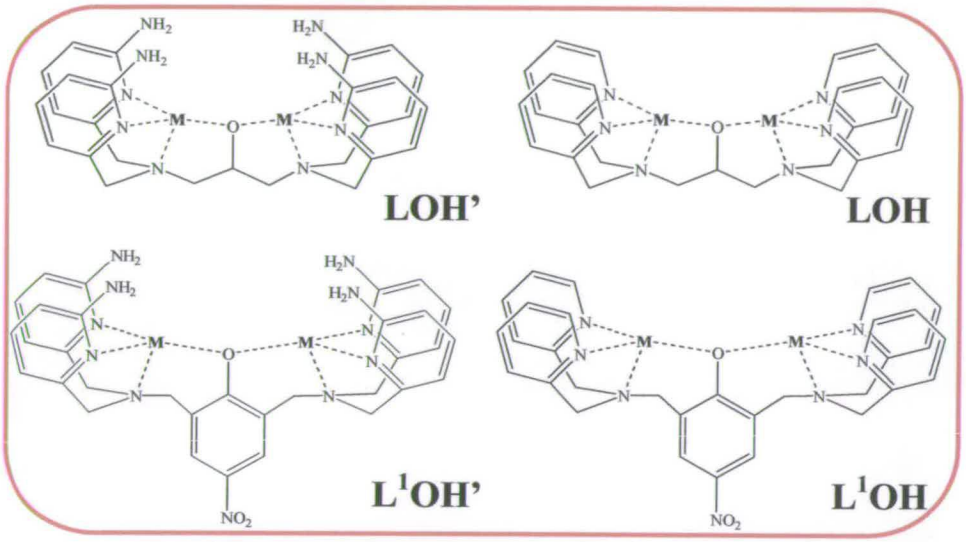

Fig. 69 Dinucleating ligands with and without amino hydrogen bond groups.

Since the intention is to test the properties of Zn(II) complexes of these ligands as catalysts for the hydrolysis of phosphate diesters (Chapter 5), in this chapter we determine the protonation and zinc complexation constants of these ligands in water.

Because dinucleating ligands can in principle afford mononuclear complexes, the complex formation mechanism between Zn(II) and these potentially dinucleating ligands was investigated by carrying out potentiometric pH titrations using different metal to ligand ratios and concentrations. We report that the metal:ligand ratio and nature of the bridging unit have a dramatic effect on the nature of the species formed. In particular it dictates whether mono or dinuclear species are formed.

In some cases the scarce solubility of the ligand (or of the zinc complexes formed) in water forced us to use binary solvent mixture of DMSO:water (67%:33%).

DMSO:water mixtures have been used quite widely in potentiometry. For example, it has been used to investigate the potential aqueous coordination chemistry of quinoline-based fluorescence Zn(II) probes for use in biological imaging applications.[103]

DMSO:water is a good solvent mixture for several reasons. Despite the different physico-chemical properties of DMSO and water, they are completely miscible. DMSO is an aprotic polar solvent which readily dissolves many water-soluble salts as well as many water-insoluble compounds. Moreover, its binary mixture with water represents an appropriate solvent for potentiometric measurements because it gives Nernstian responses over a wide pH range and the potential is highly reproducible with readily available glass electrodes.[104]

To assess the extent to which the results in DMSO:water are relevant to those in pure water we compare, where possible, the results obtained in these two different solvents. Thus, protonation constants and Zn(II) complexation constants of LOH (Fig. 69) were determined in pure water and in the binary mixture DMSO:H_2O (67%:33%). We report that for this particular ligand the solution behaviour in pure water and in the DMSO:water mixture is essentially identical.

4.2 Results and discussion.

4.2.1 Potentiometric titrations in water.

4.2.1.1 LOH.

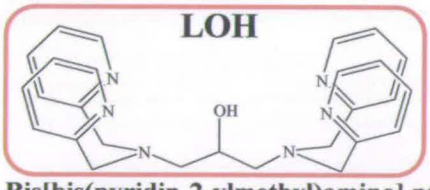

Fig. 70 1,3-Bis[bis(pyridin-2-ylmethyl)amino] propan-2-ol.

The complex formation equilibria between Zn(II) and the ligand 1,3-bis[bis(pyridin-2-ylmethyl)amino] propan-2-ol (LOH, Fig. 70) was previously investigated by Kinoshita *et al.*[105] in 0.1 M $NaNO_3$ ionic medium at 25°C. They suggested that complex formation reactions between Zn(II) and the ligand LOH result exclusively in dinuclear

complexes according to the scheme given in Fig. 71. It is important to note that they investigated only solutions with a metal:ligand ratio of 2:1.

Rather surprisingly the reported mechanism of complex formation could not be fitted to initial data collected during this work with M:L ratio of 1:1, and hence a detailed study was carried out in order to accurately define the stoichiometry and protonation state of the complexes in water solutions.

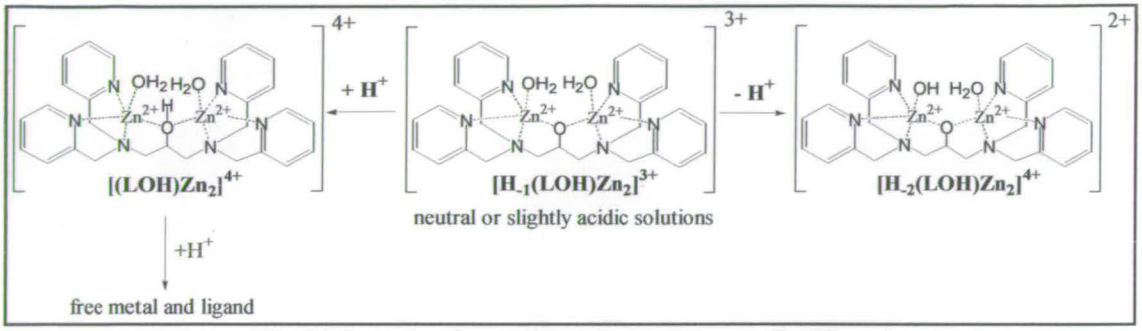

Fig. 71 Complex formation scheme between Zn(II) and 1,3-bis[bis(pyridin-2-ylmethyl)amino] propan-2-ol reported by Kinoshita *et al.*.[105]

In this work the ligand concentration was varied in the range 1-2 mM and titrated by adding small volumes of a standardized solution of 0.1 M Me_4NOH. A known amount of standardized 0.1 M $HClO_4$ was initially added to the ligand solution and data were collected up to pH slightly above 7. At this pH only the unprotonated LOH ligand exists and no further reactions were observed by increasing the pH. A typical titration curve for the ligand LOH is shown in Fig. 72.

The best values for the overall protonation constants determined for this ligand are summarized in Table 2, along with the equilibrium constants reported by Kinoshita *et al.*.

Table 2 - Protonation constants for the ligand LOH

H	LOH	log β (this work)[106]	log β (Ref. 105)
1	1	6.32 ± 0.03	6.47
2	1	11.52 ± 0.03	11.81
3	1	15.32 ± 0.04	15.62
4	1	18.47 ± 0.04	18.74

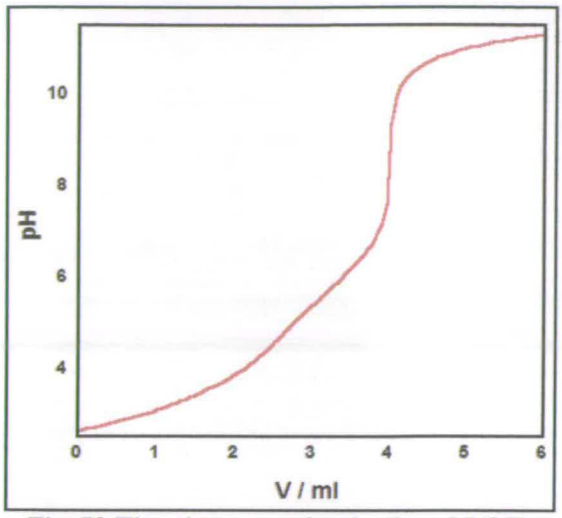

Fig. 72 Titration curve for the ligand LOH.

A diagram of species originating from the dissociation constants of $[H_4(LOH)]^{4+}$ is shown in Fig. 73. LOH behaves as a tetraprotic acid.

$$H_4LOH^{4+} \rightleftharpoons H_3LOH^{3+} + H^+ \qquad pK_{a1} = 3.15 \qquad \textbf{Eq.42}$$

$$H_3LOH^{3+} \rightleftharpoons H_2LOH^{2+} + H^+ \qquad pK_{a2} = 3.80 \qquad \textbf{Eq.43}$$

$$H_2LOH^{2+} \rightleftharpoons HLOH^{+} + H^+ \qquad pK_{a3} = 5.20 \qquad \textbf{Eq.44}$$

$$HLOH^{+} \rightleftharpoons LOH^{+} + H^+ \qquad pK_{a4} = 6.32 \qquad \textbf{Eq.45}$$

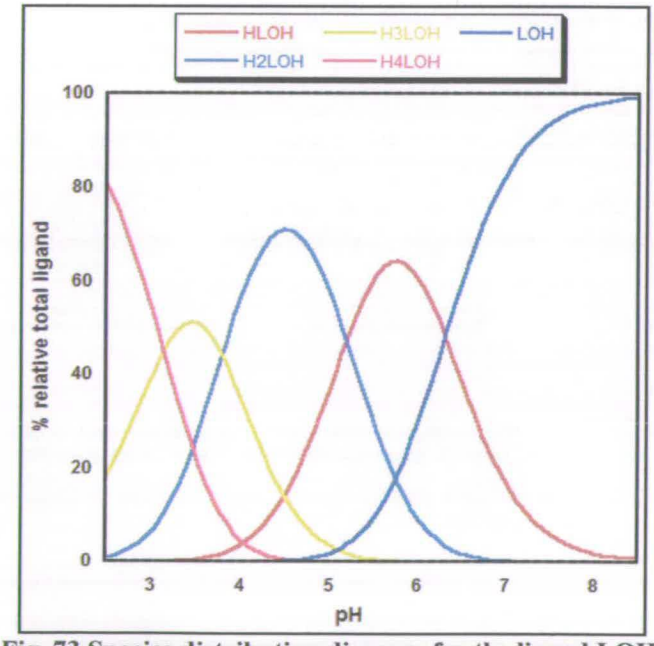

Fig. 73 Species distribution diagram for the ligand LOH.

The equilibria data associated with the complex formation reactions between Zn(II) and the ligand were collected employing two different titrations techniques. In one, the pH of the acidified solution in the titration vessel was measured after each small addition, V_{Zn}, of a titrating standardized solution of $Zn(NO_3)_2$ of composition: $T^M = C_M^0$ $Zn(NO_3)_2$, 0.1 M Et_4NClO_4. Upon addition of T^M, the pH of the titrated solution decreases due to complex formation and the titration is stopped when further addition of the titrant no longer produces appreciable pH changes. An example of data collected in this way is shown in Fig. 74, in which the measured pH is plotted as a function of the Zn(II) to ligand ratio, C_M/C_L.

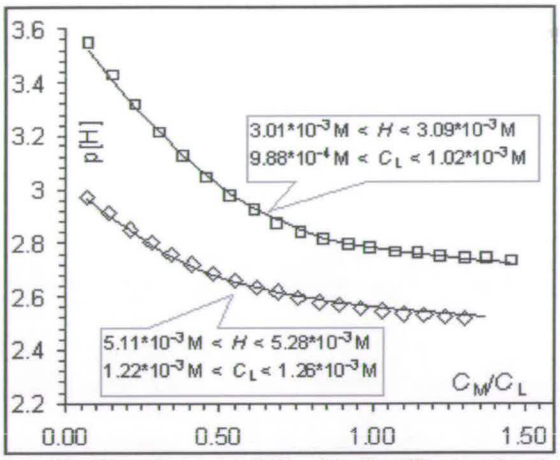

Fig. 74 pH variation during the titration of LOH with Zn(II) standard solutions. The full drawn lines have been calculated by assuming the formation of $[H(LOH)Zn]^{3+}$, $[(LOH)Zn]^{2+}$ and the formation constants given in Table 2.

In the other method, a known amount of the standardized solution of Zn(II), T^M, was added to an acidified solution of LOH. The resulting solution was then titrated alkalimetrically by adding small volumes of the Me_4NOH standard solution, T_B.

During this titration C_M/C_L is constant but the analytical excess of protons, H, defined as in Eq.46 decreases. Thus, it can be used as a convenient titration coordinate.

$$H = C_H - C_{OH} \qquad \textbf{Eq.46}$$

(C_H = analytical concentration of H^+, C_{OH} = analytical concentration of OH^-)

An example of this type of titration covering the range of C_M/C_L between 1 and 2 is shown in Fig. 75.

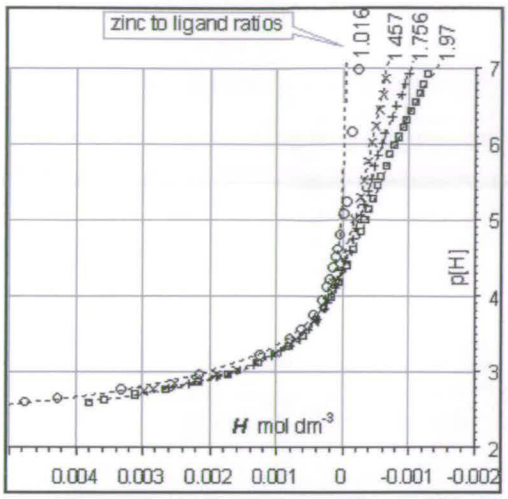

Fig. 75 Alkalimetric titration curves of solutions containing millimolar concentrations of Zn(II) and LOH in fixed ratios. The dashed curves have been calculated assuming the formation of $[H(LOH)Zn]^{3+}$, $[(LOH)Zn]^{2+}$ and $[H_{-1}(LOH)Zn]^{+}$ with the formation constants given in Table 2.

For the evaluation of the species present in solution using Hyperquad, the potential species were defined as having H^+, LOH and Zn^{2+} according to the reactions:

$$h\,H^+ + x\,LOH + z\,Zn^{2+} \rightleftharpoons H_h(LOH)_xZn_z^{(h+2z)+} \qquad \textbf{Eq.47}$$

in which *h*, *x* and *z* are integers to be found by fitting the experimental data. The species are indicated as the triplet (*h*, *x*, *z*), and their corresponding overall formation constant as β_{hxz}. The experimental points in Fig. 74 can be fitted and accurately reproduced by assuming that upon addition of Zn(II) two mononuclear complexes (1,1,1) and (0,1,1) ($[H(LOH)Zn]^{3+}$ and $[(LOH)Zn]^{2+}$) are formed.

The decrease in pH in the titration curve (Fig. 74) can be qualitatively explained and justified. Initially, the ligand is in its fully protonated form and upon addition of zinc, the formation of complexes releases protons and therefore results in a decrease of the pH. Moderate pH variations are observed up to a zinc-to-ligand ratio of around one. Any combination of the previously reported dinuclear species (0,1,2), (-1,1,2) and (-2,1,2)[105] produces large deviations between the calculated and observed pH. However, data collected during the alkalimetric titrations (Fig. 75) can only be

explained by assuming that in addition to the postulated mononuclear complexes ($[H(LOH)Zn]^{3+}$ and $[(LOH)Zn]^{2+}$), there are additional species being formed as the pH is increased during the titration. Treatment of the data with Hyperquad showed that proton deficient species have to be formed (see Fig. 75). These new species have been identified to be the dinuclear complexes $[H_{-1}(LOH)Zn_2]^{3+}$ (-1,1,2) and $[H_{-2}(LOH)Zn_2]^{2+}$ (-2,1,2).

Finally, the dashed curves in Fig. 75 have been calculated by assuming the four species (1,1,1), (0,1,1), (-1,1,2) and (-2,1,2) with the formation constants given in Table 3. The dinuclear complex $[(LOH)Zn_2]^{4+}$ (0,1,2) reported by Kinoshita *et al.*[105] was incompatible with the data collected during this work.

Table 3 - Complex formation constants between the ligand LOH and Zn(II)

H	LOH	Zn	log β (this work)[106]	log β (Ref.105)
1	1	1	14.33 ± 0.06	*not detected*
0	1	1	11.16 ± 0.06	*not detected*
0	1	2	*not detected*	14.9
-1	1	2	9.2 ± 0.1	9.6
-2	1	2	2.3 ± 0.1	2.9

The equilibrium constants determined and the different mechanism proposed here have dramatic consequences on the relative concentrations of the complexes present in water solutions containing millimolar concentrations of Zn(II) and 1,3-bis[bis(pyridin-2-ylmethyl)amino] propan-2-ol at different metal-to-ligand ratios (Fig.76a and 76b). In contrast, in the model proposed by Kinoshita *et al.* based on the existence of only dinuclear complexes (Fig.76c and 76d) the relative concentrations are practically dependent only on the pH and insensitive to the metal:ligand ratio.

The elucidation of this new mechanism involving mononuclear complexes is important because it suggests that the behaviour of mixtures of Zn(II) ions and LOH is likely to be quite different depending on the metal:ligand ratio present in solution. This should prove to be significant in elucidating the contribution of a second metal towards enhancing phosphate binding and hydrolysis (see Chapter 5), as this work shows that it is possible to find conditions under which only mono or only dinuclear complexes are present.

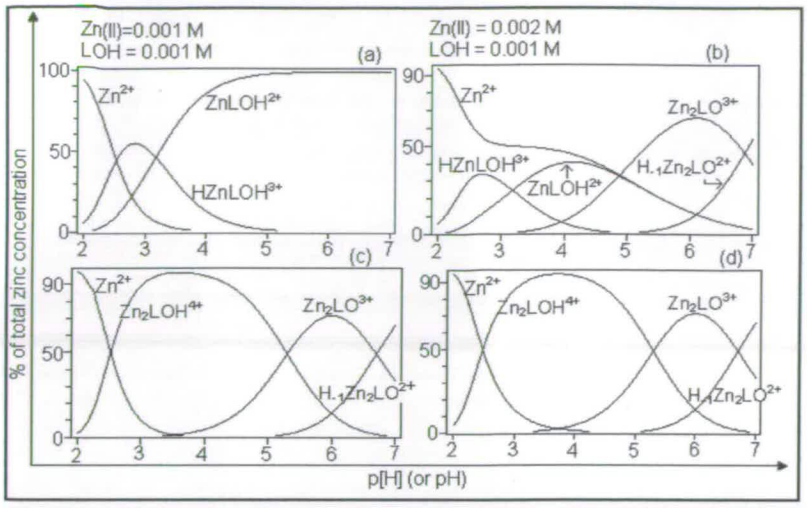

Fig.76 Distribution diagrams of Zn(II)-LOH complexes: (a) and (b) using the mechanism determined in this work and (c) and (d) the mechanism published in Ref. 105.

It should also help to interpret correctly and more accurately phosphate binding and hydrolysis data (see Chapter 5). According to the presented model the phosphate capture complex $[H_{-1}(LOH)Zn_2]^{3+}$ is not formed when the metal:ligand ratio is 1:1, but both mechanisms agree quite well in terms of predicting the prevalence of $[H_{-1}(LOH)Zn_2]^{3+}$ in slightly acidic solutions with a metal:ligand ratio of 2:1. This work shows the value of investigating metal complexation reactions using different metal:ligand ratios.

4.2.1.2 L^1OH.

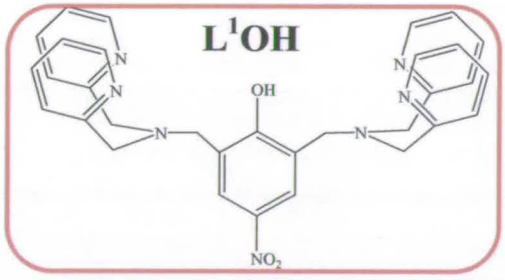

Fig. 77 *N,N,N',N'*-tetrakis[(2-pyridyl)methyl]-2,6-diamino-*p*-nitrophenol.

The protonation constant of the ligand *N,N,N',N'*-tetrakis[(2-pyridyl)methyl]-2,6-diamino-*p*-nitrophenol (L^1OH, Fig. 77) and the complex formation equilibria in the presence of Zn(II) was studied at 25°C in water with 0.1 M $KClO_4$ as the electrolyte. Several titrations were performed, and in each case, the data were collected only up to pH ≤ 8 due to the appearance of a precipitate at pH ≥ 8. The

ligand has six protonation sites but only four protonation constants were detected by fitting the *emf* data with the Hyperquad software. Since the data fit with four protonation constants was satisfactory and the error statistically acceptable (Fig. 78), the addition of further protonation constants would have been not justifiable.

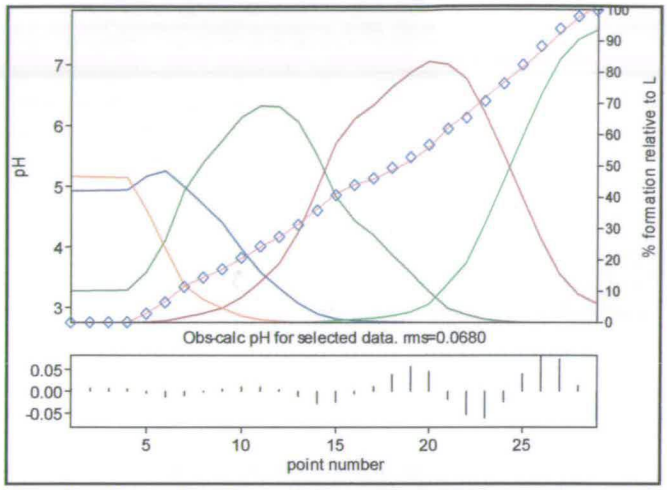

Fig. 78 Data fitting for the estimation of the protonation constants of the ligand L[1]OH using the software Hyperquad. [107]

The protonation constants found for L[1]OH are reported in Table 4. The pK_a values are very similar to those determined for LOH which has an alcohol bridging unit. Thus, the different bridging unit (nitrophenol group) does not seem to affect the basicity of the ligand. Also in this case, the ligand behaves as a tetraprotic acid and at neutral pH is present in its neutral form.

Table 4 - Protonation constants for the ligand L[1]OH

H	L[1]OH	log β	pK_a
1	1	6.79 ± 0.01	2.80
2	1	11.51 ± 0.02	3.37
3	1	14.88 ± 0.03	4.72
4	1	17.68 ± 0.05	6.79

The diagram showing the relative percentage of the different protonated species is reported in Fig. 79. This was originated using the software Hyss.[108]

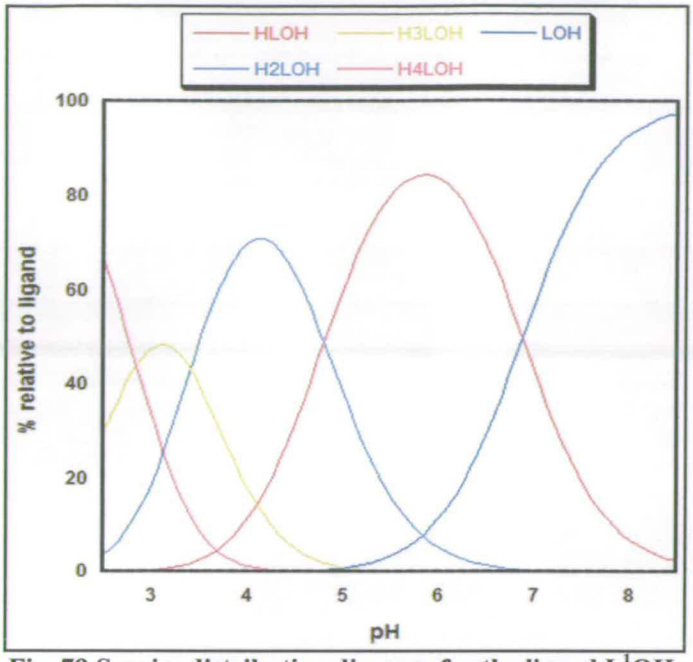

Fig. 79 Species distribution diagram for the ligand L^1OH.

$$[H_4(L^1OH)]^{4+} \overset{pK_{a1}}{\rightleftharpoons} [H_3(L^1OH)]^{3+} \overset{pK_{a2}}{\rightleftharpoons} [H_2(L^1OH)]^{2+} \overset{pK_{a3}}{\rightleftharpoons} [H(L^1OH)]^{+} \overset{pK_{a4}}{\rightleftharpoons} (L^1OH)$$

The next step was to determine the complex formation constants between L^1OH and Zn(II) ions. For this, at the end of the pH titration of the ligand, the alkaline solution was acidified with a calculated amount of standardized 0.1 M $HClO_4$ and brought back to pH around 2.5. Then, the desired stoichiometric amount (1 or 2 equivalents) of $Zn(NO_3)_2$ (solid) was added to the solution and titrated alkalimetrically with the standardized 0.1 M NaOH up to pH ≈ 8 (at this pH a copious amount of a white precipitate started to appear).

The most obvious starting point in the data processing was to fit the experimental data assuming that when the metal:ligand ratio is 2:1, only dinuclear species are formed. This was unsuccessful and data fitting with only dinuclear complexes was ruled out by the program Hyperquad. In order to obtain a good fit, it was necessary to take into account the formation of mononuclear complexes. The best fit was obtained assuming the formation of two mononuclear, (1,1,1) and (0,1,1), and two dinuclear complexes (-1,1,2) and (-2,1,2) (Fig. 80). The overall β constants for such complexes are reported in Table 5.

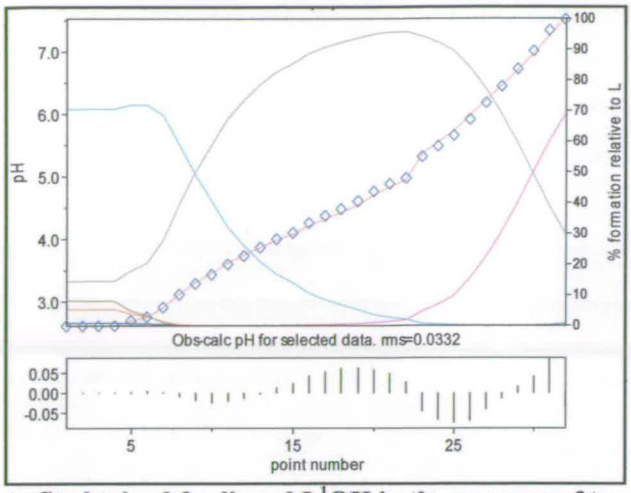

Fig. 80 Hyperquad data fit obtained for ligand L^1OH in the presence of two equivalents of Zn(II) assuming the mechanism of complex formation reported in Table 5.

Table 5 - Complex formation constants between Zn(II) and L^1OH.			
H	L^1OH	Zn	log β
1	1	1	13.8 ± 0.1
0	1	1	10.5 ± 0.1
-1	1	2	7.07 ± 0.1
-2	1	2	-2.42 ± exc*

(*the error on this constant cannot be estimated due to the small number of experimental data points)

The species distribution diagram obtained in the presence of two equivalents of Zn(II) ions (Fig. 82) assuming the equilibrium reactions of Fig. 81 indicates that the dinucleating ligand L^1OH forms both mono and dinuclear complexes in water solution.

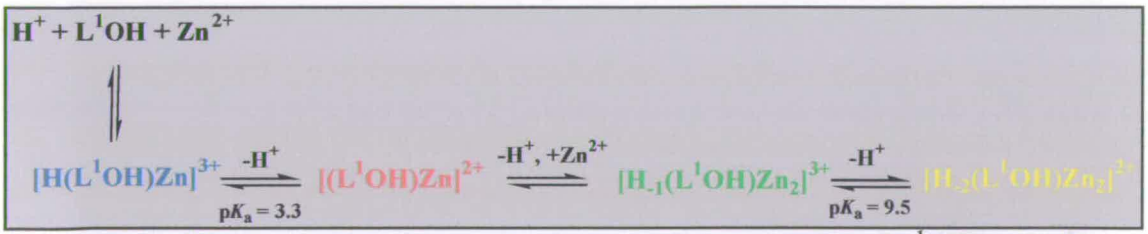

Fig. 81 Equilibrium reactions for complex formation between the ligand L^1OH and Zn(II).

The species distribution curves show that at the beginning of the titration (pH = 2.5) in the presence of two equivalents of Zn(II) ions only a mononuclear complex is present (complex represented with the triplet 1,1,1). This protonated complex, $[H(L^1OH)Zn]^{3+}$ loses a proton at pH ≈ 3.5 (pK_a = 3.3) to afford a doubly positively-

charged mononuclear complex which has maximum abundance at pH = 5. Beyond this pH, it loses a proton allowing the coordination of the second metal ion.

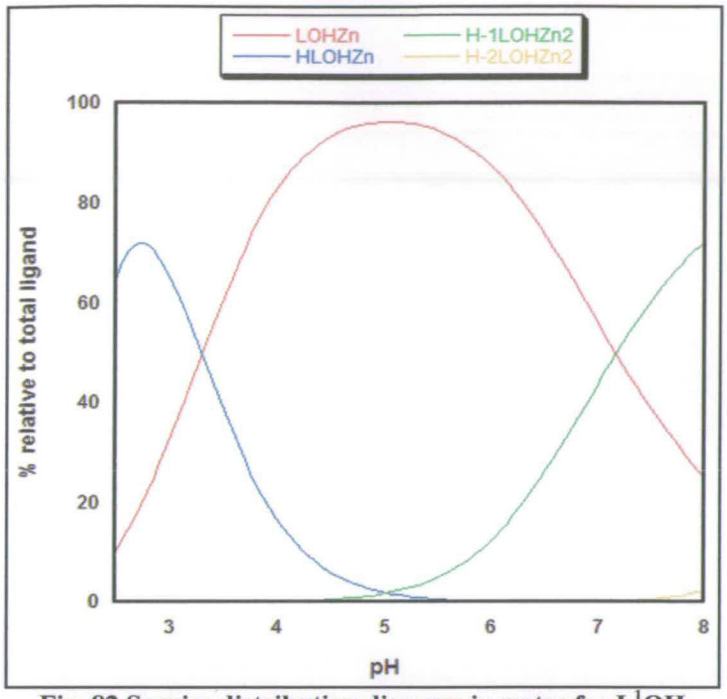

Fig. 82 Species distribution diagram in water for L^1OH in the presence of 2 equivalents of Zn(II).

Further deprotonation at higher pH (pH ≥ 9) cannot be excluded but it could not be estimated accurately due to the appearance of a precipitate. When the metal:ligand ratio goes down to 1 the distribution of the species changes, and only mononuclear complexes are present (Fig. 83). The complex $[(L^1OH)Zn]^{2+}$ is readily formed and remains the predominant complex in solution above pH = 3.5. From these results, it is evident that a proton competes with the metal for the second binding site. Unfortunately the formation of this mononuclear complex has not been confirmed in the solid state due to the impossibility of obtaining crystals suitable for X-ray diffraction studies. However similar ligand structures have been reported to form a large range of asymmetrical complexes.[109] In particular, a mononuclear complex between vanadium and the ligand 2,6-bis[bis-(2-pyridylmethyl)aminomethyl]-4-terbutylphenol (bpbp) has been characterized by X-ray diffraction (Fig. 84).[110]

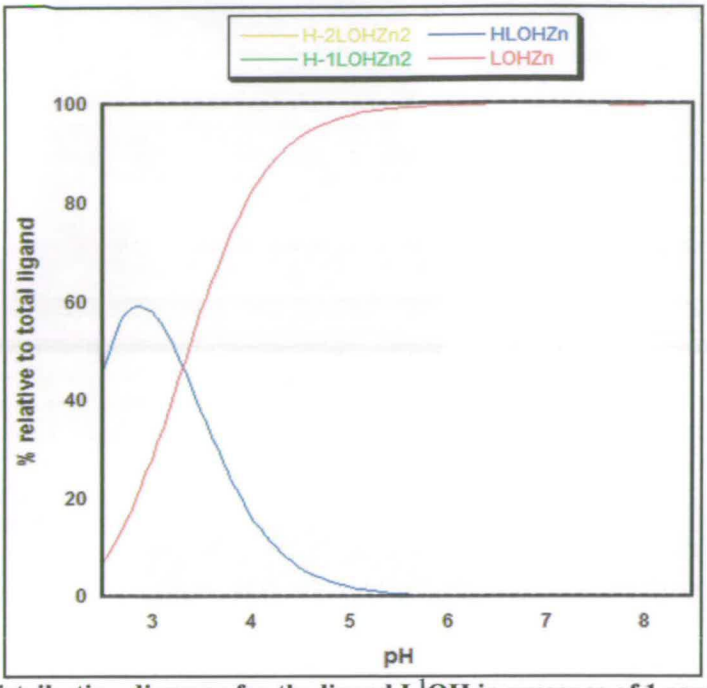

Fig. 83 Species distribution diagram for the ligand L^1OH in presence of 1 equivalent of Zn(II).

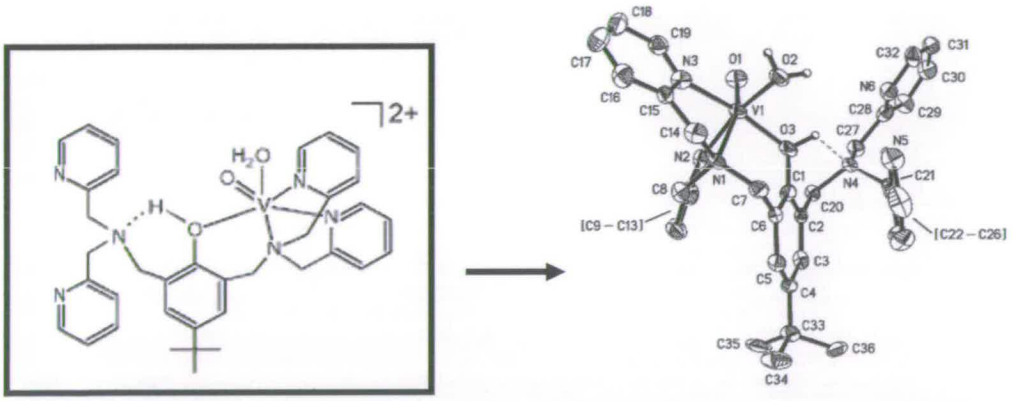

Fig. 84 Schematic representation of the $[bpbp(VOCl)_2]^{2+}$ complex (left) and its X-ray crystal structure (right).[110]

In this complex, the phenol oxygen atom remains protonated and is involved in an intramolecular hydrogen bond (2.37 Å) with the tertiary amine N atom. This means that the second binding unit is occupied by a proton which prevents coordination of a second metal ion. A similar explanation could be applied to the ligand L^1OH in solution.

4.2.1.3 L^1OH'.

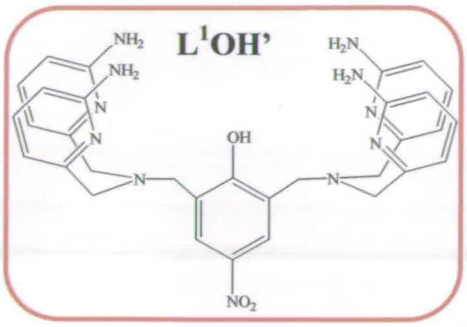

Fig. 85 *N,N,N',N'*-tetrakis[(6-amino-2-pyridyl)methyl]-2,6-diamino-*p*-nitrophenol.

The dissociation constants of L^1OH' (Fig. 85), the stoichiometry of its Zn(II) complexes and complexation constants were also determined in aqueous solution. The potentiometric pH titrations were carried out under nitrogen atmosphere at 25°C and the ionic strength of the solution adjusted to 0.1 M with $KClO_4$. A standardized solution of $HClO_4$ 0.1M was added at the beginning of the titration in order to protonate the ligand and incremental small additions of standard NaOH 0.1 M produce the titration curve (Fig. 86) from which the pK_a values can be calculated.

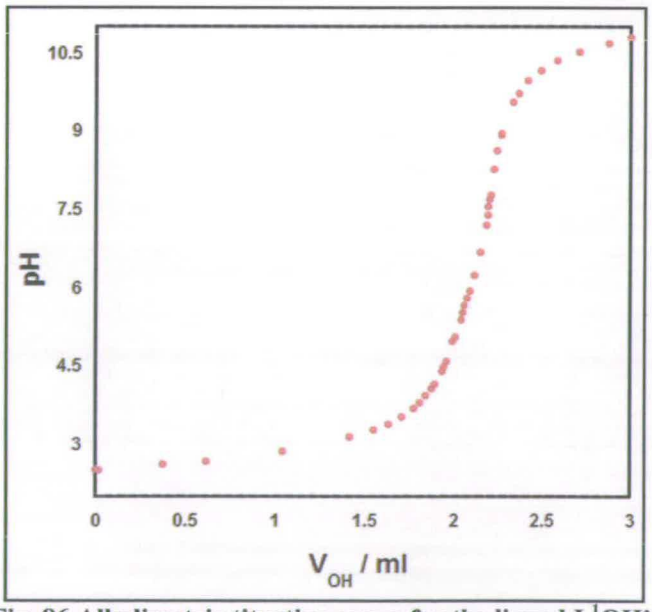

Fig. 86 Alkalimetric titration curve for the ligand L^1OH'.

The calculated protonation constants of the ligand are listed in Table 6. According to these values, in very acidic solutions L^1OH' binds up to five protons that

are then dissociated on average every two pH units (see species distribution diagram in Fig. 87).

Table 6 - Protonation constants for the ligand L^1OH'

H	LOH'	log β	pK_a
1	1	11.42 ± 0.07	2.74
2	1	21.07 ± 0.06	4.69
3	1	27.63 ± 0.06	6.56
4	1	32.32 ± 0.06	9.65
5	1	35.06 ± 0.06	11.42

The stoichiometry of the complexes formed in the presence of Zn(II) ions and their formation constants were evaluated by carrying out several alkalimetric titrations with L:M ratios in the range 1:1 to 1:2.

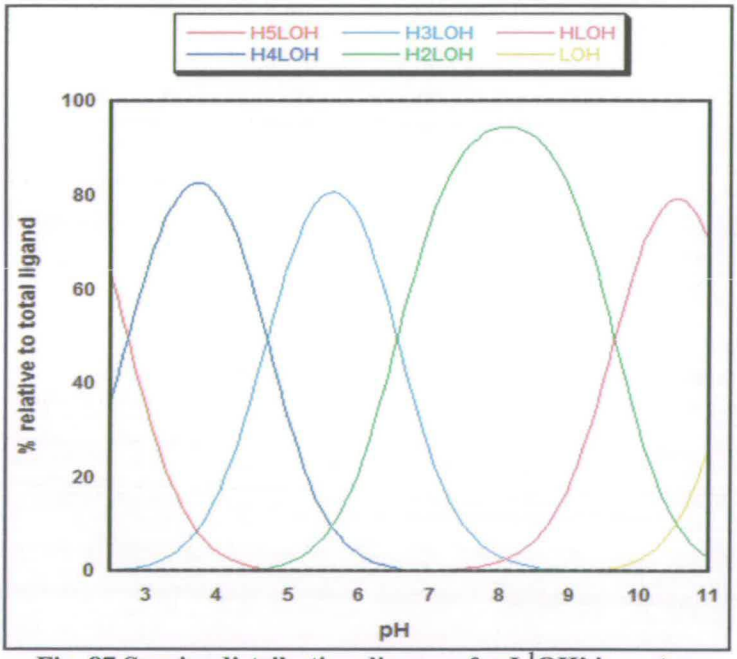

Fig. 87 Species distribution diagram for L^1OH' in water.

Despite the potential dinucleating nature of the ligand, and based on the results presented above for structurally similar ligands, both mono and dinuclear species could in principle be formed in solution. The formation of mononuclear complexes was investigated first, as knowing their nature and stability is essential to subsequently obtain the formation constants of the dinuclear complex. The experiments in the presence of Zn(II) ions were carried out under identical conditions to those used in the

determination of protonation constants of the ligand. The only difference was that in this case, the pH range explored was limited by the precipitation of zinc hydroxide at pH ≥ 8.5. The refinement of 240 experimental data points with Hyperquad allowed us to get a model for complex formation, the corresponding β constants and the pK_as for the protonated species and coordinated water molecules. The experimental data can be fully explained by assuming the following equilibrium reactions and β values:

$$2\,H^+ + L^1OH' + Zn^{2+} \rightleftharpoons [H_2(L^1OH')Zn]^{4+} \qquad \log\beta_{211} = 27.96 \pm 0.05 \qquad \textbf{Eq.48}$$

$$H^+ + L^1OH' + Zn^{2+} \rightleftharpoons [H(L^1OH')Zn]^{3+} \qquad \log\beta_{111} = 23.40 \pm 0.04 \qquad \textbf{Eq.49}$$

$$L^1OH' + Zn^{2+} \rightleftharpoons [(L^1OH')Zn]^{2+} \qquad \log\beta_{011} = 16.07 \pm 0.08 \qquad \textbf{Eq.50}$$

$$L^1OH' + 2\,Zn^{2+} \rightleftharpoons [H_{-1}(L^1OH')Zn_2]^{3+} + H^+ \qquad \log\beta_{-112} = 12.5 \pm 0.1 \qquad \textbf{Eq.51}$$

$$L^1OH' + 2\,Zn^{2+} \rightleftharpoons [H_{-2}(L^1OH')Zn_2]^{2+} + 2H^+ \qquad \log\beta_{-212} = 5.14 \pm 0.08 \qquad \textbf{Eq.52}$$

These results are the averages of three independent pairs of titration curves with L/M=1 and L/M=2. The species distribution curves for the systems (H^+ / L^1OH' / 1 Zn^{2+}) and (H^+ / L^1OH' / 2 Zn^{2+}) are shown in Fig. 88 and Fig. 89 respectively.

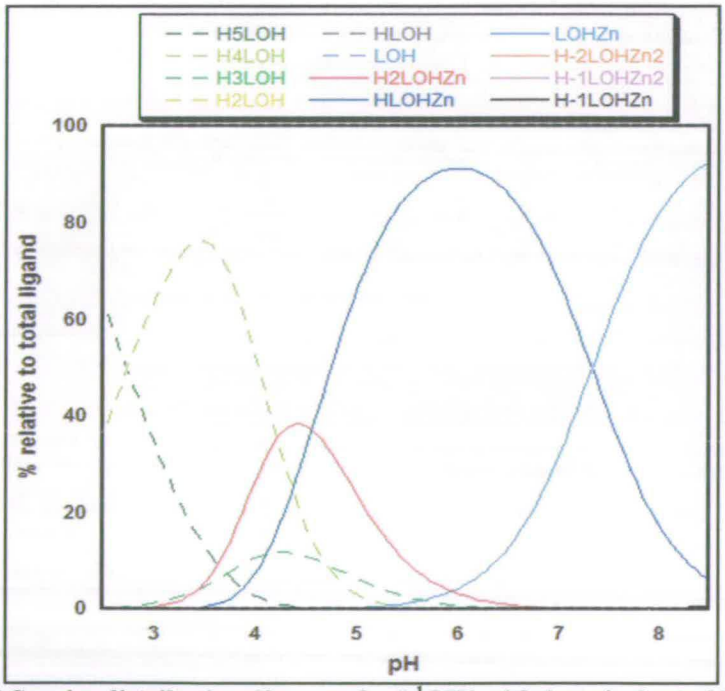

Fig. 88 Species distribution diagram for L^1OH' with 1 equivalent of Zn(II).

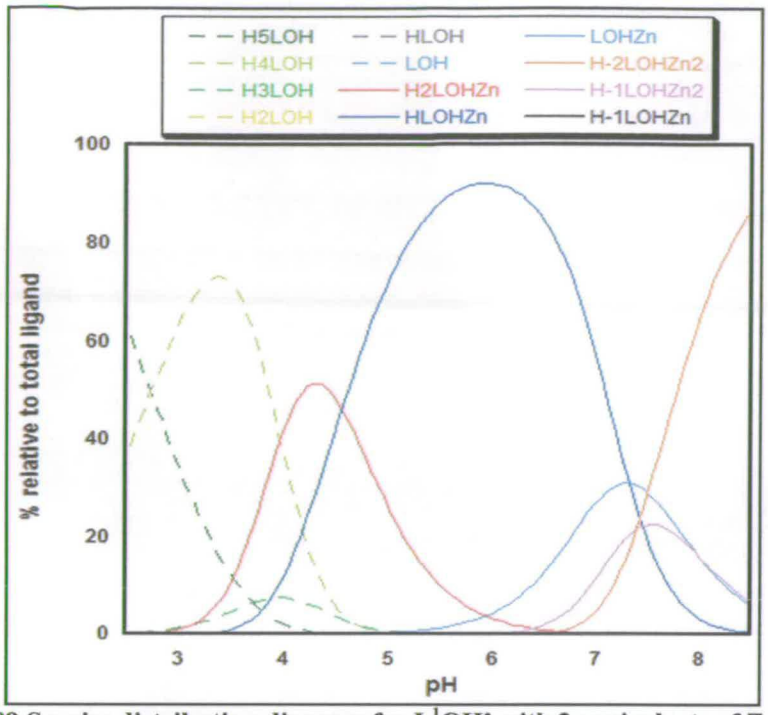

Fig. 89 Species distribution diagram for L[1]OH' with 2 equivalents of Zn(II).

They illustrate clearly the succession of complexes formed by this ligand with Zn(II) ions over the entire pH range investigated.

From a first analysis of such diagrams one aspect is immediately evident; the binding ability of the L[1]OH' towards Zn(II) is rather weak since more than 70% of a protonated form of the ligand remains present up to pH 3.5 for both L:M ratios (dashed curves in Fig. 88 and Fig. 89).

Another peculiarity of this ligand worth noting is that the speciation in solution is identical up to pH 6 in both cases (*i.e.* it makes no difference if one or two equivalents of zinc are added to the solution). Only complexes with a 1:1 stoichiometry are formed in the range pH between 3 and 6.5 and no dinuclear complexes are present when only one equivalent of zinc is added to the solution. The speciation model found was confirmed by refining the titration curves of M/L=1 and M/L=2 together. The fit was very good (Fig. 90). According to the species distribution diagrams a protonated mononuclear complex begins to form at pH 4.5. This remains as the main complex in solution up to pH 7 and reaches its maximum concentration (90%) at a pH near to 6 (Fig. 88).

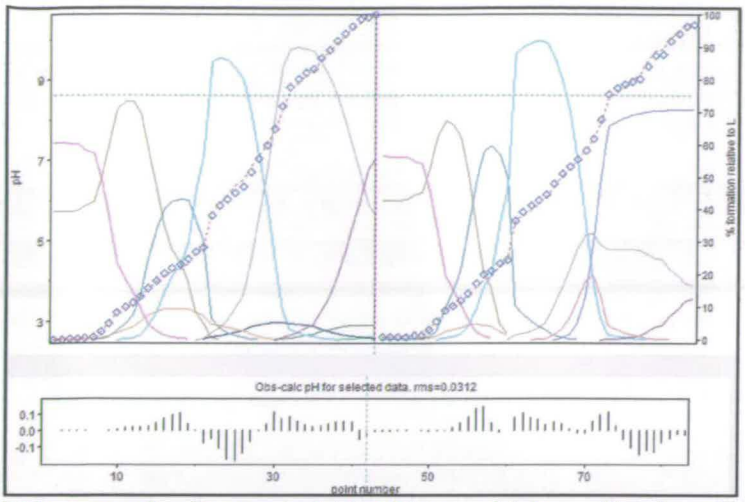

Fig. 90 Hyperquad refinement obtained by combining a titration of L^1OH' with one (left) and two equivalents of Zn(II) (right).

The formation of mononuclear complexes implies a simultaneous release of two protons in a single step according to the mechanism reported in Fig. 91.

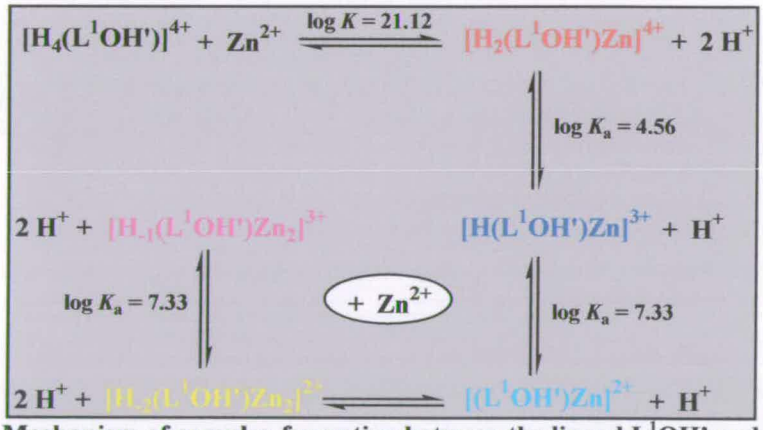

Fig. 91 Mechanism of complex formation between the ligand L^1OH' and Zn(II).

In conclusion, these potentiometric studies suggest that the ligand L^1OH' forms mainly mononuclear complexes. Dinuclear complexes are present only in solutions in which the metal:ligand ratio is at least 2:1 and the pH ≥ 7.

Fig. 92 clearly illustrates the effect of adding a second equivalent of Zn(II) ions to a solution containing a 1:1 mixture of L^1OH' and Zn(II) ions in terms of the complexes present.

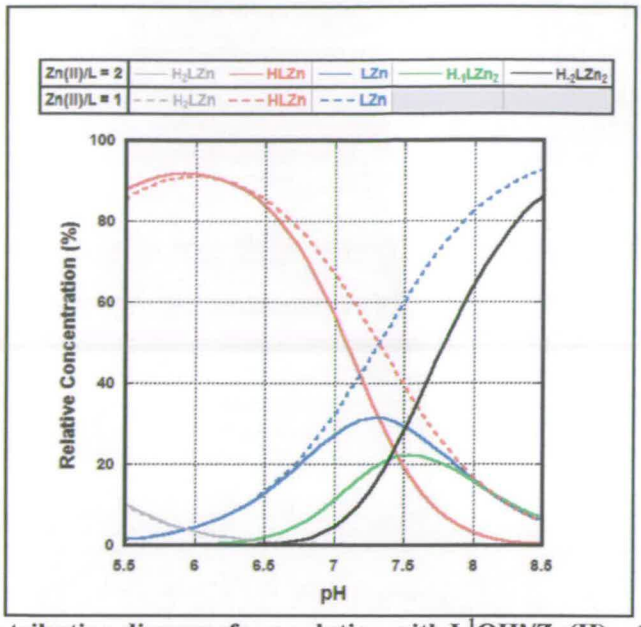

Fig. 92 Species distribution diagram for a solution with L^1OH'/Zn(II) = 1 (dashed curves) and Zn(II)/L^1OH' = 2 (full curves).

4.2.3 Potentiometric titrations in DMSO-H_2O (67%-33%).

4.2.3.1 LOH'

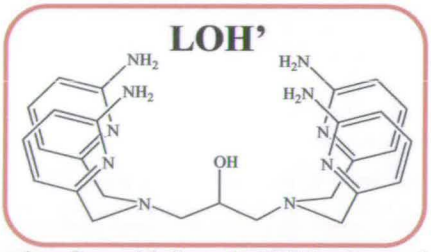

Fig. 93 *N,N,N',N'*-tetrakis[(6-amino-2-pyridyl)methyl]-2-hydroxy-1,3-diamino-propane (LOH').

The protonation constants and zinc complexation constants of LOH' were studied in DMSO:H_2O (67%:33%). The reason and benefits of this solvent choice have been outlined in the introduction of this chapter. The ionic strength of this solvent was kept constant by adding 0.1 M Et_4NClO_4, and the liquid junction between the test solution and the aqueous internal solution of the glass electrode was made by using the intermediate (bridge) solution:

67% DMSO – 33% H_2O – 0.1M $(CH_3)_4NNO_3$

The methodology and titration mode used were identical to that exployed in pure water with the only difference being that all of the solutions ($HClO_4$, $(CH_3)_4NOH$ and

$Zn(NO_3)_2$) were now prepared in the DMSO:H_2O (67%:33%) solvent mixture. The choice of Et_4NClO_4 as electrolyte was an attempt to eliminate the sodium error of the glass electrode in very alkaline solutions. However, also in this case the potential of the glass electrode drifted toward acidic pHs when the measured pH was > 9. As a result, the ionic product of water in this solvent mixture could not be accurately evaluated. The value used during the calculations was pK_w = 16.8, which is only approximate but consistent with the values used in the literature.[111] In any case this has no consequence on the evaluation of the data in the pH range of interest, where the [OH^-] is negligible. In order to determine accurately the acidity constants of the ligand, three titrations were performed using different concentrations of LOH'.

In this solvent mixture LOH' behaves as a tetraprotic acid. The best fit of the titration curves (fitted against the data from all the different titrations) was obtained with the values given in Table 7.

Table 7 - Protonation constants for the ligand LOH'

H	LOH'	log β	pK_a
1	1	6.79 ± 0.01	3.68
2	1	12.37 ± 0.04	4.38
3	1	16.75 ± 0.05	5.58
4	1	20.43 ± 0.05	6.79

The species distribution diagram (Fig. 94) shows that the deprotonation of H_4(LOH') is completed at pH ≥ 7. As previously, the complex formation in the system H^+: LOH' : Zn^{2+} is considered to take place according to the reaction:

$$h\,H^+ + x\,LOH' + z\,Zn^{2+} \rightleftharpoons H_h(LOH')Zn_z \qquad \textbf{Eq.53}$$

and the corresponding overall formation constants indicated as β_{hxz}.

Solutions with variable concentrations of Zn(II) and LOH' were investigated and the experiments were performed in the two different ways previously described.

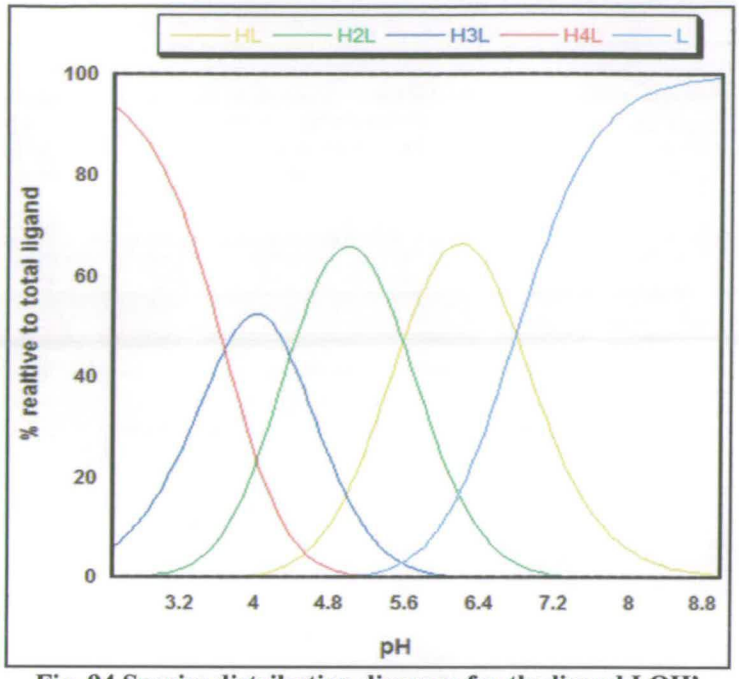

Fig. 94 Species distribution diagram for the ligand LOH' in the solvent mixture DMSO:H_2O (67%:33%).

Titration of an acidic solution of the ligand with a standardized zinc solution results in a decrease in the measured pH, denoting complex formation (Fig. 95).

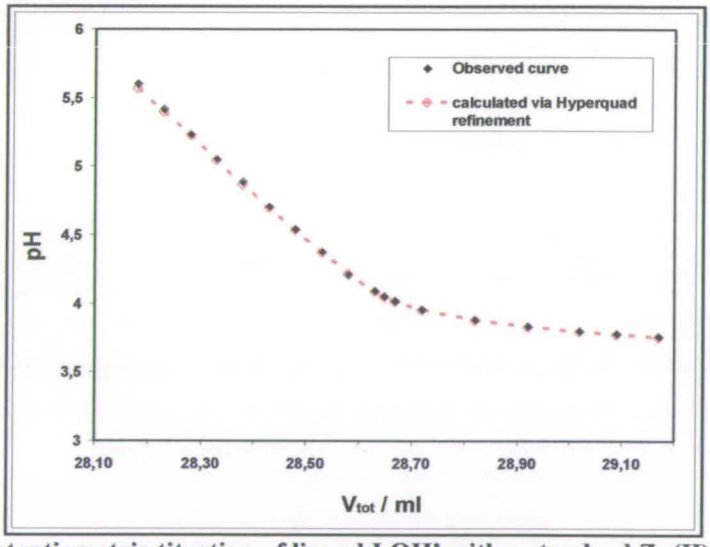

Fig. 95 Potentiometric titration of ligand LOH' with a standard Zn(II) solution.

The observed curve can be perfectly reproduced by assuming a set of mononuclear and dinuclear complexes.

To come up with a proper model, however, several alkalimetric titrations with $1 \leq$ Zn(II)/LOH'≤ 2 were performed and analyzed. This titration was useful to deduce that

possibly several mononuclear species are formed between zinc and LOH', but the composition of these mononuclear species, and their formation constants was fully elucidated only after performing titrations of solutions containing equal concentration of zinc and LOH' (M:L = 1:1).

A titration curve of this type is shown in Fig. 96 and the experimental data can be accurately reproduced by assuming only mononuclear species (dinuclear complexes can be neglected). The concentration of dinuclear species in these conditions is very low and their presence and formation constants must be determined in a different experiment in which the metal:ligand ratio is increased to 2:1. Three different alkalimetric titrations of this type were performed and analyzed.

The shape of the titration curve in Fig. 97 unambiguously shows that at this ratio additional species are formed denoted by the shoulder between pH 4 and 5 that was previously absent (see Fig. 96).

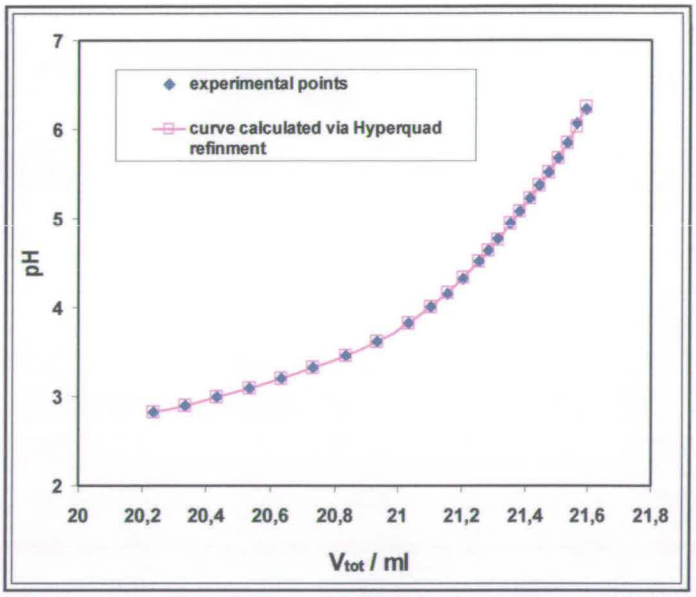

Fig. 96 Alkalimetric titration of a solution of LOH' in the presence of 1 equivalent of Zn(II).

The Hyperquad refinement and fit of three titrations with $1 \leq Zn(II)/LOH' \leq 2$ is shown in Fig. 98.

The results are excellent (σ = 1.2) and a valid model for the formation of complexes between Zn(II) and LOH' can be defined using the following reactions and formation constants (charges are omitted for simplicity):

$$2\,H^+ + LOH' + Zn^{2+} \rightleftharpoons H_2(LOH')Zn \qquad \log\beta_{211} = 17.79 \qquad \textbf{Eq.54}$$

$$H^+ + LOH' + Zn^{2+} \rightleftharpoons H(LOH')Zn \qquad \log\beta_{111} = 14.14 \qquad \textbf{Eq.55}$$

$$LOH' + Zn^{2+} \rightleftharpoons (LOH')Zn \qquad \log\beta_{011} = 9.24 \qquad \textbf{Eq.56}$$

$$LOH' + Zn^{2+} \rightleftharpoons H_{-1}(LOH')Zn + H^+ \qquad \log\beta_{-111} = 2.64 \qquad \textbf{Eq.57}$$

$$LOH' + 2\,Zn^{2+} \rightleftharpoons (LOH')Zn_2 \qquad \log\beta_{011} = 13.0 \qquad \textbf{Eq.58}$$

$$LOH' + 2\,Zn^{2+} \rightleftharpoons H_{-1}(LOH')Zn_2 + H^+ \qquad \log\beta_{-111} = 8.01 \qquad \textbf{Eq.59}$$

$$LOH' + 2\,Zn^{2+} \rightleftharpoons H_{-2}(LOH')Zn_2 + 2\,H^+ \qquad \log\beta_{-211} = 4.31 \qquad \textbf{Eq.60}$$

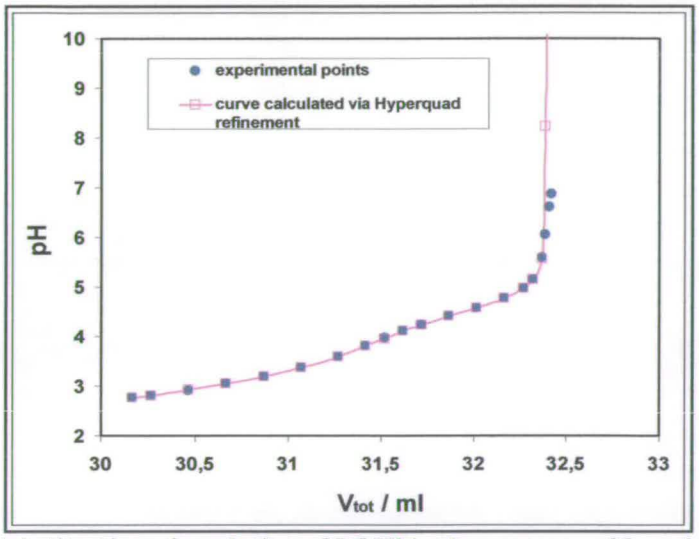

Fig. 97 Alkalimetric titration of a solution of LOH' in the presence of 2 equivalents of Zn(II).

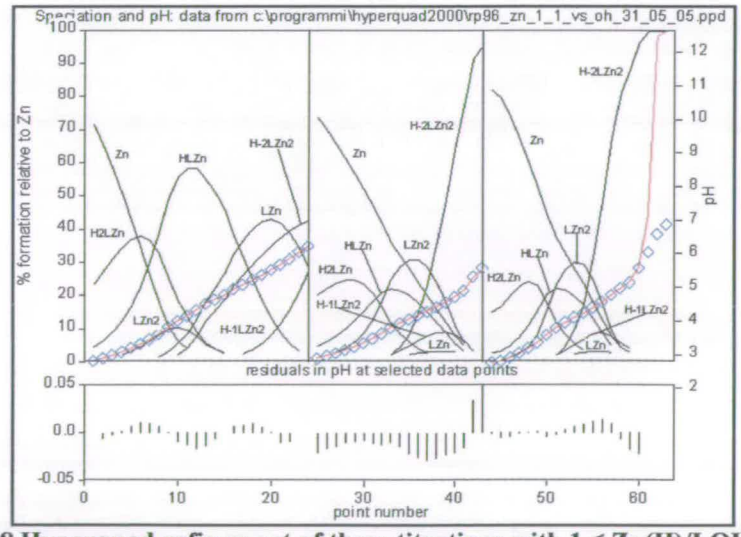

Fig. 98 Hyperquad refinement of three titrations with 1 ≤ Zn(II)/LOH'≤ 2.

The species distribution diagrams in the presence of one and two equivalents of Zn(II) ions generated by using this model are shown in Fig. 99 and Fig. 100 respectively.

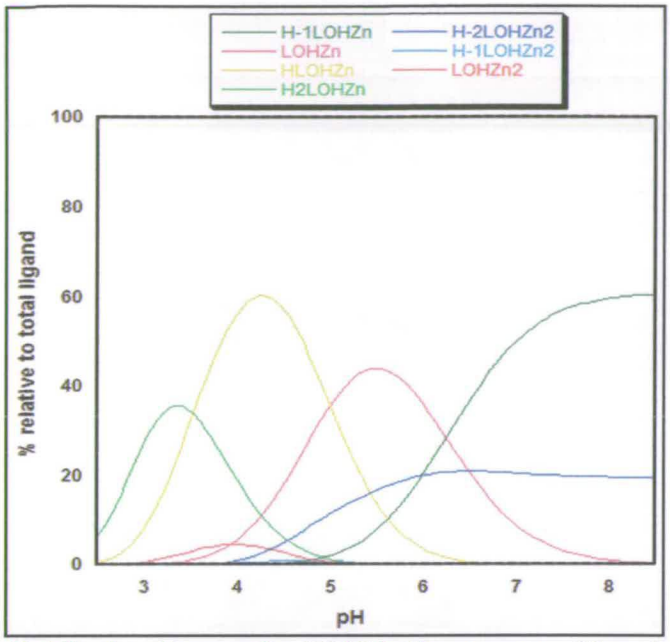

Fig. 99 Species distribution diagram for LOH' in the presence of 1 equivalent of Zn(II) in DMSO:H_2O (67%-33%).

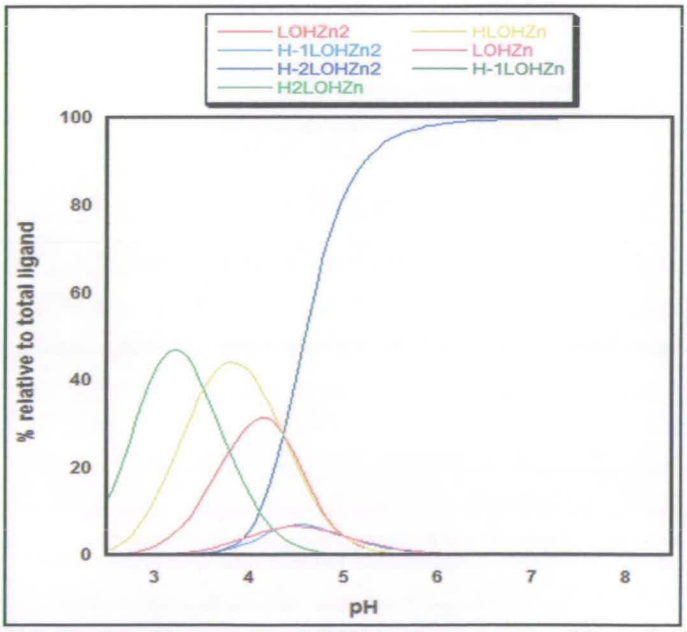

Fig. 100 Species distribution diagram for LOH' in the presence of 2 equivalents of Zn(II) in DMSO:H_2O (67%-33%).

The determination of the stability constants for the complexes and the corresponding plots showing the species present, allowed us to predict and select the best conditions (pH, concentration and M:L ratio) to obtain a complex with desired stoichiometry.

In this solvent mixture and in the presence of Zn(II) ions, the ligand LOH' forms both mono and dinuclear zinc complexes. Changing the number of zinc equivalents and pH affects the percentage of the different species. At M:L ratio of 1, a mononuclear complex is fully formed at pH ≈ 3 (Fig. 99). As the pH increases during the titration, this protonated mononuclear complex $[H_2(LOH')Zn]^{4+}$ progressively releases protons up to a total of three. Above neutral pH, and for the rest of the pH range investigated, $[H_{-1}(LOH')Zn]^{+}$ reaches maximum concentration and it is the main complex in solution. At this M:L ratio, dinuclear complexes are also formed but their relative concentration over all the pH range is only very minor. Increasing the number of equivalents of zinc from 1 to 2, does change the distribution of the species in solution but it is not sufficient to form exclusively dinuclear complexes.

In fact from the diagram in Fig. 100 it is clear that a pH of about 4.5 is necessary to form dinuclear complexes as the main species. At pH ≤ 4, although dinuclear species are formed they coexist with a significant amount of mononuclear complexes.

Finally, above pH 5 the only complex present in solution is the dinuclear complex $[H_{-2}(LOH')Zn_2]^{2+}$ (reaches 100% concentration at pH 6.5) which is presumably generated by deprotonation of a bound water molecule (Fig. 101).

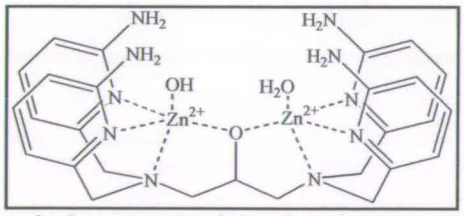

Fig. 101 Plausible chemical structure of the dinuclear complex $[H_{-2}(LOH')Zn_2]^{2+}$.

A further deprotonation of another bound water molecule was not observed in the pH range investigated, but it cannot be excluded in more alkaline solutions. The pK_a of the water bound molecule observed in this solvent mixture is therefore very low (pK_a =

3.7) probably due to the interaction with the amino hydrogen bonds and with two metal centers, and the higher basicity of DMSO compared to water.

To assess the validity of comparing the behaviour of complexes of this ligand in water and in DMSO:H_2O (67%-33%), the ligand protonation and complex formation constants for LOH (well-characterized in water) were investigated in this solvent mixture and the results compared with those obtained in 100% water (Section 4.2.1.1).

4.3.2.2 LOH.

The ligand protonation constants were determined by carrying out three titrations at different ligand concentrations. The refinement of the *emf* data with Hyperquad gave three protonation constants (Eq.61-63).

$$LOH + H^+ \rightleftharpoons [H(LOH)]^+ \qquad \log \beta_{11} = 5.16 \pm 0.05 \qquad \textbf{Eq.61}$$

$$LOH + 2\,H^+ \rightleftharpoons [H_2(LOH)]^{2+} \qquad \log \beta_{12} = 8.81 \pm 0.05 \qquad \textbf{Eq.62}$$

$$LOH + 3\,H^+ \rightleftharpoons [H_3(LOH)]^{3+} \qquad \log \beta_{13} = 10.79 \pm 0.05 \qquad \textbf{Eq.63}$$

LOH appears to be a strong triprotic acid in this solvent (Eq.64).

$$pK_{a1} = 1.98;\ pK_{a2} = 3.65;\ pK_{a3} = 5.16. \qquad \textbf{Eq.64}$$

Its first deprotonation has already started at pH ≈ 2 and above pH 5.5 it is present only in its fully deprotonated form (Fig. 102).

The formation of complexes in the presence of Zn(II) ions was carried out as previously described. During the titration of the ligand with the standardized zinc solution, the addition of Zn(II) ions produces the expected decrease of the pH denoting complex formation (Fig. 103). The pH decreases regularly until a zinc-to-ligand ratio of about 1. Further addition of zinc does not produce any further pH changes.

The fit obtained with Hyperquad is satisfactory assuming that only mononuclear species are present.

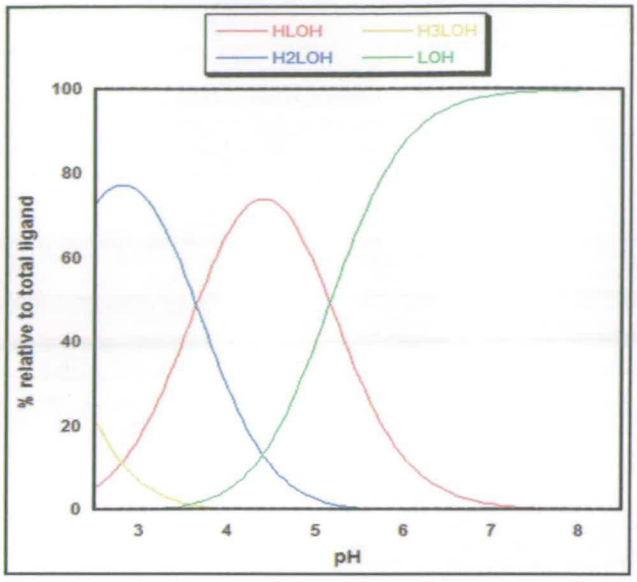

Fig. 102 Species distribution diagram for LOH in DMSO:H_2O (66%-37%).

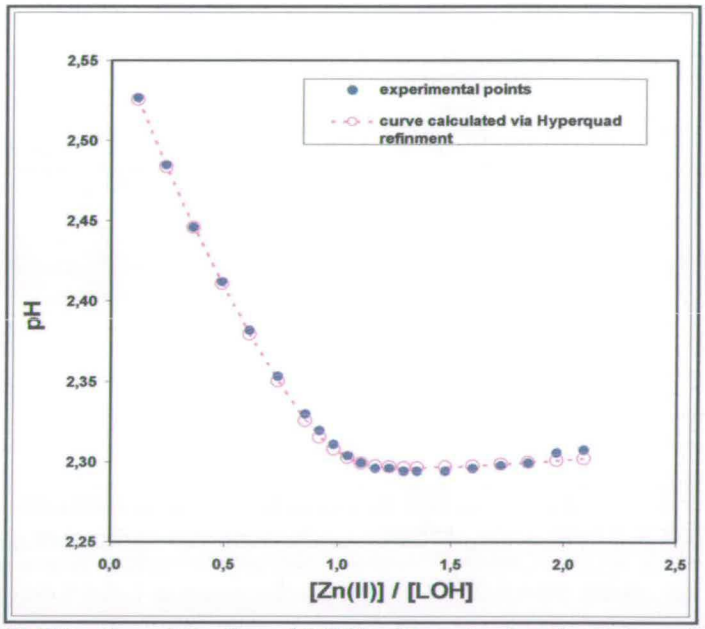

Fig. 103 Titration of the ligand LOH with a standardized zinc solution.

The mechanism of complex formation and the β constants are the following:

$$LOH + Zn^{2+} \rightleftharpoons [(LOH)Zn]^{2+} \qquad \log \beta_{011} = 9.2 \pm 0.1 \qquad \textbf{Eq.65}$$

$$H^{+} + LOH + Zn^{2+} \rightleftharpoons [H(LOH)Zn]^{3+} \qquad \log \beta_{111} = 10.9 \pm 0.1 \qquad \textbf{Eq.66}$$

From the above values it is evident that the protonated mononuclear complex $[H(LOH)Zn]^{3+}$ is formed in low concentration and only in very acidic conditions as

this complex readily loses its proton already at pH ≈ 2 ($pK_a = \log \beta_{111} - \log \beta_{011} = 1.7$). The complete mechanism of complexation between the ligand LOH' and Zn(II) ions was finally deduced by performing alkalimetric titrations on solutions with a different zinc-to-ligand ratio. The formation constants obtained from fitting the experimental data are:

$$H^+ + LOH + Zn^{2+} \rightleftharpoons [H(LOH)Zn]^{3+} \qquad \log \beta_{111} = 10.9 \qquad \textbf{Eq.67}$$

$$LOH + Zn^{2+} \rightleftharpoons [(LOH)Zn]^{2+} \qquad \log \beta_{011} = 9.21 \qquad \textbf{Eq.68}$$

$$LOH + 2\,Zn^{2+} \rightleftharpoons [H_{-1}(LOH)Zn_2]^{3+} + H^+ \qquad \log \beta_{-112} = 8.77 \qquad \textbf{Eq.69}$$

$$LOH + 2\,Zn^{2+} \rightleftharpoons [H_{-2}(LOH)Zn_2]^{2+} + 2\,H^+ \qquad \log \beta_{-212} = 1.5\text{-}2.5 \qquad \textbf{Eq.70}$$

Fig. 104 and 105 show the species distribution diagrams for the cases of Zn(II)/LOH=1 and Zn(II)/LOH = 2 respectively.

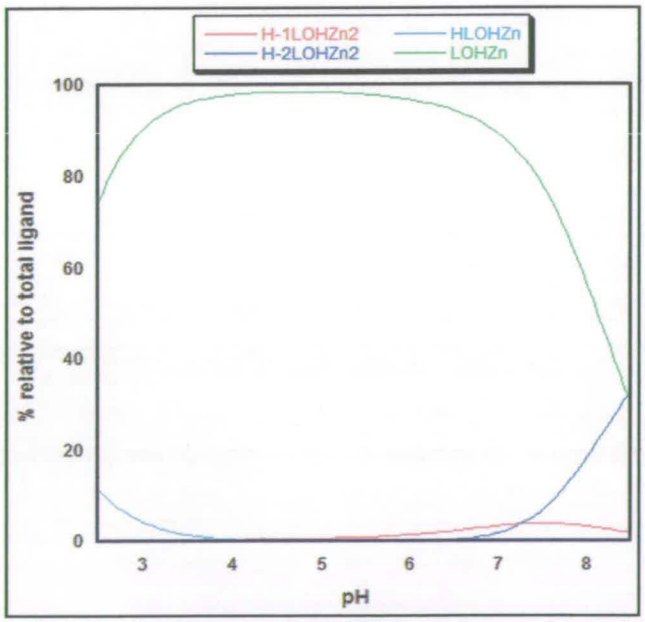

Fig. 104 Species distribution diagram for LOH in presence of 1 equivalent of Zn(II) in DMSO:H_2O (67%-33%).

In the presence of one equivalent of zinc, the solution appears mainly contain one mononuclear complex, $[(LOH)Zn]^{2+}$, which is formed by dissociating a proton

from the protonated mononuclear complex $[H(LOH)Zn]^{3+}$ present at the beginning of the titration (when the pH is only 2.5).

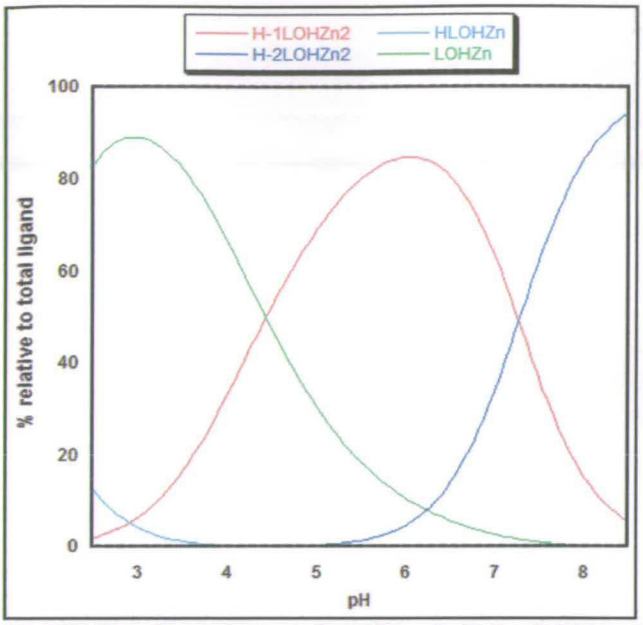

Fig. 105 Species distribution diagram as a function of pH for LOH in the presence of 2 equivalents of Zn(II) in DMSO:H_2O (67%-33%).

At this pH its concentration is 80%, but reaches its maximum at pH ≈ 4. Under these conditions, dinuclear complexes are formed only in very low concentrations (less than 10%) when the pH is higher than 6.

Only in very alkaline solutions (pH > 8.5) the dinuclear complex $[H_{-2}(LOH)Zn_2]^{2+}$ represents the main complex in solution. This complex is formed by deprotonation of a water bound molecule in the dinuclear zinc complex $[H_{-1}(LOH)Zn_2]^{3+}$.

The determination of this mechanism was not straightforward. The presence of two equivalents of zinc causes a deviation of the experimental data from the theoretical curve at pH ≥ 7 which cannot be completely reproduced by assuming the presence of the $[H_{-2}(LOH)Zn_2]^{2+}$ complex along with the other three complexes. In fact, the experimental points fall in between the curves (Fig. 106) calculated by assuming $\log \beta_{-212} = 2$ and $\log \beta_{-212} = 2.35$ (purple and green respectively).

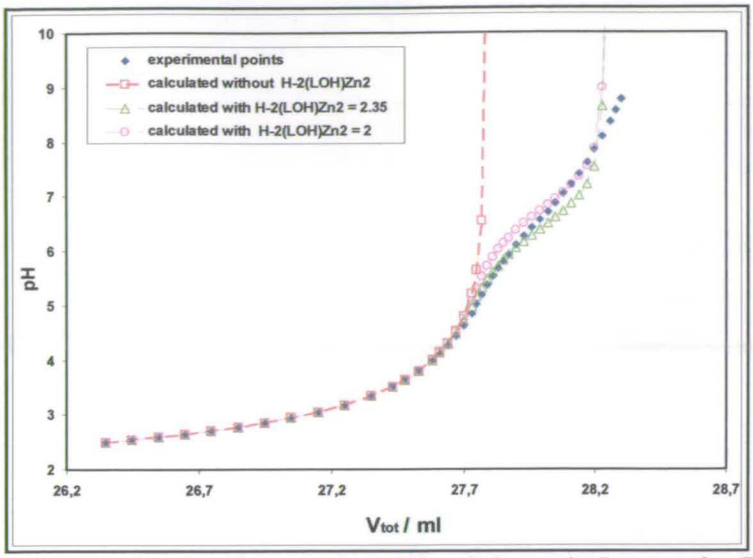

Fig. 106 Titration curve showing the experimental and theoretical curves for Zn(II)/LOH=2.

Different titrations were performed but this deviation was always observed and it is probably due to small precipitation of zinc hydroxide, which consequently acidifies the solution. This hypothesis was tested by examining the behaviour of zinc ions in this solvent mixture in the absence of the ligand. In this case, zinc hydroxide precipitation takes place at very low pH (about 4). As a result, the formation constant β_{-212} is somewhat uncertain ($1.5 \leq \log \beta_{-212} \leq 2.35$) and this produces an uncertainty on the deprotonation constant of the zinc-bound water molecule of the dinuclear complex, which can only be estimated to be in the range of $pK_{wb} = 6.5\text{-}7.3$.

When the M:L ratio is 1:1 or 1.5:1, the experimental data can be explained assuming the mechanism of complex formation mentioned above, but precipitation of zinc hydroxide caused also in these cases deviations from the theoretical curves. Despite all this, the stoichiometry of the complexes is well-established as are the differences between the formation constants (pK_as).

4.4 CONCLUSIONS.

Potentiometric pH titrations were used to determine the acid-base and Zn(II) binding properties of a series of four potentially dinucleating dipycolylamine(dpa)-based ligands. Complex formation was investigated in water and/or DMSO:H_2O (67%:33%) and a summary of the calculated protonation constants is given in Table 8.

Table 8 –Stability constants for the H^+ complexes of the ligands used in this work (T = 25°C and I = 0.1 M $KClO_4$).								
$\log \beta_{hxz}$ ($hH^+ + xL + zZn^{2+} \leftrightarrow H_hL_xZn_z$)	H	L	Zn	LOH	LOH binary solvent	L^1OH	LOH' binary solvent	L^1OH'
$H^+ + L \leftrightarrow HL^+$	1	1	0	6.32	5.16	6.79	6.79	11.42
$2\,H^+ + L \leftrightarrow H_2L^{2+}$	2	1	0	11.52	8.81	11.51	12.37	21.07
$3\,H^+ + L \leftrightarrow H_3L^{3+}$	3	1	0	15.32	10.79	14.88	16.75	27.63
$4\,H^+ + L \leftrightarrow H_4L^{4+}$	4	1	0	18.47		17.68	20.43	32.32
$5\,H^+ + L \leftrightarrow H_5L^{5+}$	5	1	0					35.06

The ligands have a total of 6 and 10 potential protonation sites (without and with amino hydrogen bonding group respectively, Fig. 107) and a dissociable OH.

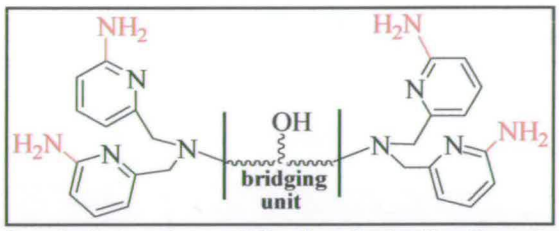

Fig. 107 General chemical structure of the dpa derivative ligands used in this work.

It was found that these ligands bind a maximum of four or five protons, and that in general they tend to be more acidic in the binary solvent (DMSO:H_2O, 67%:33%) (see Table 8). The proton dissociation constants of the ligands (pK_as) are reported in Table 9.

Table 9 – Dissociation constants of the ligands (pK_a)					
pK_a	LOH	LOH binary solvent	L^1OH	LOH' binary solvent	L^1OH'
$H_5L^{5+} \leftrightarrow H_4L^{4+} + H^+$					2.74
$H_4L^{4+} \leftrightarrow H_3L^{3+} + H^+$	3.15		2.80	3.68	4.79
$H_3L^{3+} \leftrightarrow H_2L^{2+} + H^+$	3.80	1.98	3.37	4.38	6.56
$H_2L^{2+} \leftrightarrow HL^+ + H^+$	5.20	3.65	4.72	5.58	9.65
$HL^+ \leftrightarrow L + H^+$	6.32	5.16	6.79	6.79	11.42

In general it is impossible to know the exact position of the protons from potentiometric titrations, as these only inform about the number of protons bound. However the protonation constants and proton locations had been reported[112] for LOH

(Fig. 108). This assignment can be easily justified based on the different basicities of the two different type of nitrogen atoms present in the ligand. Thus, the electron-withdrawing effect of the aromatic ring makes the pyridine nitrogen less basic.

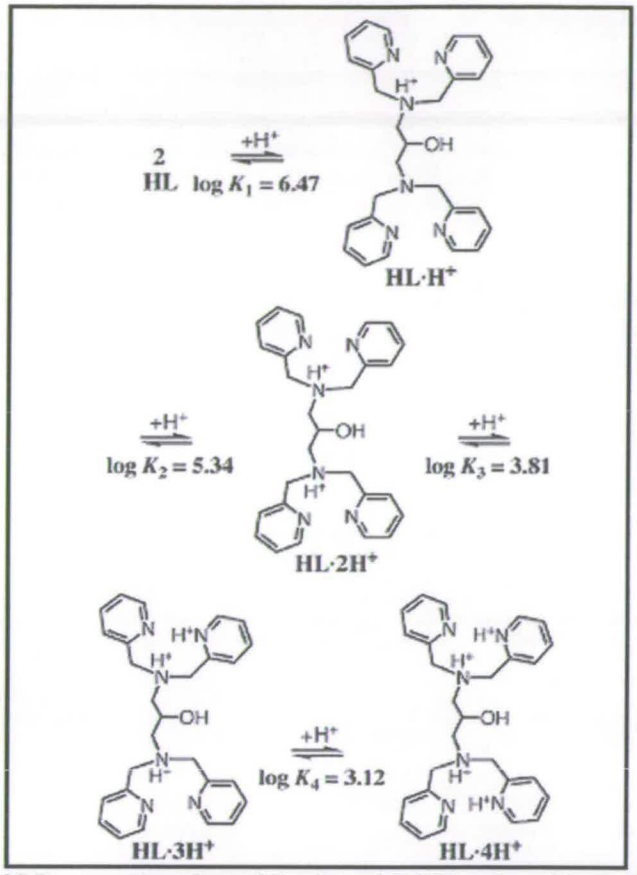

Fig. 108 Protonation sites of the ligand LOH assigned in Ref. 112.

The effect of the introducing amino groups in the dipycolinamine core can be examined by comparing the deprotonation constants of L^1OH and L^1OH'. L^1OH' binds one more proton and is deprotonated at higher pH values than L^1OH. The same occurs for LOH and LOH', albeit in DMSO:H_2O. Presumably, the enhanced basicity of the ligands with amino groups adjacent to the pyridine nitrogen is due to their electron donating properties. It is also worth noting that LOH is more basic in water than in DMSO:water. Previous studies have shown that pK_a values are typically 0.2-1 log units higher in DMSO:H_2O (80%:20%) than in aqueous solution.[113] This effect was attributed to the different solvation properties of the solvents. Characterising the ligand basicity is an important point as it will affect the complex formation constants with metal ions.

In the presence of Zn(II) all ligands investigated formed mononuclear and dinuclear complexes and a speciation model could be established (Table 10).

Table 10 – Stability constants for the Zn^{2+} complexes of the ligands used in this work (T = 25°C and I = 0.1 M $KClO_4$).

log β_{hxz} ($hH^+ + xL + zZn^{2+} \leftrightarrow H_hL_xZn_z$)	H	L	Zn	LOH	LOH binary solvent	L^1OH	LOH' binary solvent	L^1OH'
$2\ H^+ + L + Zn^{2+} \leftrightarrow [H_2LZn]^{4+}$	2	1	1				17.79	27.91
$H^+ + L + Zn^{2+} \leftrightarrow [HLZn]^{3+}$	1	1	1	14.33	10.9	13.8	14.14	23.40
$L + Zn^{2+} \leftrightarrow [LZn]^{2+}$	0	1	1	11.16	9.21	10.5	9.24	16.07
$L + Zn^{2+} \leftrightarrow [H_{-1}LZn]^{+} + H^+$	-1	1	1				2.64	
$L + 2\ Zn^{2+} \leftrightarrow [LZn_2]^{4+}$	0	1	2				13.00	
$L + 2\ Zn^{2+} \leftrightarrow [H_{-1}ZnL]^{3+} + H^+$	-1	1	2	9.2	8.77	7.07	8.01	12.5
$L + 2\ Zn^{2+} \leftrightarrow [H_{-2}ZnL]^{4+} + 2\ H^+$	-2	1	2	2.3	≈ 2	-2.42	4.31	5.14

The stability of the metal complexes can be easily compared by plotting the percentage of free Zn(II) and the p[Zn] (where p[Zn] = -log $[Zn^{2+}]$) *versus* pH. These plots are reported in Fig. 109 (L/Zn = 2) and Fig. 110 (L/Zn = 1), calculated for total concentration: [L] = 0.2 mM, $[Zn^{2+}]$ = 0.4 mM and 0.2 mM respectively.

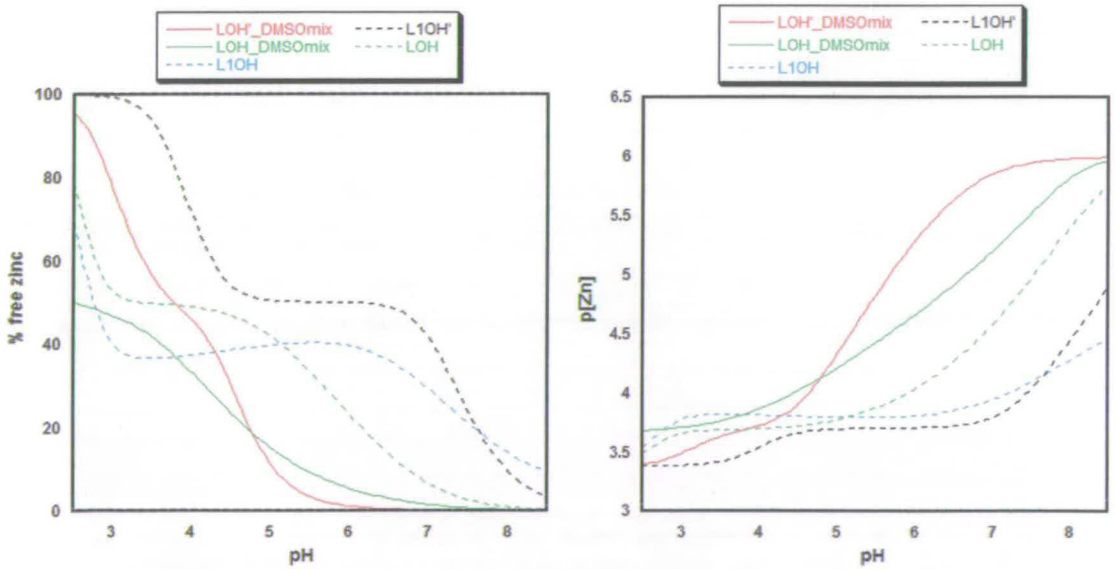

Fig. 109 Changes in the percentage of free Zn(II) (left) and p[Zn] (right) *vs* pH for M/L = 2.

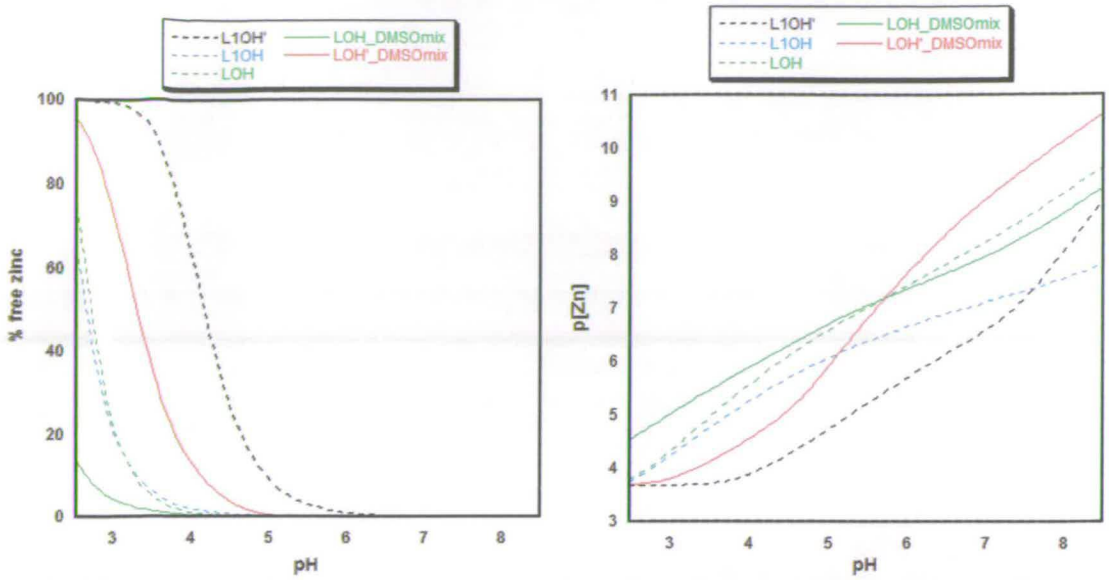

Fig. 110 Change of the percentage of free Zn(II) (left) and p[Zn] (right) *vs* pH for L/M = 1.

Under these conditions the theoretical minimum values for p[Zn], occurring when the complexes are completely dissociated (very acidic pH), would be 3.7 and 3.4 for L/M = 1 and M/L = 2 respectively.

The most acidic ligand is LOH in DMSO:H_2O, which already forms a metal complex at the beginning of the titration (pH = 2.5) leaving in solution only 50% (ratio 2) and 15% (ratio 1) of free metal. As the pH increases, the competition between metal ions and protons becomes less significant and the p[Zn] increases. At physiological pH 7.4, L^1OH' exhibits the lowest p[Zn] value. It is clear that under these conditions this ligand forms the less stable zinc complexes, whereas LOH' forms the most stable ones. Moreover LOH' is the only ligand able to reach the maximum p[Zn] value already at neutral pH and with no free zinc present in solution. It is evident that within the series of ligands examined LOH' has the optimal basicity to bind to the metal ion and to avoid proton competition.

In Chapter 1 it was mentioned that one of the strategies to catalyze the hydrolysis of phosphodiester bonds is providing a potential nucleophile at neutral pH. For such reason the pK_{wb} of a water bound molecule in these zinc complexes is an interesting parameter to estimate and compare.

The dissociation constants of the zinc complexes and of the metal-bound water molecules are reported in Table 11.

Table 11 - pK_as and pK_{wb} of a water bound molecule of Zn(II) complexes in pure water and in DMSO:H_2O (67%:33%).			
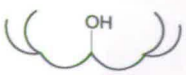 LOH	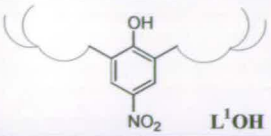 L^1OH	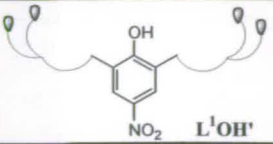 L^1OH'	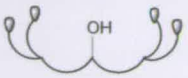 LOH'
		(211 ↔ 111) **pK_{a1} = 4.51**	(211 ↔ 111) **pK_{a1} = 3.65**
(111 ↔ 011) **pK_{a1} = 3.17**	(111 ↔ 011) **pK_{a1} = 3.30**	(111 ↔ 011) **pK_{a2} = 7.33**	(111 ↔ 011) **pK_{a2} = 4.90**
			(011 ↔ -111) **pK_{a3} = 6.60**
			(012 ↔ -112) **pK_{a4} = 4.99**
(-112 ↔ -212) **pK_{wb} = 6.90**	(-112 ↔ -212) **pK_{wb} = 9.49**	(-112 ↔ -212) **pK_{wb} = 7.36**	(-112 ↔ -212) **pK_{wb} = 3.70**

The introduction of four amino groups (represented in the schematic structure of Table 11 as "inverted drops") in the second coordination sphere of zinc complexes decreases the pK_a of the zinc-bound water molecule.[53,57a,b] The effect is notable; the pK_{wb} is more than 2 units lower with the dpa units without amino groups for both linkers (alcohol and *p*-nitrophenol). The effect is probably due to hydrogen bonds between the amino groups and the water molecule.

Although LOH' has been studied in the binary mixture DMSO:H_2O and in pure water, the effect of hydrogen bonds on the pK_{wb} seems similarly effective. In both cases, the pK_a is lowered by more than 2 units. Moreover, the pK_{wb} of LOH in DMSO:H_2O does not change dramatically in pure water (6.77 in the binary mixture and 6.90 in pure water), so extrapolations between these two solvent seem reasonable.

Table 12 – Effect of -NH_2 groups in the mixture DMSO:H_2O (67%:33%)	
LOH	**LOH'**
	(211 ↔ 111) **pK_{a1} = 3.65**
(111 ↔ 011) **pK_{a1} = 1.69**	(111 ↔ 011) **pK_{a2} = 4.90**
	(011 ↔ -111) **pK_{a3} = 6.60**
	(012 ↔ -112) **pK_{a4} = 4.99**
(-112 ↔ -212) **pK_{wb} = 6.77**	(-112 ↔ -212) **pK_{wb} = 3.70**

4.5 Experimental section.

The potentiometric studies were conducted with a Titrino 702 SM autotitrator (Brinkmann Instruments). Thermodynamic equilibrium data for all the ligands were collected potentiometrically using an ion selective electrode. A Metrohm combined pH glass electrode (Ag/AgCl) with 3M NaCl internal filling solution was used. Potentiometric pH titrations were carried out in water or in a binary mixture solvent DMSO:water, and the ionic strength of the solvent was kept constant by adding 0.1M $KClO_4$ or Et_4NClO_4 respectively as supporting electrolyte.

In such defined solvent, taking the reference state for each species as its infinitely diluted solution, activity coefficients are unitary and concentrations can be substituted for activities. All equilibrium measurements were carried out in 50 ml sample volumes with magnetic stirring under N_2 atmosphere and data collected by use of a computer-controlled automated titration system. The free concentration of protons, $[H^+]$, was measured by using a glass electrode based on the cell:

-RE / 3 M NaCl/ Test Solution (=TS) / GE

where RE represents the reference electrode (Ag / AgCl(s) / 3 M KCl) and GE a glass membrane pH electrode.

The measured *emf* of the glass electrode, E, can be expressed by the Eq.71 in which $E°$ is a constant to be determined before each experiment, and E_j is the liquid junction potential that arises at the interface between the test solution and the bridge electrolyte.

$$E = E^0 + 59.16 \log[H^+] + E_j \qquad \textbf{Eq.71}$$

E_j is relevant only when the test solution becomes very acidic (pH ≤ 2.3), while at higher pH, it is so low that it can be neglected. According to that, potentiometric measurements were limited to pH ≥ 2.3.

The $E°$ constant was determined *in situ* before each experiment (electrode calibration procedure) by titrating alkalimetrically an accurately known amount of a

standardized solution of $HClO_4$ 0.1M. The titrant (NaOH or Me_4NOH 0.1 M) was prepared by dilution of a standard 1 M FIXANAL solution (Sigma Aldrich product) with freshly boiled double de-ionized water and kept under N_2 atmosphere to prevent entry of CO_2. The temperature was kept to 25.0 ± 0.1 °C throughout the titration.

During the calibration of the electrode, the construction of a Gran plot allowed us to check the concentration of the titrating solution and the extent of contamination by carbonate, whose content must not exceed about 1%. A typical Gran's plot is shown in Fig. 111.

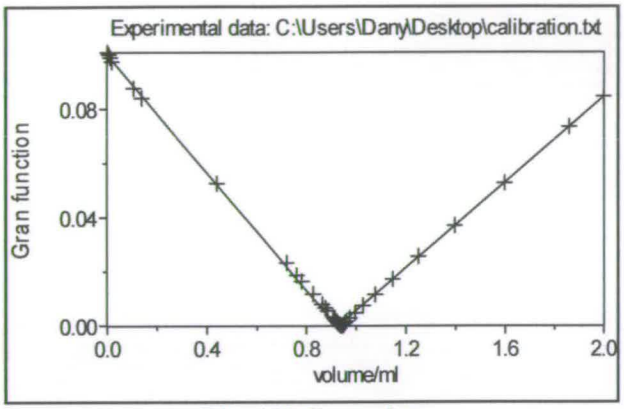

Fig. 111 Gran plot.

The ionic product of water was also evaluated during this procedure and the value of $pK_w = 13.78$ was used for all the calculations. After the electrode calibration, a weighed amount of the ligand ($0.2 \leq$ [ligand] $\leq$ 2mM) was added to the solution in the titration vessel and acidified by adding a known amount of 0.1 M $HClO_4$. At this point the analytical composition of the solution is accurately known, and the protonation constants of the ligands can be evaluated from the (pH, V_{OH}) data collected by using the least-squares program Hyperquad.

The complex formation constants between the ligands and Zn(II) were evaluated by adding the desired amount of $Zn(NO_3)_2$ (as solid or as standardized solution) to the ligand solution of known composition. The potentiometric data collected were always treated with Hyperquad. The formalism adopted during the data processing considers the formation of a general complex with formula $H_hL_xM_z$ (where M is the metal, L the ligand and H the proton) to take place according to the following reaction (charges are here omitted for convenience and L indicates in this case a general ligand):

$$hH + xL + zM \leftrightarrow M_zL_xH_h \qquad \textbf{Eq.72}$$

The formation constant of the species $H_hL_xM_z$ is defined by convention by the following equation:

$$\frac{[H_hL_xM_z]}{[H]^h[L]^x[M]^z} = \beta_{hxz} \qquad \textbf{Eq.73}$$

and β_{hxz} is the overall formation constant of the complex $H_hL_xM_z$.

Solutions with variables concentrations of Zn(II) and ligand were investigated and the experiments performed in one or both of the following two different ways:

1. An acidic solution of the ligand was titrated with a standardized solution of $Zn(NO_3)_2$.
2. An acidic solution of the ligand and Zn(II), having 2:1 or 1:1 metal to ligand ratios, was alkalimetrically titrated with the standard solution of NaOH (or Me_4NOH) employed for the titration of the ligands.

Chapter 5 – Kinetic Studies

5.1 Introduction.

The catalytic activity of the *in situ*-prepared complexes between the ligands LOH' and L^1OH' and Zn(II) ions was studied in water at 25°C for the transesterification of the activated RNA model 2-hydroxypropyl-4-nitrophenyl phophate (HPNPP). The hydrolysis reaction was followed by measuring the absorbance of the released *p*-nitrophenol at 400 nm. For LOH', cleavage of a natural and more stable dinucleotide, uridyl(3'-5')uridine (UpU), was also tested and followed by HPLC.

The work is concentrated on Zn(II) complexes, because Zn(II) is common metal choice in natural hydrolases like nucleases. Also important is the fact that it lacks redox properties, ensuring a hydrolytic rather than oxidative cleavage. This is important because the redox chemistry of the metal can produce unwanted (and very reactive) free radicals, leading to chemically modified nucleic acid fragments.

The results showed that both ligand systems provide Zn(II) complexes with very high catalytic activity for the hydrolysis of HPNPP at physiological conditions. However, significant differences were observed with respect to the nature of the active species. Interestingly, LOH' leads to complexes that are also able to activate atmospheric CO_2 to form (bi)carbonate.

The mechanism(s) of hydrolysis are discussed and they are based on the nature of the identified species in solution (Chapter 4), X-ray crystallography and a range of kinetic studies (pH profiles, saturation studies, inhibition studies and solvent kinetic isotope effects). Moreover, the potential geometries of some intermediates were investigated computationally.

The effect of changing the metal in the catalytic activity of the complexes was briefly investigated for one of the ligands and the interesting preliminary results are reported.

5.2 Experimental details.

5.2.1 Materials.

The ligands LOH' and L^1OH' were synthesized, purified and characterized as described in Chapter 3 (section 3.2.2 and 3.2.4 respectively). Zn(II) complexes were formed *in situ* by adding the appropriate amount of $Zn(NO_3)_2$ purchased from Sigma-Aldrich. HPNPP (barium salt) was synthesized according to the literature[114] and the substrate UpU was purchased from Sigma-Aldrich and used without any further purification. Buffers were prepared in fresh $Ar_{(g)}$-degassed double de-ionized distilled water by addition of the required amount of the free acid and basic components of HEPES or MES (Sigma-Aldrich) to give the desired pH.

5.2.2 Method.

The reactions were carried out in aqueous buffer media (50 mM) and the effect of pH on the catalytic activity was investigated in the pH range 5-8 (MES for $5.5 \leq$ pH ≤ 6.5 and HEPES for $7.0 \leq$ pH ≤ 8.5). The transesterification of HPNPP was monitored spectrophotometrically by following the absorbance at 400 nm of the released *p*-nitrophenol with a Cary 1 Bio spectrophotometer coupled to a thermostat cell holder to keep the temperature constant at 25°C. The absorbance values were converted into concentration of *p*-nitrophenolate as described in Section *5.2.2.1*.

Reactions were initiated by the addition of a small volume (4.5 µl or 1.25 µl) of a stock solution of substrate to 0.9 ml (or 0.5 ml, respectively) of buffer solution containing the ligand and $Zn(NO_3)_2$ in the desired ratio. All solutions were in water except the ligand stock solution (20 mM), which was made up in methanol.

The substrate stock solution was kept at -20°C to prevent autohydrolysis and heated to 4°C immediately before each kinetic study. Excellent first-order changes in absorbance were observed for at least three half lives in each case and pseudo-first-order rate constants were obtained by non-linear least squares fitting the change in absorbance with time to an exponential curve. In this case, the reaction was carried out in presence of excess of catalyst. Kinetic measurements collected under saturated

conditions were based on the initial rates method. Here, the rate of change in absorbance over the first 1-2% of reaction was fitted linearly.

The catalyzed hydrolysis of UpU was monitored by reverse phase HPLC using 9:1 acetate buffer (60 mM, pH 4.2):methanol as the eluant and detecting UpU at 260 nm.

5.2.2.1 Determination of the molar extinction coefficient of nitrophenol (ε_{NP}).

Since the hydrolysis of HPNPP was carried out by monitoring the absorbance at 400 nm of the *p*-nitrophenolate ion (NP) generated in solution, it is important to determine the molar extinction coefficient of NP at each pH.

The *p*-nitrophenolate ion is generated upon dissociation of a proton according to the equilibrium shown in Eq.74; its concentration will then depend on the pH of the solution.

$$HNP \rightleftharpoons H^+ + NP^- \qquad \textbf{Eq.74}$$

$$K_a = \frac{[NP^-][H^+]}{[HNP]} \qquad \textbf{Eq.75}$$

The dissociation constant (K_a) and the molar extinction coefficient (ε_{NP}) were determined by recording the UV-vis spectrum of a 0.1 mM solution of *p*-nitrophenol in water at different pH (Fig. 112). The absorbance at 400 nm was then plotted against the pH (Fig. 113).

According to Beer-Lambert's law:

$$A = \varepsilon_{obs} l [HNP]_{tot} = \varepsilon_{NP} l [NP] \qquad \textbf{Eq.76}$$

where ε_{obs} is the observed molar extinction coefficient at a given pH, l the cell length (1 cm), $[HNP]_{tot}$ the total concentration of *p*-nitrophenol (0.1 mM), ε_{NP} the molar extinction coefficient of the *p*-nitrophenolate generated and [NP] its concentration.

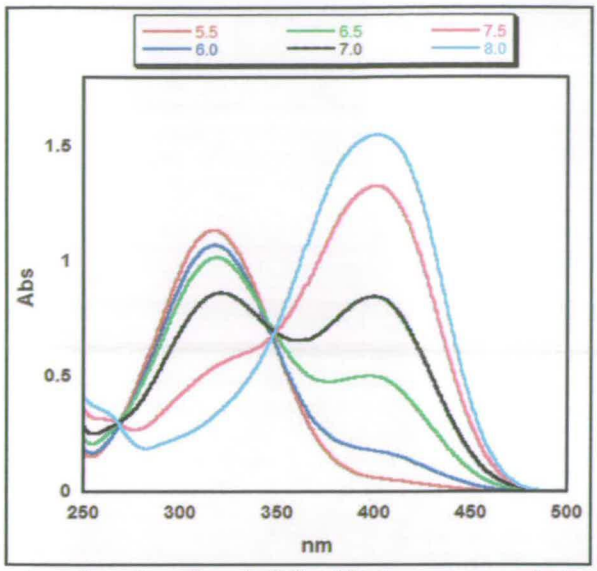

Fig. 112 UV-vis spectra of *p*-nitrophenol (0.1 mM) in aqueous solutions at different pHs.

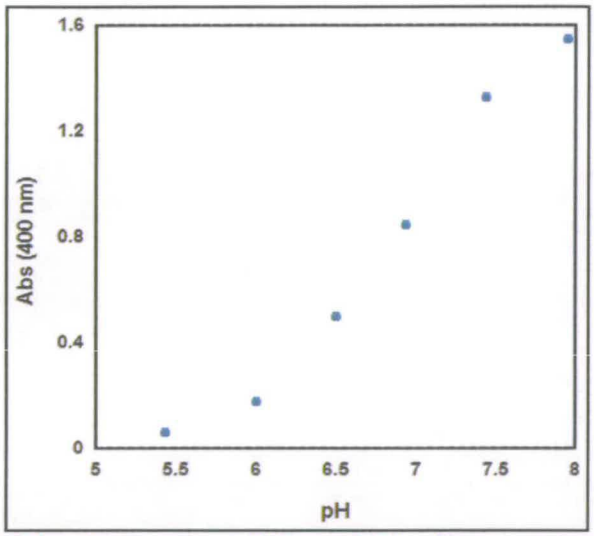

Fig. 113 Plot of the absorbance at 400 nm of 0.1 mM *p*-nitrophenol *versus* pH.

As the total concentration of *p*-nitrophenol at each point is given by:

$$[HNP]_{tot} = [HNP] + [NP] \qquad \textbf{Eq.77}$$

it is possible to combine Eq.75, 76 and 77 to obtain an expression which correlates ε_{NP} and $[H^+]$ (Eq.78).

$$\varepsilon_{obs} = \frac{\varepsilon_{NP} K_a}{K_a + [H^+]} \qquad \textbf{Eq.78}$$

The plot of $1/\varepsilon_{obs}$ versus $[H^+]$ is a straight line from which the parameters ε_{NP} and K_a can be obtained. The data collected are reported in Table 13 and plotted in Fig. 114. The linear fit of the data affords $pK_a = -\log K_a = 6.7$ and $\varepsilon_{NP} = 12953$.

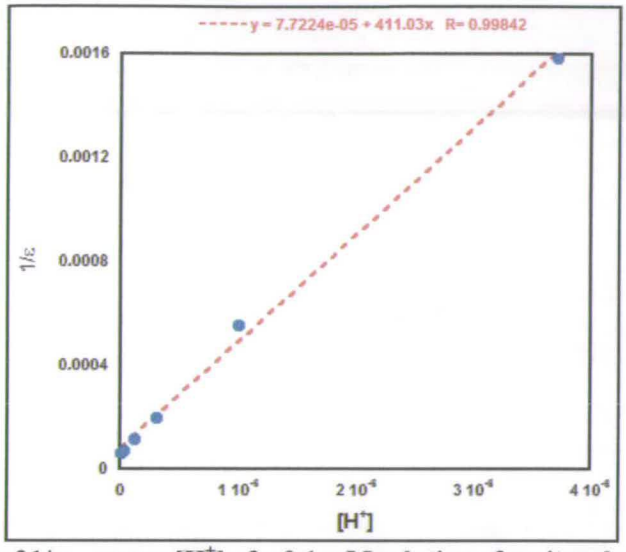

Fig. 114 Plot of $1/\varepsilon_{obs}$ *versus* $[H^+]$ of a 0.1 mM solution of *p*-nitrophenol in water.

Table 13

pH	$[H^+]$	A (400 nm)	ε_{obs}	$1/\varepsilon_{obs}$
5.43	3.71e-06	0.063	630	1.59e-03
6.00	1.00e-06	0.1799	1799	5.56e-04
6.50	3.16e-07	0.5027	5027	1.98e-04
6.93	1.17e-07	0.8488	8488	1.18e-04
7.43	3.71e-08	1.3302	13302	7.51e-05
7.95	1.12e-08	1.5494	15494	6.45e-05

5.2.3 X-Ray Crystallography.

Crystals suitable for X-ray diffraction studies were grown by slow evaporation of acetonitrile/methanol solutions containing LOH', $Zn(ClO_4)_2{\cdot}6H_2O$ and 4-nitrophenyl phosphate disodium salt hexahydrate ($Na_2NPP{\cdot}6H_2O$) in a 1:2:1 ratio. The crystals had the following composition and crystallographic parameters: $C_{35.5}H_{44.5}ClN_{11.5}O_{12.5}PZn_2$, $M = 1029.49$, colourless crystals, crystal size 0.56 x 0.28 x 0.18 mm. monoclinic, space group $P2_1/c$, $a = 10.5159(2)$, $b = 38.6134(9)$, $c = 10.3263(2)$ Å, $U = 4113.37(15)$ Å^3, $Z = 4$, $D_C = 1.662$ g cm^{-3} , $\mu = 1.349$ mm^{-1} , 48860 reflections measured, 8987 unique, $R_{int} = 0.0439$ (all data), $R1 = 0.0575$ (all data), $wR2 = 0.1105$ (all data), $S = 1.126$ (all data), largest difference peak, hole

0.926, -0.492 e $Å^{-3}$. Additional crystallographic data and the CIF file are reported in the published paper,[115] and in the supplementary material.

Unfortunately and despite exhaustive attempts, it proved impossible to obtain crystals suitable for X-ray diffraction of Zn(II) complexes of L^1OH'.

5.2.4 Computational Calculations.

Ab initio calculations were used to obtain the geometry configuration of general complexes $M_xL_yS_z$ (M = metal, L = ligand, S = substrate). All theoretical experiments were performed using the Gaussian 03 program[116] on a high performance general-purpose Linux compute cluster (*eddie*) accessed via the Edinburgh Compute and Data Facility (ECDF) service. All calculations employed the Hartree-Fock method and a 3-21G** basis set. The ArgusLab program[117] was used to prepare the input structures and visualize the results. The computations described were made possible thanks to the EaStCHEM Research Computing Facility.

5.3 Results and discussion.

5.3.1 Nuclease-like activity of metal complexes of LOH'.

5.3.1.1 Transesterification of the substrate HPNPP.

Initial experiments showed that the dinuclear Zn(II) complex of the ligand LOH' is a very efficient catalyst, with a 0.2 mM solution decreasing the half-life of HPNPP (0.05 mM) to about a minute at 25°C in water and physiological pH 7.4. This corresponds to an observed rate acceleration of about 10^6-fold. Based on the potentiometric data (Chapter 4), at this pH and in the presence of two equivalents of Zn(II), LOH' affords quantitatively a dinuclear complex. Accordingly, this dizinc complex was prepared *in situ* and it is reasonable to suggest that it is responsible for all the catalytic activity observed.

The M:L stoichiometry of the catalytically active species was confirmed by plotting k_{obs} against mole fraction of metal. The result is illustrated in Fig. 115, which

shows that the maximum activity is reached when a 2:1 metal:ligand complex is formed.

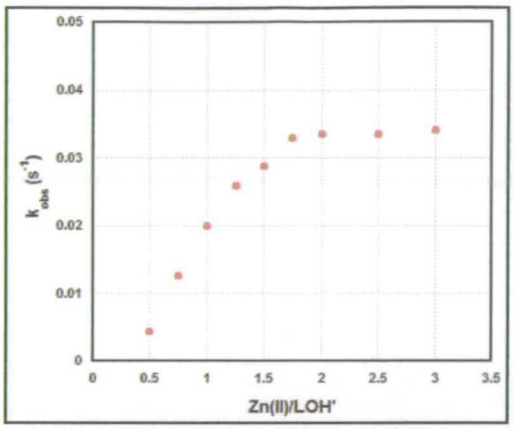

Fig. 115 Plot of k_{obs} (s^{-1}) *vs* Zn(II)/LOH' (pH 7.4, 25°C); [LOH'] = 1 mM, [HPNPP] = 0.05 mM.

Kinetic measurements were therefore restricted to a single complex and the proposed mechanism of hydrolysis is shown in Fig. 116.

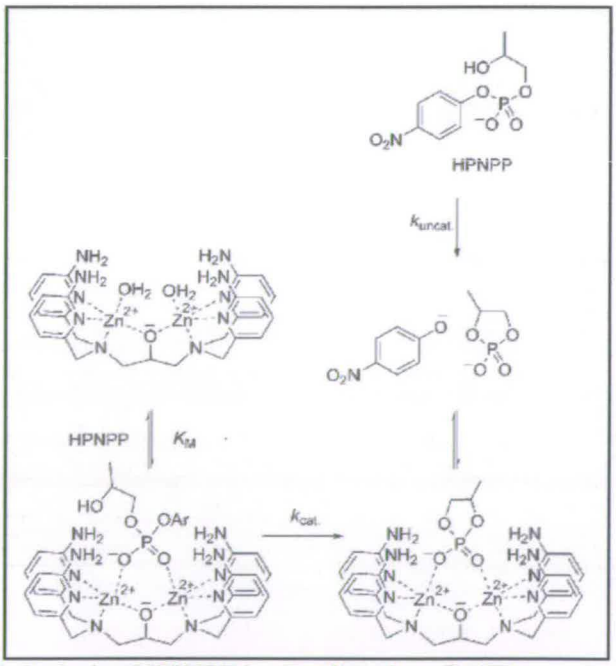

Fig. 116 Hydrolysis of HPNPP by the dinuclear Zn(II) complex of LOH'.

The pseudo first-order rate constant of the reaction was measured by following the formation of *p*-nitrophenolate in the presence of excess of catalyst. In a typical curve, the absorbance at 400 nm is plotted against time and the experiment is stopped

when no further change is observed (Fig. 117). The curve can be fitted with the following exponential equation:

$$A = A_{max} + (A_{min} - A_{max}) \times (e^{-k_{obs}t}) \qquad \textbf{Eq.79}$$

in which A is the absorbance of the *p*-nitrophenolate ion released, A_{max} and A_{min} are the maximum and minimum absorbance in the curve, k_{obs} is the observed pseudo-first order constant and t the time.

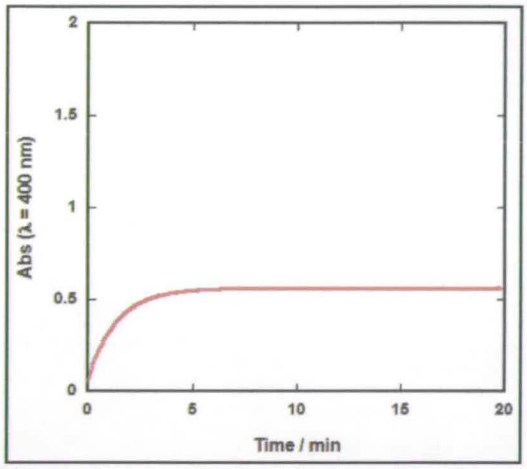

Fig. 117 Typical curve obtained during a kinetic experiment ([HPNPP] = 0.05 mM, pH = 7.5, T = 25°C, [cat] = 0.2 mM).

In order to verify if the reaction obeys the Michaelis-Menten scheme of Fig. 116, the effect of increasing the concentration of the substrate on the catalytic activity of the dinuclear Zn(II) complex of LOH' was investigated at pH 7.4. The substrate concentration was plotted against the initial rate of hydrolysis (Fig. 118). The profile reveals saturation kinetics above 5-10-fold excess of HPNPP.

This result indicated the validity of the Michaelis-Menten equation for this system; that is, the formation of the ternary [Zn_2(LOH')(HPNPP)] complex prior to the release of the cleaved product.

The experimental data points were then fitted to Eq.80:

$$v_0 = V_{max} \frac{[HPNPP]}{(K_M + [HPNPP])} \qquad \textbf{Eq.80}$$

in which v_0 is the initial rate and $V_{max} = k_{cat}\,[cat]_0$. A nonlinear least squares fit of the data points in Fig. 118 resulted in a Michaelis-Menten constant (K_M) of 0.32 ± 0.03 mM and a catalytic rate constant (k_{cat}) of 0.017 ± 0.001 s^{-1} at pH 7.4. Combining these parameters give k_{cat}/K_M, the apparent second-order rate constant for catalysis by this complex, as 53 $M^{-1}\,s^{-1}$. For comparison, the analogous dinuclear Zn(II) complex without the amino groups on the pyridine units is 0.073 $M^{-1}\,s^{-1}$. This rate constant for the triazacyclononane-based dizinc(II) complex developed by Morrow and Richards is 0.25 $M^{-1}\,s^{-1}$; previously the most reactive synthetic Zn(II) complex for HPNPP hydrolysis.[1a,40]

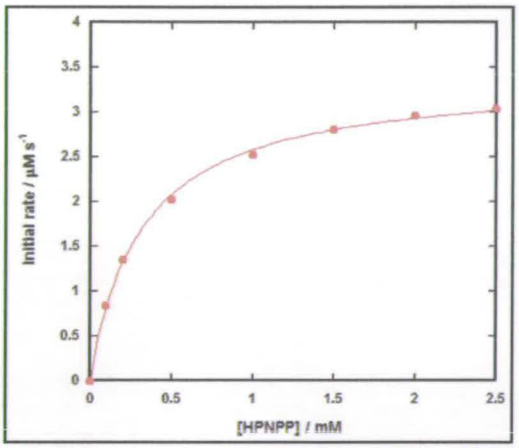

Fig. 118 Saturation kinetic curve for the hydrolysis of HPNPP catalyzed by [Zn_2(LOH')] (0.2 mM) at pH 7.4 and 25 °C.

The inverse of the Michaelis-Menten constant, $1/K_M$, represents the substrate binding constant to the metal complex catalyst (K_{HPNPP}); a small value of K_M indicates high affinity for the substrate. It is evident that the dinuclear zinc complex of LOH' binds HPNPP very tightly. The most plausible mode of interaction between the substrate and the dinuclear Zn(II) catalyst is a bridging coordination of the phosphodiester anion. This hypothesis was supported by crystallizing the dinuclear complex in the presence of 4-nitrophenyl phosphate (NPP) which revealed that the phosphate binds to the complex by bridging the two Zn(II) ions (Fig. 119).

In this way, the phosphoryl oxygen atoms are placed within hydrogen-bonding distances from the four amino groups (N---O 2.82-2.88 Å).

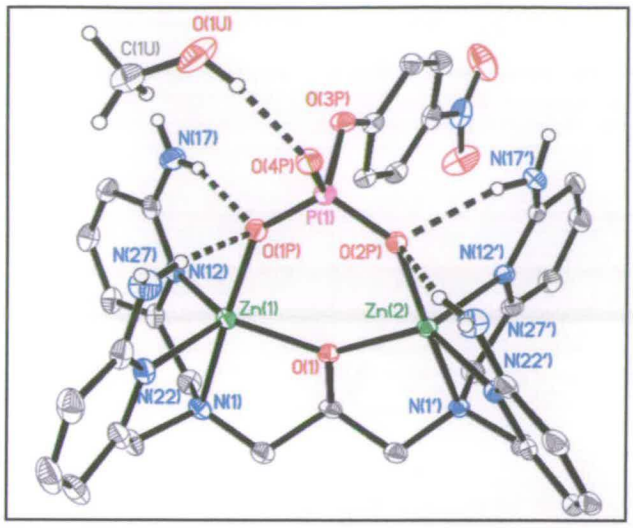

Fig. 119 Structure of the $([Zn_2(LOH')]\cdot NPP)^+$ cation. Only N-bound hydrogen atoms (white) are shown for clarity. Hydrogen-bonding interactions [Å]: N(17)···O(1P) 2.818(4), N(27)···O(1P) 2.884(4), N(17')···O(2P) 2.882(4), N(27')···O(2P) 2.872(4).

The spectacular catalytic turnover (k_{cat}) observed for this artificial Zn(II) complex is likely to be increased due to the cooperativity behaviour between the metal centres and the hydrogen bonding groups. The four amino hydrogen bonding groups can assist towards binding of the phosphate substrate to the zinc ion centres and stabilizing the reaction transition state.

^{31}P-NMR studies showed that the catalyst cleanly converts HPNPP into propylene phosphate (Fig. 116) with a complete turnover of 5 mM of substrate by 1 mM of complex (Fig. 120).

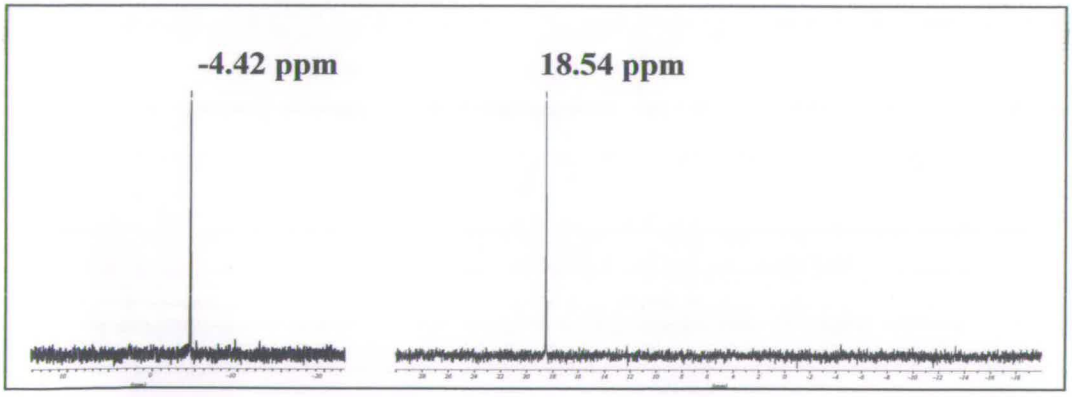

Fig. 120 ^{31}P-NMR spectra of HPNPP (5mM, in 10%D_2O in H_2O) at pH 7.1 (50 mM HEPES) and 22°C before (left) and after addition of the dizinc complex of LOH' (1 mM) and reaction for 1h (right).

The pseudo-first-order rate constants were also determined as a function of pH. The hydrolysis reaction is first order in substrate only if HPNPP is present at relatively low concentrations (< 0.1 mM, Fig. 118). For this reason the pH profile experiment was carried out with 0.05 mM substrate.

The activity increased steeply with increasing pH up to 7.5 where it reaches a plateau (Fig. 121).

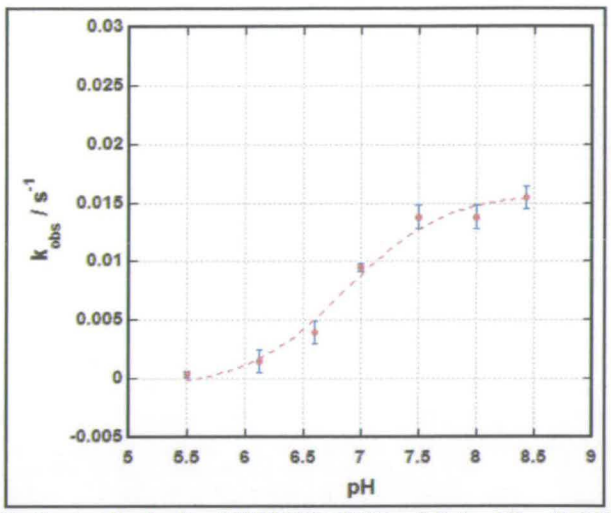

Fig. 121 pH-rate profile for hydrolysis of HPNPP (0.05 mM) by [Zn_2(LOH')] (0.2 mM) at 25°C.

Similar profiles are quite common for phosphate ester hydrolysis promoted by metal complexes.[118] In enzyme catalysis terms, it can be explained with a mechanism which involves the deprotonation of one ionising group in the enzyme-substrate complex directly involved in the catalysis:

$$HES \overset{K_{ES}}{\rightleftharpoons} ES^- + H^+ \qquad \textbf{Eq.81}$$

where HES is the protonated form of the enzyme-substrate complex and ES^- its corresponding deprotonated catalytically active form.

The pH dependence of the rate constant (k_{obs}) follows the ionization constant of the enzyme-substrate complex (K_{ES}) and it can be shown that:

$$k_{obs} = \frac{k_{HES}[H^+] + k_{ES}K_{ES}}{K_{ES} + [H^+]} \qquad \textbf{Eq.82}$$

where k_{obs} is the observed rate constant at a given pH, k_{HES} and k_{ES} are the activities of the species HES and ES respectively, and K_{ES} is the equilibrium constant for the dissociation of the proton in the enzyme-substrate complex. The data fit well to a single ionization model (Eq.82). The fit of the data in Fig. 121 was obtained using the Eq.83 and it gives a pK_{ES} value of 6.8.

$$k_{obs} = \frac{k_{ES} + k_{HES}10^{pH-pK_{ES}}}{1+10^{pH-pK_{ES}}} \qquad \textbf{Eq.83}$$

It is clear that in this case the nucleophile is deprotonated once the catalyst-substrate is formed and that this is the 2'-hydroxy group of HPNPP. The pH profile could reflect the conversion of the 2'-OH to 2'-O and/or the deprotonation of a water molecule critical for catalysis.

The potential identity and geometry of some plausible intermediates was investigated by carrying out computational studies.

A simulation of the substrate binding to the dinuclear catalyst using computational methods shows that interaction between the 2'-hydroxyl group and the ligand-based amino groups is possible (N---H—O 2.03Å, Fig. 122). This could help to activate the hydroxyl group, and together with the N-H---O hydrogen bonding to the phosphate oxygens could be responsible for the enhanced activity observed relative to the complex of the parent ligand LOH.[119] This would be consistent with several studies in which the reactivity of simple metal complexes toward phosphodiester hydrolysis was increased substantially by attachment of basic auxiliary groups to the ligand.[120]

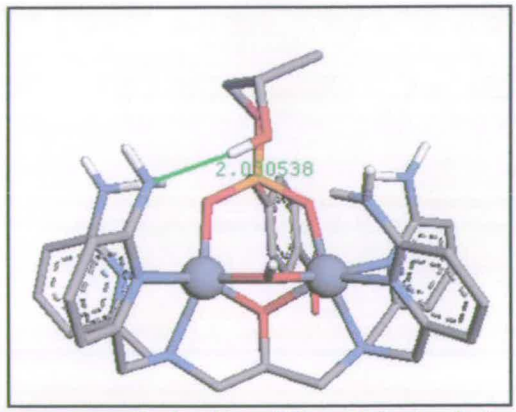

Fig. 122 Geometry optimization of the catalyst-substrate complex with a metal-bound hydroxide bridge.

Another possibility involves the deprotonation of a water molecule in the dinuclear Zn(II) complex. Computational calculations for a dinuclear complex bound to HPNPP and two hydroxide molecules converged to a structure in which one of the two hydroxides is pushed from the dinuclear metal core (Fig. 123). This hydroxide interacts with the 2-hydroxide group of the substrate and a bridging hydroxyl group.

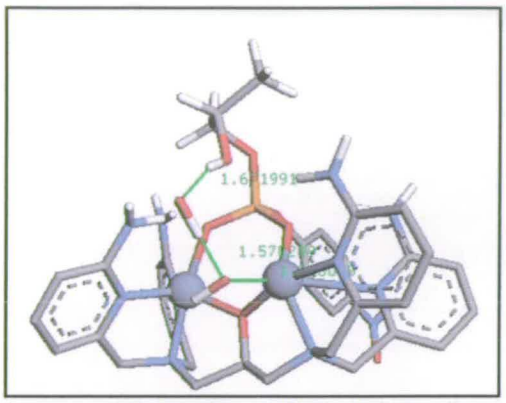

Fig. 123 Geometry optimization of the catalyst-substrate complex with two deprotonated water molecules.

Regardless of the nature of the intermediates, it is clear that the reactivity of this dinuclear catalyst is enhanced by the presence of hydrogen bonding interactions with the amino groups present in the ligand.

The effect of the hydrogen bonding groups towards substrate binding was also tested by investigating the inhibitory effect of dimethyl phosphate (DMP). For this, the rate of transesterification of HPNPP was measured at pH 7.4 in the presence of increasing concentrations of DMP. The experimental data collected are reported in Fig. 124 along with the curve fit obtained by using the following equation:

$$\frac{k}{k_0} = \frac{K_i}{(K_i + [DMP])} \qquad \textbf{Eq.84}$$

where k/k_0 is the normalized first-order rate constant and K_i the inhibition constant or binding constant to the inhibitor DMP.

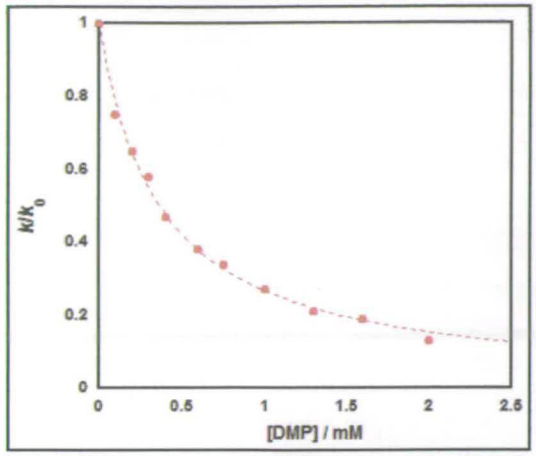

Fig. 124 Variation in the ratio of the rate constant for transesterification of HPNPP catalyzed by 0.2 mM $[H_{-2}Zn_2(LOH')]^{2+}$ in the presence of DMP (k) to the rate in the absence of DMP (k_0) at pH 7.4. The dashed line is the least-square fit to Eq.84.

The value obtained for K_i (0.37 ± 0.07 mM) is in good agreement with the value for substrate binding to the complex (0.32 mM). By comparison, the analogous complex without amino hydrogen bonding groups has $K_i \approx 9$ mM.[119] The dinuclear zinc complex of LOH' binds DMP 25 times more strongly than the dinuclear complex of the corresponding ligand (LOH) without amino groups. Thus the ca. 750-fold increase in catalytic activity for the dinuclear Zn(II) complex of LOH' relative to that of LOH is divided roughly equally between enhanced binding of the substrate and higher reactivity of the substrate-catalyst complex.

5.3.1.2 Transesterification of the substrate UpU.

Although HPNPP transesterification has been widely used as a convenient model for RNA cleavage, it has a less effective intramolecular nucleophile and a much better leaving group than RNA. These differences mean that a good catalyst for the hydrolysis of HPNPP may or may not be good for RNA cleavage.[121] For this reason, the nuclease activity of the dinuclear Zn(II) complex of LOH' was also investigated with a non-activated natural substrate; the dinucleotide uridyl(3'-5')uridine (UpU).

The experiments were carried out at pH 7.3 and 25°C and the loss of UpU was monitored by reverse-phase HPLC and fitted to a first-order curve (Fig. 125).

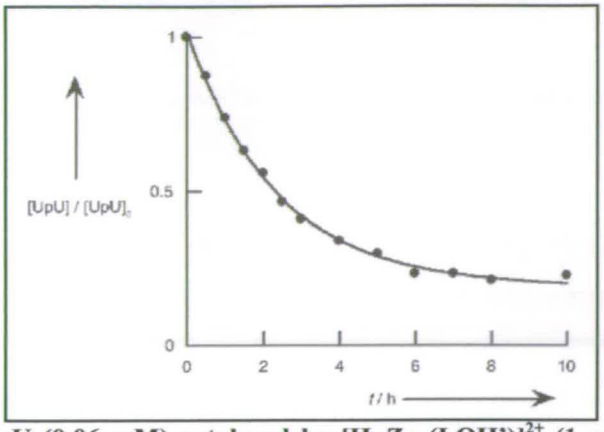

Fig. 125 Hydrolysis of UpU (0.06 mM) catalyzed by $[H_{-2}Zn_2(LOH')]^{2+}$ (1 mM) at pH 7.3 and 25°C. The solid line is the least-squares fit to a first-order decay.[116]

This study shows that 1 mM $[H_{-2}Zn_2(LOH')]^{2+}$ catalyzes the hydrolysis of UpU (0.06 mM) with an observed pseudo-first-order rate constant of $1.2 \pm 0.1 \times 10^{-4}$ s^{-1}. This corresponds to a rate acceleration of approximately 10^6-fold, which is similar to that observed for HPNPP cleavage – and so the high activity of this catalyst is not confined to activated substrates.

If we compare with the triazocyclononane-based dinuclear Zn(II) complex reported by Richard and co-workers, the k_{obs} under the same reaction condictions is 0.7×10^{-6} s^{-1}.[122] Since the reactivity of this triazacyclononane-based complex is similar to that of the pyridyl-based ligand with no amino substituents, it is possible to say that the amino groups provide an additional rate acceleration of two orders of magnitude for cleavage of inactivated natural substrates relative to double Lewis acid activation by the Zn(II) ions alone.

5.3.1.3 CO_2 activation and inhibition of phosphate diester hydrolysis.

The phosphate diester hydrolysis studies with the dizinc(II) complex of LOH' suffered from the problem of reproducibility. This problem, however, became only evident when two identical experiments were carried out consecutively in the same day. Attempts to reproduce two results back to back led to the interesting discovery that atmospheric CO_2 interferes with the phosphate diester hydrolysis reaction by acting as substrate, which can also be effectively hydrolysed by this dizinc(II) complex. This discovery is important because there is great interest in the

development of metal complexes able to promote the chemical fixation and activation of carbon dioxide.[123]

In nature the reversible hydration of carbon dioxide is catalyzed by the enzyme *carbonic anhydrase (CA)*:

$$CO_2 + H_2O \overset{CA}{\rightleftharpoons} HCO^{3-} + H^+ \qquad \textbf{Eq.85}$$

Humans express different carbonic anhydrases with varying catalytic activities. The human carbonic anhydrase II (HCA II) is the most studied and efficient hydrolases known to date; its catalytic turnover rate is 10^6 s^{-1}.[124] HCA II is a zinc-metalloenzyme and the nature of its catalytic site (Fig. 126) has been determined by X-ray diffraction.[125]

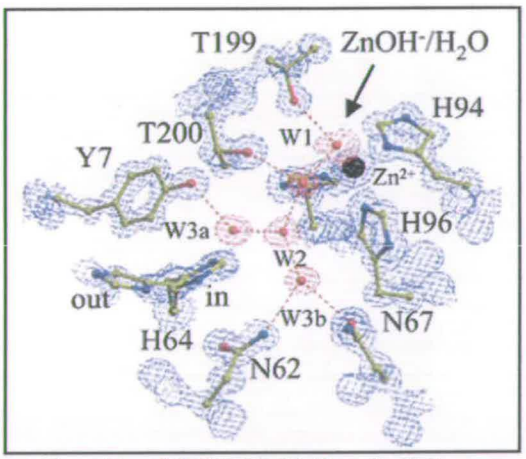

Fig. 126 Stereoview of the active site of HCA II. Ball-and-stick representation of the active site residues are as labelled, and the zinc atom and waters are shown as black and red spheres, respectively.[126]

The active site contains a pseudo-tetrahedral zinc center coordinated to three histidine imidazole groups and a water molecule or hydroxide anion, depending on the pH ($pK_a \approx 7$). The catalytic mechanism and the rate-limiting step involve an intramolecular proton transfer between the Zn-bound solvent and the side chain of His64, which has recently been proposed to occur through a hydrogen-bond water network (Fig. 127).[126]

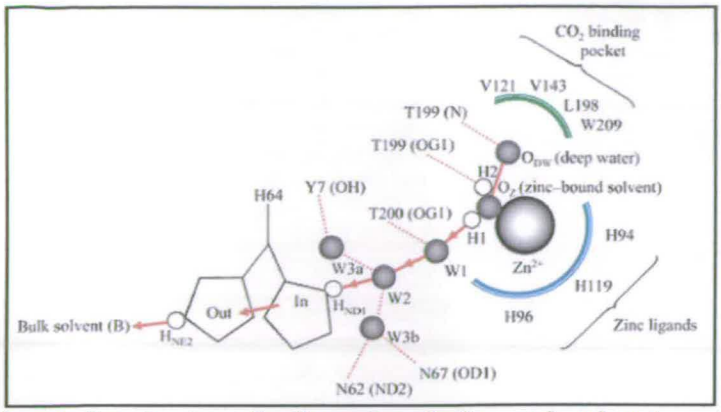

Fig. 127 The pathway of proton transfer through an hydrogen-bond water network in HCA II proposed by McKenne and co-workers.[126]

Numerous strategies and different approaches have been used for the synthesis of CA model compounds. These have been the subject of many reviews.[127] One of the approaches involves using Zn(II) complexes of ligands which are known to enhance the hydrolysis of activated esters or phosphate esters.[128] Some of these complexes, once in solution have been shown to absorb atmospheric CO_2 to give the corresponding carbonate complex.[129] Very recently, Masuda and co-workers have reported that the Zn(II) complex of a tris-pyridylamino tripodal ligand is able to fix CO_2 and generate a carbamato carboxyl group.[130] In this case CO_2 was bubbled into the solution containing the Zn(II) complex. Based on these findings, the potential ability of the Zn(II):LOH' (2:1) system to activate and hydrolyse atmospheric CO_2 was investigated.

To avoid the use of NaOH which could contain traces of CO_2 and carbonate, buffer solutions were prepared under an inert argon atmosphere by adding the appropriate proportion of the acid and basic component of the buffer. This solution was then bubbled for 30 min with $Ar_{(g)}$ and used immediately. The pH was measured with a pH-meter at the end of the experiment. When such care was taken, the activity of the catalyst for HPNPP hydrolysis at pH 7.5 was much higher and under indentical conditions reproducible. However, when the same studies were repeated only 20 minutes later, the activity of the catalyst was already only 40% of the initial one, presumably because it reacted with the CO_2 which dissolved in the buffer solution in that period. When the same studies were repeated one week later using a one-week old buffer, the activity of the complex was only 5% of the initial one (Fig. 128).

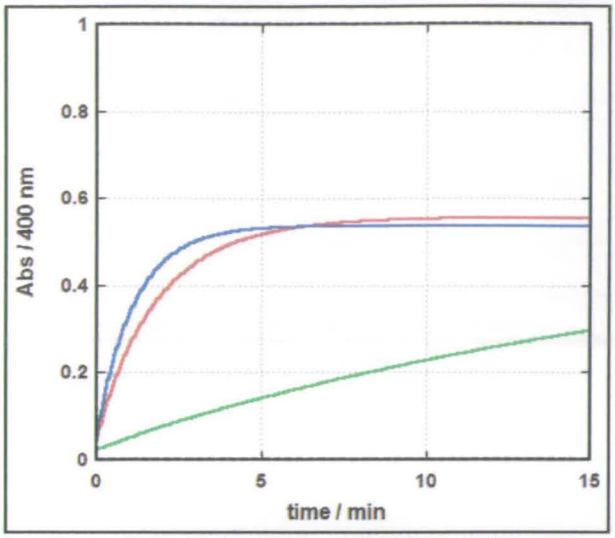

Fig. 128 Experimental curves of the hydrolysis of HPNPP (0.05 mM) at pH 7.5 catalyzed by [Zn_2(LOH')](0.2 mM) in fresh degassed buffer (blue line), in the same buffer after 20 minutes (red line) and in a week-old buffer (green line).

The k_{obs} obtained by fitting the curves in Fig. 128 and the percentage of inhibition by CO_2 are listed in Table 14.

Table 14	k_{obs} (min^{-1})	k_{obs} (s^{-1})	% inhibition
Buffer CO_2-free	0.88	0.015	0
Buffer CO_2-free after 20 min	0.53	0.009	40
Buffer CO_2-free one-week old	0.047	0.0008	95

These results suggest that the dinuclear Zn(II) complex of LOH' is capable of activating and hydrating atmospheric CO_2 as competing reaction. The product of such reaction, the (bi)carbonate anion, competes with the substrate for the catalyst binding site. The inhibitory effect is less evident in acidic solutions and increases by increasing the pH. To prove the inhibitor effect of the carbonate ion, the hydrolysis of HPNPP was monitored at neutral pH in the presence of different amounts of Na_2CO_3 and the inhibition curve is shown in Fig. 129.

The result indicates that the phosphodiester hydrolysis is strongly inhibited at very low concentration of carbonate, in fact for $[CO_3^{2-}] \sim 0.075$ mM the kinetic activity essentially dropped to zero.

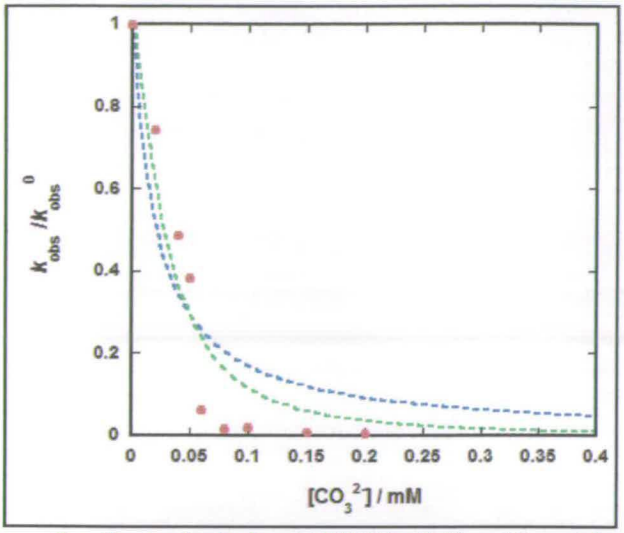

Fig. 129 Inhibition curve for the hydrolysis of HPNPP (0.05 mM) catalyzed by [Zn_2(LOH')]in presence of carbonate a pH 7.4. The dashed blue curve represents the inhibition due to one molecule of carbonate (Eq.86) and the green to two molecules (Eq.87).

$$\frac{k_{obs}}{k_{obs}^0} = \frac{k_{cat}[cat]}{1+\frac{[I]}{K_I}} \cdot \frac{1}{k_{obs}^0} \qquad \textbf{Eq.86}$$

$$\frac{k_{obs}}{k_{obs}^0} = \frac{k_{cat}[cat]}{1+\frac{[I]}{K_I}+\frac{[I]^2}{K_I^2}} \cdot \frac{1}{k_{obs}^0} \qquad \textbf{Eq.87}$$

The slope of the inhibition curve is very steep and could not be fitted to a model involving one or two molecules of carbonate binding to the catalyst (Eq.86 and Eq.87 respectively). The mechanism of CO_2 activation and subsequent carbonate inhibition must be more complex, for example, it could involve precipitation of a carbonate-ZnLOH' complex.

In enzyme catalysis terminology the atmospheric CO_2 acts in this case as a so called "suicide inhibitor". The CO_2 is chemically inactive in the absence of the catalyst but it converts into a powerful irreversible inhibitor using its target catalyst for chemical activation and binding specificity.

The formation of a carbonate complex was confirmed by ESI-MS, ^{1}H and ^{13}C-NMR. First, the ESI-MS spectrum of a solution of LOH' in MeOH/water (50:50) with two equivalents of $Zn(NO_3)_2$ was recorded. The presence of a major peak at *m/z* 702.83 Da (Fig. 130) can be considered to be indicative of the carbonate complex shown, for which the theoretical mass is 703.12 Da. For solutions left in air for longer periods of time, a mass of 766.7 Da consistent with a bis-bicarbonate complex (theoretical mass 788.13 Da) also appeared.

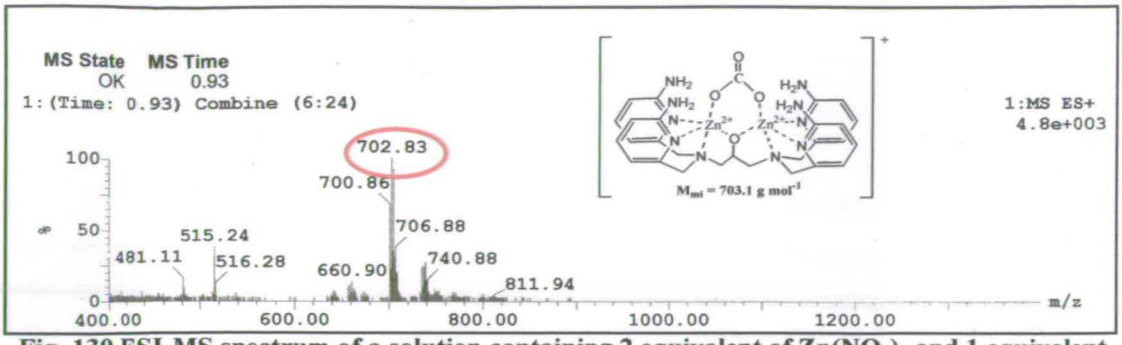

Fig. 130 ESI-MS spectrum of a solution containing 2 equivalent of $Zn(NO_3)_2$ and 1 equivalent of LOH' in MeOH/water (50:50).

To further investigate the existence of carbonate ligands, ^{1}H and ^{13}C-NMR spectra of water solutions of $[H_2Zn_2(LOH')]$ were recorded using an ava800 cryo-probe instrument. All the spectra were recorded in 5% D_2O – 95% H_2O and 50 mM HEPES buffer at pH 7.4. The stock solution of LOH' was in non deuterated methanol and the chemical shifts of MeOH (a few μL) in D_2O (^{1}H = 3.34 ppm and ^{13}C = 49.5 ppm) were used as references in all experiments.

First of all, the ^{1}H-NMR of a 0.2 mM solution of Zn(II)/LOH' (2:1), prepared under inert atmosphere and kept in a sealed NMR tube, was recorded (Fig. 131, black spectrum). In the aromatic region of the spectrum, there are a total of six signals (Table 15): two triplets (7.6 – 7.4 ppm), one broad singlet (≈ 6.8 ppm), a multiplet (≈ 6.63 ppm) (overlapping of two similar doublets) and two doublets (6.6 – 6.5 ppm). It is clear that the geometry of the complex is such that there are two types of pyridines. Then, a 50-fold excess of Na_2CO_3 was added to this sample and the spectrum was recorded again (Fig. 131, red spectrum).

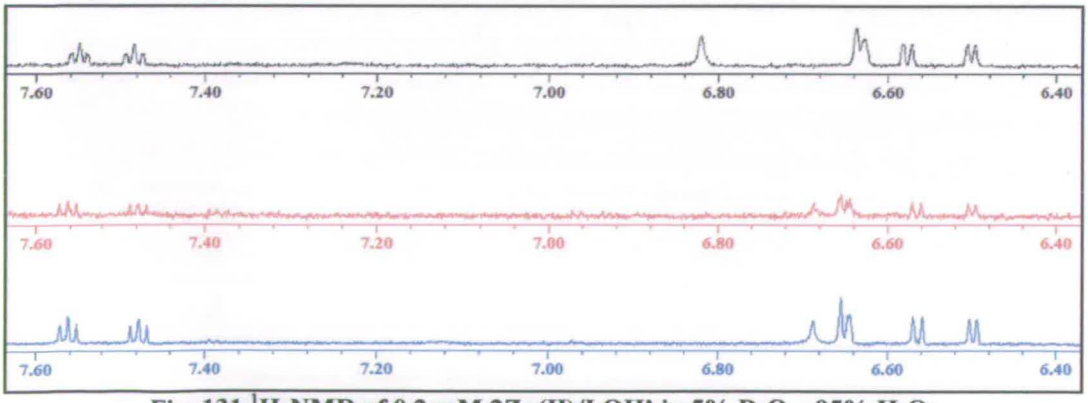

Fig. 131 ^{1}H-NMR of 0.2 mM 2Zn(II)/LOH' in 5% D_2O – 95% H_2O: ■ under Argon, ■ + 10 mM Na_2CO_3; ■ 10 mM Na_2CO_3 +100 μl MeOD.

The intensity of the pyridine signals decreased by about 66% and the singlet at ≈ 6.8 ppm is shifted upfield.

Table 15 - ^{1}H – NMR Chemical Shift / ppm			
t	7.559 - 7.549 - 7.538	7.573 - 7.563 - 7.552	7.571- 7.562 - 7.552
t	7.493 - 7.484 - 7.473	7.485 - 7.479 - 7.470	7.487 - 7.479 - 7.468
s	6.821	6.655	6.687
m	6.637 - 6.626	6.644 - 6.684	6.658 - 6.643
d	6.582 - 6.571	6.571 - 6.560	6.570 - 6.559
d	6.506 - 6.496	6.496 - 6.506	6.504 - 6.495

This suggests the formation of a new a less soluble complex, most likely a neutral carbonate complex which precipitates causing a decrease in the intensity of the NMR signals. Addition of 100 µl of MeOD to this sample restores the signal intensity (Fig. 131, blue spectrum). Similar experiments were done using ^{13}C-NMR. In this case, the spectrum of a 10 mM Na_2CO_3 solution in 50 mM HEPES at pH 7.4 was also recorded (Fig. 132, grey spectrum) and the only signal at 160.78 ppm can be attributed to free bicarbonate.

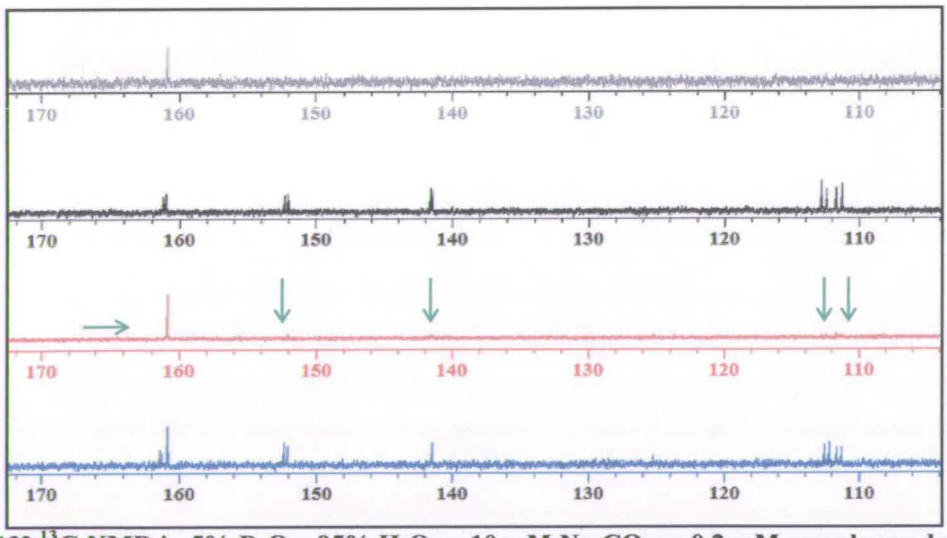

Fig. 132 ^{13}C-NMR in 5% D_2O – 95% H_2O: ■ 10 mM Na_2CO_3; ■ 0.2 mM complex under Ar; ■ 0.2 mM complex + 10 mM CO_3^{2-}; ■ 0.2 mM complex + 10 mM CO_3^{2-} + 100 µl MeOD.

The spectrum of the complex under argon atmosphere (Fig. 132, black spectrum) presents ten signals that can be assigned to specific carbons (Table 16, Fig. 133). The assignment of the chemical shifts was done with the help of a heteronuclear 2D experiment "hsqc_CH" (Fig. 134). It is clear that the signal at 160.78 which appears after the addition of carbonate and MeOD (blue spectrum in

Fig. 132) is not coupled to any hydrogen atom on the pyridine ring and therefore can be assigned to free bicarbonate. It is also clear that addition of carbonate generates a less soluble species which precipitates in water. However at this concentration a signal for the bound carbonate was not detected.

Table 16 - ^{13}C- NMR chemical shifts / ppm

	C			
	5	161.09	--------	161.31
	5	160.94	--------	161.18
160.78			160.78	160.78
	4	152.29	--------	152.29
	4	152.02	--------	152.04
	2	141.55	--------	141.46
	2	141.42	--------	141.42
	1	112.77	--------	112.50
	1	112.40	--------	112.12
	3	111.68	--------	111.64
	3	111.25	--------	111.25

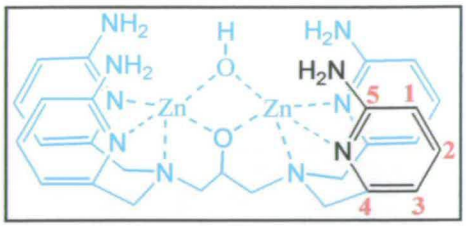

Fig. 133 Numbering scheme used for the pyridine carbon atoms.

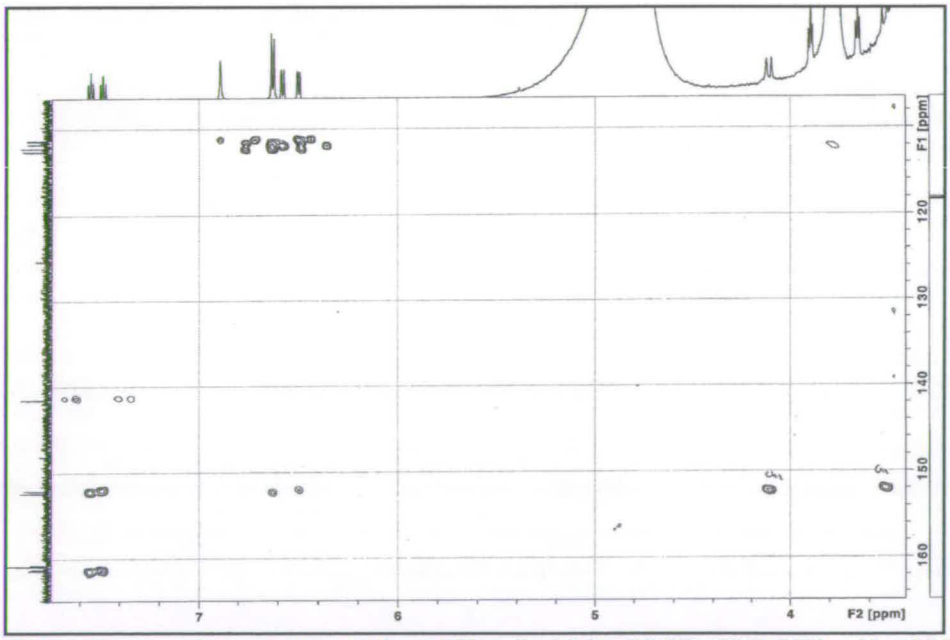

Fig. 134 Heteronuclear 2D experiment "hsqcCH_gs" of 0.2 mM 2Zn(II)/LOH' + 10 mM Na_2CO_3 in 5% D_2O – 95% H_2O + MeOD (≈ 20% of total volume).

In order to improve the intensity of the signals, the concentration of the complex was then increased to 0.5 mM and only one equivalent of Na_2CO_3 was added to the solution. The ^{13}C-NMR spectrum was recorded (Fig. 135). The signal for free (bi)carbonate is not observed, instead a new peak is present at 164.83 ppm assignable

to bound CO_3^{2-}. This confirms that carbonate can bind strongly to the dinuclear Zn(II) complex in such medium.

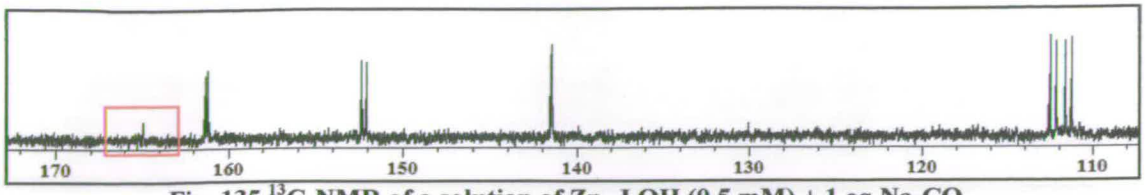

Fig. 135 ^{13}C-NMR of a solution of Zn_2-LOH (0.5 mM) + 1 eq Na_2CO_3 in 5% D_2O – 95% H_2O + 150 µl MeOD.

The chemical shifts assigned to the free bicarbonate and metal-bound carbonate are consistent with those reported in the literature.[131]

Finally, a 0.5 mM sample of Zn_2-LOH' in CO_2-free solvent was prepared under an argon atmosphere and kept in a sealed NMR tube. When this was left opened to air for 20 h the ^{13}C-NMR spectrum had a signal at 164.8 ppm (Fig. 136), consistent with the formation of the carbonate complex.

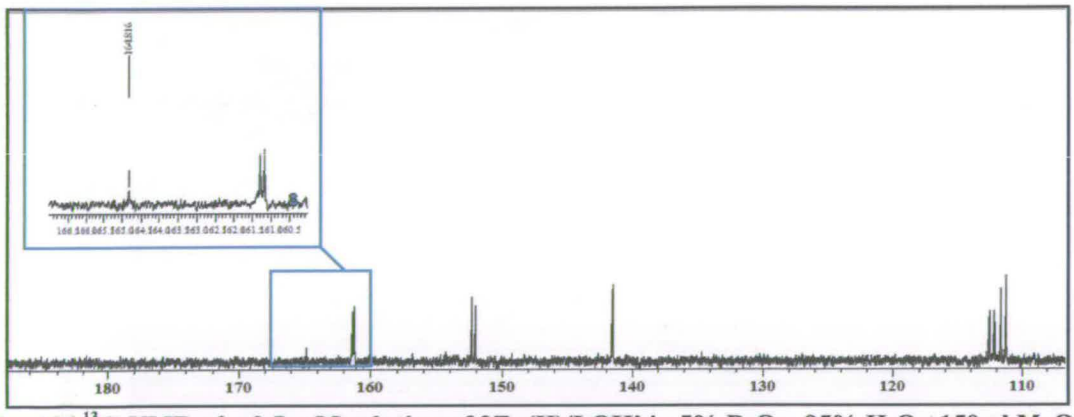

Fig. 136 ^{13}C-NMR of a 0.5 mM solution of 2Zn(II)/LOH' in 5% D_2O – 95% H_2O +150 µl MeOD after 20h of exposition to air.

From these results, it is possible to conclude that the dinuclear zinc complex of LOH' is able to activate atmospheric CO_2.

5.3.1.4 Solvent Kinetic Isotope Effect Studies.

The potential involvement of proton transfers and/or hydrogen bonding in rate determining steps was investigated by carrying out kinetic solvent isotope effects (KSIE) studies. In this case, the KSIE is expressed as the ratio of the rate constant in H_2O and D_2O. If transfer of one or more protons occurs in the rate-limiting step, the reaction rate measured in D_2O will be slower than in H_2O. Similar studies are commonly used as a tool in mechanistic studies in enzymatic reactions.[132] In the last few decades, kinetic solvent deuterium isotope effect experiments have also been applied to study phosphate transfer[133] with simple phosphate esters[134] and with ribozymes.[135] However, the interpretation of solvent isotope effects is not always straightforward, in particular when the reactions are carried out in buffer solution and in the presence of metal ions. In this case the number of protolytic equilibria and proton transfer processes in the reaction can increase.

Cleavage of HPNPP was carried out over a pL (pH or pD) range of 5.5 – 8.7 and followed by recording the absorbance at 400 nm of the released *p*-nitrophenol. The extinction molar coefficient of nitrophenolate (NP) and the pK_a in D_2O were calculated as described for water in the experimental part of this chapter.

The following equation was used to convert pH into pD:

$$pD = pH + 0.4 \qquad \textbf{Eq.88}$$

The results gave ε_{NP} (D_2O) = 9985 M^{-1} cm^{-1} and pK_a (D_2O) =7.2.

Simple visual inspection of Fig. 137 shows a large and unusual solvent KIE, the magnitude of which varies somewhat with the increasing of the pH (Table 17). Overall there is a *normal* isotope effect ($k_{obs}^{H} > k_{obs}^{D}$) that implies a loosening at hydrogenic sites upon formation of the transition state.

In D_2O one would expect a catalytic mechanism similar to that observed in water and consequently a similar pD-rate profile. However, the pD profiles seems to be almost constant over the range investigated. The cleavage reaction in D_2O is much slower than in H_2O and the magnitude of the KIE is considerable at the pL-independent region (pL ≥ 7).

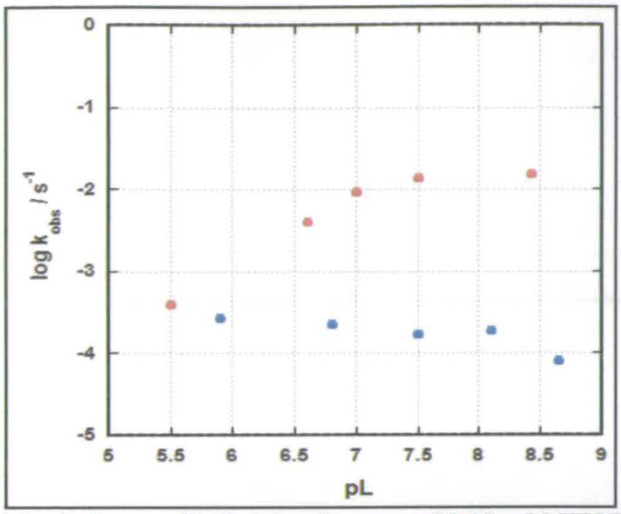

Fig. 137 pL-k_{obs} profile for the cleavage of 0.05 mM HPNPP by 0.2 mM catalyst in H_2O (red dots) and D_2O (blue dots) solutions.

Table 17 - SKIE – pL dependence	
pL	**k_H/k_D**
6	6
7	17
7.5	81
8	97
8.5	186

Such high SKIE seems unjustifiable. The presence of high carbonate concentration in the D_2O may be the reason of such difference in reactivity in the two solvents. It has been shown that CO_2 is somehow more soluble in D_2O than in H_2O ($\chi CO_2^D/\chi CO_2^H = 1.13$),[136] but this should not matter as CO_2 is eliminated from the buffer solutions (*vide supra*). High k_H/k_D KIE effects usually arise from large hydrogen transfer distances or conformational changes that affect the binding affinity of the catalyst for its substrate. Part of the anomalous magnitude of the isotope effect observed could result from the sum of different individual KIEs. The fitting of the saturation curve in D_2O (Fig. 138), however, gives a $K_M^D = 0.28$ mM. This suggests that the isotopic effect on binding is very small ($K_M^H = 0.32$ mM).

The existence of a solvent deuterium isotope effect on the rate constant permits quantification of the number of protons transferred in the rate-limiting step. In an attempt to determine this number, proton inventory experiments were performed by measuring the relative cleavage rate for different D_2O fractions (n) from 0 to 1.

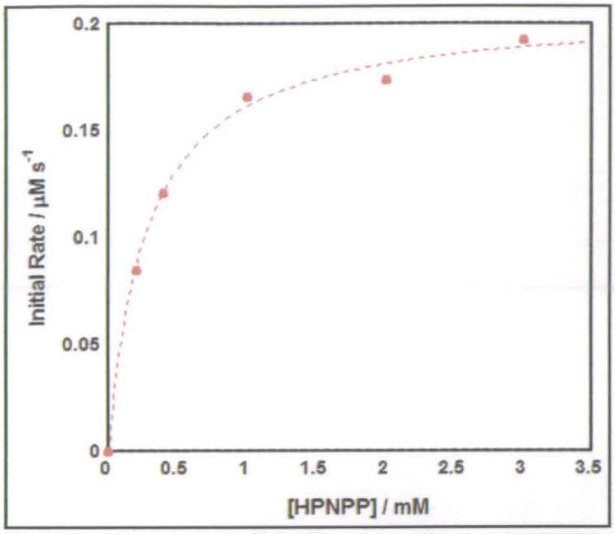

Fig. 138 Saturation curve in D_2O for the hydrolysis of HPNPP (0.05 mM) (HEPES 50 mM, pD = 7.4) in the presence of 0.2 mM catalyst.

The use of mixed isotopic waters is equivalent to separating the overall solvent isotope effect into the contributions that are produced at individual structural sites.[137] The experiments were carried out at pL 7.4 and pL determined using the following equation:

$$pL = pH_{reading} - (\Delta pH)_n \qquad \textbf{Eq.89}$$

where $(\Delta pH)_n = 0.076n^2 + 0.3314n$ and n is the deuterium fraction factor.[137]

The curvature of the plot of $k_{obs(n)}/k_{obs(0)}$ versus n is particularly informative. This can be estimated using the *midpoint* solvent isotope effects (n = 0.5). This gives an idea of which models fit the curve. Data collected for n values of 0, 0.5 and 1 gave the plot shown in Fig. 139. At this pL the overall isotope effect is 81 and the curve appears bowl-shaped. The curvature is very large, as in the middle point the activity is practically zero. For this reason the data cannot be fitted to equations involving one, two or more protons being transferred. In general, the solvent KIE can be predicted as:

$$\frac{k_D}{k_H} = \frac{\prod_i (1 - n + \phi_i^{TS} n)}{\prod_j (1 - n + \phi_j^{GS} n)} \qquad \textbf{Eq.90}$$

where $\prod_i \phi^{TS}$ and $\prod_j \phi^{GS}$ are the product of the fraction factors (φ) for all exchangeable *i* and *j* protons (H, D) in the transition (TS) and ground state (GS).

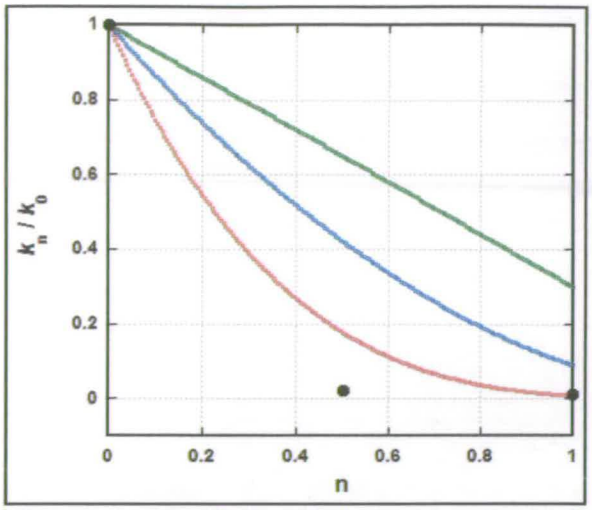

Fig. 139 Ratios of initial rates measured in mixed isotopic solvents (k_n) over the initial rate measured in water (k_0) plotted against the atom fraction of deuterium (n). The curves represent the fit to 1 (green), 2 (blue) and 4 (red) proton transfers in the TS.

The fraction factors refer to the tightness of bonding and generally the heavier isotope accumulates in the stronger bond. If one proton is transferred in the transition state, k_n/k_0 has a linear dependence on n, if two protons are transferred the dependence is quadratic and so on. The curves generated by using Eq.91-93 involving the transfer of one, two and four protons in the transition state are plotted in Fig. 139 (the fraction factor (φ) used for the plot was 0.3).

$$\frac{k_n}{k_0} = 1 - n + n\phi \qquad \textbf{Eq.91}$$

$$\frac{k_n}{k_0} = (1 - n + n\phi)^2 \qquad \textbf{Eq.92}$$

$$\frac{k_n}{k_0} = (1 - n + n\phi)^4 \qquad \textbf{Eq.93}$$

Many factors may be contributing towards this unusually large SKIE. Some could be: existence of more than a proton "in flight", geometry rearrangements, pK_a

shifts, exchangeable protons of the amino groups on the ligand and subsequent hydrogen bonds with maybe tunnelling,[138] precipitation of isoluble carbonates complexes, etc. Further studies are required to fully elucidate this aspect.

However the reliability and the singularity of the data collected for the system 2Zn(II)/LOH' was checked by carrying out solvent KIE experiments with similar ligands. The overall solvent kinetic isotope effect of two systems was examined: 2Zn(II)/LOH and Zn(II)/tpa-$(NH_2)_3$. The results gave an SKIE of 1.7 and 2 respectively and the proton inventory showed linear dependence for both systems. In this case the mechanism is simple and involves only one proton in flight.

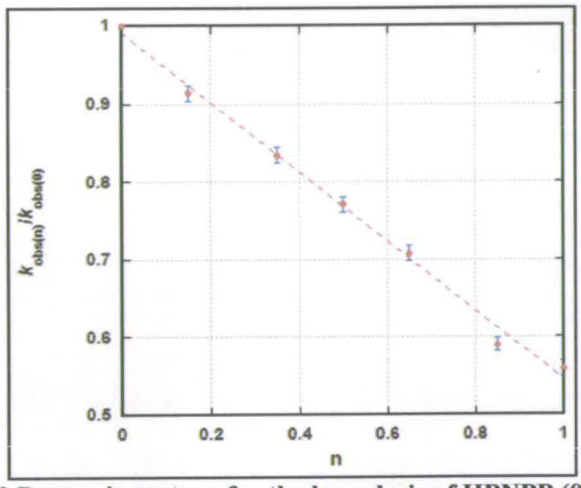

Fig. 140 Proton inventory for the hysrolysis of HPNPP (0.2 mM) catalyzed by 1 mM [Zn_2(LOH)] at pL 7.4.

5.3.1.5 Nuclease activity of the ligand LOH' with different divalent metals for HPNPP hydrolysis.

The spectacular catalytic activity of many natural and artificial nucleases is due to the presence of one or more metal ions in the active site. During the last years several examples of dinuclear complexes with Ni(II), Cu(II), Fe(II), Cd(II) and Co(II) able to hydrolyze phosphoesters bonds have been reported[139] and sometimes found to be more reactive than the corresponding Zn(II) complexes.[139b] Thus, the rate of hydrolysis of HPNPP was investigated in the presence of dinuclear complexes of the ligand LOH' with different divalent metal ions: Co(II), Cd(II), Cu(II) and Ni(II). The experiments were carried out in water, pH 7.4 (HEPES 50 mM) at 25 °C in the presence of 0.2 mM catalyst (0.05 mM in case of Ni(II)) and 0.05 mM substrate. The results are shown in Fig. 141.

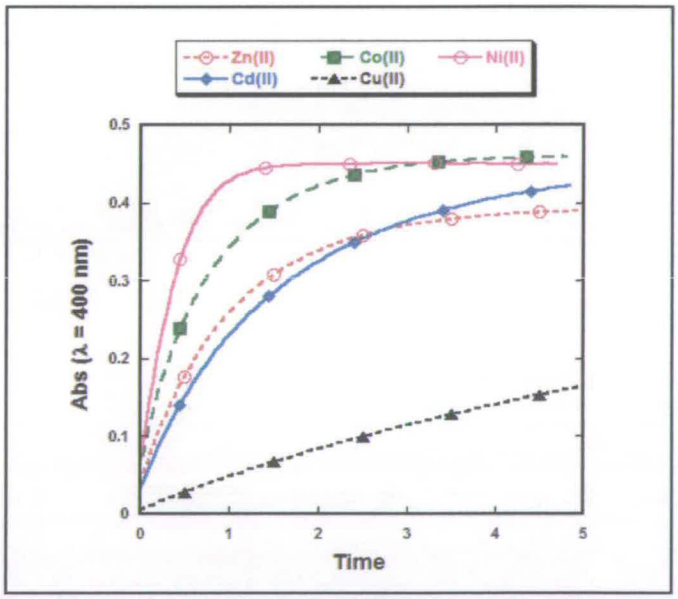

Fig. 141 Experimental curves of the hydrolysis of HPNPP catalyzed by complexes of LOH' with different divalent metals.

All metal complexes hydrolyzed HPNPP and their catalytic activity decreases in the order: Ni(II) >> Co(II) > Zn(II) > Cd(II) >> Cu(II). The least-squares fitting of the curves in Fig. 141 gives the k_{obs} values reported in Table 18.

Unexpectedly, the nickel complex is the most reactive catalyst; so effective that its concentration had to be lowered to 0.05 mM.

Table 18			
M(II)	**[cat] mM**	**k_{obs} /min^{-1}**	**K_{obs} / s^{-1}**
Ni	0.05	2.64	0.044
Co	0.2	1.20	0.02
Zn	0.2	0.94	0.016
Cd	0.2	0.64	0.011
Cu	0.2	0.10	0.002

It is interesting to find that the Zn(II) complex is only third in reactivity. SKIE was also checked for all these metal complexes and results listed in Table 19.

Table 19			
M(II)	**k_{obs} /min^{-1} H_2O**	**k_{obs} /min^{-1} D_2O**	**SKIE**
Ni	2.64	0.69	4
Co	1.20	0.01	96
Zn	0.94	0.005	176
Cd	0.64	0.25	2.5
Cu	0.10	/	/

The Co(II) and Zn(II) complexes give rise to anomalously high SKIE, whereas Ni(II) and Cd(II) lead to more normal solvent isotope effects. Interstingly, the hydrolysis of HPNPP using these metal complex catalysts was strongly inhibited by the presence of CO_2 only when the metal used is Zn(II) or Co(II). Thus, the suggestion that the large SKIE found could be due to the formation of insoluble carbonate complexes seems reasonable. The difference in reactivity found could reflect the geometrical preferences of the complexes and/or different mechanism of catalysis.

5.3.2 Nuclease-like activity of the L^1OH'-Zn(II) complex.

The hydrolysis of HPNPP by the L^1OH'-zinc complexes was carried out in water at pH 7.4 under reaction conditions similar to those used for the ligand LOH' ([cat] = 0.2 mM and [HPNPP] = 0.05 mM).

First of all, in order to identify the stoichiometry of the active species in solution, the dependence of the hydrolysis rate on the number of equivalents of Zn(II) was investigated. In this case, potentiometric titrations showed that this ligand is able to form dinuclear and mononuclear Zn(II) complexes. Moreover the mononuclear complexes are the main species at neutral pH even when the M to L ratio is 2:1 (see Chapter 4).

The dependence of the reaction rate on the Zn(II):L^1OH' ratio is illustrated in Fig. 142. It shows that zinc complexes of the ligand L^1OH' are effective catalysts for the hydrolysis of HPNPP and that the maximum reactivity is reached when the Zn(II)/L^1OH' ratio is one. This value remains constant up to Zn(II)/L^1OH' = 3, when a white precipitate appears.

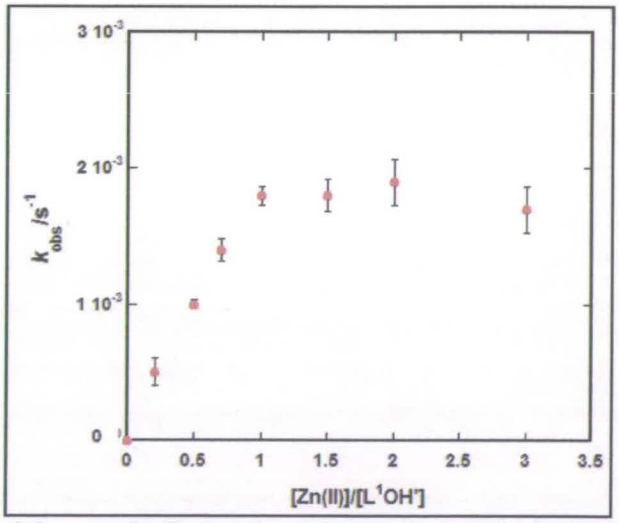

Fig. 142 Dependence of the pseudo-first-order rate constant on the Zn(II)/L^1OH' ratio at pH 7.4 and 25°C. [HPNPP] = 0.05 mM, [cat] = 0.2 mM and [HEPES] = 50 mM.

According to the potentiometric pH titrations, at pH 7.4 and M/L = 1 only a mononuclear complex is present and consequently at this ratio this species is responsible for all of the catalytic activity observed. When the ratio M/L is 2 and pH 7.4, mononuclear and dinuclear complexes are both present and the activity may therefore arise from both.

More information about the source of the catalytic activity can be obtained analysing the pH-dependence of the reaction rate at M/L =1 and M/L=2 (Fig. 143).

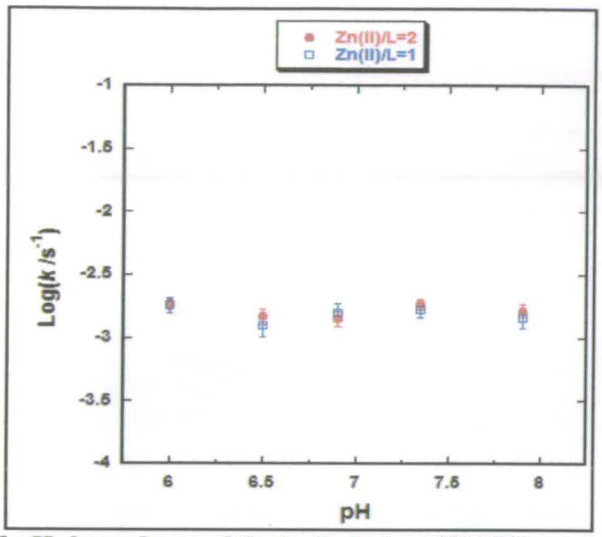

Fig. 143 pH-dependence of the hydrolysis of HPNPP catalyzed by in presence of one (□) and two (●) equivalents.

The observed rate constant k_{obs} remains constant over the entire pH range investigated. Inspection of the species distribution diagram under the conditions used for kinetic experiments (Fig. 144 and Fig. 145) reveals that there are only four species to consider:

- Mononuclear complexes: $\left[HZn(L^1OH')\right]^{3+}$ and $\left[Zn(L^1OH')\right]^{2+}$
- Dinuclear complexes: $\left[H_{-1}Zn_2(L^1OH')\right]^{3+}$ and $\left[H_{-2}Zn_2(L^1OH')\right]^{2+}$

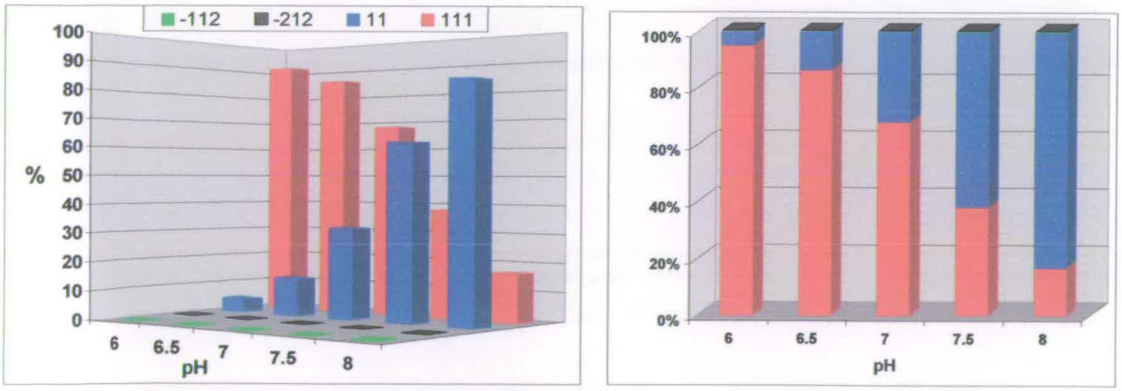

Fig. 144 Relative percentage of complexes present in a solution of Zn(II)/L^{1}OH' = 1, in water at 25°C (HEPES 50mM) in the pH 6-8 range.

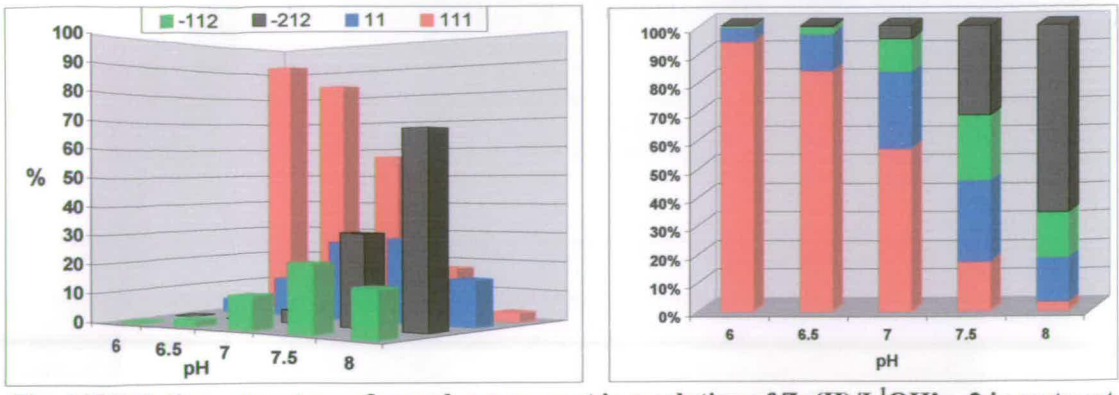

Fig. 145 Relative percentage of complexes present in a solution of Zn(II)/L^{1}OH' = 2 in water at 25°C (HEPES 50mM) in the pH 6-8 range.

When the metal:ligand ratio is 1:1, increasing the pH converts $\left[HZn(L^1OH')\right]^{3+}$ (1,1, 1) into $\left[Zn(L^1OH')\right]^{2+}$ (0,1,1). Since k_{obs} (1.9×10^{-3} s^{-1}) does not change, both mononuclear complexes must be equally active. Under identical conditions k_{obs} for the mononuclear Zn(II) complexes of tripodal ligands with two and three amino hydrogen bonding groups (Fig. 146) were 1.6×10^{-5} s^{-1} (TPA-$(NH_2)_3$) and 1.2×10^{-5} s^{-1} (BAPMAE). This is important because (prior to this work) these were the most effective mononuclear Zn(II) complexes for HPNPP hydrolysis. Thus, the metal-free DPA unit with two amino hydrogen bonding groups in L^{1}OH' provides a further two orders of magnitude increase in k_{obs}, presumably because it allows additional catalytically-important hydrogen bonding interactions.

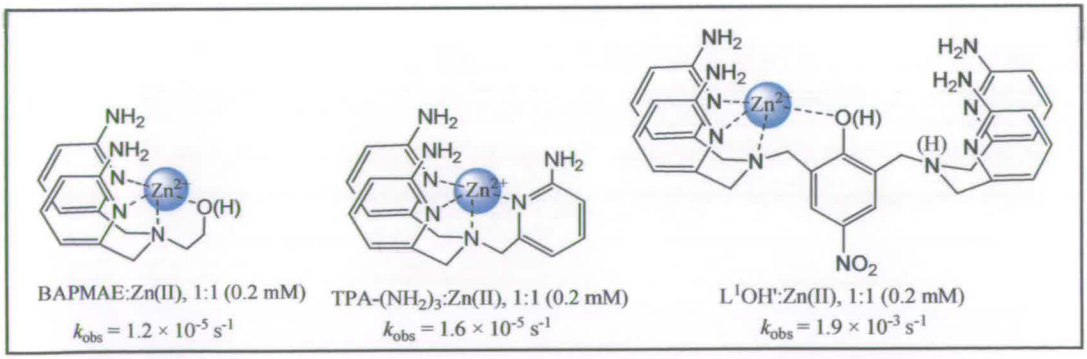

Fig. 146 Comparison of k_{obs} for ligands with amino hydrogen bonding groups.

When the metal:ligand ratio is 2:1, the activity due to $\left[Zn(L^1OH')\right]^{2+}$ under 1:1 conditions is now due to $\left[Zn(L^1OH')\right]^{2+}$ (0 1 1) and $\left[H_{-1}Zn_2(L^1OH')\right]^{3+}$ (-1 1 2) and $\left[H_{-2}Zn_2(L^1OH')\right]^{2+}$ (-2 1 2).

Since the reactivity does not change as the metal:ligand ratio changes from 1:1 to 2:1, the mononuclear complexes must be as reactive as the dinuclear complexes. The rate constant for the transesterification reaction (k_{obs}) shows first-order dependence on catalyst concentration (Fig. 147). The slope of the graph gives the second-order rate constant of 0.009 M^{-1} s^{-1}.

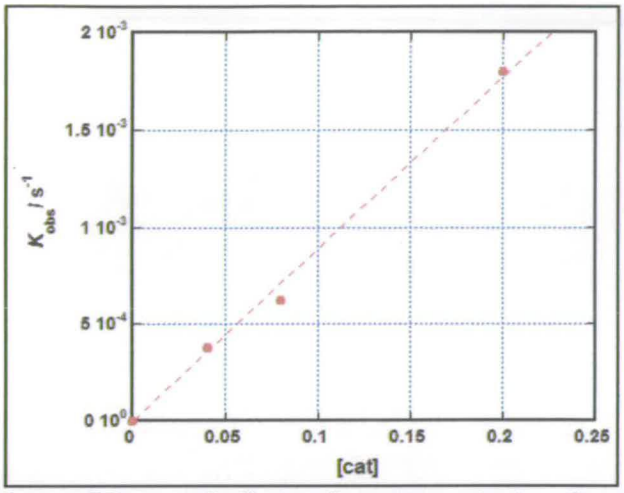

Fig. 147 Dependence of the pseudo-first-order rate constant on the concentration of [Zn(L^1OH')] at pH 7.4 and 25°C ([HEPES buffer] = 50 mM).

The same linear dependence has been observed in the presence of two equivalents of Zn(II). The plot of the initial rates as a function of substrate concentration deviates from Michaelis-Menten kinetics at high concentration of HPNPP ([HPNPP] ≥ 1 mM) (Fig. 148).

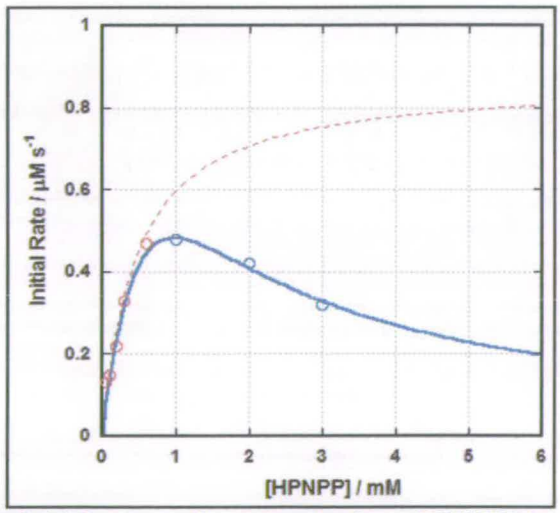

Fig. 148 Dependence of the initial rate on the concentration of HPNPP in presence of 0.2 mM [Zn(L^1OH')] at pH 7.4 and 25°C (HEPES buffer = 50 mM).

This behaviour is typical of substrate inhibition. This type of uncompetitive inhibition is quite common in natural enzymes and it is primarily caused by the binding of more than one molecule of substrate to the catalyst, which gives an inactive complex. If this assumption is valid, the experimental data can be fitted with the following equation:

$$v = \frac{V_{max}[S]}{K_M + [S]\left(1 + \frac{[S]}{K_S}\right)} \qquad \text{Eq.94}$$

where v is the initial rate ($\mu M\ s^{-1}$), V_{max} ($=k_{cat}$ [cat]) represents the maximum reaction rate without inhibition ($\mu M\ s^{-1}$), K_M is the Michaelis-Menten constant (mM) and K_S is the dissociation constant of the second molecule of substrate (mM). Fig. 148 shows the data fitting with the Eq.94 (blue curve) and the theoretical Michaelis-Menten behaviour (red curve).

The fit in presence of substrate inhibition gives $k_{cat} = 0.0063\ s^{-1}$, $K_M = 0.76$ mM and $K_S = 1.15$ mM. Substrate inhibition does not appear confined to the mononuclear system: a high concentration of substrate also inhibited the hydrolysis reaction in the presence of two equivalents of Zn(II) (Fig. 149). In this case the fit to Eq.94 gives the following parameters: $k_{cat} = 0.0036\ s^{-1}$, $K_M = 0.36$ mM and $K_S = 1.36$ mM. The decrease in K_M suggests that the dinuclear species binds the substrate more tightly.

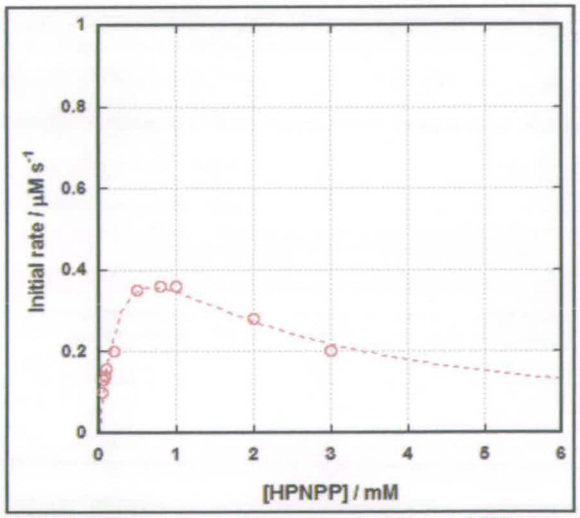

Fig. 149 Dependence of the initial rate on the concentration of HPNPP in presence of 0.2 mM [$Zn_2(L^1OH')$] at pH 7.4 and 25°C (HEPES buffer = 50 mM).

It can be assumed, however, that the observed rate constants determined at low substrate concentration ([HPNPP] < 0.1 mM) are relatively unaffected by inhibition, thus the pH profile previously shown is valid.

A summary of the kinetic parameters of solutions containing L^1OH' and one or two equivalents of Zn(II) is reported in Table 20.

Table 20	**Zn(II)/L^1OH' = 1**	**Zn(II)/L^1OH' = 2**
k_{cat} (s^{-1})	0.0063	0.0036
K_M (mM)	0.76	0.36
K_S (mM)	1.15	1.36
K_S/K_M	1.5	3.8
k_{cat}/K_M (M^{-1} s^{-1})	8.3	10

The concentration of the catalytic complex (ES) as a function of the substrate concentration depends on the ratio K_S/K_M. A low value of K_S/K_M indicates high inhibition and lower concentration of the active complex ES at the equilibrium. In this case, substrate inhibition is more significant for the mononuclear complexes although k_{cat} is higher. The catalytic efficiency k_{cat}/K_M of mono and dinuclear complexes is, however, comparable (8 and 10 M^{-1} s^{-1}).

The less tight binding of the substrate ($K_M^1 > K_M^2$) and the metal-free chelating unit could facilitate the approach and binding of a second molecule of HPNPP. The geometry optimizations obtained for mononuclear and dinuclear complexes of ligand L^1OH' are shown in Fig. 150.

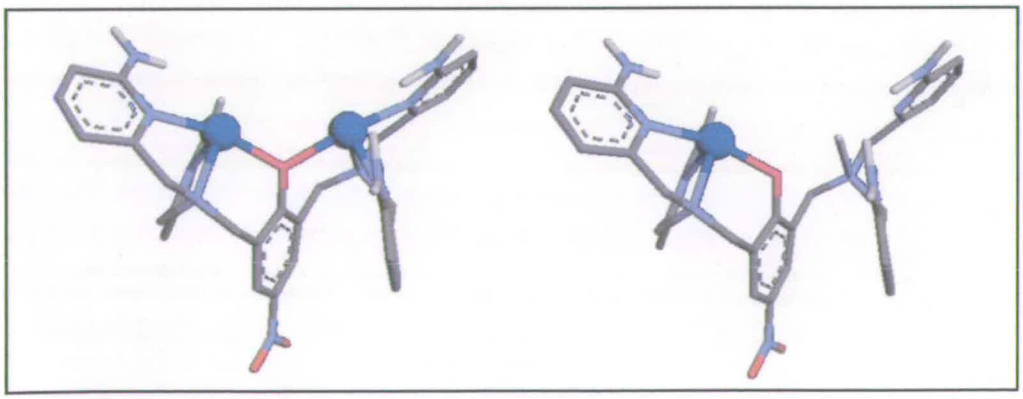

Fig. 150 Geometry optimization of dinuclear (left) and mononuclear (right) zinc complexes of ligand L^1OH'.

The ability of the Zn(II) complexes of the ligand L[1]OH' to bind another phosphate diester, DMP, was also investigated. For this, the catalytic activities toward HPNPP hydrolysis in solutions with one and two equivalents of Zn(II) were measured in the presence of increasing amounts of DMP. The inhibition curve obtained are shown in Fig. 151 and the fit give K_I^1 =2.8 mM and K_I^2 = 2.1 mM.

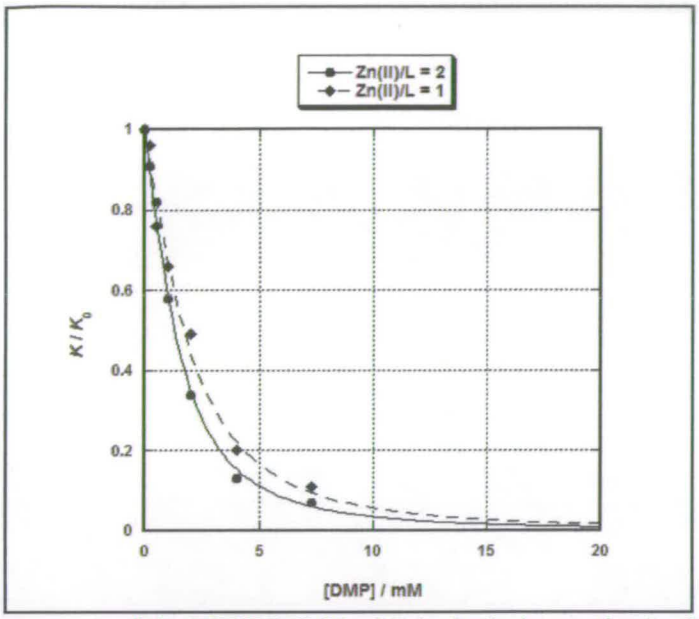

Fig. 151 Inhibition curves of the HPNPP (0.05 mM) hydrolysis reaction by 0.2 mM L[1]OH' in presence of one (♦) and two (●) equivalents of Zn(II) at pH 7.4 and 25°C.

The higher values (weaker binding) obtained for K_I compared to K_M suggests that these catalysts form additional interactions with the substrate. It is also important to note that in this case the reactivities measured in freshly prepared buffer solutions and bubbled with $Ar_{(g)}$ and old buffer solutions gave same results. This suggests that this ligand framework leads to complexes which are selective for phosphate ester hydrolysis over CO_2 activation and hydrolysis.

5.4 Conclusions.

In summary, the nuclease-like behaviour of zinc complexes of two dinucleating ligands (LOH' and L[1]OH') has been investigated on simple RNA model substrates (HPNPP and UpU).

The ligand LOH' at neutral pH forms a dinuclear zinc complex which possesses excellent catalytic ability for the hydrolysis of both substrates; a 10^6-fold rate acceleration, which makes it the most effective Zn(II) complex reported to date for phosphate diester hydrolysis. In deuterated water, the rate of hydrolysis is much slower and a very large SKIE was observed (ca. 80). The rate of phosphate diester hydrolysis is also considerably faster when the experiments are carried out under CO_2-free conditions.

^{13}C-NMR experiments showed that in water the complex $[H_2Zn_2(LOH')]^{2+}$ is able to activate atmospheric CO_2 to form an insoluble carbonate complex. When other divalent metals are used the rate of hydrolysis of HPNPP followed the order: Ni(II) >> Co(II) > Zn(II) > Cd(II) >> Cu(II). Interestingly, a 'normal' isotope effect is observed for Ni(II) or Cd(II), and with these metals atmospheric carbonic dioxide does not affect the rate of phosphate diester hydrolysis.

A general base catalysis mechanism was also found for the zinc mononuclear complex of a derivative of tpa provided with three amino hydrogen bonding functionalities. The SKIE of 2 and a linear dependence on the deuterium fraction observed during this work for such complex, indicate transferring of one proton in the rate-determining step. The corresponding reaction mechanism was studied recently by DFT methods.[140] This study suggest a mechanism involving general base catalysis in which the substrate binds to the zinc complex by coordinating to zinc and by hydrogen-bonding to the ligand. Then, the hydroxyl group of the substrate attacks the phosphorous and transfers its proton to the metal-coordinated hydroxide. Before the cleavage of the phosphodiester bond occurs, the generated coordinating water rotates and hydrogen-bonds to the phenolate oxygen. This rotation is the rate-determining step and the proton transfer through could be responsible for the observed SKIE.

Zinc complexes of the ligand L^1OH' also effectively cleave HPNPP. Interestingly, this ligand showed a different behaviour compared to LOH'. First of all, despite its dinucleating nature, L^1OH' forms a stable mononuclear zinc complex which, at neutral pH, is always present as the main species irrespective of the metal-to-ligand ratio. The rate of hydrolysis of HPNPP is two orders of magnitude faster than with previously reported mononuclear complexes with aminopyridyl hydrogen

bonding groups. When the pH is raised and the Zn(II):L^1OH' ratio is 2:1 dinuclear complexes are formed. These are as effective as the mononuclear ones. Notably, complexes of L^1OH bind the substrate HPNPP more strongly than other phosphate diesters like DMP. This suggests they form additional interactions with HPNPP, which seem to be catalytically important. Moreover, these complexes are not affected by atmospheric CO_2. Thus, these metal complex catalysts seem to be selective for phosphate diester hydrolysis.

In conclusion, for the first time the cooperation of metal ions and hydrogen bonding groups has been successfully applied to create the most effective dinuclear Zn(II) complex for phosphate diester hydrolysis. Moreover, and also for the first time the ability of dinucleating ligands to create extraordinarily effective and selective mono and dinuclear catalysts for this reaction has been reported.

5.5 Future work.

The promising results obtained during this thesis work leave plenty of scope for further investigations.

First of all, a detailed mechanistic study could be carried out with the help of computational calculations and supported by additional experimental data using isotopic solvents and/or isotopically labelled substrates and catalysts.

The nuclease-like activity of such promising catalyst needs surely be tested on natural substrates such as small oligonucleotides and RNA in view of practical applications. For this purpose, in addition to efficiency, the achievement of selectivity is an important goal. A new strategy to achive this could be using Zn(II)-Cyclen to bind specifically to uridine-rich regions of target RNA (e.g. HIV-TAR). This metal complex would then be used to bring the catalyst in close proximity to a specific phosphodiester bond (Fig. 152).

Attachment of these and related catalysts to nanoparticles, peptides and antisense oligonucleotides could also be interesting to further enhance activity and selectivity.

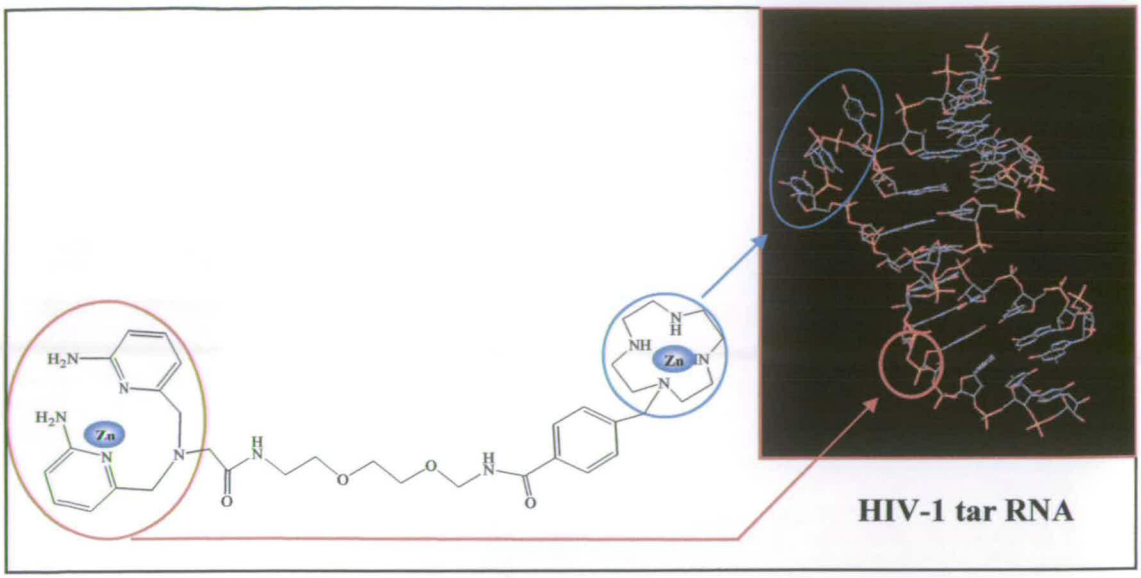

Fig. 152 Selective phosphodiester cleavage (red circle) achieved by specific metal coordination to a bulge uridine-rich of the target HIV-1 tar RNA.

Another interesting characteristic worth exploring will be the activation and hydrolysis of atmospheric CO_2 using these and similar metal complex catalysts.

References

[1] **a)** Morrow, J. R. and Iranzo, O., *Curr. Opin. Chem. Biol.*, **2004**, *8*, 192; **b)** Trawick, B. N., Daniher, A. T. and Bashkin, J. K., *Chem. Rev.*, **1998**, *98*, 939.

[2] **a)** Cowan, J. A., *Curr. Opin. Chem. Biol.*, **2001**, *5*, 634; **b)** Morrow, J. R. and Iranzo, O., *Curr. Opin. Chem. Biol.*, **2004**, *8*, 192; **c)** Lönnberg, T., *Curr. Opin. Chem. Biol.*, **2005**, *9*, 665; **d)** Mancin, F., Scrimin, P., Tecilla, P. and Tonellato, U., *Chem. Commun.*, **2005**, 2540.

[3] Krämer, R., *Coord. Chem. Rev.*, **1999**, *182*, 243.

[4] Feng, G., Natale, D., Mareque-Rivas, J. C. and Williams, N. H., *Angew. Chem. Int. Ed.*, **2006**, *45*, 7056.

[5] Williams, N. H., Takasaki, B., Wall, M. and Chin, J., *Acc. Chem. Res.*, **1999**, *32*, 485.

[6] **a)** Linn, S. and Arber, W., *Proc. Natl. Acad. Sci., USA*, **1968**, *59*, 1300; **b)** Arber, W. and Linn, S., *Annu. Rev. Biochem.*, **1969**, *38*, 467.

[7] Kimura, E., *Curr. Opin. Chem. Biol.*, **2000**, *4(2)*, 207.

[8] Chelan, W. and Hengge, A. C., *Chem. Rev.*, **2006**, *106(8)*, 3252.

[9] Sowadski, J. M., Handschumacher, M. D., Murthy, H. M. K., Foster, B. A. and Wykoff, H. W., *J. Mol. Biol.*, **1991**, *218*, 449. Crystal structure from www.phosphatase.net.

[10] Cotton, F. A., Hazen, E. E. and Legg, M. J., *Proc. Natl. Acad. Sci., USA*, **1979**, *76(6)*, 2251.

[11] Volbeda, A., Lahm, A., Sakiyama, F. and Suck, D., *EMBO J.*, **1991**, *10*, 1607.

[12] Cassano, A. G., Anderson, V. E. and Harris, M. E., *Biopolymers*, **2004**, *73*, 110.

[13] Chin, J., Banaszczyk, M., Jubian, V. and Zou, X., *J. Am. Chem. Soc.*, **1989**, *111*, 186.

[14] Bertini, I., Sigel, A. and Sigel, H., *Handbook on Metalloproteins, Marcel Dekker Inc.: New York*, **2001**.

[15] Roigk, A., Hettich, R. and Chneider, H. J., *Inorg. Chem.*, **1998**, *37*, 751.

[16] **a)** Sumaoka, J., Azuma, Y. and Kamiyama, M., *Chem. Eur. J.*, **1998**, *4*, 205; **b)** Sumaoka, J, Igawa, T., Furuki, K. and Komiyama, M., *Chem. Lett.*, **2000**, *29*, 56.

[17] Cowan, J. A., *Curr. Opin. Chem. Biol.*, **2001**, *5*, 201.

[18] Morrow, J. R., Buttery, L. A., Shelton, V. N. and Berback, K. A., *J. Am. Chem. Soc.*, **1992**, *114*, 1903.

[19] Hay, R. W. and Govan, N., *Polyhedron*, **1997**, *24*, 4233.

[20] Hayashi, N., Takeda, N., Shiiba, T., Yashiro, M., Watanaba, K. and Koniyama, M., *Inorg. Chem.*, **1993**, *32*, 5899.

[21] Bligh, S. W. A., Choi, N., Evagorov, E. G., McPartlin, M. and White, K. N., *J. Chem. Soc., Dalton Trans.*, **2001**, 3169.

[22] Igawa, T., Sumaoka, J. and Komiyama, M., *Chem. Lett.*, **2000**, *29*, 356.

[23] Spiro, T. G., Farrell, F. J. and Kjellstrom, W. A., *Science*, **1969**, *164*, 320.

[24] **a)** Chin, J, Banaszczyk, M., Jubian, V. and Zou, X., *J. Am. Chem. Soc.*, **1989**, *111*, 186; **b)** Tafesse, F., Massoud, S. S. and Milburn, R. M., *Inorg. Chem.*, **1993**, *32*, 1864; **c)** Dixon, N. E., Geue, R. J., Lamnert, J. N., Moghaddas, S., Pearce, D. A., Sargeson, A. L., *Chem. Commun.*, **1996**, 1287.

[25] Chin, J., *Acc. Chem. Res.*, **1991**, *24*, 145.

[26] Kim, J. H. and Chin, J., *J. Am. Chem. Soc.*, **1992**, *114*, 9792.

[27] De Rosch, M. A. and Trogler, W. C., *Inorg. Chem.*, **1990**, *29*, 2409.

[28] Koike, T. and Kimura, E., *J. Am. Chem. Soc.*, **1991**, *113*, 8935.

[29] Bonfà, L., Gatos, M, Mancin, F., Tecilla, P. and Tonellato, U., *Inorg. Chem.*, **2003**, *42*, 3943.

[30] Hegg, E. L. and Burstyn, J. N., *Inorg. Chem.*, **1996**, *35*, 7474.

[31] Itoh, T., Hisada, H., Sumuya, T., Hosono, M., Usui, Y. and Fujii, Y., *Chem. Commun.*, **1997**, 677.

[32] **a)** Sreedhara, A., Cowan, J. A., *Chem. Commun.*, **1998**, 1737; **b)** Sreedhara, A., Freed, J. D., Cowan, J. A., *J. Am. Chem. Soc.*, **2000**, *122*, 8814.

[33] Liu, C., Wang, M., Zhang, T. and Sun, H., *Coord. Chem. Rev.*, **2004**, *248*, 147.

[34] **a)** Chapman, W. M., Jr. and Breslow, R., *J. Am. Chem.. Soc.*, **1995**, *117*, 5462; **b)** He, C. and Lippard, S. J., *J. Am. Chem. Soc.*, **2000**, *122*, 184.

[35] Chin, J., *Curr. Opin. Chem. Biol.*, **1997**, *1*, 514.

[36] Yashiro, M., Ishikubo, A. and Komiyama, M., *J. Chem. Soc., Chem. Commun.*, **1995**, 1793.

[37] Yashiro, M., Ishikubo, A. and Komiyama, M., *Chem. Commun.*, **1997**, 83.

[38] Iranzo, O., Kovalevsky, A. Y., Morrow, J. R. and Richard, J. P., *J. Am. Chem. Soc.*, **2003**, *125*, 1988.

[39] Iranzo, O., Richard, J. P., Morrow, J. R., *Inorg. Chem.*, **2004**, *43(5)*, 1743.

[40] Iranzo, O., Elmer, T., Richard, J. P. and Morrow, J. R., *Inorg. Chem.*, **2003**, *42*, 7737.

[41] O'Donoghue, A., Pyun, S.Y., Yang, M.-Y., Morrow, J. R. and Richard, J. P., *J. Am. Chem. Soc.*, **2006**, *128*, 1615.
[42] Rossi, P., Felluga, F., Tecilla, P., Formaggio, F., Crisma, M., Toniolo, C., Scrimin, P., *J. Am. Chem.. Soc.*, **1999**, *121*, 6948.
[43] De Iuliis, G. N.; Lawrance, G. A. and Fieuw-Makaroff, S. *Inorg. Chem. Commun.*, **2000**, *3*, 307.
[44] Komiyama, M., Kina, S., Matsumura, K., Sumaoka, J., Tobey, S., Lynch, V. M. and Anslyn, E., *J. Am. Chem. Soc.*, **2002**, *124*, 13731.
[45] Molenveld, P., Engbersen, J. F. J. and Reinhoudt, D. N., *Angew. Chem. Int. Ed.*, **1999**, *38*, 3189.
[46] Cacciapaglia, R., Casnati, A., Mandolini, L., Reinhoudt, D. N., Salvio, R., Sartori, A., Ungaro, R., *J. Am. Chem. Soc.*, **2006**, *128*, 12322.
[47] Schnaith, L. M. T.; Hanson, R. S. and Que, L., *Proc. Natl. Acad. Sci. USA*, **1994**, *91*, 569.
[48] Liu, C.; Yu, S.; Li, D.; Liao, Z.; Sun, X. and Xu, H. *Inorg. Chem.*, **2002**, *41*, 913.
[49] Ragunathan, K. G.; Schneider, H.-J., *Angew. Chem., Int. Ed. Engl.*, **1996**, *35*, 1219.
[50] Zhu, B., Zhao, D.-Q., Ni, J.-Z., Zeng, Q.-H., Huang, B.-Q. and Wang, Z.-L., *Inorg. Chem. Commun.*, **1999**, *2*, 351.
[51] Farquhar, E. R., Richard, J. P. and Morrow, J. R., *Inorg. Chem.*, **2007**, *46*, 7169.
[52] Worm, K., Chu, F., Matsumoto, K., Best, M. D., Lynch, V. and Anslyn, E. V., *Chem. Eur. J.*, **2003**, *9*, 741.
[53] Wall, M., Linkletter, B., Williams, D., Lebuis, A.-M., Hynes, R. C. And Chin, J., *J. Am. Chem. Soc*, **1999**, *121*, 4710.
[54] Kövári, E. and Krämer, R., *J. Am. Chem. Soc.*, **1996**, *118*, 12704.
[55] Ait-Haddou, H., Sumaoka, J., Wiskur, S. L., Folmer-Andersen, J. F. and Anslyn, E. V., *Angew. Chem. Int. Ed.*, **2002**, *41*, 4014.
[56] Livieri, M., Mancin, F., Tonnellato, U. and Chin, J., *Chem. Commun.*, **2004**, 2862.
[57] **a)** Mareque-Rivas, J. C., Prabaharan, R. and Torres Martín De Rosales, R., *Chem. Commun.*, **2004**, 76; **b)** Mareque-Rivas, J. C.; Prabaharan, R. and Parsons, S. *Dalton Transactions*, **2004**, 1648.
[58] **a)** Feng, G., Mareque-Rivas, J. C. and William, N. H., *Chem. Commun.*, **2006**, 1845; **b)** Feng, G., Mareque-Rivas, J. C., Torres Matrin de Rosales, R. and Williams, N. H., *J. Am. Chem. Soc.*, **2005**, *127*, 13470.
[59] Raines, R. T., *Chem. Rev.*, **1998**, *98*, 1045.
[60] Anslyn, E. and Breslow, R., *J. Am. Chem. Soc.*, **1989**, *111*, 5972.
[61] Komiyama, M. and Yoshinari, K., *J. Org. Chem.*, **1997**, *62*, 2155.
[62] **a)** Jubian, V., Veronese, A., Dixon, R. P. and Hamilton, A. D., *Angew. Chem. Int. Ed. Engl.*, **1995**, *34*, 1237; **b)** Piatek, A. M., Gray, M. and Anslyn, E. V., *J. Am. Chem. Soc.*, **2004**, *126 (32)*, 9878; **c)** Scheffer, U., Strick, A., Ludwig, V., Peter, S., Kalden, E. and Göbel, M. W., *J. Am. Chem. Soc.*, **2005**, *127 (7)*, 2211.
[63] Král, V., Lang, K., Králová, J., Dvořák, M., Martásek, P., Chin, A. O., Andrievsky, A., Lynch, V. and Sessler, J. L., *J. Am. Chem. Soc.*, **2006**, *128 (2)*, 432.
[64] Avenier, F., Domingos, J. B., Van Vliet, L. D. and Hollfelder, F., *J. Am. Chem. Soc.*, **2007**, *129 (24)*, 7611.
[65] **a)** Yurchenko, L., Silnikov, V., Godovikova, T., Shishlan, G., Toulme, J.-J., Vlassov, V., *Nucleos. Nucleot. Nucl.*, **1997**, *16 (7)*, 1721; **b)** Beloglazova, N. G., Sil'nikov, V. N., Zenkova, M. A., Vlassov, V. V., *FEBS Lett.*, **2000**, *481*, 277; **c)** Verheijen, J. C., Deiman, B. A. L. M., Yeheskiely, E., van der Marel, G. A. and van Boom, J. H., *Angew. Chem. Int. Ed.*, **2000**, *39 (2)*, 369; **d)** Beloglazova, N. G., Fabani, M. M., Zenkova, M. A., Bichenkova, E. V., Polushin, N. N., Sil'nikov, V. V., Douglas, K. T. and Vlassov, V. V., *Nucleic Acids Res.*, **2004**, *32*, 3887.
[66] Erkkila, K., E., Odom, D. T. and Barton, J. K., *Chem. Rev.*, **1999**, *99*, 2777.
[67] Basile, L. A., Raphael, A. L. and Barton, J. K., *J. Am. Chem. Soc.*, **1987**, *109*, 7550.
[68] Picture derived from data submitted to the Protein Data Bank (number PDB 108D, www.rcsb.org/pdb); Spielmann, H. P., Wemmer, D. E. and Jacobsen, J. P., *Biochemistry*, **1995**, *34*, 8542.
[69] Fitzimons, M. P. and Barton, J. K., *J. Am. Chem. Soc.*, **1997**, *119*, 3379.
[70] Boseggia, E., Gatos, M., Lucatello, L., Mancin, F., Moro, S., Palumbo, M., Sissi, C., Tecilla, P., Tonnellato, U. and Zagotto, G., *J. Am. Chem. Soc.*, **2004**, *126*, 4543.
[71] Åström, H., Williams, N. H. and Strömberg, R., *Org. Biomol. Chem.*, **2003**, *1*, 1461.
[72] Whitney, A., Gavory, G. and Balasubramaniam, S., *Chem. Commun.*, **2003**, 36.
[73] Putnam, W. C. and Bashkin, J. K., *Chem. Commun.*, **2000**, 767.

[74] Verheijen, J. C., Deiman, B. A. L. M., Yeheskiely, E., van der Marel, G. A. and van Boom, J. H., *Angew. Chem. Int. Ed.*, **2000**, *39 (2)*, 369.
[75] Beloglazova, N. G., Fabani, M. M., Zenkova, M. A., Bichenkova, E. V., Polushin, N. N., Sil'nikov, V. V., Douglas, K. T. and Vlassov, V. V., *Nucleic Acid Research*, **2004**, *32(13)*, 3887.
[76] Gnaccarini, C., Peter, S., Scheffer, U., Vonhoff, S., Klussmann, S. and Göbel, M. W., *J. Am. Chem. Soc.*, **2006**, *128(24)*, 8063.
[77] Nomura, A. and Sugiura, Y., *J. Am. Chem. Soc.*, **2004**, *126*, 15374.
[78] Sigel, H., Zuberbühler, A. D. and Yamahuchi, O., *Analytica Chimica Acta*, **1991**, *255(1)*, 63.
[79] **a)** Gran, G., *Analyst*, **1952**, *77*, 661; **b)** P. Gans and B. O'Sullivan, *Talanta*, **2000**, *51*, 33.
[80] Gans, P., Sabatimi, A. and Vacca, A., *Talanta*, **1996**, *43*, 1739.
[81] Alderighi, L., Gans, P., Ienco, A., Peters, D., Sabatini, A. and Vacca, A., *Coord. Chem. Rev.*, **1999**, *184*, 311.
[82] Cornish-Bowden, A., *Fundamental of Enzyme Kinetics*, Portland Press Ltd., London **1995**.
[83] Fersht, A., *Enzyme structure and mechanism*, W. H. Freeman and Company, New York, **1985**.
[84] Boniecki, S. and Kabzinska, Z., *Ann. Pharm. Franc.*, **1964**, *22*, 685.
[85] **a)** Romary, J. K., Barger, J. D. and Bounds, J., *Inorg. Chem.*, **1968**, *7*, 1142; **b)** Gruenwedel, D. V., *Inorg. Chem.*, **1968**, *7*, 495.
[86] Groβ, F., Müllel-Hartmann, A. and Vahrenkamp, H., *Eur. J. Inorg. Chem.*, **2000**, *11*, 2363.
[87] **a)** Mito-oka, Y., Tsukiji, S., Hiraoka, T., Kasagi, N., Shinkai, S. and Hamachi, I., *Tetrahedron Lett.*, **2001**, *42*, 7059; **b)** Ojeda, A., Mito-oka, Y., Inoue, M. and Hamachi, I., *J. Am. Chem. Soc.*, **2002**, *124*, 6256; **c)** Lee, D. H., Kim, S. Y. and Hong, J. I., *Angew. Chem In. Ed.*, **2004**, *116*, 4881; **d)** Amelan, D. J., Sandhya, M., Amrita, G., Anupama, S., Sanjiv, K. M. and Amitava, D., *Org. Lett.*, **2007**, *9*, 1979; **e)** Anai, T., Nakata, E., Koshi, Y., Ojeda, A. and Hamachi, I., *J. Am. Chem. Soc.*, **2007**, *129*, 6232.
[88] **a)** Young, M. J., Wahnon, D., Hynes, R. C. and Chin, J., *J. Am. Chem. Soc.*, **1995**, *117*, 9441; **b)** Yashiro, M., Ishikubo, A. and Komiyama, M., *J. Chem. Soc., Chem. Commun.*, **1995**, *17*,1793; **c)** Yashiro, M., Kaneiwa, H., Onaka, K. and Komiyama, M. *Dalton Trans.*, **2004**, 605.
[89] **a)** Wall, M., Linkletter, B., Williams, D., Lebuis, A-M., Hynes, R. C. and Chin, J., *J. Am. Chem. Soc.*, **2002**, *124*, 10946; **b)** Livieri, M., Mancin, F., Tonellato, U. and Chin, J., *Chem. Commun.*, **2004**, 2862; **c)** Feng, G., Mareque-Rivas, J. C. and Williams, N. H., *Chem. Commun.*, **2006**, 1845.
[90] **a)** Kimura, E., Aoki, S., Koike, T. and Shiro, M., *J. Am. Chem. Soc.*, **1997**, *119*, 3068; **b)** Chin, J., Chung, S. and Kim, D. H., *J. Am. Chem. Soc.*, **2002**, *124*, 10948.
[91] Mareque-Rivas, J. C., Torres Martín de Rosales, R. and Parsons, S., *Chem. Commun.*, **2004**, 610.
[92] Mareque-Rivas, J. C., Prabaharan, R. and Torres Martín de Rosales, R., *Chem. Commun.*, **2004**, 76.
[93] Feng, G., Mareque-Rivas, J. C. and Williams, N. H., *Chem. Commun.*, **2006**, 1845.
[94] **a)** Fritz, T., Steinfeld, G., Käss, S. and Kersting, B., *Dalton Trans.*, **2006**, 3812; **b)** Adams, H., Fenton, D. E., Haque, S. R. and Spey, S. E., *Inorg. Chem. Commun.*, **2000**, *3*, 83; **c)** Wang, Z., Martell, A. E., Motekaitis, R. J. and Reibenspies, J., *J. Chem. Soc., Dalton Trans.*, **1999**, 2441.
[95] Lee, J.H., Park, J., Lah, M.S., Chin, J. and Hong, J.-I., *Org. Lett.*, **2007**, *9*, 3729.
[96] De Mendoza, J., Nieto, P. M., Prados, P. and Sànchez, C., *Tetrahedron*, **1990**, *46*, 67.
[97] Ojeda, O., Mito-oka, Y., Inoue, M. and Hamachi, I., *J. Am. Chem. Soc.*, **2002**, *124*, 6256.
[98] Horner, O., Anxolabéhère-Mallart, E., Charlot, M.-F., Tchertanov, L., Guilhem, J., Mattioli, T. A., Boussac, A. and Girerd, J.-J., *Inorg. Chem.*, **1999**, *38*, 1222.
[99] Harata, M., Hasegawa, K., Jitsukawa, L., Masuda, H. and Einaga, H., *Bull. Chem. Soc. Jpn.*, **1998**, *71*, 1031.
[100] De Mendoza, J.; Nieto, P. M.; Prados, P. and Sanchez, C., *Tetrahedron*, **1990**, *46(2)*, 671.
[101] Nishida, Y., Shimo, H. and Kida, S., *J. Chem. Soc., Chem. Commun.*, **1984**, 1611.
[102] Horner, O., Anxolabéhère-Mallart, E., Charlot, M.-F., Tchertanov, L., Guilhem, J., Mattioli, T. A., Boussac, A. and Girerd, J.-J., *Inorg. Chem.*, **1999**, *38*, 1222.
[103] **a)** Fahrni, C. J. and O'Halloran, T. V., *J. Am. Chem. Soc.*, **1999**, *121*, 11448; **b)** O'Halloran, V., *et al.*, *J. Biol. Inorg. Chem.*, **1999**, *4*, 775; **c)** Guo, Z.-J., *et al.*, *Dalton Trans.*, **2006**, *29*, 3528.
[104] Moratal, J., Julve, M. and Faus, J., *Rev. Chim. Min.*, **1982**, *19*, 72.
[105] Kinoshita, E., Takahashi, M., Takeda, H., Shiro, M. and Koike, T., *J. Chem. Soc. Dalton Trans.*, **2004**, 1189.
[106] Ciavatta, L., Mareque, J.C., Natale, D. and Salvatore, F., *Ann. Chim.*, **2006**, *96*, 317.
[107] **a)** Gans, P., Sabatini, A. and Vacca, A., *Talanta*, **1996**, *43*, 1739; **b)** Alderighi, L., Gans, P., Ienco, A., Peters, D., Sabatini, A. and Vacca, A., *Coord. Chem. Rev.*, **1999**, *184*, 311.

[108] **a)** Gans, P., Sabatini, A. and Vacca, A., *Talanta*, **1996**, *43*, 1739; **b)** Alderighi, L., Gans, P., Ienco, A., Peters, D., Sabatini, A. and Vacca, A., *Coord. Chem. Rev.*, **1999**, *184*, 311.

[109] **a)** Boisen, A., Hazell, A. and McKenzie, C. J., *Chem. Commun.*, **2001**, 2136; **b)** M. Ghilandi *et al.*, *J. Chem. Soc., Dalton Trans.*, **1999**, 2675; **c)** Ghiladi, M., Gomez, J. T., Hazell, A., Kofod, P., Lumtscher, J. and McKenzie, C. J., *J. Chem. Soc., Dalton. Trans.*, **2003**, 1320.

[110] Egdal, R. K., Larsen, F. B., Bond, A. D. and McKenzie, C. J., *Inorg. Chim. Acta*, **2005**, *358*, 376.

[111] **a)** Baughman, E. H., and Kreevoy, M. M., J. Phys. Chem., 1974, 78, 421; **b)** Georgieva, M., Velinov, G. and Budevsky, O., Anal. Chim. Acta, 1977, 90, 83; **c)** Sánchez-Lombardo, I., and Yatsimirsky, A. K., Inorg. Chem., 2008, 47, 2514.

[112] Kinoshita, E., Takahashi, M., Takeda, H., Shiro, M. and Koike, T., Dalton Trans., **2004**, 1189.

[113] **a)** Faus, J., García-España, E., Marcelino, V., Bencini, A. and Bianchi, A., *Inorg. Chim. Acta*, **1990**, *172*, 203; **b)** Edward, J. T., Farrell, F. G. and Kirchnerova, J., *J. Can. Chem.*, **1976**, *54*, 1899; **c)** Fini, A., De Maria, P., Guarnieri, A. and Varoli, L., *J. Pharm. Sci.*, **1987**, *76*, 48.

[114] Brown, D. M. and Usher, D. A., *J. Chem. Soc.*, **1965**, 6558.

[115] Feng, G., Natale, D., Prabaharan, R., Mareque-Rivas, J. C. and Williams, N. H., *Angew. Chem. Int. Ed.*, **2006**, *45*, 7056.

[116] Frish, M. J., *et al.*, *Gaussian 03*, Revision B.4, B.5, and C.1; Gaussian, Inc.: Pittsburgh, PA, 2003

[117] ArgusLab can be download for free from the website: www.planaria.software.com

[118] **a)** Albedyhl, S., Schnieders, D., Jancsó, A., Gajda, T. and Krebs, B., *Eur. J. Inorg. Chem.*, **2002**, 1400; **b)** Deal, K. A. and Burstyn, J. N., *Inorg. Chem.*, **1996**, *35*, 2792; **c)** Kady, I. O., Tan, B., Ho, Z. and Scarborough, T., *J. Chem. Soc. Chem. Commun.*, **1995**, 1137; **d)** Fritsky, I. O., Ott, R., Pritzkow, H. and Krämer, R.. *Chem. Eur. J.*, **2001**, *7*, 1221; **d)** Bauer-Siebenlist, B. *et al.*, *Inorg. Chem.*, **2004**, 43, 4189.

[119] Feng, G., Mareque-Rivas, J. C. and Williams, N. H., *Chem. Commun.*, **2006**, 1845.

[120] **a)** Breslow, R., Berger, D. and Huang, D.-L., *J. Am. Chem. Soc.*, **1990**, *112*, 3686; **b)** Chu, F., Smith, J., Lynch, V. M. and V. Anslyn, E., *Inorg. Chem.*, **1995**, *34*, 5689; **c)** Kimura, E., Kodama, Y., Koike, T. and Shiro, M.. *J. Am. Chem. Soc.*, **1995**, *117*, 8304.

[121] **a)** Molenveld, P., Engbersen, J. F. J. and Reinhoudt, D. N., *Chem. Soc. Rev.*, **2000**, *29*, 75; **b)** Worm, K., Chu, F., Matsumoto, K., Best, M. D., Lynch, V. and Anslyn, E. V., *Chem. Eur. J.*, **2003**, *9*, 741.

[122] O'Donoghue, A., Pyun, S. Y., Yang, M.-Y., Morrow, J. R. and Richard, J. P., *J. Am. Chem. Soc.*, **2006**, *128*, 1615.

[123] **a)** Belli Dell'Amico, D., Calderazzo, F., Labella, L., Marchetti, F. and Pampaloni, G., *Chem. Rev.*, **2003**, *103*, 3857; **b)** Mao, Z. W., Liehr, G. and van Eldik, R., *J. Am. Chem. Soc.*, **2000**, *122*, 4839; **c)** Kong, L.-Y. *et al.*, *Angew. Chem. Int. Ed.*, **2005**, *44*, 4352; **d)** Yamaguchi, S., Takahashi, T., Wada, A., Funahashi, Y., Ozawa, T., Jitsukawa, K. and Masuda, H., *Chem. Lett.*, **2007**, *36*, 842.

[124] Khalifah, R. G., *J. Biol. Chem.*, **1971**, *246*, 2561.

[125] **a)** Xue, Y., Vidgren, J., Svensson, L. A., Liljas, A., Jonsson B.-H. and Lindskog, S., *Proteins*, **1993**, *15*, 80; **b)** Håkansson, K., Carlsson, M., Svensson, L. A. and Liljas, A., *J. Mol. Biol.*, **1992**, *227*, 1192; **c)** Nair, S. K. and Christianson, D. W., *J. Am. Chem. Soc.*, **1991**, *113*, 9455.

[126] Fisher, S. Z. *et al.*, *Biochemistry*, **2007**, *46*, 2930.

[127] **a)** Yin, X. and Moss, J. R., *Coord. Chem. Rev.*, **1999**, *181*, 27; **b)** Leitner, W., *Coord. Chem. Rev.*, **1996**, *153*, 257.

[128] Bazzicalupi, C. *et al.*, *Inorg. Chem.*, **1996**, *35*, 5540 and references therein.

[129] **a)** N. Ueyama *et al.*, *Angew. Chem. Int. Ed.*, **2005**, *44*, 4352; **b)** Verdejo, B., Aguilar, J. and Garcia-España, E., *Inorg. Chem.*, **2006**, *45*, 3803.

[130] Masuda H. *et al.*, *Chem. Lett.*, **2007**, *36*, 842.

[131] Li, H., Sadler, P. J. and Sun, H., *J. Biol. Chem.*, **1996**, *271*, 9483; Sadler, P. J. *et al.*, *Biochem.*, **2000**, *39*, 10023; Zhing, W., Parkinson, J. A., Guo, M. and Sadler, P. J., *J. Biol. Inorg. Chem.*, **2002**, *7*, 589; Valentine, A. M. *et al.*, *PNAS*, **2008**, *105*, 3268.

[132] **a)** Cleland, W. W., M. H. O'Leary and D. B. Northrop, eds., "Isotope Effects on Enzyme-Catalyzed Reaction", University Park Press, Baltimore, Maryland, 1977; **b)** W. J. Albery, *in* "Proton Transfer Reactions" (E. Caldrin and V. Gold, eds.) p.263, Chaman & Hall, London, 1975.

[133] Virtanen, N., Polari, L., Välilä, M. and S. Mikkola, *J. Phys. Org. Chem.*, **2005**, *18*, 385 and references within.

[134] **a)** Dalby, K. N., Kirby, A. J. and Hollfelder, F., *J. Chem Soc. Perkin Trans.*, **1993**, *2*, 1269; **b)**. Bruice, T. C., Blasko, A., Arasasingham, R. D. and Kim, J., *J. Am. Chem. Soc.*, **1995**, *117*, 12070.

[135] **a)** Nakano, S., Chadalavada, D. M. and Bevilacqua, P. C., *Science*, **2000**, *287*, 1493; **b)** Pinard, R. *et al.*, *EMBO J.*, **2001**, *20*, 6434; **c)** Takagi, Y. and Taira, K., *J. Am. Chem. Soc.*, **2002**, *124*, 3850.
[136] Pocker, Y. and Biorkquist, D. W., *Biochem.*, **1977**, *16*, 5698.
[137] Schowen, K. B.and Schowen, R. L., *Methods Enzymol.*, **1982**, *87*, 551.
[138] Krishtalik, L. I., *Biochimica et Biophysica Acta*, **2002**, *1458*, 6.
[139] **a)** De Rosch, M. A. and Trogler, W. C., *Inorg. Chem.*, **1990**, *29*, 2409; **b)** Kazuya, Y. *et al.*, *Chem. Commun.*, **2001**, 375; **c)** Krebs, B. *et al.*, *Eur. J Inorg. Chem.*, **2002**, 1400; **d)** Jancsó, A. *et al.*, *Chem. Eur. J.*, **2003**, *9*, 5404.
[140] Fao, Y. and Gao, Y. Q., *J. Am. Chem. Soc.*, **2007**, *129*, 905.

Publications

1. Daniela Natale and Juan C. Mareque Rivas, The combination of transition metal ions and hydrogen-bonding interactions, *Chem. Commun.*, **2008**, *4*, 425.

2. Guoqiang Feng, Daniela Natale, Ravi Prabaharan, Juan C. Mareque Rivas, Nicholas H. Williams, Efficient phosphodiester binding and cleavage by a ZnII complex combining hydrogen-bonding interaction and double lewis acid activation, *Angew. Chem. Int. Ed.*, **2006**, *45*, 7056.

3. Liberato Ciavatta, Juan C. Mareque, Daniela Natale, Francesco Salvatore, Complex formation between Zn^{2+} ion and 1,3-bis[bis(pyridin-2-ylmethyl)amino]propan-2-ol, *Annali di Chimica*, **2006**, *96*, 317.

Other activities, awards and fellowships

Conferences attended: "UK Macrocycles and Supramolecular Chemistry Meeting" – (4-5 January 2006) – Leeds (UK) – **Poster Prize Winner**.
"DNA-Metal interaction" – (13-19 November 2006) – Athens (Greece) – **Student International Conference Grant Awarded**.
"ICBIC XIII – 13th International Conference on biological inorganic chemisty" – (15-20 July 2007) – Vienna (Austria).

Tran skills courses: "How to be an effective researcher" (2 days)
"Time Management" (1 day)